

STRATEGY FOR THE SELECTION OF GRINDING WHEEL DRESSING CONDITIONS

XUN CHEN

A thesis submitted in partial fulfilment of the requirements of Liverpool
John Moores University for the degree of Doctor of Philosophy

April 1995

Acknowledgements

The author would like to thank Professor W. Brian Rowe for his guidance and supervision, and to acknowledge the support and interest provided by Professor J. L. Moruzzi.

Thanks are also due to Professor B. Mills for permitting this work to be carried out in the School of Engineering and Technology Management.

Technical support from the technician staff in the School of Engineering and Technology Management is appreciated and particular gratitude is due to Messrs Paul Wright, Peter Moran and Stephen Ebbrell for their invaluable assistance.

Many thanks also go to Messrs David R. Allanson, Michael N. Morgan and other members of staff in the AMT Research Laboratory for their practical help.

Acknowledgements are due to the Royal Society for initial funding to visit the Liverpool John Moores University and to the Liverpool John Moores University for providing the research funding necessary to undertake the doctoral research programme.

Finally, and not least, the author would like to acknowledge the support and encouragement of his family over past years.

Abstract

The dressing process and its relationship to the mechanics of grinding are analysed. It was found that the most important parameters in single point diamond dressing are the dressing lead, the dressing depth and the diamond width. It was also found that the effects of dressing can be monitored by measuring grinding power and workpiece roughness. When a large dressing lead and a large dressing depth are employed, the grinding power decreases but surface roughness increases. It was found that a change of the diamond shape leads to large changes in grinding behaviour. Experimental results show that changes of the grinding performance due to diamond wear can be compensated by appropriate adjustments of the dressing depth and the dressing lead. To account for the inability to control diamond shape, an adaptive strategy is proposed for adjustment of dressing conditions based on the grinding performance.

Computer simulations were designed to assist in the investigation of the grinding process. Analysis showed that the grinding cycle behaviour can be characterised by the system time constant. Grinding cycles were designed and simulated based on the time constant. An adaptive control strategy was developed for maximising the metal removal rate.

Simulation showed that inputs and outputs of the grinding process could be synthesised based on the actions of individual grains. A methodology was proposed to simulate the dressing and grinding process. The grinding wheel was initially generated by means of randomly spaced grains. The shape of the grains was modified by simulating the dressing process. The grinding forces were simulated by calculating the force on every engaged grain. The workpiece surface was generated by simulating the movement of every grain of the wheel through the workpiece. Fracture of the grain, deflection of the grain centre and plastic deformation of the workpiece were considered in the simulation of each grain interaction. The effects of

the dressing conditions on grinding performance were simulated and compared with experiments.

Vibration is one of the main indicators of the need for grinding wheel dressing. A neural network was developed to identify wheel life based on vibration levels. The signal data were pre-treated by an eight band pass filter, which covered the whole frequency range of the grinding chatter. These pre-treated data were used as the inputs to the neural network. By training the neural network, an objective criterion was determined for the wheel redress life.

CONTENTS

Acknowledgements	i
Abstract	ii
Contents	iv
Nomenclature	vi
List of Illustrations	xii
1. Introduction	1
1.1. The Importance of the Dressing Operation	1
1.2. Aims and Objectives	3
1.3. Scope of the Investigation	3
2. The Mechanics of Dressing	5
2.1. The Grinding Wheel	5
2.2. The Dressing Process	7
2.3. Effects of Dressing on the Grinding Wheel Topography	10
2.4. Effects of Dressing on Grinding Behaviour	14
2.5. Evaluation and Optimisation of the Dressing Operation	17
2.6. Conclusion	19
3. Mechanics of Grinding	20
3.1. The Action of a Single Abrasive Grain	20
3.2. Empirical Grinding Process Relationships	23
3.3. Physical Grinding Process Relationships	28
3.4. Generation of the Workpiece Surface in Grinding	32
3.5. Wheel Sharpness and Wheel Wear	33
3.6. Simulation of Grinding Behaviour	38
4. Grinding Process Control	40
4.1. Basic Features of a Plunge Grinding Cycle	40
4.2. Grinding as a Control System	43

4.3. Requirements of a Dressing Strategy	45
5. Experimental Investigation of the Dressing and Grinding Performance	47
5.1. The Experimental System	47
5.2. Experimental Procedure	50
5.3. Experimental Results and Discussion	53
5.3.1. Effects of the Dressing Conditions on the Dressing Force	53
5.3.2. Effects of the Grinding Conditions on the Grinding Process	54
5.3.3. Effects of the Dressing Conditions on the Grinding Process	55
5.3.4. Correlation of Dressing Conditions and Grinding Behaviour	61
5.4. Conclusion	62
6. Empirical Models for Dressing and Grinding	64
7. Simulation of Grinding Cycles	71
7.1. The Characteristics of a Grinding Cycle	71
7.2. Development of a Simulation for Grinding Cycles	75
7.3. Simulation for Grinding Cycle Design	77
8. Simulation of the Dressing and Grinding Process	80
8.1. Generation of the Grinding Wheel Topography	80
8.2. Generation of the Ground Workpiece Surface	84
8.3. Mechanics of Grinding in the Simulation	86
8.4. Simulation Procedure	89
8.5. Simulation Results and Discussion	94
8.6. Conclusion	96
9. Formulation of Strategy for Selecting Dressing Conditions	97
9.1. Fundamentals of a Sensor Based Dressing Strategy	97
9.1.1. Selection of Initial Dressing Conditions	98
9.1.2. When the Wheel Should Be Redressed	99
9.1.3. Selection of Monitoring Parameters for Dressing	100
9.2. Development of Dressing Strategies	103
9.2.1. A Strategy Based on Stabilising the Time Constant	104
9.2.2. A Strategy Based on Stabilising the Grinding Power	106

9.3. Combination of the Dressing Strategy with a Grinding Strategy	110
10. Evaluation of the Dressing Strategy	112
10.1 Determination of the Redress life of the Grinding Wheel	112
10.2. Evaluation of the Strategy of Stabilising Grinding Power	115
11. Conclusions	120
12. Recommendations for Further Work	122
Appendices	123
A.1. References	123
A.2. Computer Program for Simulation of Dressing and Grinding	136
A.3. List of the Author's Relevant Published Papers	153

Figures

Nomenclature

A	cross sectional area of the undeformed chip;
A_o	interface area of a grain;
a	depth of cut;
a_c	engaged length of a grain;
A_d	dressing area;
a_d	dressing depth;
A_m	mean chip cross sectional area;
A_p	area of the pile-up material;
A_r	real contact area between wheel and workpiece;
b	grinding width, radius of the projected area of grain;
b_c	cutting width of a grain;
C	constant;
C'	constant of constraint;
C_0	constant;
C_1	static cutting edge density;
d_c	diameter of the equivalent grain contact circle;
d_e	equivalent diameter;
d_g	diameter of abrasive grain;
d_{geq}	diameter of the equivalent grain;
d_s	wheel diameter;
d_w	workpiece diameter;
E	energy consumption
e_c	specific energy;
e_{cc}	specific cutting energy;
e_f	specific energy due to friction;
e_g	specific energy for a single grain;
f	constant;

F_0	initial grinding force;
F_1	constant;
F_2	constant;
f_c	cutting force on a grain;
F_d	dressing force;
f_d	dressing lead;
F_e	critical grinding force at the end of the secondary grinding stage;
F_n	normal grinding force;
f_n	normal grinding force on a grain;
F_{nc}	normal grinding cutting force;
f_{nc}	normal grinding cutting force on a grain;
f_{nf}	normal grinding friction force on a grain;
F'_n	specific normal grinding force;
F'_{no}	minimum specific normal grinding force to remove metal;
F_{ns}	normal grinding sliding force;
F_r	grain retention force;
F_t	tangential grinding force;
F'_{t0}	initial specific tangential grinding force;
f_t	tangential grinding force on a grain;
F_{tc}	tangential grinding cutting force;
f_{tc}	tangential grinding cutting force on a grain;
f_{tf}	tangential grinding friction force on a grain;
F'_{te}	final specific tangential grinding force;
F_{ts}	tangential grinding sliding force;
G	grinding ratio;
H	hardness of workpiece or wheel hardness grade number;
h	amplitude of the fracture sine wave in dressing simulation, or height of plastic pile-up;
h_{eq}	equivalent chip thickness;
K	constant;

k	constant;
k_0	constant;
k_1	constant;
k_a	contact stiffness of grinding zone;
k_c	grinding force coefficient or cutting stiffness of grinding;
k_e	overall effective stiffness of the grinding system;
k_m	stiffness of the wheel and grinding machine;
k_w	stiffness of the workpiece;
$K_{\lambda w}$	constant;
l_k	kinematic grinding contact length;
l_s	the distance travelled by a grain on the wheel surface in the time the workpiece takes to travel the distance l_k ;
M	grain size number;
m	probability of grain fracture in a unit grinding cycle;
n	the number of revolutions of the workpiece;
n_d	the number of dressing passes;
n_w	workpiece rotational speed;
n_s	wheel rotational speed;
P	grinding power;
P'	specific power;
P_0	constant;
P_{ch}	the chip formation component of the grinding power;
P_{pl}	the ploughing component of the grinding power;
P_{sl}	the sliding component of the grinding power;
\bar{p}	average contact pressure between the wear flats and the workpiece;
Q_w	grinding removal rate;
Q'_w	grinding removal rate per unit wheel width;
R	force of indentation;
r	radius of the workpiece, exponent constant;
$r(t)$	workpiece radius reduction;

R_0	constant;
R_1	constant;
R_a	surface roughness;
R_c	Rockwell Hardness;
R_{pv}	theoretical peak-to-valley height of dressing trace;
S	wheel structure number;
T	period of one workpiece revolution;
t	grinding time or cutting depth of a grain;
t_{max}	maximum cutting depth of a grain;
\bar{t}	average depth of cut of the grains;
u	mean separation distance of the grains on the wheel surface;
U_d	overlap coefficient;
V_g	grain volume packing density;
VOL	volume factor for wheel;
v_s	grinding wheel speed;
v_w	workpiece speed;
v_f	wheel axis infeed rate;
$X(t)$	the position of the grinding wheel axis;
x	exponent;
y	exponent;
z	exponent;
α	proportion of grains actually cutting or coefficient of significance;
β	proportion of the groove volume removed or upward flow ratio;
γ	diamond sharpness ratio or constant;
Δ	average spacing of grains along the co-ordinate axes;
Δr	workpiece radius error;
Δr_0	initial workpiece roundness error;
$\Delta \dot{X}_0$	change of infeed rate according to the size control strategy;
$\Delta \dot{X}_1$	change of infeed rate according to the power control strategy;
δ	deflection of the grinding system;

δ_c	local workpiece deformation;
δ_d	elastic deflection of a grain in dressing;
δ_g	grain tip deformation;
δ_{rt}	rotation of the grain;
δ_w	deflection of the grain centre;
ϵ	constant;
η	constant;
θ	half-angle of the scratch or direction of action of the indent force;
λ	grinding force ratio f_n/f_t or F_n/F_t ;
$\lambda(t)$	cutting edge density during grinding;
λ_0	cutting edge density after dressing;
λ_e	cutting edge density at the end of the secondary grinding stage;
λ_w	metal removal parameter;
σ_w	strength of the grinding wheel;
τ	time constant;
ϕ	tip angle of the dressing diamond;
μ	friction coefficient

List of Illustrations

Figure

- 2.1 Kinematic description of dressing process
- 2.2 Grain surface after dressing
- 2.3 Grain fracture and bond fracture
- 3.1 Three stages of chip generation
- 3.2 Grit deflection in grinding
- 3.3 Generation of the workpiece surface in grinding
- 3.4 Cutting and sliding in the grinding process
- 3.5 Action of a spherical grain in grinding
- 3.6 Expression of material flow under a grain in grinding
- 3.7 Generation of the workpiece surface due to kinematic relationships
- 3.8 Variation of grinding force in a grinding wheel life cycle
- 4.1 Representation of the external cylindrical plunge grinding machine system
- 4.2 Process relationships in grinding
- 5.1 The experimental system
- 5.2 Acceleration signals of grinding vibration
- 5.3 Spectrum of acceleration of grinding vibrations
- 5.4 Data logging strategy
- 5.5 Flow chart of the data logging programme
- 5.6 The Butterworth filter circuit
- 5.7 Effect of the number of dressing passes
- 5.8 Measurement of dressing diamond shape
- 5.9 Diamond dressing tool shape affected by the dressing operation
- 5.10 The surface of a worn diamond
- 5.11 Effect of dressing condition on dressing force
- 5.12 Effects of equivalent chip thickness on specific power
- 5.13 Effects of equivalent chip thickness on specific energy

- 5.14 Effects of equivalent chip thickness on surface roughness
- 5.15 Effects of dressing condition on grinding power (sharp diamond)
- 5.16 Effects of dressing condition on grinding power (blunt diamond)
- 5.17 Effects of dressing condition on ground surface roughness (sharp diamond)
- 5.18 Effects of dressing conditions on ground surface roughness (blunt diamond)
- 5.19 Effects of dressing conditions on size error (sharp diamond)
- 5.20 Effects of dressing condition on size error (blunt diamond)
- 5.21 Thermal effect on size error
- 5.22 Size error generated due to variation of wheel sharpness
- 5.23 Variation of time constant with workpiece number in grinding for various dressing conditions (sharp diamond)
- 5.24 Variation of time constant with workpiece number in grinding for various dressing conditions (blunt diamond)
- 5.25 Effects of dressing condition on roundness (sharp diamond)
- 5.26 Effects of dressing condition on roundness (blunt diamond)
- 5.27 Grinding power with width of dressing diamond
- 5.28 Time constant with width of dressing diamond
- 5.29 Roundness with width of dressing diamond
- 5.30 Surface roughness with width of dressing diamond
- 5.31 Size error with width of dressing diamond
- 5.32 Effect of grinding conditions on grinding power
- 5.33 Effect of grinding conditions on surface roughness
- 5.34 Effect of grinding conditions on time constant
- 5.35 Effect of grinding conditions on roundness
- 5.36 Idealised effects of dressing conditions on grinding behaviour
- 5.37 Idealised effect of dressing conditions on size error
- 6.1 Changes of grinding force with grinding time
- 6.2 Changes of grinding power during wheel redress cycle
- 7.1 Conventional plunge grinding cycle
- 7.2 The structure of grinding cycle simulation package

- 7.3 Block diagram of the simulation relationships
- 7.4 Multi-infeed and dwell cycle simulation
- 7.5 Comparison between actual and simulated size reduction curves
- 7.6 A simulated power control grinding cycle using a non-optimal in-process power control strategy
- 7.7 The flow chart for simulation of in-process power control
- 7.8 The simulated grinding cycle after optimisation
- 7.9 Experimental power control using the cycle determined by simulation
- 8.1 Orientation of grains for simulation of grinding
- 8.2 Cutting edges generated by dressing cutting
- 8.3 Cutting edges generated by dressing fracture
- 8.4 Simplified calculation of the remaining cross sectional area of the grain
- 8.5 Kinematic relation between grinding wheel and workpiece
- 8.6 Ploughing plastic pile up
- 8.7 Relationship between grinding force components
- 8.8 The equivalent grain in simulation
- 8.9 Equivalent spherical cutting edge as in sphere shape after dressing
- 8.10 Grinding force on a spherical grain
- 8.11 Flow chart of the dressing and grinding simulation program
- 8.12 Random distribution of the grains in the simulation
- 8.13 The contour of the diamond in the simulation
- 8.14 Dressing trace in the grinding wheel co-ordinate system
- 8.15 Simulation of the dressing process on a grain
- 8.16 Simulation of the grinding process on a grain
- 8.17 Simulation of the plastic pile up of the workpiece material
- 8.18 Generation of the workpiece during grinding
- 8.19 Ground surface generated from simulation
- 8.20 Simulated effects of dressing conditions on grinding force
- 8.21 Simulated effects of dressing conditions on surface roughness
- 8.22 Simulated effects of diamond width on grinding force

- 8.23 Simulated effects of diamond width on surface roughness
- 8.24 The relationship between standard deviation of grinding force and dressing overlap coefficient
- 8.25 The relationship between standard deviation of surface roughness and dressing overlap coefficient
- 8.26 Simulated grinding power in the dwell period
- 8.27 Simulated surface roughness variations in the dwell period
- 8.28 Simulated effects of dressing conditions on grinding power
- 8.29 Simulated effects of dressing conditions on surface roughness
- 8.30 The difference between the parabola assumption and the real diamond
- 9.1 Constraints on the dressing condition
- 9.2 Variation of the time constant in the initial stage of grinding
- 9.3 A strategy of minimising time constant
- 9.4 Variation of grinding power in a redress life cycle
- 9.5 Relationship between the grinding power and dressing conditions
- 9.6 Strategy to stabilise grinding power level
- 9.7 Maximum grinding power strategy for selection of dressing conditions
- 10.1 Acceleration signals of grinding vibrations
- 10.2 Spectra of grinding vibration
- 10.3 The spectrum of grinding vibrations
- 10.4 Development of the grinding vibration
- 10.5 Distribution of acceleration density in eight band filter
- 10.6 the structure of a neural network for chatter identification
- 10.7 Grinding chatter recognition by neural network
- 10.8 Grinding performances under initial dressing conditions
- 10.9 Dressing conditions recommended by dressing strategy
- 10.10 Optimisation of dressing conditions by the dressing strategy

Chapter 1 Introduction

1.1. The Importance of the Dressing Operation

Grinding is a machining process which utilises grinding wheels containing hard abrasive particles as the cutting medium. Grinding is one of the earliest techniques learned by human beings, and can be traced to Neolithic times[1]. As grinding became a precision operation, dressing techniques were developed for preparation of the working surface of the wheel. A device for dressing a sandstone grinding wheel was first patented by Altzschner in 1860[1]. Basic principles of dressing and truing grinding wheels were laid down by Norton[2] in 1905.

The dressing operation achieves two purposes. The first is to true the wheel surface to obtain profile accuracy and the second is to resharpen or dress the abrasive grains to improve the cutting ability. Most dressing operations combine the 'truing' and 'dressing' function as one, so the term dressing generally covers both functions. The usual reasons for redressing a wheel are:

- slow removal rate,
- grinding vibration,
- workpiece burn,
- poor surface texture,
- loss of form-holding.

Conventional grinding wheels made from alumina and silica are almost exclusively dressed with diamond tools. This is because diamond is the only material hard enough to dress conventional abrasives without itself suffering excessive wear. Single point diamond dressing is commonly used for precision grinding and achieves the best grinding results if the diamond is sharp. Multi-point diamond dressing tools

and diamond disc dressers may be used to achieve longer dressing tool life since the wear is distributed over a number of diamonds. For large batch sizes and formed profiles, diamond impregnated rolls are often used. Because the diamond roll extends the full width of the workpiece, dressing is fast. The economic advantages of a diamond roll rely on the savings in cycle time. However diamond rolls are expensive due to the large quantity of diamond required and the careful setting required, particularly for profiled grinding wheels. There is therefore a continuing requirement to employ single point diamond dressing for precision grinding in batch production.

The importance of the dressing process lies in the fact that a difference in dressing conditions leads to different grinding behaviour. The problem of current interest is to develop a methodology of achieving and maintaining optimal grinding behaviour of the grinding wheel. If the dressing operation can lead to more stable behaviour of the wheel, the variations of size error, surface roughness and possibly roundness error of ground workpieces can be reduced[3]. Conversely an unstable cutting performance of the grinding wheel will make the grinding process unpredictable and uncontrollable. Stable behaviour of the grinding wheel is particularly important for operation of CNC and automatic grinding machines[4-6]. A good dressing operation minimises grinding force variations and makes grinding behaviour easier to control.

The dressing operation relies on the skill of the operator to establish the best cutting performance for an operation. Because of this, trial and error is generally employed to achieve an optimal combination of grinding and dressing parameters for a required result in precision grinding. It was therefore decided to investigate the possibility of developing an adaptive strategy for selecting dressing conditions. Because the single diamond dressing method plays an important part in CNC batch production, this research was concentrated on the single diamond dressing operation.

1.2. Aims and Objectives

The aim of the research was to develop an adaptive strategy for the selection of suitable dressing conditions in order to optimise the grinding process. Major objectives of the research were to achieve

- (i) a theoretical analysis of the dressing operation;
- (ii) a parametric study of the effects of dressing conditions on grinding behaviour;
- (iii) a simulation model of both the dressing process and the grinding process;
- (iv) an adaptive strategy for selecting dressing conditions.

1.3. Scope of the Investigation

The research programme was divided into four main parts:

- (i) A literature survey of grinding wheel dressing;
- (ii) An investigation of the mechanics of grinding and dressing;
- (iii) A simulation study of the grinding process and the dressing process;
- (iv) The development and evaluation of a dressing strategy.

The first part of the research deals with a review of previous research on the dressing operation. The review includes a description of the dressing process, effects of dressing on grinding behaviour and optimisation of the dressing operation. Grain fracture is found to be a basis for analysing the dressing process. The factors affecting the grinding behaviour are discussed with particular relevance to the effects of dressing on the wheel topography. Existing methodologies for optimising the dressing operation are considered.

The mechanics of grinding and dressing is studied in the second part of the research. The kinematics of dressing is employed to analyse the generation of the wheel topography. Fracturing and dislodging of grains from the wheel surface during

dressing are investigated. Effects of wheel sharpness on the grinding behaviour are discussed and time constant is proposed as an appropriate parameter to represent the combined effects of the grinding force and system compliance. Methods to measure and control time constant are also discussed.

An experimental study was undertaken to determine the effects of the dressing variables on grinding efficiency and productivity. Experimental results are discussed in relation to the theoretical understanding of the process. The effects of varying dressing lead, dressing depth, number of dressing passes and diamond shape are discussed in relation to grinding power, workpiece surface texture, roundness, size error and dressing power. Empirical equations for grinding force and grinding power were established to describe the effects of the dressing conditions and grinding conditions.

A grinding cycle simulation was undertaken to illustrate the effects of the sharpness of the wheel on the grinding process. Further simulations of the dressing and grinding process were developed based on the action of individual grains to illustrate the generation of the wheel surface and the workpiece surface. The simulations were used to interpret the effects of wheel surface topography on grinding behaviour.

Surface roughness, grinding power and time constant trends were investigated as techniques which could be used to indicate the required changes in dressing conditions. A methodology for selecting grinding conditions is presented. The methodology is designed to be suitable for incorporation into a CNC as a sensor based strategy for adaptation of dressing conditions.

Chapter 2 The Mechanics of Dressing

The total grinding process includes dressing as well as grinding. Most grinding research is focused on the grinding process rather than the dressing process. Because of the random nature of the grinding wheel topography, the relationships between dressing and grinding parameters are difficult to analyse deterministically. It can be argued that dressing is the least understood but one of the most influential aspects of the grinding process.

2.1. The Grinding Wheel

The behaviour of the grinding wheel depends partly on its composition and structure and partly on the dressing conditions. The wheel specification in the standard marking system is defined by the following characteristics:

- (i) the type of abrasive;
- (ii) the abrasive grain size;
- (iii) the hardness grade of the wheel;
- (iv) the structure of the wheel;
- (v) the type of bond.

Correct selection of the grinding wheel is important for the achievement of stable grinding behaviour and long wheel life. In particular, an appropriate rate of self-sharpening is usually considered to be desirable[2, 7]. The following are some considerations in the selection of the grinding wheel[8].

- (i) The type of material to be ground affects the selection of abrasive, grain size and grade. Alumina abrasives[8] are used for grinding high tensile materials such as steel and ferritic cast irons. Silicon carbide abrasives that are even more friable are

used for grinding low tensile strength materials and non-metallic materials. CBN abrasive wheels[7] are suitable for grinding high speed steel and high alloy steels. Carbide, ceramic, glass and plastic are often ground using diamond wheels[7]. The harder the workpiece, the harder the grain required. For a particular grain hardness, a hard workpiece requires a 'softer' bond than a soft workpiece[8].

(ii) The rate of stock removal and surface texture required affect the choice of abrasive size and bond type. High stock removal rates usually require coarse grain wheels[8]. Fine surface texture and small tolerances need a finer grain size. Extremely fine surface texture usually requires resinoid, rubber or shellac-bonded wheels[8].

(iii) If the cutting edges on the grinding wheel tend to glaze and are therefore less likely to be resharpened by fracture, the grinding wheel is described as acting 'hard'. When the wear of cutting edges on the grinding wheel is mostly due to the fracture of the grains or bonds, the wheel is described as acting 'soft'. The effects of the grinding condition on wheel behaviour are summarised[8] in table 2.1.

Table 2.1 Effect of grinding conditions on wheel hardness behaviour

grinding conditions	behaviour of wheel
high wheel speed	hard
high work speed	soft
high infeed rate	soft

(iv) The grinding contact area also affects the selection of wheel grade and structure. A large contact area requires a wheel of soft grade and open structure. Vitrified wheels for dry grinding need to be one or two grades softer than for wet grinding[8].

A blunted wheel tends to increase grinding force, which may result in grinding chatter or grinding burn[7, 9]. If the wheel needs to be dressed too frequently because the

grinding force rapidly increases, the wheel is said to be too hard and a softer grade or coarser grain size is required. When the surface texture and dimensional accuracy of workpiece have deteriorated, the wheel needs to be redressed. If this happens too frequently, the wheel is said to be too soft or too coarse and either a harder grade wheel or a finer grain size is required.

2.2. The Dressing Process

The wheel surface profile formed by dressing is determined by the relative motion between the diamond and the wheel, the characteristics of the wheel and the shape of the diamond. In early research, the dressing process was described as a wheel cutting process. Pahlitzsch[10] suggested that the diamond cuts through the abrasive grains to produce cutting points. It was proposed that the form of the cutting point is determined by the combination of the diamond shape, the dressing lead and the dressing depth. A representation of the kinematic relationship between the grinding wheel and the dressing tool is shown in figure 2.1.

During dressing, the dressing tool moves across the wheel surface with a dressing lead f_d per wheel revolution while removing a dressing depth a_d . A 'fine' dressing operation refers to the use of a small dressing lead and a small dressing depth. Conversely, a 'coarse' dressing operation refers to a large dressing lead and dressing depth. For a dressing diamond with a tip angle ϕ , the theoretical peak-to-valley height of the thread profile generated on the wheel can be written as

$$R_{pv} = \frac{f_d}{2 \cdot \tan(\phi/2)} \quad (2.1)$$

According to this equation, a large dressing lead f_d and a sharp dressing tool (small ϕ) should lead to a rough wheel surface. When the wheel is used for grinding, the abrasive grains transfer their profile to the workpiece surface. This grain cutting theory was agreed by many researchers [10-13] since the profile characteristics of the

surface of the ground workpiece can be directly attributed to the dressing process. Accordingly, the dressing traverse rate and the shape of the single-point diamond are particularly important. Bhateja, Chisholm and Pattinson[14] recorded wheel and workpiece profiles by stylus measurement. Dressing features clearly appeared on the workpiece surface, but could not be detected on the surface of the wheel. They suggested that this was probably because any grooves produced in the grain by the dressing process are very small compared to the roughness of the wheel.

Malkin and Cook[15] examined the grain debris produced during the dressing process. They noticed that the grain size and the wheel hardness influenced the size distribution of the dressing particles. More significantly however, the dressing particles for the wheels tested were not much smaller than the grains that went into the wheels, which indicated that the dressing diamond fractured grains to produce relatively large fragments or, possibly, dislodged whole grains from the bond. Virtually the entire weight of material dressed off the wheel consists of particles that are much bigger than the dressing depth but smaller than the original grains. Therefore it must be assumed that the wheel material is mostly removed by brittle fracture to a depth greater than the dressing depth. Although this result throws considerable doubt on the “grain cutting” theory proposed by Pahlitzsch[10], the “grain cutting” theory is still helpful in understanding the dressing process.

Abundant cracks can be found in the grain and bond on the dressed wheel surface[3, 9], which supports the conclusion that dressing is a fracture process of abrasive grains and bond. Fracture due to dressing may occur either within a grain or at a bond as shown in figure 2.2. Bhateja[16] suggested that the dressing process consisted of gross fracture and levelling effects, which may be explained by macro and micro action. The macro action cleaves grains or breaks bonds giving the gross characteristics of the wheel working surface. The micro action refers to the micro fractures on the grain surface. Tsuwa and Yashi[17] noticed that many of the non-directional micro-cracks on the flat streak of the grain were fragile. The fragile layer

has a very low mechanical strength and cannot withstand even the 0.5g load of the diamond stylus of the profilometer. This explains why the topography of the wheel cutting surface changes so rapidly during the initial stage of grinding.

Vickerstaff[18] combined these two theories. Vickerstaff confirmed that the pattern of the wheel topography produced by dressing is transferred, to some extent, to the workpiece surface. It was assumed that when the dressing diamond passes through the brittle wheel material it causes fracture of the abrasive grains or dislodges them from the bond. It was considered that the wheel profile will not indicate regular features of dressing but will probably contain some points that are coincident with the diamond locus. In grinding, a large number of grains on the wheel profile pass through the same section of the workpiece. If each grain profile contains some points that are coincident with the diamond locus, a regular pattern will gradually generate on the workpiece surface. Based on this assumption, the envelope of the wheel profile reflects the same features as the workpiece produced by the wheel. The relationship between grain shape and dressing locus is illustrated in figure 2.3.

As mentioned above, the locus traced by the diamond profile replicates onto the abrasive wheel topography which in turn affects the grinding performance. Many researchers [19-22] show that the diamond geometry has a significant effect on the stability of the dressing process and thereby influences the useful life of the dressing diamond and the efficiency of the grinding wheel in operation.

With continued use, a single-point diamond tends to become blunt at its tip and its average radius becomes bigger. This increases the dressing force and the likelihood of bond fracture instead of grain fracture, thereby leaving fewer active grains at the wheel surface. However it is reasonable to argue[9] that when a blunt dressing tool cuts plastically through a grain, the top of the remaining grain is flatter. As a consequence, the wheel is less sharp. The wheel sharpness depends on whether the prevailing effect of dressing is macrofracture or plastic deformation and

microfracture. Fracture makes the wheel sharp while plastic deformation makes the wheel blunt. There is therefore an uncontrolled variation between macrofracture and plastic deformation in the dressing process, which may cause difficulties in grinding process control, especially in automated production.

Tkhagapsoev and Khapachev[23] found that the diamond wear in dressing is mainly attributed to abrasive wear and thermal fatigue fracture. When the diamond initially acts on the wheel, the diamond point shatters on impact with the abrasive wheel and the diamond loses irregularly shaped particles from the cutting point. This happens almost instantaneously and in most instances is unpredictable. When the diamond is in contact with the wheel and it begins to wear to a shape sympathetic to the profile being traced out. A number of parallel scratches in the direction of the traces of the grains on the wheel are observed. As the wear area increases, the number of cracks on the diamond surface increases, thermal fatigue fracture becomes an important part of the diamond wear. The change of the diamond profile will trace on to the abrasive wheel topography which in turn affects the grinding performance. With diamond wear, dressing chatter may occur. In the event of dressing chatter, the dressing diamond has to be repositioned or replaced.

Malkin and Murray[24] showed that the specific energy in dressing is larger when the dressing lead and depth are decreased. The larger specific dressing energy with finer dressing conditions can be attributed to the reduced tendency to fracture and increased plastic deformation of the abrasive.

2.3. Effects of Dressing on the Grinding Wheel Topography

Because of the importance of grinding wheel topography in grinding, a number of researchers [19, 20, 25-32] focus on the description of the grinding wheel topography. In 1971 Verkerk[25] reported a co-operative work on the characterisation of grinding

wheel topography. The report reviewed previous research on the relationship between wheel topography and wheel performance. Many techniques for identifying wheel surface topography have been developed. The principal methods for measuring wheel topography are listed below:

- microscopic observation;
- taper print method;
- stylus measurement;
- scratch method;
- razor blade method;
- workpiece surface trace method;
- photo-electric sensing;
- thermocouple measurement;
- piezo-electric dynamometer method.

The last two methods can be used to monitor topography during the grinding process and can be used to measure the number of active cutting grains under the dynamic conditions of grinding.

Two dimensional measurement of wheel topography fails to relate to the three dimensional functional behaviour of the surface. Stout, Sullivan, Matsui and Tamaki[33, 34] introduced the technique of three dimensional measurement and analysis of the grinding process to allow the entire dressing and grinding function to be investigated.

By means of these 2D and 3D measurements the relationship of the topography of the wheel to the dressing condition can be discovered. A number of mathematical models[19, 35-40] were proposed to characterise the surface of the wheel. Statistical methods[35, 38, 41] were widely used to describe the texture of the wheel surface. The parameters commonly used for characterising the wheel topography are

- the number of cutting points,
- the probability density distribution of the cutting points,

the frequency distribution of the cutting points.

Koziarski and Golabczak[19] investigated the cutting surface of the grinding wheel in relation to the dressing operation. The influence of dressing on cutting edge distribution was expressed as

$$Y_i = b_0 + b_1X_1 + b_2X_2 + \dots + b_5X_5 \quad (2.2)$$

Five dressing parameters, dressing lead f_d , width of dressing tool b_d , dressing depth a_d , grain diameter d_g and number of dressing passes n_d were represented by X_1 to X_5 , where

$$X_1 = \log f_d, \quad X_2 = \log b_d, \quad X_3 = \log a_d, \quad X_4 = \log d_g, \quad X_5 = \log n_d.$$

The coefficients of equation 2.2 were determined by regression analysis at a significance level $\alpha = 0.10$. The vector Y_i is selected in relation to the output required. The total number of the static edges on the wheel surface per unit of the profile length was expressed as

$$Y_1 = 1.645 - 0.049 X_1 - 0.043 X_3 \quad (2.3)$$

The total number of the active edges on the wheel surface per unit of the profile length was expressed as

$$Y_2 = - 1.563 - 0.149 X_1 + 0.107 X_2 + 0.113 X_5 \quad (2.4)$$

The mean thickness of the undeformed chip was determined as

$$Y_3 = 0.158 + 0.174 X_1 - 0.095 X_2 - 0.0093 X_3X_5 \quad (2.5)$$

According to equations 2.3, 2.4 and 2.5,

- (i) an increase of dressing feed or dressing depth leads to a decrease in the total number of static edges;
- (ii) an increase of dressing depth causes the static cutting edge distribution to penetrate further into the depth of the wheel surface and also increases the depth of active cutting edges;
- (iii) a large diamond tip width results in a concentration of static and active cutting edges close to the nominal wheel surface and increases the number of active edges.

These equations are consistent with the hypothesis that dressing the wheel at a high

dressing feed rate or large dressing depth or with a blunt diamond leads to a wheel surface with more fractures of the grain or bond. Dressing a wheel at a slow dressing feed rate, a small dressing depth or with a sharp diamond produces more grain microfractures.

Experiments[42] showed that small grain size results in a larger proportion of bond fracture for the same dressing conditions. The reasons given were that

- (i) small grains are tougher than big ones[43, 44];
- (ii) with small grains the dressing lead and depth are larger in proportion to the grain dimensions.

Defining the active grain ratio as the ratio of the number of the active grains per unit area to the maximum number possible, Malkin and Anderson [42] found that the number of active grains on the wheel surface increased with a decreasing proportion of bond fractures. The active grains were examined by using microscope. Pattinson and Chisholm[45] confirmed the density of active grains is increased with decrease of dressing lead, which implied that the proportion of bond fractures is decreased with decrease of dressing lead. However Pande and Lal[46] gave contradictory results where the proportion of bond fractures increased as dressing lead decreased. By looking into details of their experimental conditions, it was found that the range of dressing lead used by Pattinson and Chisholm was smaller than the diameter of the grains while Pande and Lal's was larger than the diameter of the grains. Pande and Lal [46] also showed that the proportion of bond fracture increased as dressing depth increased. This is possibly because increased dressing depth and dressing lead up to the diameter of the grains increase the amount of wheel material removed during dressing, which produces a larger dressing force on the wheel and a higher probability of bond fracture. When the dressing lead is larger than the diameter of the grains, increasing the dressing lead decreases the length of the dressing path on the wheel surface and decreases the probability of bond fracture.

Besides the influence on the active grain ratio, the dressing operation also affects the shape of the cutting edges. The cutting edges of the wheel are shaped by the fracture and the plastic deformation of the grains. If the bond material is strong enough to withstand the dressing force, the dressing tool will cut through the grain, leaving a relative large plateau on the top of the grain. With finer dressing conditions, Malkin and Murray[24] observed a larger flattened area formed by plastic deformation on the top of the grains.

It is widely agreed[16, 19, 21, 22, 32, 36, 47-51] that the mechanics of the grinding process depends on the geometry and the distribution of the cutting points. Different dressing conditions with different dressing tools make great differences in the topography of the grinding wheel. Pattinson and Lyon[21] noticed that big changes occur on the wheel surface during the first few dressing passes. Further dressing passes did not yield significant benefit to the wheel surface.

Investigation of the effects of wheel wear[14, 36] showed that cutting edges are flattened and distributed closer to the wheel surface with increasing wear. Tsuwa[32] illustrated the change of cutting edge distribution in the initial stage of grinding due to different dressing conditions. The initial density of cutting edges on the grinding wheel changes and stabilises at a steady state density of cutting edges when grinding under particular grinding conditions. Makino[52] postulated that optimal dressing would make the cutting point spacing constant throughout the wheel redress life cycle.

2.4. Effects of Dressing on Grinding Behaviour

The shape of the dressing diamond and the dressing conditions have an important influence on the sharpness and topography of the grinding wheel, which subsequently affects grinding force, grinding power, specific energy, grinding temperature, metal

removal rate, grinding ratio and wheel wear. The effects of dressing may also be manifested in the quality of the ground product, as defined by size and shape accuracy, surface roughness and surface integrity. The most important dressing parameters in single diamond dressing operation are dressing lead, dressing depth and the shape of the diamond. The number of dressing passes is also important.

A number of researchers [3, 10, 12, 22, 25, 46, 53-62] discovered the effects of dressing on grinding force, power, specific energy, metal removal rate and the grinding system time constant. Most of the researchers concentrated on the effects of dressing on grinding behaviour in the steady stage. Little effort has been applied to the effect of dressing on the initial stage of grinding. As illustrated in figure 2.1, a larger dressing lead produces a more open wheel surface, leaving sharper grains on the wheel surface with a lower density of active cutting points. With a sharp wheel surface, the metal removal rate is high and grinding force and temperature are low. However, the surface roughness of the workpiece is likely to be larger than with a small dressing lead. The effect of dressing depth on grinding behaviour is similar to that of dressing lead. A large dressing depth produces a rough surface on the wheel because of more macrofractures in dressing.

The effects of dressing are not only evidenced in the grinding behaviour but also in the development of wheel wear. Pattinson and Chisholm[45] summarised the strong influence of dressing lead on the initial stage of wheel wear. It was found that a larger dressing lead increased the initial wear rate. However after the initial wear stage, the wear rate is almost independent of the dressing lead. Pacitti and Rubenstein[62] further examined the influence of the dressing depth on wheel performance. It was found that a large dressing depth reduced the rate of wheel wear. Pande and Lal[46] found that the wheel life is longer when the rate of bond fracture in dressing was high. It was also concluded that flat cutting edges cause poor cutting performance and decrease the useful life of the wheel.

Several dressing passes may be required to stabilise the wheel topography. In multi-pass dressing, the extant topography of the wheel surface is erased and replaced by each successive pass of the dressing tool. Since the second and subsequent dressing passes cannot be guaranteed to be in phase with previous passes, subsequent variations in topography may be expected. This can affect the wheel behaviour in grinding and will be discussed in chapter 4. Pattinson and Lyon[21] showed that there seemed to be little merit in a large number of dressing passes. It may be assumed that the number of dressing passes should be a minimum to achieve a satisfactory wheel surface. The experiments by Pattinson and Lyon indicated that four dressing passes are enough.

The shape of the dressing diamond has an important effect on wheel wear. More than 300% differences in wheel wear caused by the shape of the diamond were measured by Verkerk [63]. Large differences in wheel wear caused by a small change of diamond shape makes accurate prediction of grinding behaviour very difficult. Because the shape of the dressing diamond cannot be controlled, dressing remains subject to a large degree of variability. Furuichi, Nakayama and Doi[58] found that dressing with a sharp diamond gives a higher G ratio, the reason being that a sharp dressing diamond creates fewer macrofractures on the wheel surface.

The dressing operation has a strong effect on surface roughness, size error and roundness of the workpiece[3]. Many researchers[10, 11, 53, 57, 60, 64, 65] concentrated on surface roughness, because surface roughness reflects the geometrical effects of dressing. Coarse dressing gives a coarse surface texture. Scott and Baul[66] described the effect of dressing on surface roughness by using a spectral analysis method. An important result shown in many papers [3, 25, 53] is the convergence of the surface roughness with grinding time towards a constant value despite differences of the dressing conditions employed.

2.5. Evaluation and Optimisation of the Dressing Operation

Trmal and Kaliszer[64] proposed that a good dressing condition is one that does not induce rapid changes in surface roughness during the initial stage of grinding. This can be interpreted as meaning that a good dressing condition should give a stable cutting surface on the wheel and lead to a more stable grinding behaviour. The optimum dressing condition is often determined by trials for a particular grinding operation [46, 62]. Optimisation of the dressing conditions is therefore time consuming and only suitable for a limited range of grinding conditions.

Buttery, Statham and Percival[67] reviewed research on single-point diamond dressing and emphasised the effect of dressing on grinding force, specific energy, wheel wear and surface texture of the workpiece. These authors also discussed how to optimise the wheel condition by practical methods and how to monitor the wheel condition. Although Fletcher [57] had previously mentioned the effect of dressing on the efficiency of the grinding condition, dressing conditions were optimised on the grain size and wheel characteristics without considering the grinding conditions. Fletcher highlighted the importance of dressing diamond geometry and suggested the ideal dressing condition for rough grinding would be given by minimum diamond overlap in dressing. The diamond overlap in dressing can be described by an overlap coefficient U_d .

$$U_d = \frac{b_d}{f_d} \quad (2.6)$$

The overlap coefficient is a comprehensive parameter to connect diamond shape to the dressing kinematics. Oliveira, Purquerio, Coelho and Bianchi [60] agreed that the minimum diamond overlap should be used for rough grinding to achieve a small grinding force and a small variation of surface roughness. However the diamond shape is not completely controllable due to the wear process and the diamond overlap is therefore difficult to control.

Because the grinding process is not completely deterministic, the selection of dressing and grinding conditions depends to some extent on personal experience. If there is no experience for a particular grinding condition, many experiments of a trial and error nature may be required. Empirical models[68, 69] have been proposed to guide the selection of dressing conditions. Empirical models tend to be valid in a narrow range of grinding conditions. Expert system technology has been recommended as a useful tool for decision making in production grinding[70, 71], although the applications of expert system technology in grinding have been limited. Nagasaka, Kita, Kitaguchi and Tanibayashi[72] described a rule based expert system for selecting dressing conditions. If data are available to enable a data base to be established, the selection of dressing conditions can be approached by means of a neural network method[73] or a fuzzy logic method[74].

Amitay, Malkin and Koren[75] pointed out the importance of dressing in adaptively controlled grinding operations and proposed an optimising dressing procedure aimed at achieving acceptable surface roughness at maximum removal rate. The iterative computer optimisation developed by Malkin and Koren[68, 76] introduced grinding and dressing parameters into the optimisation strategy. The strategy required the measurement of grinding power and surface texture. The surface texture had to be measured by an operator. Xiao, Malkin and Danai[69] developed the strategy further. An autonomous model based control system was introduced to control cylindrical plunge grinding cycles. Because this system required the wheel surface to be dressed before every grinding cycle, the influence of initial wheel wear which has a significant effect on the wheel topography and grinding behaviour was neglected. Xiao, Malkin and Danai's method was therefore incapable of selecting conditions for a long redress life or of minimising the number of dressing operations required.

Dressing operations are usually carried out before grinding commences, which means the dressing time is non-productive. To reduce non-machining time, the method of continuous dressing was introduced[77, 78]. By using continuous dressing, the stock

removal rate on difficult-to-grind materials can be increased. Diamond roll dressing was found to be more suitable for continuous dressing operations than single diamond dressing.

2.6. Conclusion

Dressing can be described as a fracture process of grains and bonds. From the literature, it appears that a distinction can be made to dressing conditions which lead to microfractures in a grain and macrofractures which cleave or dislodge the grain. This hypothesis will be used as a basis for interpreting experimental results and will be tested for consistency in providing an interpretation of the results. The topography of the wheel is determined by wheel structure, diamond shape and dressing kinematics. A fine dressing condition generates more cutting edges and a higher density of cutting points on the grinding wheel surface than a coarse dressing condition. The cutting edge distribution is denser close to the wheel surface than with a coarse dressing condition. A fine dressing operation produces a finer workpiece surface texture. The literature survey has shown the importance of the dressing operation in the grinding process and revealed the many methods proposed to optimise dressing. However, it remains unclear how dressing conditions should be selected and there is insufficient information available on how to change dressing conditions according to changes of the grinding conditions. Previous research on selection of optimum dressing conditions has largely been conducted under fixed grinding conditions with many experiments based on trial and error. In batch manufacture the grinding parameters are frequently changed. The dressing conditions should therefore change to satisfy the grinding requirements. An adaptive strategy for the selection of optimum dressing conditions has the potential to reduce the trial and error period of testing and to maintain optimal grinding conditions.

Chapter 3 Mechanics of Grinding

3.1 The Action of a Single Abrasive Grain

As previously discussed, the grinding process is a process where numerous grains of a wheel pass through the workpiece surface. The kinematic relationship between the grinding wheel and the workpiece motions apply to each cutting grain. It is therefore proposed that analysis of the grinding process can be based on the force on an equivalent individual grain representative of the wheel surface. Some aspects of the process by which a grain grinds can be illustrated by the geometrical relationship between the grain and workpiece during the grinding process. The geometry of the undeformed chip shape is described by the theoretical path of a grain as it passes through the workpiece. The geometry of the undeformed chip is shown in figure 3.1. The undeformed chip shape can be characterised by the cutting path length of the grain l_k and the maximum undeformed chip thickness h_m . These parameters are often used as geometrical and kinematical parameters in the early study of the grinding process[79, 80].

Hahn[81] distinguished three phases in the grinding process including rubbing, ploughing and cutting. When a grain engages with the workpiece in the rubbing stage the grain slides on the workpiece surface with elastic deformation of the system and negligible plastic deformation. As the stress between the grain and workpiece is increased, plastic deformation predominates. This is called ploughing. The workpiece material piles up to the front and to the sides of the grain to form a groove. A chip is formed when the workpiece material can no longer withstand the tearing stress. The chip formation process is called cutting. From the point of view of efficient metal removal, cutting can be considered to be the most desirable deformation process. Rubbing and ploughing are inefficient, since the energy is

wasted in deformation and friction without contributing to metal removal. Furthermore a high temperature results which produces an excessive rate of wheel wear and the workpiece surface may suffer metallurgical damage.

The specific energy, defined as the energy per unit volume of material removal, is a fundamental parameter for analysing machining processes. For plunge grinding the specific energy is obtained by dividing the machining power P by the removal rate Q_w ,

$$e_c = P / Q_w = P / (\pi d_w v_f b) \quad (3.1)$$

where d_w is the diameter of the workpiece, v_f is the infeed rate and b is the grinding width. Specific energy is much larger in grinding than in turning, milling and drilling. In order to understand the material removal mechanics in grinding, an abrasive grain may be considered as a cutting tool of irregular shape. Theoretical and experimental analyses[82-84] based on the grains of an equilateral-triangular pyramid shape, a square-pyramid shape, a conical shape and a spherical shape show that the occurrence of rubbing, ploughing and cutting are strongly dependent on the shape of the grain. The shape of the grain has a strong effect on the specific energy e_c and the force ratio F_n/F_t . Based on the observation of the force ratio, Graham and Baul[84] asserted that the average effective rake angle of the grain could be expected to lie within the range -45° to -75° . They also showed that high negative rake angle, which corresponds to a blunt grain, leads to a high force ratio F_n/F_t and a high specific energy.

An important phenomenon in grinding is the size effect. The size effect was first discussed by Backer, Marshall and Shaw[85], who found that the specific energy became much larger when the undeformed chip thickness was decreased. This observation was attributed to the fact that the small chip size reduced the defects in the metal to be removed, and allowed the workpiece material to achieve its theoretical strength. However, Von Turkovich[86], Nakayama and Tamura[87] threw a doubt on Backer's description, because their researches showed that the shear strength would

not be larger as a result of the decrease of undeformed chip thickness. It has been suggested by Graham and Baul[84], Kannapan and Malkin[88] that the size effect in grinding can be attributed to the occurrence of a relatively greater proportion of sliding and ploughing energy when the undeformed chip thickness is decreased.

Another explanation due to Rowe may be given by the sliced bread analogy. The thinner the loaf is sliced, the more energy is required to slice the whole loaf. This is because a greater surface area is created. The energy required to deform material near the surface is expended more times as the number of chips is increased and the surface area of the chips is increased. For example, if a cube is cut into two equal halves the surface area is increased by at least one third. More energy is required in cutting the material into smaller chips because the surface area of the chips increases. This effect is therefore too large to ignore.

Shaw [89] suggested that an abrasive grain could be modelled as a sphere. He presented an analysis which predicted that the force per unit area of the groove will increase as the undeformed chip thickness is reduced. Based on the sphere assumption, Lortz[90] observed the dead zone in the contact area between the grain and the workpiece. There is a critical depth of cut before a chip formation process commences and metal is removed. Also using the sphere model, Malkin, Wiggins, Osman and Smalling[91] showed that a smaller proportion of the groove volume is removed with a smaller undeformed chip thickness due to the material piled up at both sides of the grain. Malkin et al asserted that the specific energy is unequal to the cutting force divided by the intercepted area of the groove. Only chip formation results in material removal. The rubbing and ploughing actions in grinding do not produce material removal. Because of the existence of rubbing and ploughing in the grinding process, the specific energy in grinding is higher than in large chip removal processes. The size effect in grinding can therefore be related to the relative proportions of sliding, ploughing and cutting that occur in addition to the effect of the greater surface area created as proposed by Rowe.

Local elastic deflection around a grain reduces the real cutting depth of the grain. The local deflections of the wheel when the grain is in contact with steel are of the same order of magnitude as the undeformed chip thickness (for example, 3µm according to [92]). Saini, Wager and Brown[92] assumed that the elastic deflection consists of four components. The four components are local workpiece deformation δ_w , grain tip deformation δ_g , variation of deflection of the grain centre δ_c and rotation δ_{rt} as shown in figure 3.2. From their results, it was concluded that grain tip deformation δ_g and rotation δ_{rt} are relatively small. The local workpiece deformation δ_w was said to be just a little more than 2 µm and could be considered as a part of the total workpiece deflection. The deflection of the grain centre δ_c was found to be up to 3 µm. The variation of the deflection of the grain centre δ_c has a trend and scale similar to the total deflection. Nakayama, Brecker and Shaw[93] described the deflection of the grain centre as following the form of a Hertz distribution,

$$\delta_c = C F_n^{2/3} \quad (3.2)$$

where C is a constant in the range 0.08 to 0.25 and has an average value 0.15, δ_c is the deflection expressed in microns and F_n is the normal force expressed in newtons.

As discussed above, only a part of the chip material at the front of a grain forms the chip because of the elastic and plastic deformation. The remaining material will be removed by successive grains. Figure 3.3 shows the material to be removed along a cross section of a grain.

3.2. Empirical Grinding Process Relationships

In this section empirical grinding progress relationships are reviewed and are used later as the basis for empirical simulation to provide a basis for selection of dressing conditions. The grinding process is often analysed by analogy with the milling process. An average grain is considered as a cutting point mounted on the wheel

surface. The grain depth of cut is recognised as the most influential parameter in grinding. Therefore the analysis of the grinding force is based on the relationship between the grain depth of cut and the grinding control parameters. Hahn[94] suggested that the normal grinding force is proportional to the metal removal rate. Therefore the grinding force may be expressed as a linear function of the grinding depth. However this model cannot take account of the size effect in grinding. An alternative way to correlate grinding force with basic process parameters is to employ empirical relationships. It was reported by Snoeys, Peters and Decneut[95] that the specific grinding force in cylindrical plunge grinding may be approximated by power function relationships of the form

$$F_t' = F_1 h_{eq}^f \quad (3.3)$$

$$F_n' = F_2 h_{eq}^f \quad (3.4)$$

where F_1 , F_2 and f are constants, and h_{eq} is the equivalent chip thickness. The equivalent chip thickness corresponds to the thickness of a continuous layer of material being removed at a volumetric rate per unit width Q_w' and cutting velocity v_s . This parameter is also equal to the volumetric removal rate per unit area of wheel surface passing through the grinding zone.

$$h_{eq} = \frac{v_w a}{v_s} = \frac{Q_w'}{v_s} \quad (3.5)$$

Where v_w is the workspeed and a is the depth of grinding. The exponent f typically lies in the range 0.4 - 0.9. From equations 3.1, 3.3 and 3.5 the specific energy is

$$e_c = F_1 h_{eq}^{f-1} \quad (3.6)$$

As a relative measure of grinding severity, the equivalent chip thickness correlates fairly well not only with grinding forces and energy, but also with other performance characteristics including surface roughness and wheel wear. However these empirical relationships tend to be of limited practical use for predicting grinding performance because the constants depend on effects which have not been taken into account, for instance the dressing conditions, grinding fluid, wheel type, dwell period and workpiece material. Although it is not immediately obvious, h_{eq} cannot take into account effects of workspeed on the plunge grinding process. This is because the

depth of cut 'a' depends on v_f/v_w so that h_{eq} depends on v_f and v_s but not on v_w .

In order to understand the effect of the grinding parameter on grinding force, Ono[96] initially assumed that the average grinding force on a grain was proportional to the mean chip cross sectional area of the grain A_m ,

$$f_t = k_c A_m \quad (3.7)$$

$$f_n = \lambda k_c A_m \quad (3.8)$$

where f_t and f_n are the tangential and the normal grinding force on a grain respectively and λ is the grinding force ratio f_n/f_t . From a survey of experiments on the grinding force, Ono discovered that the grinding force coefficient k_c can be empirically expressed as a power function. That is

$$k_c = k_0 A_m^{-\eta} \quad (3.9)$$

where k_0 and η are constant and η ranges from 0.25 to 0.5. In views of grinding energy, the grinding force coefficient is commensurate with the specific grinding energy e_c . When the wheel passes through the grinding zone of contact length l_k , the workpiece material removed by the wheel is

$$V = b l_k a \quad (3.10)$$

where b is the width of the grinding zone. During the period of contact, a grain on the wheel surface covers a distance l_s .

$$l_s = \frac{l_k v_s}{v_w} \quad (3.11)$$

If the mean separation distance of grains on the wheel surface is u , the number of the grains in the length l_s is $\frac{b l_s}{u^2}$. Therefore the mean chip volume removed by a grain

will be

$$V_c = u^2 \frac{v_w a}{v_s} \quad (3.12)$$

If the undeformed chip length is equal to the grinding contact length l_k ,

$$l_k = \left(1 \pm \frac{v_w}{v_s}\right) \sqrt{\frac{a}{\frac{1}{d_s} \pm \frac{1}{d_w}}} \quad (3.13)$$

the mean chip cross sectional area A_m is therefore

$$A_m = \frac{V_c}{l_k} = u^2 \frac{v_w}{v_s} (1 \pm \frac{v_w}{v_s})^{-1} \sqrt{a (\frac{1}{d_s} \pm \frac{1}{d_w})} \quad (3.14)$$

The total tangential grinding force F_t is the sum of the forces on each individual grain, therefore

$$F_t = \frac{b l_k}{u^2} f_t = \frac{b l_k}{u^2} k_c A_m = \frac{k_0 b l_k}{u^2} A_m^{1-\eta} \quad (3.15)$$

and

$$F_t = k_0 b u^{-2\eta} a^{1-\eta/2} (\frac{v_w}{v_s})^{1-\eta} (\frac{1}{d_s} \pm \frac{1}{d_w})^{-\eta/2} \quad (3.16)$$

Ono's equation 3.16 is the first attempt to interrelate the grinding parameters v_s , v_w , a , d_s and d_w by a single exponential coefficient η . Since the equivalent wheel diameter d_e is

$$\frac{1}{d_e} = \frac{1}{d_s} \pm \frac{1}{d_w} \quad (3.17)$$

equation 3.16 can be simplified to

$$F_t = k_0 b u^{-2\eta} a^{1-\eta/2} (\frac{v_w}{v_s})^{1-\eta} d_e^{\eta/2} \quad (3.18)$$

Werner[97] modelled the grinding force on a grain based on an empirical rule for the turning process. The cutting force on a grain was assumed to be

$$f_c = k_1 A^n \quad (3.19)$$

where k_1 is a proportionality factor, A is the cross sectional area of the undeformed chip and n lies in the range 0 to 1. Summing the grinding forces on individual cutting edges, the semi-empirical grinding force equation is given by

$$F'_n = K C_1^\gamma \left[\frac{v_w}{v_s} \right]^{2\epsilon-1} a^\epsilon d_e^{1-\epsilon} \quad (3.20)$$

where K is a constant and C_1 is the static cutting edge density. By applying the transformation $\eta = 2 - 2\epsilon$, the effects of the grinding parameters in equations 3.18 and 3.20 are the same. The difference between these two models is the spacing of the cutting edges. Ono used the average value of the dynamic cutting edge separation u , while Werner used the static cutting edge density C_1 . However these two models are otherwise the same.

The advantage of the Ono and Werner models is that if the effect of one parameter is ascertained, the effect of other parameters is also known. This suggests that wheel speed, workspeed, depth of cut, wheel diameter and workpiece diameter do not have an independent influence on the grinding force, but are closely interrelated. By studying the influence of one grinding parameter, for example depth of cut, the influence of other parameters can also be understood. The deficiency of the equations is that the mechanical significance of the exponential coefficient is not clear. Since the models are a semi-empirical models, the relationships only work for the particular range of grinding conditions.

Werner's model expresses the effects of control parameters and the wheel surface condition with two coefficients ϵ and γ respectively, which may be helpful in understanding the effect of the wheel characteristics. Werner further stated that the theoretical values of exponential coefficients γ and ϵ lie in the ranges

$$0 \leq \gamma \leq 1, \quad 0.5 \leq \epsilon \leq 1.$$

Therefore the theoretical value of η lies within the range

$$0 \leq \eta \leq 1.$$

Combining the Ono and Werner models, equations 3.18 and 3.20 can be expressed in the form

$$F_n = C_1^\gamma b [K\sqrt{a d_e}]^\eta [K(\frac{V_w a}{V_s})]^{1-\eta} \quad (3.21)$$

At the extreme condition, $\gamma = 1$ and $\eta = 1$,

$$F_n = C_1^\gamma b [K\sqrt{a d_e}]^\eta \quad (3.22)$$

At this condition the grinding force is directly related to the contact area and the specific number of the cutting edges. This may actually mean that the grinding force is generated by friction. At the other extreme, if $\gamma = 0$, and $\eta = 0$,

$$F_n = b [K(\frac{V_w a}{V_s})]^{1-\eta} \quad (3.23)$$

This equation shows the grinding force is directly related to the equivalent chip thickness. This is consistent with a situation where the grinding force is generated by chip formation. In practice[97], $0.1 < \gamma < 0.8$, $0.65 < \epsilon < 0.95$ and $0.1 < \eta < 0.7$. In a

practical situation, equation 3.21 applies which is consistent with the description of the size effect and the conclusion that the grinding force is a combination of a cutting force and a friction force.

3.3. Physical Grinding Process Relationships

In this section, physical models of the grinding process are reviewed. The equations are used later as a basis for the physical simulation of the grinding process. In order to clarify the function of cutting and friction in grinding, Malkin[98] suggested that almost all sliding energy is generated at the interface between the wear flat of the grain and the workpiece. Malkin illustrated the grinding mechanics as in figure 3.4. Both tangential and normal grinding forces consist of two components, one due to cutting and the other due to sliding on the wear flats.

$$F_n = F_{nc} + F_{ns} \quad (3.24)$$

$$F_t = F_{tc} + F_{ts} \quad (3.25)$$

It was deduced that the cutting force components were unaffected by the size of the wear flat. The sliding force components were assumed to be proportional to the area of the wear flat.

Since the tangential and normal sliding forces are both linearly related to the wear flat area, the friction coefficient μ and the average contact pressure \bar{p} between the wear flats and the workpiece were assumed to be constant. The normal friction force was assumed to be the result of the wear flat area and the average contact pressure. Defining A_r as the real contact area between the wheel and the workpiece, equations 3.24 and 3.25 become

$$F_n = F_{nc} + A_r \bar{p} \quad (3.26)$$

$$F_t = F_{tc} + \mu A_r \bar{p} \quad (3.27)$$

The tangential cutting force can be obtained from the specific cutting energy, which is defined as

$$e_{cc} = \frac{F'_{tc} v_s}{v_w a} \quad (3.28)$$

The normal force of cutting can be calculated if the cutting force ratio F_{nc}/F_{tc} is known. Although Malkin's model considers the functions of sliding and cutting to be separate in grinding, the model does not directly account for the effect of the grain shape.

Buttery[99] considered the grinding process as an interaction between two surfaces rather than as a conventional cutting process. He derived an expression for the normal force from wear theory,

$$F_n = \frac{2 v_w b a H}{v_s \alpha \beta \cot\theta} \quad (3.29)$$

where H is the hardness of the workpiece, α is the proportion of the grains actually cutting, β is the proportion of the groove volume removed and θ is the half-angle of the scratches formed on the abraded surface. This model highlights the effects of grain shape with the scratch angle and the distribution of the grains.

Shaw idealised a grain on the wheel surface as a sphere[89]. The normal force applied to a grain was assumed to be similar to the force in a Brinell hardness test or a Meyer hardness test. The deformation process is constrained by an elastic-plastic boundary. As the sphere moves horizontally, the plastically deformed zone beneath the surface becomes inclined. The workpiece material is squeezed upwards forming a chip which is subsequently sheared from the surface. The model is illustrated in figure 3.5 where the horizontal movement of a sphere at a cutting depth t is equivalent to a sphere indented into the surface to the same depth t .

In the absence of friction at the surface between the sphere and the workpiece, the force to indent the workpiece is independent of the direction in which it is loaded. This implies that the projected area of the indentation is independent of the direction of the force. If the radius of the projected area is b , the force to indent the workpiece is

$$R = \pi b^2 H \left(\frac{C'}{3} \right) \quad (3.30)$$

where C' is a constraint coefficient defined as the ratio of the average pressure \bar{P} on the contact area to the uniaxial flow stress σ_b . In most cases of grinding, C' is about 3 [89]. The specific energy may be defined as

$$e_c = \frac{f_t}{A} \quad (3.31)$$

where f_t is the tangential component grinding force on a grain and A is the cross section area of a undeformed chip. If A is approximated to

$$A = \frac{4}{3} b t$$

then

$$e_{cc} = \frac{3 R \sin\theta}{4 b t}$$

The specific energy due to cutting may therefore be expressed as

$$e_{cc} = \frac{3\pi}{4} \frac{b}{t} H \left(\frac{C'}{3} \right) \sin\theta \quad (3.32)$$

According to Shaw, the friction force is assumed to be $\mu \cdot R \cdot \cos\theta$. Where μ is the mean coefficient of friction at the contact surface. The specific energy due to friction is

$$e_f = \frac{3\pi}{4} \mu \frac{b}{t} H \left(\frac{C'}{3} \right) \cos\theta \quad (3.33)$$

Therefore the total specific energy for a single grain is

$$e_g = \frac{3\pi}{4} \frac{b}{t} H \left(\frac{C'}{3} \right) (\sin\theta + \mu \cos\theta) \quad (3.34)$$

Generally only a portion of the workpiece material engaged by the grain is removed in grinding. In a hardness test, the material flows upward along the sides of the indenter. This can be expressed by the upward flow ratio β [89],

$$\beta = \frac{\text{Volume rising above original surface}}{\text{Total volume displaced}} \quad (3.35)$$

In grinding, some material is removed so that the volume rising above the original surface is less than the total volume displaced. The volume rising above the original surface is commensurate with the material bulge at the sides of a grain and chip

formation. Therefore the upward flow ratio is a measure of the cutting efficiency of a grain. In grinding, the upward flow ratio β may be expressed in terms of a cross section perpendicular to the path of a grain[100, 101],

$$\beta = \frac{A_1 - A_2}{A_1 + A_3} \quad (3.36)$$

where A_1 , A_2 and A_3 are areas illustrated in figure 3.6. The parameters in this definition may be easily measured in laboratory.

For an upward flow ratio β less than one, the specific energy for a single grain is

$$e_g = \frac{3\pi}{4} \frac{b}{t} \frac{H}{\beta} \left(\frac{C'}{3}\right) (\sin\theta + \mu\cos\theta) \quad (3.37)$$

If the average diameter of the grains is d_g and the average depth of cut of the grains is \bar{t} , from figure 3.5

$$b = \sqrt{\left(\frac{d_g}{2}\right)^2 - \left(\frac{d_g}{2} - \bar{t}\right)^2} = \sqrt{\bar{t}(d_g - \bar{t})}$$

$$\sin\theta = \frac{2b}{d_g} = \frac{2\sqrt{\bar{t}(d_g - \bar{t})}}{d_g}$$

$$\cos\theta = \frac{\sqrt{d_g^2 - (2b)^2}}{d_g} = \frac{\sqrt{d_g^2 - 4\bar{t}(d_g - \bar{t})}}{d_g}$$

Therefore the specific energy of grinding is

$$e_c = \frac{3\pi}{4} \frac{\sqrt{\bar{t}(d_g - \bar{t})}}{\bar{t}} \frac{H}{\beta} \left(\frac{C'}{3}\right) \left(\frac{2\sqrt{\bar{t}(d_g - \bar{t})}}{d_g} + \mu \frac{\sqrt{d_g^2 - 4\bar{t}(d_g - \bar{t})}}{d_g}\right) \quad (3.38)$$

For most practical cases, $d_g \gg \bar{t}$, so that

$$e_c \approx \frac{3\pi}{4} \frac{H}{\beta} \left(\frac{C'}{3}\right) \left(2 + \mu\sqrt{\frac{d_g}{\bar{t}}}\right) \quad (3.39)$$

The mechanics of grinding can also be investigated by monitoring and analysing the grinding power. In plunge grinding the grinding power P can be expressed in terms of the tangential force

$$P = F_t (v_s \pm v_w) \quad (3.40)$$

The positive sign is for upcut grinding and the minus sign is for downcut grinding.

When the workpiece speed is much smaller than the wheel speed, the grinding power

can usually be simplified with less than 2% error to

$$P = F_t v_s \quad (3.41)$$

Based on the simplification that grinding consists of rubbing, ploughing and chip formation phases, Malkin[9] suggested that the grinding power P can be partitioned into chip formation, ploughing and sliding components

$$P = P_{ch} + P_{pl} + P_{sl} \quad (3.42)$$

Malkin proposed that the chip formation component P_{ch} can be estimated based on a constant specific chip formation energy. The ploughing component P_{pl} was assumed to be based on a constant ploughing force per unit width. The sliding power P_{sl} was assumed to be proportional to the area of the wear flats on the surface of the wheel. A linear relationship was found between the grinding force and the area of the wear flats on the wheel. The proportionality factor depends on the grinding conditions and the particular wheel-workpiece-fluid combination.

3.4. Generation of the Workpiece Surface in Grinding

Generation of the ground surface of the workpiece may be illustrated theoretically from the geometrical relationships and the mechanics of the grinding process. Geometrical effects depend on the kinematics of the grinding situation and the topography of the wheel surface. It is commonly agreed[52, 67, 84, 100] that the mechanics of the grinding process depends critically on the geometry and the distribution of the cutting points on the wheel surface, both of which are affected by dressing. In grinding, abrasive grains transfer their profile to the workpiece surface. When a grain passes through the workpiece surface, workpiece material is removed, leaving a trace on the workpiece surface. Because the cutting edges are randomly positioned on the wheel surface, the path of each grain is different. Only the outermost active cutting edges on the grinding wheel surface actually cut through the workpiece to generate the workpiece profile. The action leaves an irregular rough

surface along the direction of grinding as shown in figure 3.7. The surface roughness is therefore determined both by the grinding kinematics and the distribution of the cutting edges on the wheel surface.

In view of the physical mechanism involved in the generation of the ground surface, both the elastic and plastic deformations have to be considered. The side-flow material ploughed into ridges increases the workpiece roughness, while rubbing in the grinding zone may improve the surface roughness. Due to the elastic and plastic deformation in grinding, only a proportion of the material in the groove is removed by the grain as shown in figure 3.3. A rough surface can therefore be attributed to the accumulation of grooves, which are generated according to the grinding kinematics and the deformation which occurs in grinding.

Empirical models may also provide a basis for further understanding of the workpiece surface generation in grinding. In cylindrical plunge grinding, the surface roughness may be expressed approximately as a function of equivalent chip thickness[95].

$$R_a = R_1 h_{eq}^r \quad (3.43)$$

where R_1 and r are constant for a particular system. The exponent r typically lies in the range 0.15 - 0.6. Malkin and Murray[24] found that there is a logarithmic linear relationship between specific energy and surface roughness. This indicates that the generation of the workpiece surface cannot be fully understood without considering the mechanics of the grinding process.

3.5. Wheel Sharpness and Wheel Wear

It is important to minimise the cutting force coefficient and to achieve optimum grinding performance. Sharpness of the grinding wheel depends not only on the geometry of the wheel but also on the physical process. A sharp wheel is related to sharp grains on the wheel surface. This means the apex angle of the grains is small.

A sharp wheel or a blunt wheel is an ambiguous concept. Sometimes in the literature[13], a sharp wheel is taken to mean that a high metal removal rate can be achieved, and other times[102] to the condition where a good surface integrity can be obtained. However it can be argued that a sharp wheel contributes to all of the features listed below:

- a high metal removal rate;
- a low grinding force;
- a low energy consumption;
- a small residual stock at the end of the cycle;
- a high size accuracy
- a low temperature in grinding;
- good surface integrity

Since the wheel sharpness influences grinding force, grinding temperature, productivity, accuracy and surface integrity, the wheel sharpness is clearly very important. Although there is no standard definition of wheel sharpness, many parameters and methods have been proposed.

The metal removal parameter λ_w was introduced to describe the wheel sharpness on the basis of grinding force and stock removal rate[103]. The metal removal parameter is defined as:

$$\lambda_w = \frac{Q'_w}{F'_n - F'_{no}} \quad (3.44)$$

where Q'_w is the volumetric removal rate per unit width, F'_n is the specific normal grinding force, F'_{no} is the threshold value of the specific normal force required to remove metal. By studying the effects of the grinding parameters, dressing parameters and wheel characteristics, Lindsay[103] developed the following equation for the metal removal parameter in British Imperial Units.

$$\lambda_w = K_{\lambda_w} \frac{\left(\frac{v_w}{v_s}\right)^{\frac{3}{19}} \left(1 + \frac{2}{3} \frac{a_d}{f_d}\right) f_{d19}^{\frac{11}{19}} v_s}{d_e^{\frac{43}{304}} (\text{VOL})^{0.47} d_g^{\frac{5}{38}} R_c^{\frac{27}{19}}} \quad (3.45)$$

where

$$K_{\lambda_w} = 0.021 \frac{\text{inch}^{819/304}}{\text{lb,ft}},$$

d_g is the grain size,

R_c is the Rockwell Hardness,

VOL is a volume factor for the wheel, $\text{VOL} = 1.33H + 2.2S - 8$,

H refers to the grade of the wheel hardness, and $H = 0, 1, 2$, etc. corresponding to a wheel hardness of H, I, J, etc..

S is the wheel structure number, 4, 5, 6, etc..

Equation 3.45 indicates that an increase in the dressing depth improves the wheel sharpness. The effect of dressing lead indicated in the equation is questionable. The previous experimental results[104] showed that λ_w increased with increases of f_d and a_d . The grinding conditions also have a strong effect on wheel sharpness.

The time constant τ of the grinding system is another commonly used parameter to indicate the wheel sharpness. The time constant reflects the dynamic response of the system. Time constant therefore represents the combined effect of wheel sharpness and the system stiffness on grinding behaviour. A small value of time constant corresponds to a sharp grinding wheel and a stiff machine-workpiece system.

The force ratio F_n/F_t and the specific grinding energy e_c are also used to indicate the wheel sharpness. A sharp wheel corresponds to a small value of F_n/F_t and a small value of e_c .

The sharpness of a grinding wheel changes during the grinding process. This is indicated by the wear of the grinding wheel. The wear of a grinding wheel in grinding is the combined effect of the wear of individual grains in the wheel. When the wheel is rotated at grinding speed and applied to the workpiece, the abrasive

grains cut the material and remove small chips. Under the action of the forces imposed during grinding, flats are worn on the abrasive cutting points. This causes an increase in friction, workpiece heating and the magnitude of the forces imposed on the wheel. An increase in the magnitude of grinding force increasingly causes the abrasive to fracture, exposing new cutting edges, or fractures the bond bridges to expose fresh abrasive grains. If the fracture wear allows the wheel to remain sharp, the grinding wheel is said to be self-sharpening. If the wheel is not self-sharpening, the wheel has to be dressed more frequently.

Three principal mechanisms of wheel wear were commonly identified[5, 105-110] as:

- (i) Attritious wear. This occurs on a microscopic scale and enlarges the wear flat area of a grain.
- (ii) Grain fracture. This is the sharpening mechanism whereby a new cutting edge is formed by fracture of an individual grain.
- (iii) Bond failure. This is a process where dull individual grains break away to reveal fresh grains.

In grinding, the abrasive grains are subject to high temperatures and pressures. In consequence, chemical reaction, mechanical wear and material adhesion all play a part. The sharpness of a wheel is reduced by attritious wear of the grains and adhesion of workpiece material. Attritious wear of the grains is attributed to chemical corrosion and mechanical wear. Although the consumption of the wheel caused by attritious wear is relatively small, grinding quality and productivity are affected. Where possible, the abrasive should be considerably harder than the material being ground and should not demonstrate chemical affinity for the workpiece material.

It is known that grain fracture wear consists principally of the detachment of fragments from the sliding surface of the grains. The fracture properties of single abrasive grains engaging a metal surface have been found to be different after a number of engagements [98, 111]. This observation was made on a statistical basis

and no physical mechanism was suggested. Furthermore fracture was found to depend on crystallographic orientation. Because of the random orientation of grains in a grinding wheel, prediction of grain fracture is not possible. A thermal analysis of grinding indicates that the thermal gradient along the grain can be as high as 4×10^5 K°/mm[81, 112]. Under such extreme conditions, it is evident that thermal stress can cause grain fracture. The occurrence of these temperature gradients during grinding followed by rapid cooling during the free path around the wheel periphery causes thermal fatigue. It is apparent that the fracture wear of the grains during grinding is a complex process, which has not yet been fully explained.

In precision grinding, the wheel wear is mainly attributed to attritious wear and grain fracture. The proportion of attritious wear and grain fracture in grinding depends on the grinding conditions and the wheel hardness[113, 114]. Large stock removal rate tends to fracture grains. Excessive bond fracture leads to a large volume of wheel wear, which is not usually allowable in precision grinding operations. To avoid severe bond fracture, a harder grade wheel and slower grinding conditions are used.

It is commonly accepted[5, 45, 104, 105, 115, 116] that the wheel wear process may be divided into three stages, an initial wear stage(I), a steady stage(II) and a final stage where the wheel surface rapidly deteriorates(III). The grinding force in different stages of wheel wear is shown in figure 3.8.

The initial stage is characterised by intensive wheel wear and the shape of the grinding force characteristic is strongly dependent on the dressing operation. There are many cracks in the wheel surface after dressing, which cause grains to fracture or dislodge from the wheel surface when the wheel engages to the workpiece. In the second stage, the wheel wear is mainly due to a combination of attritious wear and grain fracture. Grinding wheel wear is slower and a steady grinding behaviour is experienced. The steady stage is desirable for predictable control of the grinding process. The first and second wear stages represent the useful redress life of the

grinding wheel.

In the final stage, either grinding forces become excessive or excessive vibration develops and the wheel has to be redressed. Wheel wear in this stage is due to bond post rupture and whole grains are dislodged from the wheel. This leads to rapid deterioration in surface texture, workpiece form and size tolerance. If the surface roughness, roundness and size errors of the workpiece fall outside the tolerance limits, the wheel should be redressed.

Although only 2-10% of wheel consumption is attributed to the wear during grinding[5], the grinding behaviour can change greatly as the wheel wears. As the grinding wheel wears towards the third wear stage, the profile and distribution of the active grain edges on the wheel become increasingly irregular[52, 117]. This can lead to a loss of form accuracy. Irregular wear of the grinding wheel is often associated with the build up of vibration on the wheel, a phenomenon known as 'wheel regenerative chatter'. This causes poor roundness and surface roughness. Grinding force may either be increased associated with excessive glazing or decreased accompanied by intensive bond fracture, leading to increased size errors.

The maximum machine power may be exceeded due to a blunt wheel. The constraint infringement may be overcome by either reducing material removal rate or redressing the wheel. A reduction of removal rate may increase the specific energy because of the size effect and the increased tendency towards attritious wear of the grains. This can increase the possibility of thermal damage to the workpiece. Redressing the grinding wheel becomes essential to restore the wheel sharpness.

3.6. Simulation of Grinding Behaviour

Simulation can be used to check the consistency of models of the grinding process

with actual grinding behaviour. There are two kinds of models, physical and empirical, used in grinding simulations. Though assumptions made in physical models may introduce errors, simulations based on physical models may illustrate the physical behaviour in grinding and express the effects of influential factors. Simulations based on empirical models may be more easily matched with grinding behaviour. However they cannot easily be used to control industrial applications[118]. The reason may be attributed to the many tests required to establish empirical models covering an appropriate range of conditions.

Suto and Sata[119] measured the number and worn area of the active cutting edges and developed empirical models to simulate grinding behaviour. The results of the simulations showed good agreement with experimental results. However, the grain size was not involved as a parameter in the simulation models.

Steffens[120] simulated the grinding process based on measurements of the wheel surface. After the cutting edge radius and the distribution of the cutting edges were obtained from the measurement, the shape of the grinding chips were calculated. Subsequently, the grinding force, grinding temperature and generation of the workpiece surface were simulated. A key requirement of the simulation technique was the need to accurately measure the wheel surface.

Due to the difficulty of measurement of the wheel surface, some researchers generated the distribution of the cutting edges by the Monte Carlo method[36, 121-123]. Simulations using the Monte Carlo method also showed good agreement with experiments. However a difficulty still remained since the density function of the cutting edge distribution is also difficult to obtain in practice. The practical application of the simulation technique is therefore limited by the need to describe the wheel surface.

Chapter 4 Grinding Process Control

In this chapter, dressing and grinding are considered in terms of process control. The relationships between grinding behaviour and process parameters are examined for the external cylindrical plunge grinding process. The dressing and grinding process is analysed drawing from previous work to form a basis for the later design of a process simulation and the formulation of an objective for the optimisation of dressing conditions. This chapter draws attention to the particular importance of time constant as a measure of cutting efficiency and its relationship to size-holding. This provides the basis for consideration of the use of time constant in an adaptive dressing strategy.

4.1. Basic Features of a Plunge Grinding Cycle

As illustrated in figure 4.1, a plunge grinding process is usually controlled by wheel speed v_s , workpiece speed v_w and wheel infeed rate v_f . As the grinding wheel grinds the workpiece, a grinding force is induced between the wheel and the workpiece. The faster the stock removal, the larger is the grinding force. The grinding force causes deflection of the machine and generation of heat. The ability of the grinding wheel to remove stock is often described in terms of wheel sharpness. When the grinding force rises for a given infeed rate, the wheel sharpness is said to reduce. Increased forces result in more deflection of the machine and sometimes in thermal damage or grinding chatter.

Simplified as figure 4.1, the machine structure supports the wheel with a linear spring of stiffness k_m and the workpiece with a linear spring of stiffness k_w . The stiffness of the grinding wheel at the contact with the workpiece is k_a . An expression for the overall effective stiffness k_e is

$$\frac{1}{k_e} = \frac{1}{k_m} + \frac{1}{k_w} + \frac{1}{k_a} \quad (4.1)$$

When the infeed rate v_f is applied to the cross slide of the machine, the wheel advances towards the workpiece. The wheel and the workpiece mutually 'machine' each other, generating the grinding interface force and the deflection in the grinding system. The deflection δ is given by

$$\delta = F_n / k_e \quad (4.2)$$

where F_n is the normal component of the grinding force and k_e is the stiffness of the grinding system. The normal force is approximately proportional to the real depth of cut[94]:

$$F_n = k_c a = \frac{k_c \dot{r}}{n_w} \quad (4.3)$$

where k_c is the grinding force coefficient, a is the real depth of cut, \dot{r} is the rate of reduction of the workpiece radius and n_w is the workpiece rotational speed. If grinding wheel wear is neglected, the difference between the command infeed velocity \dot{X} and the actual infeed velocity \dot{r} can be attributed to the changing radial elastic deflection $\dot{\delta}$ in the grinding system.

$$\dot{X} - \dot{r} = \dot{\delta} \quad (4.4)$$

The parameter r is the reduction in radius of the workpiece and thus expresses the radial shape. Combining equations 4.2, 4.3 and 4.4 leads to the controlling equation of the grinding system.

$$\dot{X} - \dot{r} = \frac{k_c}{k_e n_w} \dot{r} \quad (4.5)$$

So that,

$$\tau \dot{r} + \dot{r} = \dot{X} \quad (4.6)$$

where τ is the time constant of the system and is a measure of the relationship between stiffness and grinding force coefficient.

$$\tau = \frac{k_c}{k_e n_w} \quad (4.7)$$

The time constant is affected by the wheel speed and workpiece speed through the rotational speed n_w and the grinding force coefficient k_c .

The grinding model can be readily modified to include the effect of wheel wear, if a grinding ratio G is defined as the volumetric ratio of material removal rate to the wheel wear rate[7]:

$$G = \frac{\pi d_w b \dot{r}}{\pi d_s b \dot{w}} = \frac{d_w \dot{r}}{d_s \dot{w}} \quad (4.8)$$

where \dot{w} is the radial wear rate of the grinding wheel. If wheel wear is taken into account, the continuity condition given by equation 4.4 is modified to

$$\dot{X} - \dot{r} - \dot{w} = \dot{\delta} \quad (4.9)$$

Let

$$\tau' = \frac{\tau}{1 + \frac{d_w}{d_s G}} \quad (4.10)$$

and

$$\dot{X}' = \frac{\dot{X}}{1 + \frac{d_w}{d_s G}} \quad (4.11)$$

Equation 4.9 can then be modified to

$$\tau' \dot{r} + \dot{r} = \dot{X}' \quad (4.12)$$

which has the same form as equation 4.6. In terms of process control, equation 4.6 and 4.12 are the same. Therefore the grinding system behaves approximately as a first order system despite wheel wear. When the time constant is estimated from experimental data, the result will be affected by the rate of wheel wear. When the rate of wheel wear is small in comparison to the radial penetration rate, the wheel wear can be neglected, enabling equation 4.6 to be used.

A commonly used grinding cycle consists of a roughing stage and a sparking-out stage. Solving equation 4.6[6] for the roughing stage ($\dot{X} = v_f$) gives

$$r(t) = v_f \{ t - \tau [1 - \exp(-\frac{t}{\tau})] \} \quad (4.13)$$

for the sparking out stage ($\dot{X} = 0$) gives

$$r(t) = v_f \{ t_1 - \tau \exp(-\frac{t-t_1}{\tau}) \} \quad (4.14)$$

where t is the grinding time and t_1 is the rough grinding period. From equations 4.13

and 4.14, the time constant is found to be the characteristic parameter. The removal rate and the deflection of the grinding system are different for different values of time constant even if the same infeed rate is applied. The rate of size change of the workpiece in the sparking-out stage is also characterised by the time constant. Accordingly the time constant is considered to be a valid parameter to represent the cutting ability of the grinding system[6]. For a particular grinding system and a particular set of grinding conditions, the only cause of variations in time constant is the wheel sharpness. Therefore changes of the time constant of a grinding system are indicative of changes in the grinding wheel sharpness.

4.2. Grinding as a Control System

It is proposed that the mechanism of the total grinding process may be investigated by considering the grinding process in terms of process control. From the point of view of control, the total grinding process includes dressing and grinding. The basic relationships in grinding can be interpreted by the interdependency existing between the inputs and outputs of the process as in figure 4.2. In figure 4.2, the grinding process is assumed to be affected by the grinding wheel, the dressing tool, the workpiece, the dressing conditions and the grinding conditions. These influential aspects are considered as the inputs of the grinding process. The grinding behaviour is characterised mainly by grinding force, vibration, temperature, wheel wear and quality of the ground workpiece. These parameters may therefore be considered as the outputs of the grinding process.

It is proposed that the grinding wheel and the dressing tool combine with the dressing kinematic conditions to generate the wheel cutting surface. The volume of material removed by each grain is associated with its kinematic action. The force on a single grain depends on the characteristics of the workpiece and the cutting motion of the grain. The relationship between the inputs and outputs of the grinding process may

be defined from the action of a single representative grain. The grinding behaviour results from the aggregation of the effects of each individual grain. Therefore the basis of grinding behaviour is the performance of a single grain. Based on this analysis, the relationships between the inputs and outputs of the grinding process can be investigated by considering relationships with the action of a single grain.

The grinding wheel is characterised by many parameters, such as wheel grade, grain size, structure number, grain material and bond material. The dressing conditions affect the topography of the working surface of the wheel, which in turn affects the grinding behaviour after dressing[3]. The diamond tip shape also affects the wheel topography. The tip shape cannot be controlled due to the effect of diamond wear. The effects of dressing can therefore be very different for the same dressing conditions. A dressing strategy for CNC grinding should, therefore, be capable of compensating for diamond wear. The characteristics of the workpiece affect the load on the grain. The machine control parameters for plunge grinding are grinding wheel speed, workpiece speed and wheel infeed rate. The principal grinding parameter is the infeed rate v_f which directly controls removal rate.

The outputs of the grinding process are those parameters which represent the grinding behaviour and the workpiece quality. The grinding force and the grinding vibration are outputs from the viewpoint of the mechanics. The grinding temperature is an output from the viewpoint of thermal effects. The wear of the grinding wheel is an output of the grinding process from the view point of tribology. The specific energy of grinding is the main output from considerations of energy efficiency. Because the specific energy is affected by grinding force, temperature, vibration and wheel wear, it can be considered as a more comprehensive parameter of the grinding process. Other outputs of the grinding process from the viewpoint of workpiece quality are the size errors, roundness errors, surface roughness and surface integrity.

A key point linking inputs and outputs of the grinding process is the individual grain

load as shown in figure 4.2. The grinding behaviour can be separated into two aspects relating to the physics of material removal and the geometry of the grinding process. The physical behaviour of the wheel may be related to the grinding force. Because the topography of the wheel reflects its shape onto the workpiece surface, the roughness of the workpiece under ideal conditions may be considered as the geometrical expression of the behaviour of the grinding wheel. The effect of dressing on grinding behaviour can be mainly described by the effects on the grinding force and surface roughness.

4.3. Requirements of a Dressing Strategy

In evaluating the effects of the dressing operation on the grinding process, the following criteria need to be satisfied.

- (i) The values of surface roughness after grinding should always lie within the product design limits. In particular the surface roughness must be less than the upper limit. Higher values of surface roughness will be rejected. Lower values of surface roughness are unnecessary for component function and it is possible that lower values of surface roughness will lead to increased production costs, because of decrease in productivity.
- (ii) The values of workpiece size generated by the process with a high removal rate should fall within the size limits.
- (iii) The grinding wheel should wear as uniformly as possible across the face. The wheel wear rate must not be too high nor too low. If the grinding wheel wears too rapidly, the deterioration of the wheel form will occur prematurely[52]. If the fracture process in the grinding wheel occurs too slowly, grinding chatter or grinding burn will occur due to bluntness of the grains of the grinding wheel resulting in high grinding forces[124-126].
- (iv) The redress life of the grinding wheel should be as long as possible. Usually grinding cannot be carried out at the same time as dressing is in progress. Frequent

dressing therefore decreases productivity.

For a fixed grinding cycle these requirements imply that the working surface of the grinding wheel should be stable. Therefore a good dressing operation is one which leads to stable grinding behaviour. For different grinding conditions, different dressing conditions may be required in order to optimise the grinding process.

Large variations in the initial grinding behaviour are often due to inadequate dressing which leads to a large initial change of the wheel surface. It has been found[3, 10, 38] that the effects of dressing in the initial stage of grinding are much stronger than in later stages, and these effects continue until the next dressing operation. Therefore dressing conditions should be selected to lead to stable grinding behaviour or at least to reduce the behavioural variations in the initial stage of grinding. It may be further argued that a good dressing operation should provide stable grinding behaviour at the maximum material removal rate without offending the constraints of the grinding operation.

The important influence of diamond tip width is commonly ignored when dressing conditions are selected. The reason is due to the difficulty of measuring or controlling the diamond tip width and also due to lack of knowledge on the effect of the diamond shape. Due to the lack of a suitable method of controlling diamond shape, the results of dressing become unpredictable. The objective is therefore to achieve a dressing strategy for the selection of dressing conditions to compensate for the effects of the variation of diamond tip width. If the variation of the shape of the dressing diamond causes the grinding force to increase, a larger dressing depth or dressing lead may be used to reduce the grinding force. Similarly the dressing depth or dressing lead may be adjusted to improve the surface roughness. The methodology of how to adjust the dressing conditions to compensate for the variation of the shape of the dressing diamond will be detailed in following chapters.

Chapter 5 Experimental Investigation of Dressing and Grinding Performance

5.1 The Experimental System

The aim of the experiments was to investigate dressing and the subsequent grinding behaviour. The grinding experiments were undertaken on a Jones & Shipman Series 10 cylindrical grinding machine with an A-B 8200 CNC. The minimum programmable increment of the wheelhead was 0.0001 mm and the servo input resolution was 0.0002 mm. The resolution of the optical scale used for position feedback was 0.1 μm . The standard wheel peripheral speed was maintained at 33 m/s. An automatic wheel balancing unit was used. The workpiece was held between dead centres on the workhead and tailstock. The parameters v_s , v_w and v_f were checked and found to be controlled to an accuracy approximately 1%.

A grinding wheel type A465-K5-V30W was used. The diameter of the wheel in the experiments varied progressively from 410 ± 1 mm to 360 ± 1 mm due to wheel wear. The workpiece material was oil hardened cast steel with a hardness of HRC 60 - 62. The diameter of the workpieces varied between 15 ± 0.0005 mm and 18.5 ± 0.0005 mm, depending on the number of times the specimens were ground. The width of the workpieces was in the range of 23 mm to 25 mm. Single diamond dressing tools were used for dressing. The coolant used for dressing and grinding was Arrow Synthetic Cutting Fluid with a dilution ratio of 16:1.

Workpiece size measurements were carried out on a Taylor-Hobson Talymin 4-10 comparator (0.2 μm resolution). Workpiece surface texture and diamond shape were measured on a Taylor-Hobson Form Talysurf 120. Workpiece roundness was measured on a Taylor-Hobson Talyrond 210. The measurement accuracy of the

Talymin, Talysurf and Talyrond were better than $\pm 0.5 \mu\text{m}$. Wheel wear was measured by the razor blade method, by which the accuracy was judged to better than $1 \mu\text{m}$.

A schematic arrangement of the on-line measurement system is shown in figure 5.1. During the grinding process, the workpiece size, grinding power and vibration were logged by a multifunction, high-speed, A/D, I/O expansion board (MetraByte Model DAS-20[127]) using a personal computer. The MetraByte board enabled the computer to be used as a high-speed, high-precision, data-acquisition and signal-analysis instrument. The board was designed as a multilayer construction with integral ground plane to minimise noise and crosstalk at high frequencies. The maximum sampling rate was 100,000 samples per second. For A/D conversion, one unit of the signal was equivalent to the full scale input range divided by 4096.

A Tektronix 2211 digital storage oscilloscope was used as a visual monitor. The oscilloscope was capable of storing 4,000 data on each channel. The resolution was 256 units for full range. The accuracy in the range of use was better than 3%.

On-line size measurement was undertaken by using a Movomatic size gauging system built into the Jones & Shipman Series 10 cylindrical grinding machine. The resolution of the diameter gauging system was $0.1 \mu\text{m}$. The accuracy of the measurement was within $\pm 0.5 \mu\text{m}$.

Grinding power was assumed to be the difference between grinding wheel spindle power when grinding and when running under no load. The grinding power signals were obtained from a Deemstop power meter. The power data from the Deemstop were calibrated with a Siemens Function Meter B 1081. The calibration was found to be linear at 0.75 W/unit at a significance level $\alpha = 0.01$. The coefficient of determination of the regression was 0.97. The accuracy in the range of use was better than 5%.

Where a wide frequency band vibration measurement is made, the choice of measurement parameter is very important if the signal has components at many frequencies. There are three main parameters for monitoring vibration, which are acceleration, velocity and displacement. Measurement of displacement gives the low frequency component the most weight while measurement of acceleration weights the level towards high frequency components. The vibration of a grinding system consists of many components in a wide frequency band. Therefore acceleration was selected as the parameter to be monitored. A Brüel & Kjær type 4332 piezoelectric accelerometer was used which gave a constant frequency response from 0 to 10 kHz. An FE-128-CA Fylde Charge Amplifier was used to provide a voltage signal indicative of the level of vibration from the accelerometer. For the range of experiments, a typical grinding acceleration signal detected by the oscilloscope at a sampling rate of 80 kHz is illustrated in figure 5.2. As shown in figure 5.3, the characteristic frequency of the grinding chatter was found by spectral analysis to be between 2.5 and 3.5 kHz, which is higher than the normally expected frequency. The vibration frequency of the coolant pump was identified at about 350 Hz.

The grinding power and size data were sampled at 100 Hz. However, since the characteristic frequency of the grinding chatter was about 2.5~3.5 kHz, the vibration data were logged at a very high frequency of 10 kHz based on the Nyquist sampling theorem. Due to the limit of the computer memory, it was impossible to log both size and vibration data at 10 kHz for the whole grinding cycle. Therefore, the data logging strategy shown in figure 5.4 was used. The strategy was to record vibration signals at high frequency for a short time during the steady state period within a grinding cycle. The steady stage was assumed to be achieved after a 3 time constant period.

The program for data logging was written in 'C' language. The data logging process was carried out in two ways. Slow data logging was undertaken in the foreground during the whole grinding cycle, and fast data logging was undertaken in the

background during steady grinding. The slow logging frequency was controlled by the PC system clock interrupt. The fast logging frequency was controlled by the MetraByte on-board clock. The fast logging data were transferred to memory using the DMA(Direct Memory Access) method. Because only one board was available, the slow data logging was stopped when the fast data logging was being undertaken. The slow logging data were set to zero while the fast logging was carried out. This allowed the successive data from the slow logging to be maintained in order as a continuous array. The flow chart of the data logging program used is shown in figure 5.5.

In order to prevent aliasing errors, low pass Butterworth filters were applied to all signals before they were recorded. A Butterworth cascaded filter was used to provide a maximally flat magnitude response in the pass band combined with a high attenuation rate. It makes voltage control and wide-range tuning easier because it sets the low-pass cut-off frequencies in all cascaded sections to the same frequency. The normalised third-order low-pass active filter circuit employed is shown in figure 5.6.[128] For a low pass filter of critical frequency 4000 Hz, the parameters in figure 5.6 were $R = 51\Omega$, $C_1 = 2670 \text{ pF}$, $C_2 = 1050 \text{ pF}$ and $C_3 = 150 \text{ pF}$.

5.2 Experimental Procedure

Before the experimental investigation on dressing and grinding was undertaken, the number of dressing passes required was determined. Many dressing passes were found to be required in order to clean the wheel working surface effectively and achieve a stable dressing result. Figure 5.7 shows the effect of the number of dressing passes on grinding behaviour. One dressing pass was undertaken before every workpiece grinding cycle. Grinding power became steady after approximately 8 grinding cycles. Therefore it was assumed that eight dressing passes were needed to clean the wheel surface in this particular case. In the further grinding experiments,

eight dressing passes were employed each time the wheel was redressed.

The diamond shape was measured before and after dressing. The diamond was carefully replaced in its previous position after measurement so as to present the same aspect to the grinding wheel each time dressing was performed. A typical diamond shape measured is shown in figure 5.8. The active diamond width b_d was defined as the engaged width in the horizontal plane. The shape of the diamond can also be characterised by the diamond sharpness ratio γ , which is defined as the dressing depth a_d divided by the active width of the diamond b_d as shown in figure 2.1. The diamond shape measurement was carried out using a chisel stylus on the Talysurf. A significant change in diamond shape was often found after dressing as shown in figure 5.9. It was found that diamond wear can either make the diamond sharp or make the diamond blunt which indicates that the diamond shape is unpredictable during the dressing process.

The plateau surface of a worn diamond is very rough and irregular as illustrated in figure 5.10. This makes it difficult to achieve accurate measurement of the active diamond width. For this reason the measurements shown in figure 5.9 can only be used as approximate indications.

The single diamond dressing operations were defined by dressing depth, dressing lead, dressing diamond shape and number of dressing passes. Experiments were carried out to examine the effects of these dressing conditions. The effects of grinding conditions, workspeed and wheel infeed rate, were also investigated. In relation to dressing, the shape of the dressing diamond tip and the dressing power were measured. The diameters of the wheel and workpieces were measured for each experiment. Grinding power, grinding vibration and size changes of the workpiece were monitored during the grinding process. After grinding, surface texture, size error and roundness of the workpieces were measured. The wheel wear was also measured.

Four fundamental experiments sets were carried out in the research, which were

- i effects of dressing conditions on dressing force;
- ii effects of grinding conditions on grinding behaviour;
- iii effects of dressing conditions on grinding behaviour;
- iv correlation of dressing conditions and grinding conditions.

The basic dressing and grinding procedure for these experiments was as follows.

The stock removed from the workpiece was $300 \pm 10 \mu\text{m}$ on diameter. Dressing diamonds with different wear flats were used for dressing. Eight dressing passes were made before each set of trials to achieve a consistent wheel surface. After the infeed phase of the cycle was completed, the wheelhead was held stationary for a dwell period of 5 seconds in most cases. For experiment ii, the dwell time was 10 seconds. The number of workpieces ground in each set of trials depended on the wheel redress life. The redress life was considered to be finished when evidence was found of grinding chatter.

According to equation 3.5, the equivalent chip thickness is dependent on metal removal rate and wheel speed. In plunge grinding the metal removal rate is equal to $\pi \cdot d_w \cdot v_f \cdot b$. Therefore in plunge grinding, the equivalent chip thickness is normally controlled by varying the infeed rate and is independent of workpiece speed. Due to the large momentum of the wheel in external grinding, the grinding wheel speed is normally maintained constant. Therefore considering the comparatively weak effect of workpiece speed on specific energy, the main grinding control parameter is the infeed rate of the wheelhead.

Dressing and grinding conditions were decided depending on the nature of the investigation. The effects of dressing were investigated by varying dressing depth a_d and dressing lead f_d under fixed grinding conditions as in experiments i and iii. The wheel speed v_s was 33 m/s. The workspeed v_w was 0.25 m/s. The infeed rate v_f was

10 $\mu\text{m/s}$. In experiment ii, the effects of equivalent chip thickness were investigated by varying wheel infeed rate and workspeed under the dressing conditions, $a_d = 0.010$ mm, $f_d = 0.10$ mm/rev. In experiment iv, the effects of infeed rate and workspeed were investigated under the fixed dressing conditions, $a_d = 0.015$ mm, $f_d = 0.15$ mm/rev.

All dressing and grinding operations were carried out with the coolant supply turned on fully. Maximum grinding power was read from the Function Meter. The dressing force was determined by measuring dressing power. After grinding, the workpieces were left to "soak" in a controlled temperature environment of 20°C for a period of 24 hours before measurement. Workpiece size error, surface roughness and roundness were measured. Size error variations were obtained by comparing the workpiece size with the size of the first workpiece. The size error reading was an average of 5 readings at different positions around the workpiece taken half way between the two ends. Wheel wear was measured after each set of grinding trials using the razor blade method. The wheel profile was replicated onto a razor blade by grinding it. The razor blade profile was then measured using the Form Talysurf.

5.3. Experimental Results and Discussion

5.3.1. Effects of Dressing Conditions on the Dressing Force

The relationship between the dressing force and the dressing parameters was determined and illustrated in figure 5.11. An empirical dressing force model was obtained by least mean squares regression of the experimental results shown in figure 5.11 to a straight line. The coefficient of determination was 0.89. The significance level of regression was 0.01. The dressing force model was thus expressed as

$$F_d = 724 a_d \cdot f_d + 0.281 \quad (5.1)$$

where the units of a_d and f_d are in millimetres and the unit of dressing force is newtons. This model shows that dressing force increases linearly with cross-sectional area of the diamond path in the range investigated.

5.3.2. Effects of Grinding Conditions on the Grinding Process

As mentioned in chapter 3, a fairly good correlation exists between grinding force, specific energy and surface roughness with equivalent chip thickness. In order to evaluate the effects of equivalent chip thickness on the grinding process, the experiments were arranged by varying workpiece speed v_w and wheel infeed rate v_f . The wheel speed was fixed at 33 m/s. Two dressing passes with $f_d = 0.10$ mm/rev and $a_d = 0.010$ mm were completed before each trial. In order to make the wheel surface stable ten grinding cycles were completed before making measurements. The specific power and the specific energy are illustrated in relation to equivalent chip thickness as in figure 5.12 and figure 5.13 respectively. Figure 5.13 demonstrates the size effect. The specific energy decreases with increasing equivalent chip thickness. The effect of workpiece speed is not so strong as that of equivalent chip thickness. By curve fitting the experimental results, empirical equations were obtained

$$P' = 3.86 h_{eq}^{0.831} \quad (5.2)$$

$$e_c = 11.4 h_{eq}^{-0.169} \quad (5.3)$$

where the units for h_{eq} was mm, for specific power was W/mm and for specific energy was J/mm³.

There was no obvious effect of equivalent chip thickness and workpiece speed on surface roughness. This is shown in figure 5.14. The reason for this may be the use of a long dwell time which reduces the surface roughness. The wheelhead dwell time in this particular trial was 10 seconds.

5.3.3. Effect of Dressing Conditions on the Grinding Process

Experiments were undertaken in order to understand the effect of dressing on the grinding behaviour throughout the redress life cycle. The effects of dressing on grinding power, workpiece surface roughness, size error, roundness and time constant were studied. The grinding results after dressing with sharp and blunt single point diamonds are considered. The sharpness of the diamond was expressed by the diamond sharpness ratio γ as shown in figure 2.1. The sharpness ratios of the sharp and blunt diamonds were approximately 0.05 and 0.02 respectively.

Figure 5.15 and figure 5.16 show the effect of dressing on grinding power. Figure 5.17 and figure 5.18 show the effects of dressing on surface roughness. It can be seen that grinding power and surface roughness in the initial stage of grinding were strongly affected by the dressing operation. A coarse dressing operation, large a_d and f_d , produced a sharper and more open wheel cutting surface. With a coarse dressing operation a small initial grinding power and larger surface roughness resulted irrespective of whether a sharp or a blunt diamond was used. Comparing figure 5.15 with figure 5.16 and figure 5.17 with figure 5.18, grinding power was smaller and surface roughness was larger when a blunt diamond was used. It was shown that the sharp diamond gave a more stable grinding behaviour than the blunt diamond. It was inferred that a blunt diamond introduced more bond fractures on the wheel surface. If coarse dressing conditions were applied, surface roughness was very rough and unstable with a blunt diamond. This was particularly apparent under the conditions where $a_d = 25 \mu\text{m}$ and $f_d = 0.25 \text{ mm/rev}$ in figure 5.18.

From the results of the grinding experiments, it can be seen that the effect of dressing on grinding behaviour is strong in the early stage of grinding and reduces afterwards. The grinding power and workpiece roughness progressed towards similar values whatever dressing condition was applied after a large amount of metal is ground. This is consistent with other published work[57, 61] which suggests that it may be

generally true. This may be attributed to the self-sharpening action of the grinding wheel. As grinding proceeds, both attritious wear and fracture wear occur in the wheel surface and the wheel topography becomes either more open or more closed depending on the severity of grinding[61]. If the wheel surface generated by the dressing operation is similar to its equilibrium state, the excessive change of grinding behaviour can be avoided and the grinding outputs will be steady.

Figure 5.19 and 5.20 show the effect of dressing on size errors. It was found that the effect on the size can be very different using different dressing conditions. Comparing figure 5.19 and 5.20, it was found that with a blunt diamond the size errors increased in a positive sense, while with a sharp diamond the size errors increase in either a positive sense or a negative sense. Workpiece size errors are commonly attributed to wheel wear, thermal effects and variations in wheel sharpness[6]. Wheel wear causes successive workpiece diameters to become larger. Thermal effects cause successive workpiece diameters to become either larger or smaller. Variations in wheel sharpness affect the final size of the workpiece because of the effect of changing force on machine deflection. The sharper the wheel, the smaller will be the residual stock remaining as a result of deflection. The result of reducing deflections is to reduce the size of successive workpiece diameters. By using a sharp diamond, the initial decrease of workpiece size can be attributed to the fact that the effects of changes of wheel sharpness and thermal deformation are stronger than the effect of wheel wear. This implies that the wheel wear with a sharp diamond was relatively small. A good dressing operation is assumed to be one which balances the effects of wheel wear, thermal expansion and wheel sharpness variations, leading to small size errors.

Comparing the size errors with the changes of grinding power shown in figure 5.19 and 5.15, 5.20 and 5.16, it was found that the size errors in a wheel life cycle were relatively small if the initial power was approximately equal to the final grinding power.

Wheel wear can be expressed by grinding ratio (G ratio), which is the ratio of the removed volume of the workpiece to the wear volume of the wheel. The effect of dressing conditions on G ratio are illustrated in table 5.1 and table 5.2. It was found that G ratio decreased with increasing dressing depth. The effect of dressing lead on G ratio was found to be relatively weak. In order to investigate the effect of diamond shape on G ratio, a constant volume of material was ground with the wheel dressed by different diamonds. For the dressing condition, $a_d = 0.015$ mm, $f_d = 0.15$ mm/rev and the same metal volume removed by grinding, about $490 \text{ mm}^3/\text{mm}$, the G ratio was 75 for the blunt dressing tool and 115 for the sharp dressing tool. From the results, it appears that when a blunt dressing tool is used, the G ratio will be smaller and wheel wear and size increase of successive workpieces will be larger. However, if the dressing conditions are very fine, there is little difference between a sharp dressing tool and a blunt dressing tool.

Table 5.1 Effect of dressing on G ratio (sharp dressing tool)

Experimental conditions: Grinding Machine: Jones & Shipman Series 10 Wheel type: A465-K5-V30W Workpiece material: Oil hardened cast steel, HRC 60-62 Coolant: Arrow Synthetic Cutting Fluid, dilution rate 16:1 Diamond sharpness ratio: $a_d/b_d \approx 0.05$ $v_s = 33 \text{ m/s}$, $v_w = 250 \text{ mm/s}$, $v_f = 10 \text{ } \mu\text{m/s}$ $d_s \approx 370 \text{ mm}$, $d_w \approx 17 \text{ mm}$, $V_w \approx 245 \text{ mm}^3/\text{mm}$			
Dressing Lead / Dressing Increment	0.05 mm/r	0.15 mm/r	0.25 mm/r
0.005 mm	109.8	97.8	111.7
0.015 mm	77.8	92.9	72.0
0.025 mm	71.5	66.0	69.2

Table 5.2 Effect of dressing on G ratio (blunt dressing tool)

Experimental conditions: Grinding Machine: Jones & Shipman Series 10 Wheel type: A465-K5-V30W Workpiece material: Oil hardened cast steel, HRC 60-62 Coolant: Arrow Synthetic Cutting Fluid, dilution rate 16:1 Diamond sharpness ratio: $a_d/b_d \approx 0.02$ $v_s = 33 \text{ m/s}$, $v_w = 250 \text{ mm/s}$, $v_f = 10 \text{ } \mu\text{m/s}$ $d_s \approx 390 \text{ mm}$, $d_w \approx 17 \text{ mm}$, $V_w \approx 490 \text{ mm}^3/\text{mm}$			
Dressing Lead \ Dressing Increment	0.05 mm/r	0.15 mm/r	0.25 mm/r
0.005 mm	114.3	84.1	66.3
0.015 mm	99.1	75.5	79.3
0.025 mm	63.1	52.5	53.0

A sharp cutting surface of the wheel is obtained when a coarser dressing operation is applied, leading to lower specific energy and temperature in grinding. With a sharp wheel, thermal expansion was expected to be reduced. The effect of thermal expansion in the initial stage of grinding was easily observed if the wheel wear was small. To confirm this, an experiment was arranged with a wheel working in the steady wear stage. In this case the wheel wear was small. The results of the experiment are illustrated in figure 5.21, in which it can be seen that workpiece size decreased. The variation of the distance between the wheelhead and the tailstock was only about 1 μm in the experiments as measured using dial test indicator. It was considered that the size variations were due to thermal expansion of the wheel, which arises because the wheel is warmed up by the additional friction in the bearings during grinding. The trend of size variations is similar to a thermal stabilisation process, that is the size changes rapidly at the beginning and then the change slows down exponentially. The initial size reduction found in figure 5.19 occurred because a sharp diamond was used, which reduced initial wheel wear. If a blunt dressing tool

is used, the initial wheel wear is increased and the thermal effect is masked by wheel wear. Using a blunt diamond the sizes of successive workpieces always increased as in figure 5.20.

The size errors are also affected by wheel sharpness. As mentioned in section 3.3.4, the sharpness can be expressed by the time constant. A sharper wheel gives a smaller value of time constant. Effects of time constant on the grinding cycle are illustrated in figure 5.22. When the dwell time is unchanged, a blunt wheel with a large time constant gives a large difference between the programmed wheel position and the actual wheel position at the end of a grinding cycle. Consequently, variations of wheel sharpness introduce size errors and roundness variations between each grinding cycle. However, if the dwell period is longer than three time constants the size variations are limited to 5% of maximum depth of cut.

Figure 5.23 and figure 5.24 illustrate the effect of dressing conditions on the time constant. Coarse dressing conditions produce a sharp wheel and give a small value of time constant in the initial grinding stage. It was also found that the time constant was smaller if a blunt dressing diamond was used. This was attributed to the fact that a blunt dressing diamond induces more macrofractures during dressing[9] thus making the wheel sharper.

Effects of dressing conditions on roundness are shown in figure 5.25 and figure 5.26. Large variations of roundness are found under some dressing conditions. Most of the roundness variations occurred when a large dressing lead was used. The reason for this effect remains unclear. The possible reason may be attributed to the fact that a large value of f_d leaves more space for the diamond to make a distinctly different groove in a succeeding pass and causes the grinding wheel to be out of round.

Figures 5.27 to 5.31 show that large differences of the grinding behaviour are experienced when the wheel is dressed with different diamond widths. It was found

that a sharp dressing tool generated high grinding power as shown in figure 5.27. It might suggest that a sharp dressing tool with small active width would produce less macrofractures, leaving more cutting edges on the wheel surface. This is consistent with the theory that more cutting edges lead higher grinding force as discussed previously. The rapid initial fall in grinding power might be attributed to the change of cutting edge density in the initial wheel wear stage.

It was found in figure 5.28 that small values of time constant were obtained with both sharp and blunt dressing diamonds. This is possibly explained by a sharp dressing tool giving a sharp shape when it cuts through the grain. On the other hand, a blunt dressing diamond causes grains and bonds to break, also creating sharp cutting edges. This variability of the effect of dressing makes it difficult to control the wheel sharpness. Comparing figure 5.28 and figure 5.29, it was found that a larger time constant was associated with larger roundness errors. This is discussed in chapter 7.

Figure 5.30 indicated that the active width of the diamond had a strong effect on the surface roughness. Geometrical analysis suggests that a blunt dressing diamond should reduce surface roughness. However if the blunt dressing diamond increases the number of bond fractures on the wheel surface, the surface roughness will be increased. This implies that the dressing width of the diamond may not fully illustrate the effect of diamond shape on the grinding process. Figure 5.31 shows that a sharp diamond tends to give size errors of a negative sense, which would be expected due to the higher initial grinding force followed by reducing forces associated with a sharp diamond used for dressing. This condition was considered to be associated with the thermal expansion of the wheel.

5.3.4. Correlation of Dressing Conditions and Grinding Conditions

The grinding behaviour is dominated both by dressing conditions and grinding

conditions. Optimal grinding requires an appropriate combination of dressing conditions and grinding conditions. A change in grinding conditions requires a change in dressing conditions in order to achieve the required grinding behaviour. Some effects of grinding conditions on grinding behaviour are shown in figure 5.32 to 5.35.

Figures 5.32 and 5.33 show that the specific grinding power and surface roughness increase with increasing infeed rate v_f . The effect of v_f on surface roughness is relatively weak, which may be due to the fact that surface roughness improves during the dwell period. Figure 5.32 suggests that the effect of v_w on the specific power at the end of wheel life depends on v_f . When $v_f = 10 \mu\text{m/s}$, the specific power decreased with increase of workspeed. When $v_f = 20 \mu\text{m/s}$, the specific power slightly increased with increase of workspeed. Workpiece speed has a weak influence on surface roughness as shown in figure 5.33.

It can be seen in figure 5.33 that the surface roughness for $v_f = 20 \mu\text{m/s}$ remained more nearly constant throughout the wheel redress life than for $v_f = 10 \mu\text{m/s}$. In figure 5.32, it can be seen that the initial grinding power was approximately equal to the final grinding power for $v_f = 20 \mu\text{m/s}$. Accordingly, it was concluded that surface roughness remained more closely at the same level when the initial grinding power was approximately equal to the final grinding power in the wheel life cycle. It is therefore proposed to use this conclusion as a basis for an optimisation strategy. If grinding conditions change a stable grinding process can possibly be achieved by changing the dressing conditions in such a manner as to make the initial grinding power level in the wheel life cycle approximately equal to the final grinding power level. Because the surface roughness is influenced both by the dressing and the grinding conditions, it should be possible to obtain optimal results for grinding by applying a suitable combination of dressing and grinding conditions.

The effect of grinding conditions on time constant is shown in figure 5.34. Because

of the variations of time constant, the stock remaining on the workpiece after grinding changes and the roundness of the workpiece also changes, as demonstrated in figure 5.35. Because the dwell time of 5 seconds was more than three times the time constant, the roundness variations were small. As discussed previously the variance of the time constant represents the variance of the cutting ability of the grinding wheel. Figure 5.34 shows that the time constant decreased when grinding infeed rate was increased. For the particular dressing conditions, a rapid decrease of the time constant were found in the initial stage when grinding under a lower workspeed. From the observation in this section, it is concluded that the dressing condition should be selected according to a strategy which tends to stabilise the grinding behaviour.

5.4. Conclusion

From the results of the grinding experiments shown in this chapter, the effects of dressing on grinding behaviour may be idealised as in figure 5.36. A very important feature illustrated in figure 5.36 is the convergence of grinding performance for different dressing conditions. Grinding power, time constant, surface roughness and roundness converge with grinding time despite differences in the dressing conditions employed. This implies that dressing has most effect on the initial grinding stage, while the grinding conditions affect the whole wheel life cycle. Based on this observation, it is proposed that selections of dressing conditions and grinding conditions may be separated. The dressing conditions may be selected to adjust the initial grinding behaviour after dressing and the grinding conditions selected to adjust the grinding behaviour in other stages of a wheel redress life cycle. This conclusion is considered to be important for the design of a dressing strategy.

The effects of dressing on grinding size errors can be contradictory as idealised in figure 5.37. When dressing with very coarse conditions or with a very blunt dressing diamond, more bond fractures are generated on the wheel surface. The result is that

wheel wear is increased and workpiece size errors are increased in a positive sense. After dressing with very fine conditions, the wheel wear may mainly be attributed to attritious wear and microfracture. The wheel wear volume was small. Force and deflection reduction and thermal expansion cause the workpiece size errors to increase in a negative sense. It is concluded that a good dressing operation makes grinding behaviour more stable and gives better grinding quality.

One of the most interesting aspects of the grinding process is that the grinding behaviour can be very different even for the same value of control parameters, such as v_s , v_w , v_f , a_d and f_d . This is attributed to uncontrollable parameters involved in the grinding operation. For example, the dressing width of the diamond is an uncontrollable parameter and has a strong effect on grinding behaviour. Due to insufficient control of the shape of the dressing diamond, it is necessary to develop a strategy for the selection of dressing parameters a_d and f_d , so that the effect of the width of the dressing diamond can be compensated.

Chapter 6 Empirical Models for Dressing and Grinding

Empirical equations for the grinding output parameters were required to make it possible to control the dressing and grinding process rationally. Empirical equations for the effect of grinding conditions were discussed in section 5.3.2. Grinding power, specific energy and surface roughness were directly related to equivalent chip thickness. In order to take the dressing effect into account, the grinding outputs may also be expressed as a function of dressing parameters. Malkin[68] suggested that surface roughness can be expressed in the form

$$R_a = R_0 a_d^{1/4} f_d^{1/2} h_{eq}^r \quad (6.1)$$

where the exponent r lies typically in the range $0.15 < r < 0.6$, R_0 is a constant. Similarly, because a logarithmic linear relationship exists between surface texture and specific energy, the specific grinding power may be expressed as

$$P' = P_0 a_d^x f_d^y h_{eq}^z \quad (6.2)$$

where P_0 , x , y and z are constants.

The influence of the dressing conditions on grinding power appears to be more complex. According to the results shown in figure 5.15 and 5.16, a large change of grinding power can be observed in the initial stage of grinding. This means that equation 6.2 does not apply for the whole redress life cycle. Variations of grinding power in relation to the grinding wheel wear were idealised as shown in figure 5.36. The trends of grinding power in the initial wear stage of grinding are dominated by dressing. Too fine a dressing condition leads to a high initial grinding power which rapidly decreases during the initial stage of grinding. Too coarse a dressing condition leads to a large increase of grinding power in the initial stage. In the steady wear stage, the grinding power gradually increases because of the attritious wear of the grains. As grinding proceeds, the grinding power for different dressing conditions

tends to converge to the same value. This phenomenon indicates that the effects of the dressing conditions on grinding power are mainly experienced in the initial stage of grinding and gradually become less obvious.

Grinding performance is dependent on the cutting surface of the grinding wheel generated by the dressing operation. The number of cutting points on the wheel surface will be different if different dressing conditions are used. The cutting edge density may be defined as the number of static cutting edges per unit area of the grinding wheel surface. Based on equation 2.3 the cutting edge density after dressing λ_0 may be expressed as

$$\lambda_0 = C_0 a_d^x f_d^y \quad (6.3)$$

Where C_0 , x and y are constants. With regard to grinding force or grinding power, the number of the active edges on the wheel surface and the mean thickness of the undeformed chips should also be considered. According to equations 2.4 and 2.5, the grinding force is mainly affected by the dressing lead, diamond tip width, dressing depth and the number of non-incremented dressing passes. The effect of the diameter of the grains is relatively insignificant.

According to the principles of grinding described in chapter 3, the grinding force is the summation of individual grain forces. The grinding force due to an individual grain is related to undeformed chip thickness and cutting speed. The total grinding force is the accumulated effect depending on the density of cutting edges on the wheel. Werner's grinding force model equation 3.20 gives two exponents, ϵ and γ , to describe the effects of grinding conditions and wheel characteristics respectively. In grinding, ϵ lies in the range 0.5 to 0.95 and γ lies in the range 0.1 to 0.8. If the concept of equivalent chip thickness is applied and F_n/F_t is a constant, the tangential specific grinding force becomes

$$F_t' = k C_1^\gamma \left[\frac{v_s}{v_w} \right]^{1-\epsilon} d_e^{1-\epsilon} h_{eq}^\epsilon \quad (6.4)$$

where k is a constant. Based on equation 6.4, the more cutting points there are on the

wheel surface, the larger will be the force generated in grinding. Because finer dressing generates more cutting points on the wheel surface, a large grinding force and a high grinding power are expected. As grinding proceeds, the grinding force or power tends to converge to the same level as for coarse dressing. This phenomenon of the convergence of the grinding force in grinding process was also observed in the experimental results of Umino and Shinozaki[61]. Umino and Shinozaki expressed the grinding force as,

$$F(t) = F_0 - (F_0 - F_e)(1 - e^{-m n_s t}) \quad (6.5)$$

where F_0 is the initial grinding force, F_e is the critical grinding force at the end of the secondary grinding stage, m is the probability of grain fracture in a grinding cycle and n_s is the wheel rotational speed. Changes of grinding force expressed by equation 6.5 are illustrated in figure 6.1. If $F_0 > F_e$, the grinding force will initially decrease. If $F_0 < F_e$, the grinding force will initially increase. The reason for the convergence of the grinding force was explained by the change of the density of the cutting edges on the wheel surface.

Umino and Shinozaki[61] suggested that the initial cutting point density after dressing will converge to a critical density in the grinding process. The variation of the cutting edge density was expressed as

$$\lambda(t) = \lambda_e + (\lambda_0 - \lambda_e)e^{-m n_s t} \quad (6.6)$$

where λ_e is the cutting edge density at the end of the secondary grinding stage, λ_0 is the cutting edge density after dressing. Combining equations 6.4 and 6.6, the time dependent force may be expressed as

$$F'_t = k [\lambda_e + (\lambda_0 - \lambda_e)e^{-m n_s t}]^\gamma \left[\frac{V_s}{V_w} \right]^{1-\varepsilon} d_e^{1-\varepsilon} h_{eq}^\varepsilon \quad (6.7)$$

Equation 6.7 has the same disadvantage as equation 6.4. The density of the cutting edges on the wheel surface is not normally available by measurement. To overcome this problem, two special cases may be considered. These are the grinding behaviour at the beginning and at the end of the grinding wheel redress life cycle. At the beginning of the wheel life cycle, the time t in equation 6.7 is zero, so the initial

specific tangential grinding force is

$$F'_{t0} = K_0 \lambda_0^\gamma \left[\frac{V_s}{V_w} \right]^{1-\varepsilon} d_e^{1-\varepsilon} h_{eq}^\varepsilon \quad (6.8)$$

Combining equations 6.3 and 6.8,

$$F'_{t0} = K_0 [C_0 a_d^\alpha f_d^\gamma]^\gamma \left[\frac{V_s}{V_w} \right]^{1-\varepsilon} d_e^{1-\varepsilon} h_{eq}^\varepsilon \quad (6.9)$$

Let $k_0 = K_0 C_0^\gamma$, $\alpha = x \gamma$, and $\beta = y \gamma$, then

$$F'_{t0} = k_0 a_d^\alpha f_d^\beta \left[\frac{V_s}{V_w} \right]^{1-\varepsilon} d_e^{1-\varepsilon} h_{eq}^\varepsilon \quad (6.10)$$

At the end of the wheel life cycle, the value of $e^{-mns t}$ in equation 6.7 is very small and near to zero, so that the final specific tangential grinding force is

$$F'_{te} = K_e \lambda_e^\gamma \left[\frac{V_s}{V_w} \right]^{1-\varepsilon} d_e^{1-\varepsilon} h_{eq}^\varepsilon \quad (6.11)$$

Let $k_1 = K_e \lambda_e^\gamma$, then

$$F'_{te} = k_1 \left[\frac{V_s}{V_w} \right]^{1-\varepsilon} d_e^{1-\varepsilon} h_{eq}^\varepsilon \quad (6.12)$$

Combining equations 6.5, 6.10 and 6.12, the grinding force may be expressed as

$$F'_t(t) = \{k_1 + [k_0 a_d^\alpha f_d^\beta - k_1] e^{-mns t}\} \left[\frac{V_s}{V_w} \right]^{1-\varepsilon} d_e^{1-\varepsilon} h_{eq}^\varepsilon \quad (6.13)$$

To explain the rise of the grinding force in the steady grinding stage, Malkin[98] observed that the grinding force was proportional to the wear flat area, which can be expressed as equations 3.26 and 3.27. From Malkin's results[98], it can be seen that the wear area increases linearly with the number of encounters of the wheel and the workpiece during the steady grinding stage. Therefore it is reasonable to assume that the grinding force increases linearly with the number of the wheel encounters with the workpiece. Based on this assumption and equation 6.13, the time dependant grinding force can be expressed as

$$F'_t(t) = \{k_1 + [k_0 a_d^\alpha f_d^\beta - k_1] e^{-mns t}\} \left[\frac{V_s}{V_w} \right]^{1-\varepsilon} d_e^{1-\varepsilon} h_{eq}^\varepsilon + k_2 n_s t \quad (6.14)$$

where k_2 is the constant representing the effect of wheel wear. The tangential grinding force can be obtained from the grinding power, when the facility for

measuring grinding force is unavailable. The specific grinding power can be expressed as

$$P' = F_t' v_s \quad (6.15)$$

Therefore the time dependant specific grinding power in a wheel redress cycle may be expressed as

$$P'(t) = P_e' + (P_0' - P_e')e^{-m n_s t} + k_2 v_s n_s t \quad (6.16)$$

where

$$P_0' = k_0 a_d^\alpha f_d^\beta \left[\frac{v_s}{v_w} \right]^{1-\epsilon} d_e^{1-\epsilon} h_{eq}^\epsilon v_s \quad (6.17)$$

and

$$P_e' = k_1 \left[\frac{v_s}{v_w} \right]^{1-\epsilon} d_e^{1-\epsilon} h_{eq}^\epsilon v_s \quad (6.18)$$

Since in most grinding operations the grinding speed is constant and the value of $(1 - \epsilon)$ is small in this work, the specific grinding power can be expressed in the simple form

$$P'(t) = [C_1 + (C_0 a_d^\alpha f_d^\beta - C_1) e^{-m n_s t}] h_{eq}^p + C_2 n_s t \quad (6.19)$$

where $C_0 = k_0 \left[\frac{v_s}{v_w} \right]^{1-\epsilon} d_e^{1-\epsilon} v_s$, $C_1 = k_1 \left[\frac{v_s}{v_w} \right]^{1-\epsilon} d_e^{1-\epsilon} v_s$ and $C_2 = k_2 v_s$. At the beginning of grinding, where $m n_s t$ is very small, the grinding power can be approximated by

$$P_0' = C_0 a_d^\alpha f_d^\beta h_{eq}^p \quad (6.20)$$

which is the same as equation 6.2. After the initial stage of grinding, if $m n_s t$ is large enough, the grinding power is given by

$$P'(t) = C_1 h_{eq}^p + C_2 n_s t \quad (6.21)$$

By regression analysis of the experimental data in figure 5.12, the value of p is 0.831.

By regression analysis of the experimental data in figure 5.15, $x = -0.358$ and $y = -0.068$. Therefore the initial specific grinding power for the experiments may be expressed as

$$P_0' = C_0 a_d^{-0.358} f_d^{-0.068} h_{eq}^{0.831} \quad (6.22)$$

where C_0 can be determined by measuring initial grinding power after dressing. C_2 in

equation 6.19 represents the effect of wheel wear on grinding power. C_2 is determined by the slope of the grinding power results plotted against numbers of the wheel revolutions during the second stage of grinding. After C_2 is calculated, C_1 can be obtained from equation 6.21. Once C_0 , C_1 and C_2 are decided, changes of grinding power in a wheel life cycle can be matched by varying the constant m . A particular change process of the grinding power in a wheel life cycle is illustrated in figure 6.2. To match the change of the grinding power, the empirical model is expressed as

$$P'(t) = [26.6 + (7.31 a_d^{-0.358} f_d^{-0.068} - 26.6) e^{-0.035 t}] h_{eq}^{0.831} \times 10^4 + 2.05 \times 10^{-4} t \quad (6.23)$$

The units used in the equation 6.23 are W/mm for $P'(t)$, millimetres for a_d , f_d and h_{eq} , seconds for the time. Figure 6.2 indicates that equation 6.23 gives a good expression of the change of the grinding power. It has been known that the wheel wear is affected both by dressing and grinding conditions, so that the constants, m and C_2 , may change if the dressing and grinding conditions change. Therefore equation 6.19 has a limited ability to illustrate of the changes of the grinding power in a wheel life cycle. Even so, because of the convergent feature of the grinding power, equation 6.19 can still be used to give the initial and the final grinding power of a wheel life cycle.

Because the effect of dressing is stronger at the initial stage, the process of selection of dressing conditions should be concentrated on the initial stage. The conclusions which can be drawn from equations 6.1 and 6.22 are that surface roughness is mainly affected by dressing lead f_d and grinding power is mainly affected by dressing depth a_d . These relationships can be used to develop a dressing strategy.

The empirical equations developed here have not taken into consideration the effects of the width of the dressing diamond. If the shape of the dressing diamond does not change too rapidly, the equations will give a good estimate. According to equations

2.4 and 2.5 the width of the diamond is indispensable to a description of the influence of dressing, especially for grinding force. Due to the lack of an effective way to measure and control the width of the diamond, it is very difficult to quantify the effects of diamond width. Because of this difficulty, the constant C_0 in equation 6.19 has to be obtained by regression analysis between each dressing operation, so that the influence of the diamond wear on the equations can be minimised.

Chapter 7. Simulation of Grinding Cycles

As discussed in chapter 4, grinding power, size error and roundness are directly affected by grinding cycle design. In order to grind workpieces accurately and efficiently, it is necessary to determine appropriate values of feed-rate, target position and dwell time in a grinding cycle. The selection of optimum values depends on the deflection behaviour of the machine-workpiece system as represented by the system time constant. In this chapter, results from simulated grinding cycles are compared with results from experimental measurements. Simulation techniques allow the effects of modelling assumptions on grinding behaviour to be investigated. The objectives of employing simulation were therefore to test the extent to which modelling assumptions can be used to predict grinding behaviour and provide a basis for further investigation of the grinding process.

7.1. The Characteristics of a Grinding Cycle

The magnitude of the deflection between the grinding wheel and the workpiece is not always fully appreciated. Typically the deflection is of the same order of magnitude as the depth of cut in precision grinding[93, 129]. Sometimes the deflections measured are considerably larger than the depth of cut. The deflection causes a delay between the command signal for position and the system response. A basic plunge grinding cycle consists of an infeed period and a dwell period as illustrated in figure 7.1. Deflections are generated during the transient at the beginning of the infeed period. The deflections have to be removed during the dwell period when the workpiece size approaches the value corresponding to the command position of the infeed. The roundness also improves during the dwell period.

A mathematical model of the process should be broadly capable of describing these effects, so that the controller can predict the machine-workpiece deflection and apply the appropriate compensation in advance. In chapter 4, a cylindrical plunge grinding process was represented as a first order linear system. Equation 4.6 gave the relationship between command infeed rate and the rate of radius reduction of the workpiece as

$$\ddot{r} = \frac{1}{\tau} (\dot{X} - \dot{r}) \quad (7.1)$$

Therefore the grinding system is characterised by the time constant of the grinding system τ and it is possible to simulate the system response. The most important requirement is to determine an accurate value of the time constant from experiment to characterise the system.

The time constant can be derived from a data log of either size or power level during the dwell period by using a curve fitting technique. When the wheel infeed rate \dot{X} is selected as a constant v_f , the solution of equation 7.1 is:

$$r(t) = v_f \cdot (t - \tau + \tau \cdot e^{-t/\tau}) \quad (7.2)$$

If the grinding cycle is selected as in figure 7.1, the solution of equation 7.1 during the dwell period ($t > t_1$) is

$$r(t) = v_f \cdot (t_1 - \tau \cdot e^{-\frac{t-t_1}{\tau}}) \quad (7.3)$$

$$\dot{r}(t) = v_f \cdot e^{-\frac{t-t_1}{\tau}} \quad (7.4)$$

If grinding speed remains as a constant, the grinding power is approximately proportional to the normal grinding force. Therefore equation 4.3 and 7.4 lead to:

$$P(t) = P(t_1) \cdot e^{-\frac{t-t_1}{\tau}} \quad (7.5)$$

At any time t_2 on the decay curve in the dwell period

$$\frac{P(t_2)}{P(t_1)} = e^{-\frac{t_2-t_1}{\tau}} \quad (7.6)$$

$$\tau = \frac{\log P(t_2) - \log P(t_1)}{t_2 - t_1} \quad (7.7)$$

An alternative method, which is convenient when used with data logging on a computer, involves integration of the power signal. This refinement automatically filters noise. Integration of equation 7.5 leads to

$$\int_{t_1}^t P(t) dt = \tau P(t_1) (1 - e^{-\frac{t-t_1}{\tau}}) \quad (7.8)$$

When t is big enough, $e^{-\frac{t-t_1}{\tau}}$ is much smaller than 1, so that the time constant can be expressed as

$$\tau = \frac{\int_{t_1}^t P(t) dt}{P(t_1)} \quad (7.9)$$

Equations 7.3 and 7.5 can also be used for evaluation of the time constant by means of least mean squares regression analysis of the data from size and power measurement.

Roundness errors mainly result from machine vibration and from geometrically generated errors. Geometrically generated errors are primarily due to variations in the differences between $r(t)$ and $r(t - T)$ expressed by equation 7.2, where T is the period of one workpiece revolution. In the absence of significant vibrations and at high feedrates, roundness errors are mainly caused by geometrically generated errors. Roundness errors also occur due to the residual effects of the initial workpiece roundness errors Δr_0 . A simplified analysis of the rounding process relates roundness errors after n workpiece revolutions to the initial roundness error. This analysis is very much over-simplified and is only applicable if the frequencies represented by the combined effects of the roundness errors and the workpiece speed are much lower than the first resonant frequency of the grinding system. However the process broadly reflects the rounding process for large low frequency errors[130].

Δr_0 is denoted as an initial radius error of the workpiece. After the first revolution of grinding, Δr_0 will be reduced by a_1 . The remaining error is equal to the deflection caused by Δr_0 . Therefore

$$\Delta r_0 = a_1 + \delta_1 = \frac{\delta_1 \cdot (k_e + k_c)}{k_c} \quad (7.10)$$

where $k_e = F_n / \delta$, and $k_c = F_n / a$. So,

$$\Delta r_1 = \delta_1 = \Delta r_0 \cdot \left(\frac{k_c}{k_e + k_c} \right) \quad (7.11)$$

Similarly,

$$\Delta r_1 = a_2 + \delta_2 = \delta_2 \cdot \left(\frac{k_e + k_c}{k_c} \right) \quad (7.12)$$

$$\Delta r_2 = \delta_2 = \Delta r_1 \cdot \left(\frac{k_c}{k_e + k_c} \right) = \Delta r_0 \cdot \left(\frac{k_c}{k_e + k_c} \right)^2 \quad (7.13)$$

Continuing the same procedure, the roundness error of the nth revolution is obtained as

$$\Delta r_n = \Delta r_0 \cdot \left(\frac{k_c}{k_e + k_c} \right)^n \quad (7.14)$$

Combining equations 4.7 and 7.14 gives

$$\Delta r_n = \Delta r_0 \cdot \left(\frac{1}{1 + \frac{1}{\tau n_w}} \right)^n \quad (7.15)$$

Therefore the effect of the initial workpiece roundness errors is only $\Delta r_0 \cdot \left(\frac{k_c}{k_e + k_c} \right)^n$ for low frequency Fourier shape harmonics and can be neglected. Here n is the number of revolutions of the workpiece during grinding. Considering only the effects of feed-rate and static compliance, the roundness error of the workpiece at any time in the grinding process is approximately given by the maximum variation of $r(t) - r(t - T)$ during any period T/2.

Grinding power and grinding force are important parameters of the grinding process which can be directly controlled if the technology is available. Usually, the infeed rate is controlled and the process monitored by sensing the spindle power. Equation 6.19 may be used to indicate the size effect. For simplicity, the equation used to express the variation of grinding power during grinding for a simulation of a grinding cycle was

$$P = k \dot{r}^p \quad (7.16)$$

where p is a constant.

7.2. Development of a Simulation for Grinding Cycles

Simulation of the grinding cycle was undertaken to illustrate the effects of the various cycle parameters. Figure 7.2 illustrates the structure of the grinding cycle simulation developed using Simnon a commercial software package[131]. The grinding cycle simulation mimics a CNC controller and was used to simulate various grinding cycles with various combinations of values of grinding cycle parameters. Thus the simulation was able to predict the final workpiece size and cycle time that a selected cycle would achieve.

The elements of the simulation in control terms are listed below:

- (i) The wheel axis model, which gives the axis position, is

$$\frac{X(s)}{\dot{X}(s)} = \frac{1}{s} \quad (7.17)$$

- (ii) The workpiece size model, which gives the radius of the workpiece, derived from equation 7.1 is

$$\frac{r(s)}{\dot{X}(s)} = \frac{1}{s(s\tau + 1)} \quad (7.18)$$

where $X(s)$, $\dot{X}(s)$ and $r(s)$ are the Laplace transforms of the wheel axis position, wheel axis infeed rate and workpiece size. When the wheel wear rate is large, the G ratio should be used in the size model as in equations 4.10, 4.11 and 4.12.

- (iii) The power model is

$$\frac{P}{\dot{r}^f} = k \quad (7.19)$$

This relationship is shown as $T(P(t))$ in figure 7.3. The exponent f can easily be updated according to the grinding condition. From the power model, the variation of grinding power during grinding can be clearly predicted. In addition, if the information is entered to allow burn to be predicted for the materials being used[132, 133], there is the potential for the system to give a warning when damage is likely to

occur.

(iv) **Simulation control program.** The simulation control program supervises the simulation and contains the simulation algorithm. Various grinding cycles were simulated by varying the algorithm. How this simulation program simulates the grinding cycle is shown as a block diagram in figure 7.3, where $T(P(t))$ is the transfer function of the grinding power model. Either a constant feedrate control strategy may be employed or a power control strategy depending on the type of cycle to be simulated. The constant feedrate control strategy is described by the following set of conditional statements.

$$\Delta\dot{X}_0 = \left\{ \begin{array}{ll} 0 & \text{If size threshold not crossed} \\ \Delta\dot{X}_c & \text{If within coarse infeed stage} \\ \Delta\dot{X}_m & \text{If within the medium infeed stage} \\ \Delta\dot{X}_f & \text{If within the fine infeed stage} \\ \dot{X}_0 & \text{If the command size is achieved} \end{array} \right\} \quad (7.20)$$

The power control strategy is described by the following set of conditional statements.

$$\Delta\dot{X}_1 = \left\{ \begin{array}{ll} 0 & \text{If power threshold not crossed} \\ -\Delta\dot{X}_i & \text{If the initial action level is crossed} \\ -\Delta\dot{X}_h & \text{If the higher power threshold is crossed} \\ +\Delta\dot{X}_l & \text{If the lower power threshold is crossed} \end{array} \right\} \quad (7.21)$$

The above strategies are further discussed and explained in relation to simulated and experimental results for particular grinding cycles.

7.3. Simulation for Grinding Cycle Design

A standard grinding cycle consisting of coarse infeed, medium infeed, fine infeed and a dwell was simulated in figure 7.4. The response of the system in bringing the workpiece to size was simulated and the overall cycle time, the final size errors and

the final roundness were predicted. The grinding cycle was optimised to control errors within the required tolerances for size and roundness by adjusting the infeed rate, infeed period, overshoot and dwell period. All changes caused by adjusting parameters were clearly evident in graphical representations of the grinding cycle. A significant degree of accuracy in the simulation can be achieved when the grinding system is characterised by a time constant. Figure 7.5 shows that the values of the reduction of workpiece radius from the simulation and from experiment are in close agreement for a plunge grinding cycle consisting of a single infeed and a dwell. The largest size error observed in this simulation was only 1.7 μm .

In order to fully utilise the capabilities of the simulation the time constant of the grinding system and the maximum power to be employed have to be available. In principle, the best strategy is to control the power level rather than the infeed rate in order to achieve a minimum cycle time consistent with specified quality requirements. This strategy requires that the power is increased to the set power limit as quickly as possible and the controller adjusts the infeed rate adaptively to maintain the power setting [75, 94, 133]. However the implementation of in-process power control presents a difficulty, because of deflections in the system. It is difficult to know when and how the infeed rate should be reduced to prevent the grinding power overshooting the power setting. This problem is illustrated in figure 7.6 which indicates that the grinding power, which should approach the power limit, takes an appreciable time to react to decreases in infeed rate and a power "overshoot" occurs. This situation could be unacceptable if the power limit setting has been set to avoid poor size accuracy and possible burn. To avoid the occurrence of this phenomenon, the infeed rate needs to be reduced at an appropriate time before the power limit is reached. This was achieved by setting an initial action level which was lower than the lower power threshold. When the grinding power was higher than the initial action level, the infeed rate was decreased. In this way, the shape of the grinding power curve was adjusted to prevent power overshoot.

Figure 7.7 illustrates the procedure employed for simulating and developing an in-process power control cycle. In this grinding cycle control strategy, the grinding process begins with the fastest infeed rate. When the grinding power is higher than the initial action level, the infeed rate decreases with set change steps. When the grinding power is between the required power control limits, the infeed rate is varied to constrain the power within this power control band. This is achieved by decreasing infeed rate when power is higher than the upper power threshold and increasing infeed rate when the power is lower than the lower power threshold.

The grinding cycle was optimised by adjusting the upper power threshold, the lower power threshold, and the initial action level together with the infeed rate change steps. Figure 7.8 illustrates a simulation of a grinding cycle developed using the above procedure. The grinding power was controlled to remain under the set limit of 1.5 kW. It was found that the power reached its limit in about one second with no overshoot. Providing the data base values are appropriate the simulation indicated that burn will not occur and the cycle time will be close to the shortest possible. In principle, the dwell time can also be minimised, if the system time constant is known. The effectiveness of the control strategy developed by the simulation technique was evaluated by using the parameters determined by these means on a real machine fitted with an appropriate adaptive control system.

Figure 7.9 illustrates the grinding process control achieved in a real grinding experiment using the values developed by simulation. Power overshoot was avoided and maximum power was reached in the shortest time possible for the particular system. In this trial the wheel speed was 33 m/s and the workpiece speed was 0.25 m/s. Because the infeed rate was frequently varied during the power control cycle, the control of size accuracy and roundness was worse than that of the cycle using a constant infeed rate. This means a longer dwell period was required to achieve the same accuracy. This problem could also be solved by using an over-shoot and retract strategy[135, 136]. However further research is required on this subject to determine

the practical problems and benefits of attempting to achieve a controlled retraction.

It has been shown by grinding experiments and by simulations that grinding power, size error and roundness are strongly affected by the time constant. The time constant plays an important part in grinding cycle simulation. A stable time constant is essential for predicting and controlling grinding cycle behaviour. Therefore it is necessary to employ a suitable dressing operation to ensure a stable time constant in grinding.

Chapter 8 Simulation of the Dressing and Grinding Process

In order to clearly understand the grinding process, a basic study of the interactions occurring between the abrasive grains and a workpiece is needed. In this chapter, a method of simulating the dressing and grinding process is described. With the help of computer simulation, the various phenomena in dressing and grinding can be visually presented and understood more easily. Simulation of the grinding process requires information concerning the wheel topography which is difficult to obtain in practice. The wheel topography depends on both the wheel characteristics and the dressing operation. An attempt is therefore made to describe the grain-workpiece interactions from fundamental grinding parameters, including the spacing of effective cutting points or grains and the geometry of undeformed chips, associated with the generation of a representative workpiece profile.

The generation of workpiece profiles in grinding is illustrated in relation to the fundamental grinding parameters associated with the wheel working surface profile. The workpiece topography is represented by the surface roughness R_a . The interaction between the wheel working surface and the workpiece is based on the effective cutting point spacing and chip cross sectional area. The grinding force is considered as the most important parameter to describe the grinding mechanism. The grinding force is therefore used to evaluate the grinding process. The effect of changes both of dressing and grinding parameters are discussed.

8.1. Generation of the Grinding Wheel Topography

In practice, wheel performance depends on the grain-workpiece interactions generated from the grain distribution and the kinematic conditions of dressing and grinding. A

quantitative description of these interactions is therefore used to provide a basis for an evaluation of grinding wheel performance. The grinding wheel is composed of a large number of grains which are randomly spaced in the wheel. For simplicity, the grains are approximated as uniform spheres of diameter d_g [89] randomly distributed throughout the wheel volume. The grain diameter is given as[9]

$$d_g = 15.2 M^{-1} \quad (8.1)$$

where M is the grain size number. The grain volume packing density V_g as a percentage is given by

$$V_g = 2 \cdot (32 - S) \quad (8.2)$$

where S is the structure number of the wheel. Based on the above values, the location of the grains in the grinding wheel can be expressed by the following matrix:

$$\{\Phi\} = \{G_{i,j,k}\}_{I \times J \times K} \quad (8.3)$$

where the vector $G_{i,j,k}$ represents the location of each individual grain centre in three dimensional space.

$$\{G_{i,j,k}\} = \begin{pmatrix} G_{i,j,k}^x \\ G_{i,j,k}^y \\ G_{i,j,k}^z \end{pmatrix} = \begin{pmatrix} G_{0,0,0}^x + i \cdot \Delta x + R_x \\ G_{0,0,0}^y + j \cdot \Delta y + R_y \\ G_{0,0,0}^z + k \cdot \Delta z + R_z \end{pmatrix} \quad (8.4)$$

In the simulation, the spatial probability distribution of the grains is assumed to be uniform, so the average spacing Δx , Δy and Δz are the same. Let $\Delta x = \Delta y = \Delta z = \Delta$, where Δ is determined by the density of the grains in the grinding wheel V_g , then

$$\frac{\pi}{6} d_g^3 = V_g \cdot \Delta^3$$

Therefore the average grain spacing Δ is

$$\Delta = \sqrt[3]{\frac{\pi \cdot d_g^3}{6 \cdot V_g}} \quad (8.5)$$

To randomise the grain positions, the random numbers R_x , R_y and R_z between 0 and Δ were introduced as a bias. These random numbers were generated by a standard Turbo Pascal random number generator. So that

$$\{G_{i,j,k}\} = \left\{ \begin{array}{l} G_{0,0,0}^x + i \cdot \Delta + R_x \\ G_{0,0,0}^y + j \cdot \Delta + R_y \\ G_{0,0,0}^z + k \cdot \Delta + R_z \end{array} \right\} \quad (8.6)$$

A restraint on grain location is that the distance between two grains should be larger than the diameter of the grains d_g . Following the sequence of grain allocation the distance between shadowy grains and the black grain shown in figure 8.1 should be larger than d_g . Therefore the following rules have to be satisfied.

$$\left\{ \begin{array}{l} d(G_{i,j,k}, G_{i-1,j-1,k-1}) > d_g \\ d(G_{i,j,k}, G_{i-1,j-1,k}) > d_g \\ d(G_{i,j,k}, G_{i-1,j-1,k+1}) > d_g \\ d(G_{i,j,k}, G_{i-1,j,k-1}) > d_g \\ d(G_{i,j,k}, G_{i-1,j,k}) > d_g \\ d(G_{i,j,k}, G_{i-1,j,k+1}) > d_g \\ d(G_{i,j,k}, G_{i-1,j+1,k-1}) > d_g \\ d(G_{i,j,k}, G_{i-1,j+1,k}) > d_g \\ d(G_{i,j,k}, G_{i-1,j+1,k+1}) > d_g \\ d(G_{i,j,k}, G_{i,j-1,k-1}) > d_g \\ d(G_{i,j,k}, G_{i,j-1,k}) > d_g \\ d(G_{i,j,k}, G_{i,j-1,k+1}) > d_g \\ d(G_{i,j,k}, G_{i,j,k-1}) > d_g \end{array} \right. \quad (8.7)$$

Where $d(G_{i,j,k}, G_{l,m,n})$ is the distance between the grain $G_{i,j,k}$ and grain $G_{l,m,n}$. If the rules are not all satisfied, the black grain has to be reallocated until the rules are satisfied. The grain is reallocated by applying equation 8.6 with new random numbers R_x, R_y, R_z .

To clarify the mechanism of formation of a ground surface, it is necessary to know the distribution of the cutting edges after dressing. The cutting surface of the grinding wheel is generated by the interaction of the dressing diamond with the grinding wheel. A geometrical interaction was initially used as the basis of the dressing process. Subsequently the fracture of the bonds or grains was considered. Equation 3.2 was used for the local elastic deflections of the grains in the simulations of both dressing and grinding.

The assumptions for the simulation of dressing were as follows:

- Vibration of both the grinding wheel and the dressing tool is negligible.
- The shape of the dressing tool tip is assumed to be a paraboloid.
- The adjacent grains are mounted on springs but are uncoupled, which means that force applied to one grain does not deflect the adjacent grains.

The contour of the wheel surface is determined both by the dressing movement and the grain location. When a single diamond passes helically over the surface of a grinding wheel, the shape of the resulting cutting edge is shown by the dressing trace lines as in the figure 8.2. After several dressing passes, the shape of the grain cutting surface is as shown by the bold lines. The final contour of the cutting edges is decided by the largest values removed from the grain surface by the dresser.

In practice, the shape of the cutting surface after dressing can be erratic and not conform precisely to the shape of the dressing tool due to fracture of the grains on the wheel surface or due to vibration of either the dressing tool or the wheel. It is assumed that only a few points of the cutting path traced by the dressing tool remain on the surface after each dressing pass. Therefore a sine wave function $h \cdot [\sin(\omega x + \alpha) + 1]$ with random frequency ω and random initial angle α was superimposed on the cutting edge shape. The random frequency ω was selected to fall into the range from $4\pi/(f_d + b_d)$ to $8\pi/(f_d + b_d)$ so as to ensure there are only one or two points of the grain surface in touch with the dressing tool. The amplitude of the sine wave h depends on the extent of the grain fracture. A large value of h represents a large extent of grain fracture in dressing. If the cutting path traced by the dressing tool is expressed as a function of position along the x axis, the cut surface of a grain may be expressed as

$$z_g(x) = f(x) + h [\sin(\omega x + \alpha) + 1] \quad (8.8)$$

where $f(x)$ is the grain cut surface after dressing according to the cutting action in dressing and $h \cdot [\sin(\omega x + \alpha) + 1]$ represents the additional grain material removed by the fracture action in dressing. The function $f(x)$ is decided by the largest value of dressing traces and the grain surface. The superimposed area of the sine wave is

assumed to be proportional to the nominal dressing area A_d and the overlap ratio U_d .

Therefore h is expressed as

$$h = k \frac{A_d U_d}{f_d} \quad (8.9)$$

The proportionality factor k was chosen by trial and error so as to match real grinding results with results from the simulation. The simulation of the grain fracture is illustrated in figure 8.3. This process is repeated for each grain in turn.

It was assumed that during dressing, the dressing force will pull out the grain if the cutting force is larger than the grain retention strength. The retention force was determined by the strength of the wheel, which was deduced from the dressing force model. According to the experimental results shown in section 4.3.1, the dressing force F_d can be considered as a composite of the friction force F_{fri} and fracture force F_{fra} . Equation 5.1 can therefore be expressed as

$$F_d = F_{fra} + F_{fri} = \sigma_w \cdot A_d + F_{fri} \quad (8.10)$$

where A_d is the nominal dressing area (equal to $a_d \cdot f_d$) and the strength of the grinding wheel σ_w was assumed to be

$$\sigma_w = \frac{F_{fra}}{A_d} \quad (8.11)$$

Therefore σ_w can be determined from the dressing experiments, as illustrated in figure 5.11 σ_w is the gradient of the dressing force curve. For the purposes of simulation, the grain retention force was then calculated from

$$F_r = \sigma_w \cdot A_{i,j,k} \quad (8.12)$$

where $A_{i,j,k}$ is the cross sectional area of the grain $G_{i,j,k}$ remaining on the wheel after dressing as illustrated in figure 8.4.

8.2. Generation of a Ground Workpiece Surface

During the grinding process the grain cutting points pass through the workpiece.

Workpiece material was assumed to be removed if the grain engages the workpiece. The principle of generation of the workpiece topography was based on the grinding kinematics. During grinding, the grains on the wheel cutting surface pass through the workpiece and cut a portion of the workpiece material as shown in figure 8.5. In the simulation when the workpiece passes through the length of the grinding contact zone l_c , the distance travelled by the wheel surface is l_s .

$$l_s = \frac{v_s}{v_w} l_c \quad (8.13)$$

This means that all grits in the range of l_s (ACDD'C'A') engage with the cross section of the workpiece ABB'A'. When a cutting edge passes through a cross section of the grinding zone, the material of the workpiece higher than the cutting edge was assumed to be removed. Assuming the grain $G_{i,j,k}$ passes through the grinding zone at abb'a', the dark area will be removed. After the grinding wheel passes through the cross section ABB'A', the remaining surface contour is the ground surface of the workpiece. The simulation is carried out by each grain in turn.

Local elastic deflections of the grinding wheel have a very important influence on the chip formation process as discussed in chapter 3. Since the local workpiece elastic deformation is approximately a constant[92], it can be considered as a part of the total workpiece deflection. The variation of the deflection of the grain centre has a trend similar to the total local deflection[92]. Therefore the deflection of the grain centre was assumed to be the local deflection in the simulation of both the dressing and the grinding process. The deflection of the grain centre was calculated from equation 3.2.

In grinding, only a portion of the undeformed chip material is removed by a grain. The remaining material is plastically piled-up on the sides of the grain as shown in figure 8.6. It was therefore assumed that the area of the material removed is proportional to the undeformed cutting area of the grain. When a grain cuts through the workpiece, the ratio of material removed by the grain to the volume of undeformed chip is defined as the cutting efficiency ratio β in the simulation. The

remaining material will be $1 - \beta$ of the volume of the undeformed chip. For simplicity, the shape of the displaced material was approximated by a parabola expressed as follows.

$$x^2 = \frac{a^2}{h} (h - z) \quad (8.14)$$

The area of the remaining material is

$$A_p = \frac{4}{3} a h \quad (8.15)$$

The remaining material is superimposed on the workpiece surface at both sides of the grain trace.

8.3. Mechanics of Grinding in the Simulation

The grinding force acting on the grinding wheel is distributed between the individual grains in the grinding zone. The grinding force F can be separated into a tangential component F_t and a normal component F_n or into a horizontal component F_h and a vertical component F_v as illustrated in figure 8.7. When the diameter of the grinding wheel is much larger than the grinding depth, the angle α is very small. Under these conditions the horizontal component is almost identical to the tangential component and the vertical component is almost identical to the normal component. The horizontal component and the tangential component were therefore assumed to be the same. The vertical component was assumed to be the same as the normal component.

The total grinding force was obtained by integrating the grinding force on the individual grains in the grinding zone. Due to the random distribution of the grains in a grinding wheel, it is difficult to know the real number or the orientation of the grits in the grinding zone. An alternative method to obtain the total grinding force is to consider the energy consumption of the grinding process. When the area ABCD is removed as illustrated in figure 8.7, the grinding energy consumption

$$E = F_t \cdot l_s \quad (8.16)$$

The energy consumption to remove area $AC \cdot \Delta x$ is

$$\Delta E = \sum_i^n f_{t,i} v_s \Delta t = \sum_i^n f_{t,i} \frac{v_s}{v_w} \Delta x \quad (8.17)$$

where $f_{t,i}$ is the tangential grinding force on a grain i as it passes the section AC , Δt is the time for a grain to travel a distance Δx . To remove the area $ABCD$ the energy consumption is

$$E = \sum_{l_c} \Delta E = \sum_{l_c} \left(\sum_i^n f_{t,i} \frac{v_s}{v_w} \Delta x \right) = \sum_i^n f_{t,i} \frac{v_s}{v_w} l_c \quad (8.18)$$

Combining equations 8.11, 8.13 and 8.15, the tangential grinding force is

$$F_t = \sum_i^n f_{t,i} \quad (8.19)$$

The grinding force can therefore be simulated by considering the action of each individual grain as it passes a section such as AC .

As discussed in chapter 3, Shaw deduced the specific energy in grinding using a single grain approach. In Shaw's analysis the grain was assumed to be a sphere, each grain was assumed to be one cutting edge. The cutting depth was assumed to be much smaller than the diameter of the grain, an assumption which is suitable for the case where the grain is not dressed. After dressing, the cutting edges on a grain are of complex shape, which made it difficult to analyse grinding force on each grain. Therefore it was proposed that the cutting edges on a grain were assumed to be equivalent to a spherical cutting edge based on the assumption that one grain only acts as one cutting edge[25]. As in figure 8.8, the interface area was assumed to be equivalent to the shaded oval area, which was expressed as

$$A_o = \frac{\pi}{4} a_c b_c \quad (8.20)$$

where a_c is the contact length of the grain and b_c is the cutting width of the grain. The equivalent spherical grain was assumed to have the same interface area as the shaded oval area with the workpiece. So the diameter of the engaged circle of the

equivalent grain is

$$d_c = \sqrt{a_c b_c} \quad (8.21)$$

When the maximum cutting depth of a grain t_{\max} is available, the diameter of the equivalent grain d_{geq} can be determined as figure 8.8.

$$d_{\text{geq}} = \frac{t_{\max}^2 + \left(\frac{d_c}{2}\right)^2}{t_{\max}} \quad (8.22)$$

The size of the dressed grain is smaller than the original one, but the equivalent diameter of the cutting edge may be larger or smaller than the original diameter of the grain. The equivalent grain diameter depends on the shape of the grain and the depth of cut of the grain as illustrated in figure 8.9.

After the diameter of the equivalent grain has been determined, equation 3.39 can be used to determine the specific energy of the grinding. If the action of a grain in grinding is idealised as in figure 3.5, the indentation force of the grain R can be expressed by equation 3.30. The cutting force on a grain can be assumed to be equal to the indentation force R acting in direction θ as shown in figure 8.10. Therefore the tangential cutting force on a grain is

$$f_{tc,i} = \frac{3\pi}{4} \frac{b}{t} H \left(\frac{C'}{3}\right) A \sin\theta \quad (8.23)$$

and the normal cutting force on a grain is

$$f_{nc,i} = \frac{3\pi}{4} \frac{b}{t} H \left(\frac{C'}{3}\right) A \cos\theta \quad (8.24)$$

where A is the area of cross section of the undeformed chip as shown in figure 8.10.

If the friction coefficient is μ , the tangential and normal friction forces will be

$$f_{if,i} = \frac{3\pi}{4} \frac{b}{t} H \left(\frac{C'}{3}\right) \mu A \cos\theta \quad (8.25)$$

$$f_{nf,i} = \frac{3\pi}{4} \frac{b}{t} H \left(\frac{C'}{3}\right) \mu A \sin\theta \quad (8.26)$$

Combining the cutting and friction action, the force models for each grain were

represented as follows.

$$f_{t,i} = \frac{3\pi}{4} \frac{b}{t} H \left(\frac{C'}{3} \right) (\sin\theta + \mu \cos\theta) A \quad (8.27)$$

$$f_{n,i} = \frac{3\pi}{4} \frac{b}{t} H \left(\frac{C'}{3} \right) (\cos\theta - \mu \sin\theta) A \quad (8.28)$$

8.4. Simulation Procedure

Simulation of dressing and grinding was carried out to demonstrate the dressing and grinding process and to corroborate the relationships between the inputs and outputs of the total grinding process. The simulation was developed based on the relationships illustrated in figure 4.2. As discussed previously, the key point of a grinding process is the load on each single grain in the wheel. Therefore the simulation concentrated on the behaviour of each individual grain in dressing and grinding. The final grinding behaviour was obtained by accumulation of the grinding behaviour of all grains involved in dressing and grinding.

With specifications of the grinding wheel and workpiece, grinding conditions and dressing conditions, the simulation was designed to simulate the dressing and grinding process and give the outputs of grinding such as surface roughness, grinding force and grinding power.

Three functions were represented in the simulation. The first was the simulation of the dressing process, which provides the location of the grains and the shape of the cutting edges. The second was the simulation of the cutting process by a grain in grinding according to the kinematics and the deformations in the process. The third function in the simulation was to represent the action of each individual grain as it contributed to the total grinding process. The basic steps of the simulation are therefore as shown in figure 8.11.

In order to simulate a real situation of dressing and grinding, the conditions selected for the simulation were as close as possible to measured experimental conditions. For the grinding wheel A465-K5-V30W, the average diameter of the grains was about 0.293 mm and the density of the grains in the wheel was approximately 54%. Equation 5.1, which was derived empirically, was used to determine the dressing force used in the simulation. Based on these values the strength of the wheel σ_w from equations 8.9 and 5.1 was approximately 724 N/mm². To match the grinding results, the proportionality factor k in equation 8.9 was selected as 0.25.

After the input parameters were specified, the distribution of the grains in the wheel were determined. The co-ordinate axis system for grains in the grinding operation was set up as in figure 8.5. The subscripts i, j and k in the grain location vector $G_{i, j, k}$ represent the position of the grain along the X, Y and Z axes respectively. The number of grain layers along the X axis determined by the grinding width is 'I'.

$$I = \frac{b}{\Delta} + 1 \quad (8.29)$$

For the simulation of the ground surface roughness and the specific grinding force and power, a simulation along the full grinding width is unnecessary. Six layers along the X axis were found to be sufficient. The number of grain layers along the Y axis is 'J', which is determined according to the distance travelled by a point on the wheel surface in contact with the workpiece.

$$J = \frac{l_s}{\Delta} + 1 \quad (8.30)$$

The number of grain layers along the Z axis is 'K', which must ensure there are sufficient grains for the generation of the wheel working surface. Three layers are in most cases enough for simulation. Since the grains in the wheel are assumed to be spherical in shape, the distribution of the grains is determined from equations 8.6 and 8.7, which give the co-ordinate positions of the centre of the grain. The distribution of the grains in the wheel is sketched in figure 8.12.

Because adjacent grains are assumed to be independent of each other, the dressing

and grinding process were simulated by considering each single grain in sequence. The sequence of the grains in the simulation of dressing and grinding takes place in order of the Z, Y and X directions. The cutting action in dressing is determined by the engagement between the grain and the diamond according to the kinematic relationship of dressing. The material of the grains interfering with the diamond locus was assumed to be removed. The diamond shape assumed in the simulation was a paraboloid which is determined by b_d and a_d as shown in figure 8.13. The contour of the diamond can therefore be expressed as

$$z_d = -\frac{4 a_d x_d^2}{b_d^2} \quad (8.31)$$

Since the top point of the diamond was selected as the origin in the simulation, the values of the co-ordinates in equation 8.31 need to be adjusted accordingly. For the situation shown in figure 8.14, where the XOZ co-ordinate system is the same as the co-ordinate system in figure 8.5, the dressing trace can be expressed as

$$z_d(x) = \Delta z z_d - \frac{4 a_d (x - \Delta x x_d)^2}{b_d^2} \quad (8.32)$$

where $\Delta z z_d$ depends on the dressing depth. $\Delta x x_d$ depends on the position the diamond engages with the wheel and is expressed as

$$\Delta x x_d = R + n f_d \quad (8.33)$$

where R is a random number in the range from 0 to f_d and n is the number of wheel rotations when the diamond passes through. If b_d is smaller than f_d , there will be some parts of the wheel surface which do not engage with the diamond. This increases uncertainty in the simulation. Therefore the overlap ratio U_d in the simulation was assumed to be at least equal to or larger than one.

The fracture action of dressing was determined from equations 8.8 and 8.9. The elastic deflection was determined from equation 3.2. The shape of a grain after dressing was therefore determined by a combination of the cutting, elastic deflection and fracture actions in dressing. Figure 8.15 illustrates the simulation of the

generation of the grain cutting surface under the wheel co-ordinate system. The centre of the grain $G_{i,j,k}$ may be expressed as $(x_{G_{i,j,k}}, y_{G_{i,j,k}}, z_{G_{i,j,k}})$ in the wheel co-ordinate system. The z values of the cutting surface of the grain are stored in an array $z_g(x)$, where x is addressed in the range $[x_{G_{i,j,k}} - d_g/2, x_{G_{i,j,k}} + d_g/2]$. This allows further dressing passes to be simulated. The cutting surface of the grain was initially determined from the centre of the grain and the diameter of the grain.

$$z_g(x) = z_{G_{i,j,k}} + \sqrt{\left(\frac{d_g}{2}\right)^2 - (x - x_{G_{i,j,k}})^2} \quad (8.34)$$

Once the diamond cuts through the grain, the z values of the grain contour after dressing are the larger values taken from the diamond contour $z_d(x)$ and the grain contour $z_g(x)$. Therefore

$$z_g(x) = \max\{z_g(x), z_d(x)\} \quad (8.35)$$

The effects of fracture of the grain are added to the z values as in equation 8.8. The elastic deflection δ_d in dressing may be determined from equation 3.2 and needs to be subtracted from the z values as shown in figure 8.15.

The chip to be cut by a grain was determined from the kinematic relationships of grinding as shown in figure 8.5. When a grain $G_{i,j,k}$ passes across the section AA'B'B, the grain centre rises by a distance $\Delta_{i,j,k}$ in the workpiece co-ordinate system.

$$\Delta_{i,j,k} = d_e - \sqrt{d_e^2 - \left(l_c - \frac{l_c}{l_s} y_{G_{i,j,k}}\right)^2} \quad (8.36)$$

Therefore the z' value for the centre of the grain in the workpiece co-ordinate system is

$$z' = z_{G_{i,j,k}} + \Delta_{i,j,k} + \Delta_{z'z} \quad (8.37)$$

where $\Delta_{z'z}$ is the distance between the two system origins. Figure 8.16 shows the grinding process of the grain under the combination of the workpiece co-ordinate system and the wheel co-ordinate system. The cutting, the elastic deflection and the plastic pile-up are considered. The initial workpiece surface was set into an array $z'(i')$, $i' = 0, 1, 2, 3, \dots$, where i' represents the positions of the workpiece to be simulated. The value of each element in the array represents the z' value of the

workpiece point i' . The number of elements in the array depends on the precision required of the simulation. A larger number of elements give more precision. The interval between elements used in the simulation was one micron.

The cutting process was simulated by comparing the cutting surface of the grain with the relevant surface points of the workpiece. If a grain $G_{i,j,k}$ passes through the grinding zone, the surface points of workpiece in the area $[x_{G_{i,j,k}} - d_g/2, x_{G_{i,j,k}} + d_g/2]$ are involved in the cutting simulation. If the workpiece surface is higher, then the material higher than the cutting face of the grain will be removed. Values of elastic retrieval and plastic pile-up were assigned to the relevant workpiece points after each grain passed through the workpiece. The compliance of the grain centre was determined from equation 3.2 and the value selected for the compliance constant of the equation was 0.15. The material piled up along the sides of the grain path was given by the cutting efficiency ratio β . The cutting efficiency ratio varies with the cutting depth and grain shape[89]. Since a practical value was not available, β was assumed to be 0.75 in the simulation. Therefore 25% of the undeformed chip remains on the workpiece surface. The determination of the contour of the piled up material is detailed in figure 8.17. The material was assumed to pile up in the direction of α at both sides of the grain path, where the angle α is determined by the equivalent diameter and the maximum depth of cut of the grain. After the area of piled up material is determined, the parameters for determination of the contour of the piled up material can be given as

$$a = \sqrt{\frac{3 A_p}{2 \tan \alpha}} \quad (8.38)$$

and

$$h = \sqrt{\frac{3 A_p \tan \alpha}{8}} \quad (8.39)$$

Therefore

$$z'' = \left(1 - \frac{2 \tan \alpha}{3 A_p} x''^2\right) \sqrt{\frac{3 A_p \tan \alpha}{8}} \quad (8.40)$$

Since $\tan \alpha = \frac{t_{\max}}{b}$, then

$$z'' = \left(1 - \frac{2 t_{\max}}{3 A_p b} x''^2\right) \sqrt{\frac{3 A_p t_{\max}}{8 b}} \quad (8.41)$$

The final workpiece topography is the material remaining on the workpiece after the passage of all the engaged grains through the grinding zone. The generation of the workpiece surface is sketched in figure 8.18, where the numbers represent the sequence of the grains passing through the section under consideration. A simulated ground surface is illustrated in figure 8.19.

The total grinding force is determined by summing up the loads for all grains involved in grinding as expressed in equation 8.19. The forces on each grain were calculated from equation 8.27 and 8.28. There were five parameters to be determined, the grain shape ratio b/t , the material hardness, the constraint factor C' , the friction coefficient μ and the direction of the chip flow θ . The grain shape ratio was determined from the kinematic relationship between the grain and the workpiece in the simulation. The material hardness was determined from a Rockwell hardness test and was HRC 61. In most cases the cutting depth was much smaller than the diameter of the grain. Following Shaw's assumption[89], the constraint factor C' was assumed to be 3. The friction coefficient was assumed to be 0.4 for a reasonable value of F_n/F_t . The chip flow direction determined by Shaw's spherical grain model is shown in figure 3.8. Using the diameter and the cutting depth of a grain, the direction of the chip flow θ can be calculated

$$\theta = \arcsin \frac{2b}{d_g} = \arcsin \frac{2\sqrt{t(d_g - t)}}{d_g} \quad (8.42)$$

8.5. Simulation Results and Discussion

Following the simulation procedure, simulated results of dressing and grinding were generated. The effects of dressing conditions on specific grinding force based on the simulation are illustrated in figure 8.20. The effects of dressing depth on grinding

force are found to be stronger than the effects of dressing lead. The effects of dressing conditions on surface roughness are shown in figure 8.21. The surface roughness increases with increase of dressing lead. The dressing depth has a relatively weak influence on surface roughness and the nature of the influence is less clear. The tendency of the simulation results is similar to that of the experimental results as given by equations 6.1 and 6.22.

By changing the diamond active width only, the simulated effects of the diamond active width on grinding force and roughness are as in figures 8.22 and 8.23. The grinding force initially increases with increases of the diamond width and then decreases. The surface roughness decreases with an increase in the diamond width. It is interesting to note that the variation of the simulation results decreases with an increase of diamond width. The dressing overlap coefficient provides the connection between the diamond and the dressing conditions. With the same diamond shape, different dressing conditions give different dressing overlap coefficients. As shown in figure 8.24 and 8.25, the standard deviation of the simulation results decreases with an increase of dressing overlap coefficient. This may attributed to the fact that a small diamond overlap leaves more scope for variations in the diamond trace.

During the spark-out stage of the grinding cycle the grinding depth decreases, so that the grinding power decreases. The rate of decrease of grinding depth during the dwell period depends on the time constant of the grinding system. Decrease of grinding depth is equal to the change in the workpiece radius in one revolution as expressed by equation 7.15. The simulation also shows that grinding power in the dwell period decreases following an exponential decay function as illustrated in figure 8.26. This is in agreement with equation 7.5. Simulation results indicate that surface roughness during dwell improves as illustrated in figure 8.27. However the improvement of surface roughness does not follow an exponential decay as might be expected from the power results. This tendency is in agreement with experimental results which were found in previous work by Rowe[129].

The values of specific grinding power from the simulation and from the experiments illustrated in figure 8.28 show good agreement in the trends observed. Values of surface roughness from simulation and from experiment after a dwell of 5 seconds are illustrated in figure 8.29. The experimental results in most cases fall within the range of values given by the simulation. For those results where the agreement is less satisfactory, the error may possibly be attributed to the assumption of the parabolic diamond shape in the simulation. The real diamond shape is very rough as shown in figure 5.9 and 5.10. As illustrated in figure 8.30, the height of the dressing trace simulated using the parabolic assumption will be different from that of the real diamond dressing trace, when b_d is much different from f_d . If the overlap coefficient U_d is very large, the assumption of a parabola gives a diamond shape which is too smooth. If the overlap coefficient U_d is very small, the assumption of a parabola gives a diamond shape which is too rough.

8.6. Conclusion

The results from the simulation give good agreement for most parameters with experimental results. Although clearly this is not a proof that the underlying assumptions are correct, it is clear evidence that the assumptions are consistent with the facts in so far as the investigation went. This is evidence that a reasonable working model has been obtained for the effects of dressing on the grinding process. It is tentatively concluded that the understanding of causation achieved so far provides a reasonable basis for the formulation of an adaptive dressing strategy.

Chapter 9. Formulation of Strategies for Selecting Dressing Conditions

9.1. Fundamentals of a Sensor Based Dressing Strategy

Previous chapters show that the active width of the dressing tool has a strong effect on grinding behaviour. Models and so-called AI techniques which do not take account of the active width of the dressing tool will not be reliable for selection of dressing conditions for single diamond dressing. The active width of the dressing tool is almost uncontrollable in industry. However it can be assumed that the change in width of the dressing tool occurs progressively. It is therefore proposed that the grinding behaviour over a wheel redressing life cycle can be used as a reference for selection of improved dressing conditions for the next dressing operation. Based on this assumption, it is proposed to develop an adaptive sensor based strategy to select and modify dressing conditions. The formulation of the sensor based dressing strategy is discussed in the following sections.

In order to develop an adaptive strategy for selection of dressing conditions, the ability to monitor the effects of dressing on the grinding process must first be established. It is necessary to decide what grinding output parameters should be selected to monitor the process. This decision relies on whether the parameters employed to monitor the process are sensitive to the dressing operation and capable of reliably predicting grinding performance. The selection of the initial dressing conditions is also important. A good initial dressing condition will make optimisation of the dressing operation more efficient. It is also important to know when the wheel needs to be redressed because wheel life affects productivity. Key issues for the development of a strategy are

- (i) how to recognise what dressing conditions are suitable for the specified grinding

operation;

(ii) how to utilise sensor outputs to improve the dressing operation.

The strategy for the selection of dressing conditions is discussed in three parts,

- (i) selection of the initial dressing conditions,
- (ii) identification of the grinding wheel life cycle,
- (iii) sensor based adaptation of dressing conditions.

9.1.1. Selection of Initial Dressing Conditions

The initial dressing conditions for the first grinding operation are usually selected according to experience. If there is no experience available, a conservative dressing condition will probably be applied to satisfy quality requirements. A large dressing depth produces an open wheel surface leading to a small grinding force. A small dressing lead gives a good surface roughness as shown in equation 2.1. Therefore a combination of large a_d and small f_d may be considered to be a conservative dressing condition in order to achieve efficient grinding and low values of surface roughness. These conditions however remove a large amount of the wheel and require a long dressing time.

With the development of AI technologies it is possible that initial dressing conditions could be selected on a more rational basis. In some cases a database may be used to decide the initial dressing conditions. If the grinding requirement is similar to a case in the database, the dressing conditions in the database can be used as the initial dressing condition. For a new grinding operation, a similar case may not be available from the database. The fuzzy logic method or the neural network method may be helpful to find a closely corresponding condition for the specific grinding requirement. Expert systems might also be useful in selection of the initial dressing conditions. Any of these methods could be integrated into a strategy for the selection

of initial dressing conditions.

9.1.2. When the Wheel Should Be Redressed

Redressing the wheel at the right time is important for the optimisation of the total grinding process. If dressing is applied too late, the material removal rate may be reduced and the grinding quality may be worse than specified. On the other hand if dressing is applied too often, increased wear of the diamond and the increased volume removed from the wheel increases cost. Unnecessary dressing also increases non-productive time which lowers productivity and increases production expense.

The grinding wheel should be redressed when any of the grinding constraints is offended. Typical grinding constraints are as follows:

- (i) machine power capacity or maximum allowable operative power;
- (ii) maximum permissible surface roughness;
- (iii) maximum size error;
- (iv) maximum roundness error;
- (v) onset of workpiece burn;
- (vi) onset of grinding chatter;

Besides direct detection of the violation of grinding constraints, many indirect methods have been proposed to identify the need to redress. Wheel wear glazes the wheel surface, which causes a change in the relationship between the normal grinding force and the tangential grinding force. Based on this, Pacitti and Rubenstein[62, 137] suggested that the wheel life could be determined by plotting a graph of the normal grinding force versus the tangential force, where the grinding force is expressed as

$$F_n = \frac{1}{\mu} F_t + C \quad (9.1)$$

A significant decrease of the friction coefficient μ was found between the second stage and the third stage of the wheel wear process. Therefore a decrease in μ was proposed as an objective measure of redress life. However the decrease in μ was obtained only when the grinding forces in both the second and the tertiary stages were available. If the grinding wheel produces reject parts in the tertiary stage, this method may be considered unsuitable.

Grinding force increases as flats develop on the wheel surface. This is because the flats on the grains increase the friction force in grinding. Based on the relationship between grinding force and total plateau area of the wheel surface, Yoshikawa[124] proposed the plateau area as a measure of wheel life. Yoshikawa suggested the wheel needed to be redressed when the plateau area reaches 8% of the wheel surface. The difficulty of applying this indirect method is that the threshold for the plateau area varies with different grinding conditions, workpiece materials and coolants.

Grinding vibration is normally considered to be an adverse condition in grinding. As the amplitude of vibration increases, surface texture often deteriorates and errors in workpiece form and size increase. The grinding wheel has to be redressed when chatter develops. Based on grinding noise, an experienced operator can recognise whether the wheel is worn or not. Identification of the onset of grinding chatter from machine vibration was used to achieve an objective measure of redress life. This is detailed in chapter 10.

9.1.3. Selection of Monitoring Parameters for Dressing

There are many parameters which can be used to demonstrate the effect of dressing on the grinding process. Possibilities include grinding force, grinding power, grinding temperature, workpiece surface texture and wheel redress life. Parameters which represent the quality of the ground workpiece may also be chosen to evaluate

the grinding operation. Parameters in this category may include size error, surface roughness and roundness. These parameters demonstrate the effects of the dressing conditions directly but only to a limited extent. For example size errors indicate the effect of dressing on wheel wear and normal grinding force but do not give direct information on the effect of dressing on the grinding wheel surface topography.

Grinding force was considered to be the best parameter to comprehensively reflect the grinding behaviour and the effect of the dressing operation. Almost all grinding behaviour can be related explicitly to the grinding force. However, force is a vector parameter which is dependent on the position of the sensor, and the specific grinding operation. Force measurement is therefore inflexible in operation. Furthermore to install a grinding force sensor is expensive and often affects the stiffness of the grinding system, which degrades the machine performance. More importantly manufacturers are reluctant to increase the number of sensors on machines which has implications for reliability. Grinding power is an easily measured parameter which does not affect the grinding system. Grinding power represents the tangential grinding force and relates well with other grinding parameters. For example, the specific energy which may be calculated from grinding power has a logarithmic linear relationship with surface roughness[24]. Accordingly it was decided that grinding power would be investigated as a parameter for monitoring the dressing operation.

The time constant is another parameter which is indicative of differences in the grinding contact condition after dressing. If the grinding wheel cutting surface is unchanged, the interaction between the wheel and the workpiece as characterised by the time constant should be stable. Wheel sharpness will be stable too. The results of the experiments in chapter 5 showed minimal variations of time constant and best grinding results were achieved when the most appropriate dressing conditions were applied.

Both the grinding power and the time constant can be used to interpret the cutting

ability of the grinding wheel. Equations 3.41, 4.3 and 4.7 show that the grinding power is proportional to the tangential grinding force while time constant depends on the normal grinding force. The time constant also depends on the stiffness of the grinding system which is relevant to the contact situation between the wheel and the workpiece. As mentioned in chapter 5, when appropriate dressing conditions are employed, the time constant remains more nearly constant as grinding progresses. The grinding power, however, initially decreases with time and then increases. The difference in behaviour for the two parameters is partly because time constant can indicate the grinding contact situation but power cannot. The other reason is that time constant depends on the normal force and power depends on the tangential grinding force. The variation of the grinding force ratio F_n/F_t in the wheel life cycle was observed by many researchers[57, 62, 138]. Rubenstein[137] gave equation 9.1 for the relationship between F_n and F_t . In equation 9.1, C is a constant under stable conditions. C depends on the geometric characteristics of the wheel surface, the hardness of the workpiece, the strength of the workpiece, the friction coefficient between the grit and/or bond sliding against the workpiece, the grinding contact area and the grinding conditions. According to Rubenstein's equation, if $C \neq 0$, the grinding force ratio changes with the tangential grinding force. The initial stage of grinding is characterised by a high rate of wheel wear. A rapid change in the topography of the wheel surface results in a considerable change in the grinding force ratio, leading to a change in the constant C .

Surface roughness of the workpieces reflects the influence of the dressing and grinding conditions as well as the geometric characteristics of the wheel surface. Too coarse or too fine a dressing operation induces a large change of surface roughness in the initial stage of wheel wear as shown in chapter 5. A small variation of surface roughness in a narrow band can only be realised when suitable dressing conditions are applied. Hence the surface roughness is assumed to be one of the most sensitive parameters for monitoring the dressing operation. Surface roughness values are usually provided by an operator. Therefore it is inconvenient to rely completely on

surface roughness. However, it is reasonable for an operator to indicate when the surface roughness is too rough or too smooth and enter R_a values. It is not usually necessary to make frequent measurements of surface roughness. Occasional measurements are usually sufficient to check the surface roughness quality.

The analysis above shows that grinding power, time constant and surface roughness can be used to demonstrate the effects of dressing on grinding behaviour and these three parameters will therefore be used in the evaluation of dressing strategies.

9.2. Development of Dressing Strategies

Adaptive sensor based learning strategies for selection of dressing conditions should aim to make the grinding process stable and satisfy the quality requirements. The grinding power and surface roughness should not be so high as to degrade grinding quality, nor so small as to lead to a loss of productivity. The parameters most often used to control grinding are those parameters which are most easily adjusted. For plunge grinding, the main control parameter is the infeed rate v_f , because of its strong effect on grinding process. In dressing, the control parameters are the dressing lead f_d and the dressing increment a_d . Other parameters are chosen from experience. For example, the type of wheel is often selected from experience and in many case is rarely changed after the wheel is mounted on the machine. Some input parameters are not subject to control. Parameters in this category include the shape of the diamond dressing tool and the character of the workpiece.

A large dressing lead reduces the dressing time. This implies that the dressing lead should be as large as possible. However if the dressing lead is larger than the average diameter of the grains, some grains on the wheel surface will not be dressed. Therefore the dressing lead must not be larger than the average diameter of grains. A large dressing lead and dressing depth will lead to a large value of surface roughness.

Dressing lead and dressing depth should be selected so that the resulting values of surface roughness lie within the specified range. Consumption of the wheel is due much more to dressing than wheel wear[139]. Therefore the depth of dressing should be as small as possible to reduce the wheel consumption. The constraint on the depth of dressing is that dressing should make the apertures in the wheel surface big enough to contain the grinding chips. It has been argued that if the pores in the wheel surface are not large enough to contain the grinding chips, the grinding power will be very high[140]. Therefore a constraint on minimum dressing depth could relate to a constraint on grinding power. Based on the above discussion, constraints on the dressing operation are illustrated in figure 9.1. The dressing conditions in shadowed area are applicable.

9.2.1. A Strategy Based on Stabilising the Time Constant

As shown in chapter 4, a good dressing operation gives a smaller variation of the time constant in the initial grinding stage. This implies a stable grinding wheel working surface after dressing. The strategy proposed here is to minimise the variation of the time constant during the initial stage of grinding. Variations of time constant in the initial grinding stage are illustrated in figure 9.2. The standard deviation σ_{τ} and the residual deviation σ_{cf} of a straight line fit of the measured values of time constant during the initial stage of wear are defined as

$$\sigma_{\tau} = \sqrt{\frac{1}{n-1} \sum_{i=1}^n (\tau_i - \bar{\tau})^2} \quad (9.2)$$

$$\sigma_{cf} = \sqrt{\frac{1}{n-2} \sum_{i=1}^n (\tau_i - \hat{\tau}_i)^2} \quad (9.3)$$

where n is the number of workpieces ground during the initial stage of wheel wear, i refers to the sequence of workpieces ground, $\bar{\tau}$ is the mean value of time constant in the initial stage of wheel wear, $\hat{\tau}_i$ is the estimated value of time constant from the straight line fit. At the end of the wheel life, the standard deviation of the time

constant σ_τ and the residual deviation σ_{cf} of the time constants during the initial stage of wear were calculated. If $\sigma_\tau \leq \sigma_{cf}$, no trend is apparent in the time constant series. This means the wheel sharpness is stable and the dressing operation is acceptable. If $\sigma_\tau > \sigma_{cf}$, there is a trend in the time constant series, which means the dressing operation could be either too coarse or too fine. If the time constant trend has a negative slope, the dressing is too fine and an increase of dressing lead or dressing increment should be applied. If the time constant trend has a positive slope, the dressing is too coarse and a decrease of dressing lead or dressing increment should be applied.

The strategy for selecting optimal dressing conditions to minimise the variation of the time constant is shown in the figure 9.3. The initial dressing conditions may be determined from experience or by one of the methods discussed previously. The strategy for selection of dressing conditions should not only make the time constant trend level, but should also minimise the variation of the time constant. It is reasonable to assume that a larger value of σ_{cf} means more bond fractures in dressing, because the variation of time constant arises from the variation in the density and shape of the cutting edges on the wheel surface. A good dressing operation should minimise the bond fractures in the dressing operation and make the time constant steady. Pande[46] found that the proportion of bond fractures during dressing was increased with an increase of dressing depth or a decrease of dressing lead. Based on Pande's observation, a small dressing depth or a large dressing lead might be expected to reduce the variation of time constant, because these conditions introduced less fractures on the wheel surface. It was found in figure 5.23 that the effect of dressing depth on the time constant is stronger than that of dressing lead. Therefore it was proposed that the time constant trend was to be adjusted by varying dressing depth. Larger dressing depth gives a more open wheel surface and decreases the initial time constant. Decreasing the dressing depth increases the time constant and reduces the wheel consumption. On the other hand the surface roughness is to be

adjusted by varying dressing lead. A smaller dressing lead gives a better surface roughness. If the values of surface roughness are far smaller than its upper limit, the dressing lead should be increased to reduce the dressing time and to reduce the number of bond fractures.

The strategy of minimising the variations of the time constant is suitable where the grinding conditions remain the same and the grinding power level is not crucial. The efficiency of the strategy is dependent on how accurately the time constant can be measured. Normally when the initial wear stage of the wheel finishes is determined by experience. This is a disadvantage of the strategy of minimising the variations of the time constant.

9.2.2. Strategy of Stabilising the Grinding Power

As discussed previously the error of the estimation of the time constant limits the ability to demonstrate the effects of the dressing operation. The changes in grinding power were found to be much larger than the changes in time constant as shown in chapter 5. The grinding power can therefore be concluded to be more sensitive to the dressing operation than the time constant. The strategy of stabilising grinding power is to minimise the changes of grinding power in the grinding wheel cycle, so that the grinding behaviour will be stable.

It was observed that the grinding power initially decreased then gradually increased until the end of the wheel life cycle as shown in figure 9.4. Changes of grinding power depend on the dressing operation. If the initial grinding power is equal to the grinding power at the end of the wheel life cycle, the change of grinding power is approximately at a minimum, and the grinding performance can be considered to be approximately constant. Similarly the initial surface roughness should be controlled so as to be at the same level at the beginning and the end of the wheel life. If

empirical models of surface roughness and grinding power, such as equations 6.1 and 6.2, are available, the dressing conditions may be directly determined.

When the surface roughness is not critically important, good dressing conditions may be defined by the conditions which achieve steady grinding power and stable grinding behaviour. For a specific power level, combinations of a_d and f_d to be used follow the loci shown in figure 9.5. Combinations of dressing parameters follow a different locus if the specified grinding power level is changed. For low wheel consumption and short dressing time, dressing with small a_d and large f_d should be employed. Furthermore, as mentioned previously, the combination of small a_d and large f_d creates less fractures on the wheel surface, which may make grinding behaviour more stable. If a maximum surface roughness constraint is involved, the dressing conditions should be selected within the boundary for surface roughness. The best dressing conditions correspond to the point B in figure 9.1.

Because of the wear of the dressing tool, the boundaries of dressing conditions for maximum surface roughness and power control locus may shift. This makes it difficult to use the models to determine the dressing conditions. However based on the assumption that the change of the width of the dressing tool occurs progressively, the outputs of the grinding behaviour in a wheel redress life cycle can be used as a reference for selection of the next values of dressing conditions. Therefore the effects of a change in dressing conditions can be gained from equations 6.1 and 6.2 obtained from real grinding data. Based on the empirical grinding power model, equation 6.22, the effects of the dressing depth a_d is stronger than the effects of the dressing lead f_d . The dressing depth is therefore selected as the main parameter for controlling grinding power. Because the dressing lead f_d has a stronger influence on surface roughness than dressing depth a_d according to equation 6.1, the dressing lead is selected as the main parameter to control the surface roughness. Therefore the grinding power and surface roughness may be controlled separately.

A gradual approach to selection of dressing conditions is proposed as shown in figure 9.6. Because the objective of selection of the dressing conditions is to obtain the required quality with a stable grinding process, selection of dressing lead takes priority over selection of dressing depth to ensure the surface roughness falls just below the limit. The first layer controls the dressing feed rate to achieve the required surface roughness. The second layer controls dressing depth to minimise the variations of grinding power.

The procedure for achievement of the strategy is as follows. The first step is the selection of the initial values of dressing parameters. This relies on experience or on a method discussed in section 9.1.1. After dressing and grinding with the initial dressing conditions, the surface roughness is examined and the grinding power is recorded. The dressing lead is adjusted until the surface roughness is acceptable, which means the surface roughness should be just below its tolerance limit. If the surface roughness is too coarse, the dressing lead should be decreased. If the surface roughness is too fine, the dressing lead should be increased.

By reference to the optimal grinding power change locus, it is possible to decide whether the dressing operation is too fine or too coarse. If the initial grinding power is much higher than the final grinding power in the wheel life cycle, the dressing operation is too fine, and the dressing depth needs to be increased. Conversely, if the initial grinding power is much lower than the final grinding power in the wheel life cycle, the dressing operation is too coarse, and the dressing depth needs to be decreased. When the initial grinding power level is similar to the final grinding power level in the wheel life cycle, and the surface roughness is acceptable, the dressing conditions employed are acceptable.

Consideration should be given to the maximum power threshold for the onset of grinding burn. The dressing depth and dressing lead may have to be adjusted when the grinding power and surface roughness are larger than their constraints. In this

situation, dressing depth has to be increased to reduce grinding power and the dressing lead has to be decreased to improve surface roughness. The changes of the dressing conditions should be small enough to ensure the grinding behaviour changes progressively and grinding qualities are acceptable.

By using the strategy shown in figure 9.6, dressing conditions were adjusted step by step to achieve optimal conditions. In order to determine the optimum dressing conditions more effectively, empirical equations for grinding power and surface roughness can be used. If the shape of the dressing tool does not change severely, equations 6.1 and 6.2 will be sufficiently accurate to assist in the selection of the dressing conditions. The constants in the empirical equations are updated with the data extracted from the most recent grinding results. By consulting the empirical equations, the dressing lead and dressing depth can be adjusted more rationally.

The adjustments of dressing depth and dressing lead in the strategy can, in most cases, be made either for the same wheel life cycle, or for separate wheel life cycles. However if the initial values of surface roughness and grinding power are both larger than their values at the end of the wheel life cycle, the increase of a_d and the decrease of f_d will need to be applied at the same time to prevent the violation of grinding constraints. By applying the strategy, dressing conditions are shifted according to the grinding behaviour. When the recommended dressing lead is smaller than the machine capability or the recommended dressing depth is too large leading to excessive wheel consumption, the diamond has to be relocated.

Compared with the strategy of minimising the time constant, the strategy of stabilising the grinding power is more sensitive, though the wheel life has to be detected because the grinding power at the end of the wheel life cycle is involved in the strategy. The wheel life cycle time can be determined either by experience or by the techniques mentioned in section 9.1.2 and will be further discussed.

9.3. Combination of the Dressing Strategy with Grinding Strategy

The dressing strategies developed in the previous section are based on the situation where the grinding conditions do not change. If the grinding conditions change according to the adaptive optimisation of the grinding operation, the dressing conditions may also need to be changed. For example in order to maximise the grinding productivity, the grinding process should be carried out with the maximum power available, providing chatter or thermal damage do not occur. Therefore an adaptive dressing strategy of maximising stable grinding power is needed to achieve an optimal grinding process within the maximum grinding power constraint.

Dressing mainly affects grinding in the initial stage of the wheel life. No matter what dressing conditions are employed, the grinding power at the end of the wheel redress life cycle is not of much difference if the grinding conditions remain the same. When the grinding power level at the end of the wheel redress life cycle is much lower than the machine power capacity or the grinding power constraint of grinding burn, the grinding conditions might need to be changed to improve the grinding productivity.

Figure 5.32 shows that the grinding power level at the end of the wheel redress life cycle changes with the grinding conditions. When the grinding conditions change, the dressing conditions should also be changed to make the initial grinding behaviour the same as the final grinding behaviour of the grinding wheel life cycle in order to achieve the most stable grinding behaviour between two dressing operations. According to equation 6.22, the grinding power level at the end of the wheel life cycle can be adjusted to its constraint by changing undeformed chip thickness h_{eq} . For plunge grinding, the infeed rate v_f is usually used as the control parameter to adjust the undeformed chip thickness. Dressing conditions can be selected in the same way as described in section 9.2.2.

The strategy of maximising stable grinding power is achieved by combining the grinding condition adjustment into the power stabilising strategy as shown in figure 9.7. The first wheel redress life cycle is run conservatively with parameters recommended by experience or from a data base. These parameters ensure the grinding operation is within the constraints of the grinding power and the grinding quality. After grinding to the end of the wheel life cycle, the power stabilising strategy shown in figure 9.6 is applied to achieve the stable grinding performance within the grinding constraints. Then the grinding conditions are adjusted to make the grinding power at the end of the wheel life cycle just below the maximum power allowable. Thereafter, the power stabilising strategy is used to make initial grinding power equal to final grinding power and the surface roughness remain constant. The optimal dressing and grinding conditions are obtained when the grinding operation produces a maximal metal removal rate and a constant acceptable surface roughness at the maximum power allowable.

The dressing and grinding conditions may more efficiently be selected according to equation 6.1 and 6.22. If the constants in the empirical equations are not available for a new set of grinding conditions, the changes of dressing and grinding conditions can only be taken in small steps, so that the constraints of the grinding process will not be violated. After several adjustments of dressing and grinding conditions, the constants of the empirical equations may be obtained by curve fitting from the grinding results.

The grinding power constraint may be dominated by the maximum power available from the machine. It is known that the specific grinding energy is more relevant than power in prevention of grinding burn. By using the constraint of the specific grinding energy to substitute for the grinding power constraint, the strategy might be linked with the CNC adaptive control strategy for grinding. The key issue might then be how to monitor the effects of dressing and grinding separately.

Chapter 10 Evaluation of the Dressing Strategy

It is proposed that the strategy of stabilising grinding power is the most efficient strategy for stabilising grinding performance. An essential part of the strategy is how to determine the wheel redress life. In this chapter, the determination of the wheel redress life is discussed and the strategy of stabilising grinding power is evaluated.

10.1. Determination of the Redress Life of the Grinding Wheel

The grinding wheel should be redressed when grinding behaviour becomes poor due to wheel wear. The wheel redress life needs to be determined for the dressing strategy. During the course of the investigation, it was found that grinding chatter was the main determinant of the need for wheel dressing. Therefore the wheel redress life was determined by monitoring the onset of grinding chatter.

The workpiece and the grinding wheel tend to wear in the form of a polygon[117]. Wheel regenerated grinding chatter is related to the development of a polygonal shape on the wheel. The predominant vibration frequency of the grinding chatter depends on a characteristic frequency of the grinding system. Because a non-linear relationship exists between the deflection of the wheel and the grinding force, the contact stiffness of the grinding wheel could not be a constant. It was found that the chatter frequency of the grinding system increases with radial force between the wheel and workpiece[141]. Therefore when the grinding force increases due to wheel wear, the chatter frequency increases too. A decrease of the grinding force is often found when chatter occurs[61, 103, 139, 142]. It was found that as grinding chatter develops, the predominant vibration frequency shifts from a low value to a high value and then from high to low[61, 141-143]. It can be assumed that when the amplitude

of vibration at the characteristic frequency begins to increase, grinding chatter has begun. When the amplitude of the vibration at the characteristic frequency increases to an unacceptable level, the wheel has to be redressed. Szekeres[141] proposed that the vibration amplitude-time function could be used to measure the wheel life. The second inflection point of the amplitude-time function was assumed to mark the end of the wheel life.

Grinding chatter due to wheel wear is a gradually developing vibration process. Figure 10.1 shows the difference of acceleration signals between the chatter and non-chatter conditions, where a is the acceleration signal and the sampling rate is 10 kHz. By means of FFT data processing, the distribution of the acceleration density is obtained as illustrated in figure 10.2. In figure 10.2 the distribution of the acceleration density is varying with the time. The average acceleration density distribution is illustrated in figure 10.3. It can be seen that the characteristic frequency of grinding chatter in the experimental system is around 3100 Hz. When the grinding chatter developed, the acceleration density at the characteristic frequency increased. When this acceleration density increased to a certain level, the wheel had to be dressed. By monitoring the grinding vibration in the characteristic frequency zone, the need to redress the wheel can be determined. Figure 10.4 shows a typical pattern of development of grinding chatter, where a' is the acceleration density at the characteristic frequency of the chatter. By setting an acceptable acceleration density level at the characteristic frequency, the wheel redress life could be determined. However it is difficult to decide on an objective basis for the vibration level at which the wheel should be dressed.

A neural network is a powerful tool for process identification[144]. It was therefore proposed that grinding chatter might be identified objectively by using a neural network technique. The distribution of acceleration density in the frequency domain provides useful information concerning grinding chatter and was used to derive inputs to the neural network. Combining FFT analysis and neural network techniques, Mori,

Kasashima and Yamane[145] established a system to identify the type of grinding vibration. In their system, 106 selected values from the FFT spectrum were used as inputs to the neural network.

The number of inputs to the neural network affects the speed of the network in operation. Though more inputs may give more information about the chatter process, the speed of the neural network will reduce. For real-time monitoring of a vibration situation, a huge number of calculations are often undesirable. The problem here is only to identify when grinding chatter begins and therefore the number of inputs to the neural network may be reduced. In order to reduce the number of inputs without losing the ability to identify chatter, the acceleration signal was taken through a small number of band pass filters covering the frequency range of interest. For a set of 16 samples, a FFT process can act as eight band pass filters of equal band width. For the sampling rate of 10 kHz, the filter covers the frequency range between 0 - 5000 Hz. Using the filter, the acceleration signals are distributed into eight bands. With the same signals in figure 10.3, the distributions of acceleration density in eight band filter are changed as shown in figure 10.5. The difference between chatter and non-chatter is manifest. In figure 10.5, the acceleration density in the lowest band included DC signal. The distribution of acceleration density at each band provides important information for determining the wheel redress life. Though the 8 band pass filter was realised by FFT processing in experiment, the physical hardware approach is easier and cheaper.

The software package 'NeuralDesk'[146] was used to establish a neural network to determine the wheel redress life. The recommended structure using NeuralDesk is shown in figure 10.6. The network is of the feedforward type with a back-propagation learning structure. The acceleration densities from the eight band pass filter are used as inputs to the network. There is only one output from the network, which displays whether grinding chatter has begun or not. There is one hidden layer of four artificial neurons in the neural network.

Judgement of the existence of grinding chatter was initially identified based on experience. Seventy five cases of vibration were used to train the neural network. Where grinding chatter was identified, the output of the neural network was set to one, otherwise the output was set to zero. After training, the filtered grinding vibration signals are fed into the network. If the value of the network output is larger than 0.5, grinding chatter is assumed to have commenced. Analysing the example for the case shown in figure 10.4, the output of the neural network is illustrated in figure 10.7. According to the output value from the neural network, the acceleration density threshold for objective identification of chatter is about $8 \text{ m}/(\text{s}^2\text{Hz})$. After the acceleration density at the characteristic frequency reaches this level, the vibration begins to increase significantly and erratically.

Development of grinding chatter due to wheel wear can be expressed as the increase of the vibration amplitude in the characteristic frequency zone. By measuring the increase of the acceleration in a narrow band of characteristic frequency, the development of chatter can be monitored. However the monitoring frequency zone has to shift due to the characteristic frequency differences with different grinding systems. Although the FFT data process can give the spectrum of the vibration, it requires a huge amount of calculation. By distributing the vibration signals into an eight band pass filter which covers the whole frequency range of the vibration, a neural network can easily recognise when chatter begins. Because the neural network works as a black box, which can be trained for each particular situation, it can adjust itself when the characteristic frequency changes. The other advance of the neural network technique is that neural networks can more clearly recognise when chatter begins.

10.2. Evaluation of the Strategy of Stabilising Grinding Power

A series of experiments was carried out to evaluate the strategy of stabilising grinding

power. The trials were undertaken on a Jones & Shipman Series 10 cylindrical grinding machine. The grinding wheel, workpieces and coolant used in the trials were as described in chapter 5. The grinding conditions were fixed: $v_s = 33$ m/s, $v_w = 250$ mm/s and $v_f = 10$ μ m/s. At the beginning of chatter under these grinding conditions the specific grinding power was about 32.6 W/mm and surface roughness was about 0.316 μ m based on the observation in chapter 5. Therefore the target of the dressing strategy was to make grinding performance stable, which means that the initial specific grinding power should be approximately 33W/mm and the initial surface roughness R_a approximately 0.31 μ m.

The dressing conditions in the trials were determined by the strategy shown in figure 9.6. Initial dressing conditions were selected according to the experience from the trials described in figures 5.15 and 5.17. The initial dressing depth was 15 μ m. The initial dressing lead was 0.15 mm/rev. The average grain diameter of the wheel type A465-K5-V30W was 0.293 mm, so the maximum dressing lead was 0.29 mm to avoid non-dressing of some grains. To avoid excessive change of grinding behaviour in the evaluation trials, the change in dressing depth was limited to 0.005 mm and the change in dressing lead was limited to 0.05 mm/rev.

To make the strategy more efficient, equations 6.1 and 6.2 were used to assist selection of dressing conditions. Therefore the constants in equations 6.1 and 6.2 were required to be determined. Since the grinding conditions remained constant in the trials, equations 6.1 and 6.2 were simplified as

$$R_a = R_0 a_d^{r_1} f_d^{r_2} \quad (10.1)$$

$$P' = P_0 a_d^{p_1} f_d^{p_2} \quad (10.2)$$

The exponents of dressing depth and dressing lead in the equations were determined by curve fitting the data from the experiments shown in figures 5.15 and 5.17. Therefore

$$R_a = 0.797 a_d^{0.113} f_d^{0.290} \quad (10.3)$$

$$P' = 7.34 a_d^{0.358} f_d^{-0.068} \quad (10.4)$$

Employing the initial dressing conditions to dress the wheel, the grinding behaviour was as illustrated in figure 10.8. To match the grinding performance the constants in equations 6.1 and 6.2 were determined by using the constants obtained from curve fitting the grinding performance in the last wheel redress life cycle. To match the grinding performance in figure 10.8, it was found that $R_0 = 0.724$ and $P_0 = 7.38$, so that

$$R_a = 0.724 a_d^{0.113} f_d^{0.290} \quad (10.5)$$

$$P' = 7.38 a_d^{0.358} f_d^{-0.068} \quad (10.6)$$

New dressing conditions were recommended by equations 10.5 and 10.6. Because the surface roughness after dressing in figure 10.8 was far smaller than $0.31 \mu\text{m}$ and had a trend to increase, the dressing lead was required to be increased. To achieve initial surface roughness values similar to those at the end of the wheel redress life, the recommended dressing conditions were $a_d = 0.015 \text{ mm}$ and $f_d = 0.20 \text{ mm/r}$. Following this procedure, a series of dressing conditions were determined according to grinding behaviour. The selected dressing conditions are illustrated in figure 10.9. The specific grinding power and surface roughness were measured during these trials. Diamond shape was measured between the tests. The constant P_0 and R_0 were calculated. The results are shown in the table 10.1. The estimated specific grinding power \hat{P}' and the estimated surface roughness \hat{R}_a are also expressed in table 10.1.

Table 10.1 grinding results and constant for equations

No	a_d (mm)	f_d (mm/rev)	\hat{P}' (W/mm)	\hat{R}_a (μm)	P' (W/mm)	R_a (μm)	P_0	R_0
1	0.015	0.15	37.56	0.274	37.76	0.260	7.38	0.724
2	0.015	0.20	37.03	0.282	28.76	0.312	5.73	0.800
3	0.013	0.20	30.26	0.307	33.50	0.267	6.35	0.696
4	0.013	0.24	33.12	0.282	34.47	0.307	6.61	0.759
5	0.014	0.23	33.67	0.306	23.74	0.427	4.66	1.059
6	0.014	0.18	24.14	0.398	27.18	0.302	5.25	0.804
7	0.009	0.18	31.86	0.287	34.63	0.322	5.71	0.902

Errors in estimating the grinding power and surface roughness can be observed in table 10.1. The errors may be due to the random nature of the grinding process and may also be attributed to the fact that the empirical equations are only valid over a limit range of experimental conditions. Table 10.1 also shows that constants P_0 and R_0 have considerable variations in the trials. These variations are the reflection of the effects of the diamond wear and introduce a considerable error in the estimation of the grinding behaviour. Because of this uncertainty of the grinding behaviour, the empirical equations can only be used as a guide. Therefore the extent of change of dressing parameters has to be limited within a certain range to avoid excessive change of grinding performance from one batch to the next. The optimal dressing conditions can only be achieved progressively. For a more efficient selection of dressing conditions, the exponents of the empirical equations need to be updated according to the grinding performance.

Trials 1 to 4 show how the procedure led to recommendations for better dressing conditions without degrading grinding performance. The grinding performance under the dressing conditions No. 2 to No. 4 is illustrated in figure 10.10. It can be seen that the variations of grinding performance are similar, since the effect of the change of diamond shape was compensated by adjustments of dressing conditions. In figure 10.10, the values of the specific power after dressing were found to be approximately equal to those at the end of the wheel redress cycle. The surface roughness R_a stabilised at approximately $0.3 \mu\text{m}$. The new dressing conditions result in shorter dressing time and less wheel consumption.

When the grinding behaviour deteriorates due to diamond wear, the strategy can also recommend new dressing conditions to bring the grinding performance back to normal. Figure 10.11 shows the surface roughness in trial 5 was too high with $a_d = 0.014 \text{ mm}$ and $f_d = 0.23$. The surface roughness decreased during the wheel redress cycle and the specific power after dressing was much lower than at the end of the

wheel life. Based on the procedure mentioned previously, the dressing conditions were suggested as shown for trial 6 and then trial 7. As shown in figure 10.12, the surface roughness and grinding power were brought back to stable conditions.

Experimental results discussed in this chapter demonstrated that the grinding power stabilising strategy can compensate for the effects of the variation of diamond shape and make grinding behaviour stable. In the maximum power stabilising strategy shown in figure 9.7, the key element is the power stabilising strategy. Therefore there should be little problem to execute the maximum power stabilising strategy.

Chapter 11. Conclusions

Grinding behaviour with single point diamond dressing is not fully controllable without consideration of the dressing operation. The dressing diamond shape was found to have a strong influence on both dressing and grinding. The variation of the dressing diamond shape is uncontrollable in practice, hence the grinding behaviour can be very different even when the same kinematic dressing and grinding conditions are applied.

The dressing conditions have an important influence on the grinding wheel performance. Empirical models were established to assist in the selection of dressing conditions.

A strategy for selecting dressing conditions to compensate for variation of diamond width was developed. The strategy selected the dressing conditions according to the grinding wheel performance in the previous wheel redress life cycle to stabilise grinding performance. The aim of the strategies developed was the efficient selection of dressing conditions to achieve an optimal stable grinding behaviour within the grinding constraints. With given grinding conditions, the recommended dressing operation will give a stable grinding behaviour without losing grinding productivity.

Simulation of grinding cycles shows that the time constant of the grinding system is important for controlling grinding performance. A stable time constant makes grinding performance more predictable. The simulation technique is also useful in determination of an adaptive control strategy. With the help of the simulation, an adaptive power control strategy achieved the maximal removal rate in grinding at the maximal power threshold.

In order to understand the dressing and grinding process, a methodology was developed to simulate the dressing and grinding process. The simulation was based on the behaviour of each grain on the wheel surface in the dressing and grinding operations. The simulated results were found to be similar to the experimental results in most cases.

A neural network method was developed to identify grinding chatter and hence wheel redress life objectively.

Chapter 12. Recommendations for Further Work

The following areas need further investigation:

All the dressing strategies developed in this research are concerned with situations where the grinding conditions remain the same between two dressing operations. If changes of the grinding conditions are required within a wheel redress life cycle, a new method is required to identify the effects of dressing and grinding conditions on grinding behaviour separately, so that the recommended dressing operation can match the wheel self-sharpening action and maintain the grinding wheel behaviour stable.

The methodology for simulating the dressing and grinding process needs to be further modified. The grains of the wheel in the simulation were assumed to be a constant diameter. For further research the diameters of the grains should conform to the real distribution of the diameters of the grains. As mentioned previously, the parabola assumption may introduce large errors in the simulation. Therefore the measurement of the diamond shape and simulation with the real diamond shape should improve the results. For simulation of the grinding process, the wear process of the grains needs to be further studied. The model for the effect of grinding conditions on the grinding force of a single grain needs to be investigated further.

Appendices

A.1. References

- [1] Woodbury, Robert S., History of the Grinding Machine, The Technology Press, Massachusetts Institute of Technology, 1959.
- [2] Norton, C. H., Emery Wheel 'Dresser' and Grinding Wheel 'truing', American Machinist, 1905, 2, 142-143.
- [3] Rowe, W. B., Chen, X., Morgan, M. N., The Identification of Dressing Strategies for Optimal Grinding Wheel Performance, Proceedings of the 30th Int. MATADOR conference, 1993, 195-202.
- [4] Kegg, R. L., Industrial Problems in Grinding, Annals of the CIRP, 1983, v. 32, 2, 559-561.
- [5] Loladze, T.N., Bokuchava, G.V., Tribological Aspects of the Grinding Process, ASME, PED, 1985, v. 16, 401-407.
- [6] Chen, X., Allanson, D., Thomas, A., Moruzzi, J. L., Rowe, W. B., Simulation of Feed Cycles for Grinding Between Centres, Int. J. Mach. Tools Manufact., 1994, v. 34, 5, 603-616.
- [7] King, R. I., Hahn, R. S., Handbook of Modern Grinding Technology, Chapman and Hall, 1986.
- [8] The Grinding Data Book, Universal Grinding Wheel Company Limited, 1992.
- [9] Malkin, S., Grinding Technology — Theory and Applications of Machining with Abrasives, Ellis Horwood Limited, 1989.
- [10] Pahlitzsch, G., Appun, J., B., Effect of Truing Conditions on Circular Grinding, Industrial Diamond Review, 1954, v. 14, 185-189, 212-217.
- [11] Vickerstaff, T. J., Diamond Dressing — Its Effect on Work Surface Roughness, Industrial Diamond Review, July, 1970, v. 30, 260-267.

- [12] Lindsay, R. P., Dressing and Its Effect on Grinding Performance, Am. Soc. Tool Manuf. Eng., Technical Paper, MR 69 - 568, 1969.
- [13] Hahn, R. S., Lindsay, R., The Influence of Process Variables on Material Removal, Surface Integrity, Surface Finish and Vibration in Grinding, Proceedings of 10th Int. MTDR Conference, The Macmillan Press, 1969, 95-117.
- [14] Bhateja, C. P., Chisholm, A. W. J., Pattinson, E. J., The Influence of Grinding Wheel Wear and Dressing on the Quality of Ground Surfaces, Proceedings of the International Grinding Conference, 1972, 685-707.
- [15] Malkin S., Cook, N. H., The wear of grinding wheels, Part 2 — Fracture Wear, Journal of Engineering for Industry, Trans. ASME, 1971., v. 93, 1129-1133.
- [16] Bhateja, C. P., On the Mechanism of the Diamond Dressing of Grinding Wheels, Proceedings of the International Conference on Production Engineering, 1974, 733-739.
- [17] Tsuwa, H., Yasui, H., Micro-Structure of Dressed Abrasive Cutting Edges, Proceedings of the International Grinding Conference, Pittsburgh, Pennsylvania, 1972, 142-160.
- [18] Vickerstaff, T. J., The Influence of Wheel Dressing on the Surface Generated in the Grinding Process, Int. J. Mach. Tool Des. Res., 1976, v. 16, 145-152.
- [19] Koziarski, A., Golabczak, A., The Assessment of the Grinding Wheel Cutting Surface Condition After Dressing with the Single Point Diamond Dresser, Int. J. Mach. Tool Des. Res., 1985, 25, 4, 313-325.
- [20] Fletcher, N. P., Maden, H., The Influence of Diamond Geometry on the Stability of the Grinding Wheel Dressing Process, Proceedings of 19th Int. MTDR Conference, 1979, 607-614.
- [21] Pattinson, E. J., Lyon, J., The Collection of Data for the Assessment of a Grinding Wheel Dressing Treatment, Proceedings of 15th Int. MTDR Conference, The Macmillan Press, 1975, 317-323.
- [22] Matsui, S., Tamaki, J., Effect of Dresser Type on the Surface Topography of

- Grinding Wheel, Bull. Japan Soc. of Precision Engineering., 1986, v. 20, 2, 135-137.
- [23] Tkhasapsoev, Kh. G., Khapachev, B. S.,...Diamond Wear in Dressing Abrasive Wheel, Soviet Journal of Superhard Materials,1987, v. 9, 2, 38-44.
- [24] Malkin, S., Murray, T., Comparison of Single Point and Rotary Dressing of Grinding Wheels, Proceedings Fifth North American Metalworking Research Conference, 1977, 278-283.
- [25] Verkerk, J., Final report concerning CIRP Cooperative work on the characterization of grinding wheel topography, Annals of the CIRP, 1977, v. 26, 2, 385-395.
- [26] Huang, Y.Y., Wu, S. M., Grinding Surface Characterization by CEST, Int. J. Mach. Tool Des. Res., 1986, v. 26, 4, 431-444.
- [27] Yoshida, T., Nagasaka, K, Kita, Y., Hashimoto, F., Identification of a Grinding Wheel Wear Equation of the Abrasive Cut-off by the Modified GMDH, Int. J. Mach. Tool Des. Res., 1986, v. 26, 3, 283-292.
- [28] Matsui, S., Study on Measurement of Grinding Wheel Surface Topography — Razor Blade Method, Technology Reports, Tohoko Univ., 1987, v. 52, 1, 1-14.
- [29] Matsui, S., Tamaki, J., Studies on Measurement of Wheel Surface Topography (5th Report) — Termal-couple Method, J. Japan Soc. Prec. Engg., 1987, v. 53, 2, 301-307(in Japanese).
- [30] Matsui, S., Tamaki, J., Studies on Measurement of Wheel Surface Topography (3th Report) — Razor Blade Method, J. Japan Soc. Prec. Engg., 1983, v. 49, 12, 1652-1657(in Japanese).
- [31] Matsui, S., Tamaki, J., Study on Measuring Method of Wheel surface Topography — Stylus Method, Technology Report, Tohoku Univ., 1984, v. 49, 2, 129-145.
- [32] Tsuwa, H., An Investigation of Grinding Wheel Cutting Edges, Trans of the ASME, Journal of Engineering for Industry, 1964, v. 86, 371-382.
- [33] Stout, K. J., Sullivan, P. J., The Analysis of the Three Dimensional

- Topography of the Grinding Process, *The Annals of the CIRP*, 1989, v. 38, 1, 545-548.
- [34] Matsui, S., Tamaki, J., Measurement of Grinding Wheel Surface Topography Using Three-dimensional Stylus Instrument, *J. Japan Soc. Prec. Eng. Seimitsu Kogaku Kai Shi*, 1988, v. 54, 5, 871-876(in Japanese).
- [35] Stralkowski, C. M., Wu, S. M., DeVor, R. E., Characterization of Grinding Wheel Profiles by Autoregressive-Moving Average Models, *Int. J. Mach. Tool Des. Res.*, 1969, v. 9, 145-163.
- [36] Baul, R. M., Shilton, R., Mechanics of Metal Grinding with Particular Reference to Monte Carlo Simulation, *Proceedings of the 8th International MTDR Conference*, Pergamon Press, 1967, 2, 923-946.
- [37] Baul, R. M., Graham, D., Scott, W., Characterization of the working surface of abrasive wheels, *Tribology*, 1972, 8, 169-176.
- [38] Verkerk, J., Pekelharing, A. J., The Influence of the Dressing Operation on Productivity in Precision Grinding, *Annals of the CIRP*, 1979, v. 28, 2, 487-495.
- [39] Pandit, S. M., Suratkar, P. T., Wu, S. M., Mathematical Model of a Ground Surface Profile with the Grinding Process as a Feedback System, *Wear*, v. 39, 2, 205-217.
- [40] Sathiamoorthy, P., Radhakrishnan, V., Rehman, J. F., A Stochastic Analysis of Grinding Wheel and Workpiece Surfaces, *Wear*, v. 54, 2, 303-313.
- [41] Bhateja, C. P., Chisholm, A. W. J., Pattinson, E. J., A Computer-Aided Study of the Texture of the Working Surfaces of Grinding Wheels, *Proceedings of the 12th Int. MTDR Conference*, The Macmillan Press, 1971, 535-541.
- [42] Malkin, S., Anderson, R. B., Active Grains and Dressing Particles in Grinding, *Proceedings of the International Grinding Conference*, Pittsburgh, Pennsylvania, 1972, 161-181.
- [43] Brecker, J. N., The Fracture Strength of Abrasive Grains, *Trans. of the ASME, J. of Eng. for Ind.*, 1974, 11, 1253-1257.
- [44] Goepfert, G. J., Williams, J. L., The Wear of Abrasives in Grinding, *ASME*

Paper 58-A-157, 1-5.

- [45] Pattinson, E. J., Chisholm, A. W. J., The Effect of Dressing Techniques on Grinding Wheel Wear, Proc. Int. Conf. on Manufacturing Technology, A. S. T. M. E., Univ. of Michigan, 1967, 601-616.
- [46] Pande, S. J., Lal, G. K., Effect of dressing on grinding wheel performance, Int. Jnl MTDR, 1979, v. 19, 171-179.
- [47] Bhateja, C. P., Chisholm, A. W. J., Pattinson, E. J., The Influence of Grinding Wheel Wear and Dressing on the Quality of Ground Surfaces, Proceedings of the International Grinding Conference, 1972, 685-707.
- [48] Yoshikawa, H., Peklenik, J., Three Dimensional Simulation Techniques of the Grinding Process — II. Effect of grinding Conditions and Wear on the Statistical Distribution of Geometrical Chip Parameters, Annals of the CIRP, 1970, Vol. XVIII, 361-365.
- [49] Makino, H., Suto, T., Fukushima, E., An Experimental Investigation of Grinding Process, Journal of Mechanical Laboratory of Japan, 1966, v.12, 1, 17-25.
- [50] McAdams, H. T., The Role of Topography in the Cutting Performance of Abrasive Tools, Trans. of the ASME, Journal of Engineering for Industry, 1964, v. 86, 75-81,
- [51] Hasegawa, M., Statistical Analysis for the Generating Mechanism of Ground Surface Roughness, wear, 1974, 29, 1, 31-39.
- [52] Makino, H., Roughness of Finished Surface in Grinding Operation of Hardened Steel, Bull. the Japan Soc. of Prec. Engg., 1965, v. 1, 4, 281-286.
- [53] Chalkley, J. R., Jennings, C. P., Some Observations on the Working Surfaces of Grinding Wheels, Proceedings of 18th Int. MTDR Conference, The Macmillan Press, 1978, v. 18, 431-438.
- [54] Dhawan, U. P., Sachdev, A. S., Rao, U. R. K., Power Measurement as a Criterion for Appropriate Selection of Grinding Conditions, 12th AIMTDR Conference, IIT Delhi, Tata McGraw-Hill Pub. Co. Ltd., New Delhi, 1986, 343-346.

- [55] Hahn, R. S., The Effect of Wheel — Work Conformity in Precision Grinding, *Trans. ASME*, 1955, v. 77, 1325-1329
- [56] Fielding, E. R., Vickertaff, T. J., The prediction of grinding forces in cylindrical plunge grinding, *Int. J. Prod. Res.*, 1986, v. 24, 1, 167-186.
- [57] Fletcher, N. P., Single Point Diamond Dressing of Aluminium Oxide Grinding Wheels and Its Influence in Cylindrical Traverse Grinding, *Int. J. Mach. Tool Des. Res.*, 1980, v.20, 55-65.
- [58] Furuichi, R., Nakayama, M., Doi, T., Influence of Dressing Conditions of Grinding Wheel on Grinding Fluid Performance in Free Infeed Plunge Grinding, *Bulletin of JSME*, 1967, v. 10, 38, 411-417.
- [59] Foellinger, H., Optimum Parameters for Dressing Process of Conventional Grinding, *Superabrasives 85 Proceedings*, 8, 22-37.
- [60] Oliveira, J. F. G. De., Purquerio, B. De. M., Coelho, R. T., Bianchi, E. C., Grinding Process Dominance by Means of the Dressing Operation, *Proceedings of the 29th Int. MATADOR conference*, 1992, 547-550.
- [61] Umino, K., Shinozaki, N., One Aspect of Variation of Grinding Wheel Surface Based on Grinding Force Analysis — Studies on Wear and Redress Life of Grinding Wheel (1st report), *Semishu Kikai*, 1976, v. 42, 4, 299-305(in Japanese).
- [62] Pacitti, V., Rubenstein, C., The Influence of the Dressing Depth of Cut on the Performance of a Single Point Diamond Dressed Alumina Grinding Wheel, *Int. J. Mach. Tool Des. Res.*, 1972, v. 12, 267-279.
- [63] Verkerk, J., Characterization of wheelwear in plunge grinding, *Annals of the CIRP*, 1977, v. 26, 1, 127-131.
- [64] Trmal, G., Kaliszer, H., Optimization of a Grinding Process and Criteria for Wheel Life, *Proceedings of 15th Int. MTDR Conference*, The Macmillan Press, 1975, 311-315.
- [65] Hahn, R. S., Graham, G., An Application of Force-Adaptive Grinding, *Tech. Pap. Soc. Mnu. Eng.*, MR84-530, 1984.
- [66] Scott, W., Baul, R. M., Relationship Between Wheel and Workpiece Surface

- Topographies in Plunge Grinding, The third International Conference on Manufacturing Engineering 1986, National Conference Publication — Inst. Engineers, Australia, 1986/7, 44-48.
- [67] Buttery, T. C., Statham, A., Percival, J. B., Some Effects of Dressing on Grinding Performance, *Wear*, 1979, v. 55, 2, 195-219.
- [68] Malkin, S., Practical Grinding Optimization, Proceeding of Abrasive Engineering Society 24th International Grinding conference, 1986, 93-103.
- [69] Xiao, G., Malkin, S., Danai, K., Intelligent Control of Cylindrical Plunge Grinding, *Proc. American Control Conf.*, 1992, v. 1, 391-398.
- [70] Venk, S., Govind, R., An Expert System Approach to Optimization of the Centerless Grinding Process, *Annals of the CIRP*, 1990, v. 39, 1, 489-492.
- [71] Venk, S., A Systems Approach for Decision Making in Production Grinding, *Annals of the CIRP*, 1991, v. 40, 1, 445-449.
- [72] Nagasaka, K., Kita, Y., Kitakuchi, Y., Tanibayashi, A., The Construction of Expert System for Grinding Process, *J. Japan Soc. Precis. Eng. Seimitsu Kogaku KaiShi*, 1991, v. 57, 9, 1661-1666(in Japanese).
- [73] Sakakura, M., Inasaki, I., A Neural Network Approach to the Decision-Making Process for Grinding Operations, *Annals of the CIRP*, 1992, v. 41, 1, 353-356.
- [74] Sakakura, M., Inasaki, I., Intelligent Data Base for Grinding Operations, *Annals of the CIRP*, 1993, v.42, 1, 379-382.
- [75] Amitay, G., Malkin, S., Koren Y., Adaptive Control Optimization of Grinding, *Journal of Engineering for Industry*, 1981, v. 103, 103-108.
- [76] Malkin, S., Koren, Y., Off-Line Grinding Optimization with a Macro-Computer, *Annals of the CIRP*, 1980, v. 29, 1, 213-216.
- [77] Pearce, T. R. A., The Effect of Continuous Dressing on the Occurrence of Chatter in Cylindrical Grinding, *Int. J. Mach. Tool Des. Res.*, 1984, v.24, 2, 77-86.
- [78] Andrew, C., Howes, T. D., Pearce, T. R. A., *Creep Feed Grinding*, Holt, Rinehart and Winston Ltd, 1985.

- [79] Guest, J. J., *Grinding Machinery*, Edward Arnold, London, 1915.
- [80] Alden, Geo. I., *Operation of Grinding Wheels in Machine Grinding*, ASME Trans., 1914, v. 36, 451-460.
- [81] Hahn, R. S., *On the Nature of the Grinding Process*, Proc. of the 3rd MTDR Conf., 1962, 129-154.
- [82] Goddard, J., Wilman, H., *A Theory of Friction and Wear During the Abrasion of Metals*, Wear, 1962, v. 5, 114-135.
- [83] Sedriks, A., Mulhearn, T. O., *Mechanics of Cutting and Rubbing in Simulated Abrasive Processes*, Wear, 1963, v. 6, 457-466.
- [84] Graham, D., Baul, R. M., *An Investigation into the Mode of Metal Removal in the Grinding Process*, Wear, 1972, v. 19, 301-314.
- [85] Backer, W. R., Marshall, E. R., Shaw, M. C., *The Size Effect in Metal Cutting*, Trans. ASME, 1952, v. 74, 61-72.
- [86] Von Turkovich, B. F., *Shear Stress in Metal Cutting*, Trans. ASME Journal of Engineering for Industry, 1970, v. 92, 151-157.
- [87] Nakayama, K., Tamura, K., *Size Effect in Metal-Cutting Force*, Trans. of the ASME, Journal of Engineering for Industry, 1968, v. 90, 119-126.
- [88] Kannappan, S., Malkin, S., *Effects of Grain Size and Operating Parameters on the Mechanics of Grinding*, Journal of Engineering for Industry, Aug. 1972, 833-842.
- [89] Shaw, M. C., *A New Theory of Grinding*, Int. Conf. Proc. Sci. in Ind., Australia, 1971, 1-16.
- [90] Lortz, W., *A Model of the Cutting Mechanism in Grinding*, Wear, 1979, v. 53, 115-128.
- [91] Malkin, S., Wiggins, K. L., Osman, M., Smalling, R. W., *Size Effects in Abrasive Processes*, Proceedings of 13th Int. MTDR Conference, The Macmillan Press, 1973, 291-296.
- [92] Saini, D. P., Wager, J. G., Brown, R. H., *Practical Significance of Contact Deflections in Grinding*, Annals of the CIRP, 1982, v. 31, 1, 215-219.
- [93] Nakayama, K., Brecker, J., Shaw, M. C., *Grinding Wheel Elasticity*, Trans.

- of the ASME, Journal of Engineering for Industry, May,1971, 609-614.
- [94] Hahn, R. S., Controlled-Force Grinding — a New Technique for Precision Internal Grinding, Trans. ASME, Journal of Engineering for Industry, 1964, v. 86, 287-293.
- [95] Snoeys, R., Peters, J., Decneut, A., The Significance of Chip Thickness in Grinding, The Annals of the CIRP, 1974, v. 23, 2, 227-237.
- [96] Ono, K., Analysis on the Grinding Force, Bulletin of the Japan Society of Grinding Engineers, 1961, 1, 19-22.
- [97] Werner, G., Influence of Work Material on Grinding Force, The Annals of the CIRP, 1978, v. 27, 1, 243-248.
- [98] Malkin, S., Cook, N. H., The wear of grinding wheels, Part 1 — Attritious Wear, Journal of Engineering for Industry, Trans. ASME, 1971, v. 93, 1120-1128.
- [99] Buttery, T. C., Grinding Force Predictions Based on Wear Theory, Proceedings of 13th Int. MTDR Conference, The Macmillan Press, 1973, 283-289.
- [100] Hemed, M. S., Grinding Mechanics — Single grit Approach, PhD Thesis, Leicester Polytechnic, 1977.
- [101] Torrance, A. A., The Correlation of Process Parameters in Grinding, Wear, 1990, v. 139, 383-401.
- [102] Hahn, R. S., On the Loss of Surface Integrity and Surface Form due to Thermoplastic Stress in Plunge Grinding Operations, The Annals of the CIRP, 1978, v. 25, 1, 203-207.
- [103] Lindsay, R., Principles of Grinding, Handbook of Modern Grinding Technology, composed by R. I. King and R. S. Hahn, Chapman and Hall, 1986, 30-71.
- [104] Lin, Z. B., Chen, X., Monitoring of Grinding Wheel Sharpness, Abrasive and Grinding, 1989, 5, 7-12(in Chinese).
- [105] Graham, W., Voutsadopoulos, C. M., Fracture Wear of Grinding Wheels, Int. J. Mach. Tool Des. Res., 1978, v. 18, 95-103.

- [106] Grisbrook, H., Hollier, R. H., Varley, P. G., Related Patterns of Grinding Forces, Wheel Wear and Surface Finish, *Int. Jnl. of Prod. Res.*, 1962, v. 1, 3, 57-74.
- [107] Backer, W. R., Merchant, M. E., On the Basic Mechanics of the Grinding Process, *ASME Paper No 56-A-43*, 1957, 1-6.
- [108] Koloc, J., On the Wear of Grinding wheels, *MicroTechnic*, 1959, v. 8, 1, 13-15.
- [109] Yoshikawa, H., Fracture Wear of Grinding Wheels, *International Research in Production Engineering*, 1963, 209-217.
- [110] Bhattacharyya, S. K., Grisbrook, H., Moran, H., Analysis of grit fracture with change in grinding conditions, *Microtechnic*, 1968, v. 22, 114-116.
- [111] Tsuwa, H.; Yasui, H., Micro-Structure of Dressed Abrasive Cutting Edges, *Proceedings of the International Grinding Conference, Pittsburgh, Pennsylvania*, 1972, 142-160.
- [112] Wetton, A. G., A Review of Published Fundamental Research of the Grinding of Metals, *Research Report No. 38, The Machine Tool Industry Research Association (MTIRA)*, 1970.
- [113] Bhattacharyya, S. K., Moffatt, V. L., Characteristics of Micro Wheel Wear in Grinding, *Int. J. Mach. Tool Des. Res.*, 1976, v.16, 325-334.
- [114] Chen, X., Lin, Z. B., Probe into the Characteristic of the Wear of Grinding Wheel, *Journal of Fuzhou University*, 1989, 2, (in Chinese).
- [115] Rowe, W. B., Stout, K. J., Review of Grinding-Process Parameters, *Engineers' Digest*, 1971, v. 32, 10, 41-48.
- [116] Pande, S. J., Halder, S. N., Lal, G. K., Evaluation of Grinding Wheel Performance, *Wear*, v.58, 2, 237-248.
- [117] Landberg, P., Experiments on Grinding, *Microtechnic*, 1957, v. 11, 1, 18-25.
- [118] Tönshoff, H. K., Peters, J., Inasaki, I., Paul, T., Modelling and Simulation of Grinding Processes, *Annals of the CIRP* , 1992, v. 41, 2, 677-688.
- [119] Suto, T., Sata, T., Simulation of Grinding Process Based on Wheel Surface Characteristics, *Bull. Japan Soc. of Prec. Engg.*, Mar. 1981, v. 15, 1, 27-33.

- [120] Steffens, K., König, W., Closed Loop Simulation of Grinding, *Annals of the CIRP*, 1983, v. 32, 1, 255-259.
- [121] Yoshikawa, H., Sata, T., Simulated Grinding Process by Monte Carlo Method, *Annals of the CIRP*, 1968, Vol. XVI, 297-302.
- [122] Yoshikawa, H., Peklenik, J., Three Dimensional Simulation Techniques of the Grinding Process — II. Effect of grinding Conditions and Wear on the Statistical Distribution of Geometrical Chip Parameters, *Annals of the CIRP*, 1970, Vol. XVIII, P.361-365.
- [123] Law, S. S., Wu, S. M., Simulation Study of the Grinding Process, *Journal of Engineering for Industry, Transaction of the ASME*, Nov. 1973, v. 95, 972-978.
- [124] Yoshikawa, H., Criterion of Grinding Wheel Tool Life, *Bull. Japan Soc. of Grinding Engineers*, 1963, v. 3, 29-32.
- [125] Yoshikawa, H., Process of Wear in Grinding Wheel with Fracture of Bond and Grain, *Semishu Kikai*, 1960, v. 26, 11, 691-700(in Japanese).
- [126] Malyshev, V. I., Levin, B. M., Kovalev, A.V., Grinding with Ultrasonic Cleaning and Dressing of Abrasive Wheels, *Soviet Engineering Research*, 1990, v. 19, 9, 111-114.
- [127] DAS-20 Manual, MetraByte Corporation, 1989.
- [128] Tompkins, W. J., Webster, J. G., *Interfacing Sensors to the IBM PC*, Prentice-Hall Inc., 1988.
- [129] Rowe, W. B., An Experimental Investigation of Grinding Machine Compliance and Improvements in Productivity, *Proceedings of the 14th Int. MTDR Conference*, 1974, 479-486.
- [130] Rowe, W. B., Willmore, J. L., Hulton, L. J., A Technique for Simulation of Cylindrical Grinding Processes by Hybrid Computation, *Int. J. Mach. Tool Des. Res.*, 1973, v. 13, 111-121.
- [131] Elmqvist, H., Åström, K. J., Schönthal, T., Wittenmark, B., *Simnon User's Guide for MS-DOS Computers*, SSPA Systems, Sweden, March 1990,.
- [132] Rowe, W. B., Bell, W. F., Brough, D., Limit charts for high removal rate

- centreless grinding, *Int. Jnl Mach Tools Manuf.*, 1987, v 27, 1, 15-25.
- [133] Rowe, W. B., Pettit, J. A., Boyle, A., Moruzzi, J. L., Avoidance of thermal damage in grinding and prediction of the damage threshold, *The Annals of the CIRP*, 1988, 37, 1, 327-330.
- [134] Malkin, S., Thermal Aspects of Grinding, Part 2, — Surface temperatures and workpiece burn, *ASME Trans. Journal of Engineering for Industry*, 1974, 11, 1184-1191.
- [135] Malkin, S., Koren, Y., Optimal Infeed Control for Accelerated Sparking-out in Plunge Grinding, *Trans. ASME, Journal of Engineering for Industry*, Feb. 1984, v. 106, 70-74.
- [136] Chung, Y., Inasaki, I., A study on Time Constant in Grinding Process, *J. Japan Soc. Precis. Engg. Semishu Kikai*, 1984, v. 50, 6, 67-71(in Japanese).
- [137] Rubenstein, C., The Mechanics of Grinding, *Int. J. Mach. Tool Des. Res.*, 1972, v. 12, 127-139.
- [138] Davis, C.E., The Dependence of Grinding Wheel Performance on Dressing Procedure, *Int. J. Mach. Tool Des. Res.*, 1974, v. 14, 33-52.
- [139] Hornung, A., Tool Life Variation of Grinding Wheel as a Function of Vibration Amplitude, *Proceedings of the 10th Int. MTDR Conference*, Pergamon Press Ltd., 1970, 127-135.
- [140] Tawakoli, T., High Efficiency Deep Grinding, *Mechanical Engineering Publications Limited*, London, 1993.
- [141] Szekeres, F., Objective Method for Determining Grinding Wheel Life, *Proceedings of 12th Int. MTDR Conference*, The Macmillan Press, 1972, 229-233.
- [142] Chen, X., Study on the Sharpness of Grinding Wheel, Master Thesis, Fuzhou University, 1989(in Chinese).
- [143] Makino, H., Chattering Phenomena as the Criterion of Redress life of Grinding Wheel: a Study on the Establishment of Optimum Operational Condition in Precision Grinding of Hardened Steel, *Proceedings of the 15th International MTDR Conference*, 1974, 325-332.

- [144] Schalkoff, R. J., Pattern Recognition: Statistical, Structural and Neural Approaches, John Wiley & Sons, Inc., 1992.
- [145] Mori, K., Kasashima, N., Yamane, T., Nakai, T., An Intelligent Vibration Diagnostic System for Cylindrical Grinding, Japan/USA Symposium on Flexible Automation, ASME, 1992, 2, 1097-1100.
- [146] NeuralDesk User's Guide, Neural Computer Sciences, 1992.

A.2. Computer Program for Simulation of Dressing and Grinding

```

/*****
      DRESSING AND GRINDING SIMULATION PROGRAM _____by XUN CHEN
                                          17th November, 1994.

file name: xphdsimu.c
The following processes can be simulated:
  Topography of the wheel after dressing;
  The successive cutting point length;
  The dressing force, the model comes from experiments;
  The surface texture Ra during grinding;
  The effects of dwelling on Ra;
  The grinding force;
The following functions have been considered
  grains pull off
  grain broken
  plastic pile-up
  elastic deflection
*****/

#include <stdlib.h>
#include <time.h>
#include <stdio.h>
#include <string.h>
#include <alloc.h>
#include <math.h>
#include <graphics.h>
#include <conio.h>
#include <dos.h>

#define PI 3.1415927

typedef struct
    {
        float x, y, z;
    } grit_matrix;
grit_matrix huge *gp;

float *dresser;
int *x_rand;
int max_x, max_y;
float wear_top, kd, kd0, bd, dg, ds, dw, fd, ad, vf, vs, vw, kel, kpl, kchip;

float get_datum(char parameter[], char file_name[]);
void dresser_shape(float *dresser, float dres_top);
void init_grit_position(int I, int J, int K, float delta);
void grit_position(int I, int J, int K, float delta);
float dstn(float x1, float y1, float z1, float x2, float y2, float z2);
float grit_strength(int n, int nd);
float grit_force(float cut_incre, int nd, int n, int xrand, float wly, float far *work_surface,
                float far *wheel_surface_x, float F0, float ff, int iwr, float gpof, float *F1);
float Ra(float far *z, int n);
float grit_length(float far *wel_face, int n, float cut);
int grainface(float *cut, int ixb, int ix, int n, int id, float gpof, int xrand);
void wheelcutface(float far *wheel_surface, float delta, int wl_x, int I, int J, int K); /* produce wheel surface */
void pileup(int ixb, int ix, int iwr, float heap_area, float kslp, float far *work_surface);
int set_graph(void);
void calc_coords(void);
void draw_background(void);
void draw_graph(float far *yy, int n, float x_gain, float y_gain);
void draw_Ra(float far *yy, int n);
void get_key(void);

void main (int argc, char *argv[])
{
float far *wheel_surface, far *work_surface, far *wheel_surface_x;

```

```

int ix, idx, ii, z, dwell_No, nd, iwr, i, j, k, n, I, J, K;
char parameter[12], file_name[10];
unsigned long nl;
size_t an;          /* array number */
float wlx, wly, api, nw, dwell_time, dres_top, Vg, cut_depth, cut_incre, dlta, tau, wear;
float gf, FORCE, F0, ff, gpof, de, ap, lc, ls, ra, Fd, Fn, F1[2];
struct date today;
struct time now;

if (argc != 2)
{
    printf("Command Error!");
    exit(1);
}

printf("SIMULATION OF DRESSING AND GRINDING by Xun Chen ");
getdate(&today);
gettime(&now);
printf(" %d-%d-%d, ", today.da_day, today.da_mon, today.da_year);
printf("%02d:%02d.\n", now.ti_hour, now.ti_min);

/*----- SIMULATION CONDITION DATA INPUT -----*/

strcpy(file_name, argv[1]);
strcat(file_name, ".DAT");
printf("simulation conditons: %s\n", file_name);

    strcpy(parameter, "ra");          /* um, initial Ra */
ra=get_datum(&parameter[0], &file_name[0]);

    strcpy(parameter, "ds");          /* um, diameter of wheel */
ds=get_datum(&parameter[0], &file_name[0]);

    strcpy(parameter, "dw");          /* um, workpiece diameter */
dw=get_datum(&parameter[0], &file_name[0]);

    strcpy(parameter, "dg");          /* um, diameter of grain */
dg=get_datum(&parameter[0], &file_name[0]);

    strcpy(parameter, "Vg");          /* proportion of grain in wheel */
Vg=get_datum(&parameter[0], &file_name[0]);

    strcpy(parameter, "fd");          /* um/r, feed rate of dressing */
fd=get_datum(&parameter[0], &file_name[0]);

    strcpy(parameter, "ad");          /* um, increment of dressing */
ad=get_datum(&parameter[0], &file_name[0]);

    strcpy(parameter, "bd");          /* um, active width of diamond */
bd=get_datum(&parameter[0], &file_name[0]);

    strcpy(parameter, "nd");          /* No. of dressing passes */
nd=get_datum(&parameter[0], &file_name[0]);

    strcpy(parameter, "vf");          /* um/s, infeed rate of wheel */
vf=get_datum(&parameter[0], &file_name[0]);

    strcpy(parameter, "vs");          /* wheel speed um/s */
vs=get_datum(&parameter[0], &file_name[0]);

    strcpy(parameter, "vw");          /* um/s, workpiece speed */
vw=get_datum(&parameter[0], &file_name[0]);

    strcpy(parameter, "dwell_time"); /* second */
dwell_time=get_datum(&parameter[0], &file_name[0]);

    strcpy(parameter, "tau");          /* second, time constant */
tau=get_datum(&parameter[0], &file_name[0]);

    strcpy(parameter, "kpl");          /* plastic parameter, beta */
kpl=get_datum(&parameter[0], &file_name[0]);

```

```

        strcpy(parameter,"kel");          /* elastic parameter of grain */
kel=get_datum(&parameter[0], &file_name[0]);

        strcpy(parameter,"F0");          /* force constant, depends on workpiece hardness */
F0=get_datum(&parameter[0], &file_name[0]);

        strcpy(parameter,"ff");         /* exponent of force, from experiment */
ff=get_datum(&parameter[0], &file_name[0]);

        strcpy(parameter,"kd");         /* strength of the wheel */
kd=get_datum(&parameter[0], &file_name[0]);

        strcpy(parameter,"kd0");        /* slide dressing force */
kd0=get_datum(&parameter[0], &file_name[0]);

        strcpy(parameter,"kchip");      /* grain fracture parameter */
kchip=get_datum(&parameter[0], &file_name[0]);

printf ("\n");

/***** BASIC PARAMETERS CALCULATION *****/
nw = vw/PI/dw;
ap = vf/nw;
de=ds*dw/(ds+dw);
dlt=PI/(6*Vg);
dlt=dg*pow(dlt,1/3);          /* um matrix distant between grains */
Fd=kd*fd*ad+kd0;           /* dressing force */
printf("Dressing Force = %f(N)\n", Fd);
wlx=2.5*dlt;                /* um position for wheel topography */
wly=2.5*dlt;                /* um position for wheel topography */
lc= 2*sqrt(ap*de);          /* contact length */
ls=lc*vs/vw;

I= 6;                       /* No. of X axis layers, minimum is 4 */
J= ls/dlt+1;                /* No. of Y axis layers */
K= 3;                       /* No. of Z axis layers */

n= I * J * K;
printf ("gp array size: %d\n",n);
nl=n;                        /* int turn to long */
if ((gp = farcalloc(nl, sizeof( grit_matrix)))==NULL) /* grit position */
    printf ("error allocating gp\n");
nl=5000;
if ((wheel_surface = farcalloc(nl, sizeof(float)))==NULL)
    printf ("error allocating wheel_surface\n");
iwr=(I+2)*dlt;
nl=iwr+1;
if ((work_surface= farcalloc(nl, sizeof(float)))==NULL)
    printf ("error allocating work_surface\n");
if ((wheel_surface_x = farcalloc(nl, sizeof(float)))==NULL)
    printf ("error allocating wheel_surface\n");

    randomize();

/***** dressing tool surface *****/
dres_top=1.5*dg;             /* 1.5*dg is dresser position */
an = fd+1;
if ((dresser = calloc(an, sizeof(float)))==NULL)
    printf ("error allocating dresser\n");
an = nd;
if ((x_rand = calloc(an, sizeof(int)))==NULL)
    printf ("error allocating x_rand\n");

dresser_shape(&dresser[0], dres_top);

idx= fd;
for (i= 0; i< nd; i++)
    {

```

```

        z=random(idx);
        x_rand[i]=z;
    }
    dres_top += (nd-1)*ad;

    i=0;
    do
        {
            work_surface[i] = ra*random(100)/25;
            work_surface[i] += dres_top;
            wheel_surface_x[i] = 5*dg;
        }while (i++, i<iwr);
        /* initializing workpiece surface, 1 μm/unit */
        /* ra is initial surface roughness */

    i=0;
    do
        {
            wheel_surface[i] = 5*dg;
        }while (i++, i<5000);
        /* initializing wheel surface, 10 μm/unit */

    wear = 0;
    FORCE =0;
    Fn=0;

    /* ----- Grinding Processing ----- */
    for(ii=0; ii<6; ii++)
    {
        wear_top = dres_top + wear*ii;
        cut_depth = ap;

        i=0;
        do
            {
                work_surface[i] += cut_depth;
            }while (i++, i<iwr);
        /* positioning workpiece surface, 1 μm/unit */

        init_grit_position(I, J, K, dlt);
        grit_position(I, J, K, dlt);
        idx=fd+1;
        z = random(idx);
        FORCE=0;
        Fn=0;
        for (i=1; i<I; i++)
        {
            for (j=1; j<J; j++)
            {
                for (k=1; k<K; k++)
                {
                    /* -----judge if grit pull-off ----- */
                    n=i*J*k+j*K+k;
                    gpof = grit_strength(n, nd);
                    if (gpof <= Fd)
                    {
                        gp[n].z= 5*dg;
                        continue;
                    }
                    /* grain dug out when truing */
                    /* depend on bond strength */

                    /* -----produce workpiece surface during grinding----- */
                    cut_incre = lc - lc*(gp[n].y/l);
                    cut_incre = de - sqrt(de*de-cut_incre*cut_incre);
                    gf = grit_force(cut_incre, nd, n, z, wly, &work_surface[0], &wheel_surface_x[0], F0, ff, iwr, gpof,&F1[0]);
                    FORCE += gf;
                    Fn+=F1[0];
                }
            }
        }
        FORCE /= (I-1)*dlt/1000;
        Fn /= (I-1)*dlt/1000;
        printf ("Ft= %6.4f N/mm, Fn= %6.4f N/mm, P'= %7.4f W/mm, ", FORCE, Fn, FORCE*vs*1e-6);
        ra= Ra(&work_surface[dg], (I-3)*dlt);
        printf ("Ra= %5.3f um.\n", ra);

        printf ("Press any key to continue");
        getch();
        printf("\n");

```

```

if (set_graph() !=1)
    {
        printf ("This programme needs EGA or VGA \n");
        exit (0);
    }
calc_coords();
draw_background();

        setcolor(1);
draw_graph(&work_surface[0], iwr, 0.1, 0.1);
draw_Ra(&work_surface[dg], (I-3)*dlt);
        setcolor(5);
draw_graph(&dresser[0], fd, 0.1, 0.1);

if(ii==0)
    {
        wheelcutface(&wheel_surface[0], dlt, wlx, I, J, K);
        setcolor(57);
        draw_graph(&wheel_surface[0], 5000, 0.1, 0.1);
        setcolor(4);
        draw_graph(&wheel_surface_x[0], iwr, 0.1, 0.1);
    }

get_key();
closegraph();
}

/*-----Grinding Process finished-----*/

cut_depth= dres_top + ap;
printf ("Successive cutting point length: %f um\n", grit_length(&wheel_surface[0], min(J*dlt,5000), cut_depth));

cut_depth= dres_top + ap;
printf ("wheelhead dwelling\n");

        /* ----- surface texture versus dwelling ----- */
dwell_No = dwell_time * nw;
api= ap;
for (ii = 0; ii < dwell_No; ii++)
    {
        api=api/(1+1/(tau*nw));
        /* depth of cut by the decrease of
        1/(1+1/(tau*nw))=Kc/(Kc+Ke),
        tau*nw=Kc/Ke
        tau is the time constant got from trial */

cut_depth = api;

i=0;
do
    {
        work_surface[i] += cut_depth;
    }while (i++, i< iwr);

        /* positioning workpiece surface, 1um/unit */

lc= 2*sqrt(api*de);
ls=lc*vs/vw;
J=ls/dlt+1;
        /* contact length */
        /* wheel cutting length */

init_grit_position(I, J, K, dlt);

grit_position(I, J, K, dlt);
        /*locating grits position*/

FORCE = 0;
Fn = 0;
ix = fd;
z = random(ix);
for (i=1; i<I; i++)
    {
        for (j=1; j<J; j++)
            {
                for (k=1; k<K; k++)
                    {
                        /* -----judge if grit pull-off ----- */

```

```

        n=i*J*K+j*K+k;
gpof = grit_strength(n, nd);
if (gpof <= Fd)
    {
        gp[n].z = 5*dg;          /* grain dug out when truing */
        continue;              /* depend on bond strength */
    }
    /* -----produce workpiece surface----- */
cut_incre = lc - lc*(gp[n].y/lc); /* kinematic cutting increment of grain */
cut_incre = de - sqrt(de*de-cut_incre*cut_incre);
gf = grit_force(cut_incre, nd, n, z, wly, &work_surface[0], &wheel_surface_x[0], F0, ff, iwr, gpof, &F1[0]);
FORCE += gf;
Fn += F1[0];
}
}
}

if (set_graph() !=1)
    {
        printf ("This programme needs EGA or VGA \n");
        exit (0);
    }
calc_coords();
draw_background();
setcolor(1);
draw_graph(&work_surface[0], iwr, 0.1, 0.1);
draw_Ra(&work_surface[dg], 500);

get_key();
closegraph();

FORCE /= (I-1)*dlt/1000;          /* N/mm */
Fn /= (I-1)*dlt/1000;
printf ("Ft= %6.4f N/mm, Fn= %6.4f N/mm, P= %7.4f W/mm, ", FORCE, Fn, FORCE*vs*1e-6);
ra= Ra(&work_surface[dg], (I-3)*dlt);
printf ("Ra= %5.3f um, time= %4.2f s.\n", ra, ((float)ii+1)/nw);

}

printf ("Press any key to continue");
getch();
printf("\n");

if (set_graph() !=1)
    {
        printf ("This programme needs EGA or VGA \n");
        exit (0);
    }
calc_coords();
draw_background();

        setcolor(1);
draw_graph(&work_surface[0], iwr, 0.1, 0.1);
draw_Ra(&work_surface[dg], 500);

get_key();
closegraph();

free(wheel_surface);
free(wheel_surface_x);
free(work_surface);
free(dresser);
free(x_rand);
}

    /****** main programme finished *****/

    /*----- DATA INPUT -----*/
float get_datum(char *parameter, char *file_name)
{
    FILE *in;

```

```

int i;
char para[12];
float value;

if ((in=fopen(file_name, "r"))==NULL)
    {
    printf ("Cannot open the Data File\n");
    exit(1);
    }
value=0;
i=0;
do
    {
    i++;
    if (fscanf (in,"%s %f\n", &para, &value) == EOF)
        {printf ("parameter %s was not found!",parameter);
        break;
        }
    }while (strcmp(para, parameter)!=0);
printf ("%10s %8g ", para, value);
fclose(in);
return(value);
}

```

```

void dresser_shape(float *dresser, float dres_top)
{
int idx;
float h, x;
h = ad-ad*fd*fd/(bd*bd);
h = max(h, 0);
h = dres_top-h;
for (idx= 0; idx<= fd; idx++)
    {
    x=idx-fd/2;
    dresser[idx] = (h + ad - 4*ad*x*x/(bd*bd));
    }
}

```

```

/* initialing grit position */
void init_grit_position(int I, int J, int K, float dlta)
{
int i, j, k, n;

for (i=0; i < I; i++)
    {for (j=0; j < J; j++)
        {for (k=0; k < K; k++)
            {
            n=i*J*K+j*K+k;
            gp[n].x=i*dlta;
            gp[n].y=j*dlta;
            gp[n].z=k*dlta;
            }
        }
    }
}

```

```

void grit_position(int I, int J, int K, float dlta)
{
float d1, d2, d3, d4, d5, d6, d7, d8, d9, d10, d11, d12, d13, dmi, x, y, z;
int i, j, k, n, m, rdt;

dmi=dg; /* limit of grit distance */
rdt=dlta;
for (i=1; i<I; i++)
    {
    for (j=1; j<J; j++)
        {
        for (k=1; k<K; k++)
            {

```

```

n=i*J*K+j*K+k;
x=gp[n].x;
y=gp[n].y;
z=gp[n].z;
if (j==J-1)
do
{
gp[n].x= random(rdt) + x;
gp[n].y= random(rdt) + y;
gp[n].z= random(rdt) + z;
m=(i-1)*J*K+(j-1)*K+k-1;
d1=dstn(gp[n].x, gp[n].y, gp[n].z, gp[m].x, gp[m].y, gp[m].z);
m=(i-1)*J*K+(j-1)*K+k;
d2=dstn(gp[n].x, gp[n].y, gp[n].z, gp[m].x, gp[m].y, gp[m].z);
m=(i-1)*J*K+(j-1)*K+k+1;
d3=dstn(gp[n].x, gp[n].y, gp[n].z, gp[m].x, gp[m].y, gp[m].z);
m=(i-1)*J*K+j*K+k+1;
d4=dstn(gp[n].x, gp[n].y, gp[n].z, gp[m].x, gp[m].y, gp[m].z);
m=(i-1)*J*K+j*K+k;
d5=dstn(gp[n].x, gp[n].y, gp[n].z, gp[m].x, gp[m].y, gp[m].z);
m=(i-1)*J*K+j*K+k-1;
d6=dstn(gp[n].x, gp[n].y, gp[n].z, gp[m].x, gp[m].y, gp[m].z);
m=i*J*K+(j-1)*K+k-1;
d10=dstn(gp[n].x, gp[n].y, gp[n].z, gp[m].x, gp[m].y, gp[m].z);
m=i*J*K+(j-1)*K+k;
d11=dstn(gp[n].x, gp[n].y, gp[n].z, gp[m].x, gp[m].y, gp[m].z);
m=i*J*K+(j-1)*K+k+1;
d12=dstn(gp[n].x, gp[n].y, gp[n].z, gp[m].x, gp[m].y, gp[m].z);
m=i*J*K+j*K+k-1;
d13=dstn(gp[n].x, gp[n].y, gp[n].z, gp[m].x, gp[m].y, gp[m].z);
} while ((d1<dmi) || (d2<dmi) || (d3<dmi) || (d4<dmi) || (d5<dmi) ||
(d6<dmi) || (d10<dmi) || (d11<dmi) || (d12<dmi) || (d13<dmi));
else
if (k==K-1)
do
{
gp[n].x= random(rdt) + x;
gp[n].y= random(rdt) + y;
gp[n].z= random(rdt) + z;
m=(i-1)*J*K+(j-1)*K+k-1;
d1=dstn(gp[n].x, gp[n].y, gp[n].z, gp[m].x, gp[m].y, gp[m].z);
m=(i-1)*J*K+(j-1)*K+k;
d2=dstn(gp[n].x, gp[n].y, gp[n].z, gp[m].x, gp[m].y, gp[m].z);
m=(i-1)*J*K+j*K+k;
d5=dstn(gp[n].x, gp[n].y, gp[n].z, gp[m].x, gp[m].y, gp[m].z);
m=(i-1)*J*K+j*K+k-1;
d6=dstn(gp[n].x, gp[n].y, gp[n].z, gp[m].x, gp[m].y, gp[m].z);
m=(i-1)*J*K+(j+1)*K+k;
d8=dstn(gp[n].x, gp[n].y, gp[n].z, gp[m].x, gp[m].y, gp[m].z);
m=(i-1)*J*K+(j+1)*K+k-1;
d9=dstn(gp[n].x, gp[n].y, gp[n].z, gp[m].x, gp[m].y, gp[m].z);
m=i*J*K+(j-1)*K+k-1;
d10=dstn(gp[n].x, gp[n].y, gp[n].z, gp[m].x, gp[m].y, gp[m].z);
m=i*J*K+(j-1)*K+k;
d11=dstn(gp[n].x, gp[n].y, gp[n].z, gp[m].x, gp[m].y, gp[m].z);
m=i*J*K+j*K+k-1;
d13=dstn(gp[n].x, gp[n].y, gp[n].z, gp[m].x, gp[m].y, gp[m].z);
} while ((d1<dmi) || (d2<dmi) || (d5<dmi) || (d6<dmi) || (d8<dmi)
|| (d9<dmi) || (d10<dmi) || (d11<dmi) || (d13<dmi));
else
do
{
gp[n].x= random(rdt) + x;
gp[n].y= random(rdt) + y;
gp[n].z= random(rdt) + z;
m=(i-1)*J*K+(j-1)*K+k-1;
d1=dstn(gp[n].x, gp[n].y, gp[n].z, gp[m].x, gp[m].y, gp[m].z);
m=(i-1)*J*K+(j-1)*K+k;
d2=dstn(gp[n].x, gp[n].y, gp[n].z, gp[m].x, gp[m].y, gp[m].z);
m=(i-1)*J*K+(j-1)*K+k+1;
d3=dstn(gp[n].x, gp[n].y, gp[n].z, gp[m].x, gp[m].y, gp[m].z);

```

```

m=(i-1)*J*K+j*K+k+1;
d4=dstn(gp[n].x, gp[n].y, gp[n].z, gp[m].x, gp[m].y, gp[m].z);
m=(i-1)*J*K+j*K+k;
d5=dstn(gp[n].x, gp[n].y, gp[n].z, gp[m].x, gp[m].y, gp[m].z);
m=(i-1)*J*K+j*K+k-1;
d6=dstn(gp[n].x, gp[n].y, gp[n].z, gp[m].x, gp[m].y, gp[m].z);
m=(i-1)*J*K+(j+1)*K+k+1;
d7=dstn(gp[n].x, gp[n].y, gp[n].z, gp[m].x, gp[m].y, gp[m].z);
m=(i-1)*J*K+(j+1)*K+k;
d8=dstn(gp[n].x, gp[n].y, gp[n].z, gp[m].x, gp[m].y, gp[m].z);
m=(i-1)*J*K+(j+1)*K+k-1;
d9=dstn(gp[n].x, gp[n].y, gp[n].z, gp[m].x, gp[m].y, gp[m].z);
m=i*J*K+(j-1)*K+k-1;
d10=dstn(gp[n].x, gp[n].y, gp[n].z, gp[m].x, gp[m].y, gp[m].z);
m=i*J*K+(j-1)*K+k;
d11=dstn(gp[n].x, gp[n].y, gp[n].z, gp[m].x, gp[m].y, gp[m].z);
m=i*J*K+(j-1)*K+k+1;
d12=dstn(gp[n].x, gp[n].y, gp[n].z, gp[m].x, gp[m].y, gp[m].z);
m=i*J*K+j*K+k-1;
d13=dstn(gp[n].x, gp[n].y, gp[n].z, gp[m].x, gp[m].y, gp[m].z);
} while ((d1<dmi) || (d2<dmi) || (d3<dmi) || (d4<dmi) || (d5<dmi) ||
(d6<dmi) || (d7<dmi) || (d8<dmi) || (d9<dmi) || (d10<dmi) ||
(d11<dmi) || (d12<dmi) || (d13<dmi));
}}}
}

```

```

/**** distance between two grain centres ****/
float dstn( float x1, float y1, float z1, float x2, float y2, float z2)
{
return (sqrt((x1-x2)*(x1-x2)+(y1-y2)*(y1-y2)+(z1-z2)*(z1-z2)));
}

```

```

float grit_strength(int n, int nd)
{
int i;
float dresser_top, dp, thta, Agrit;

dresser_top = 0;
i=0;
while (i<fd)
{
dresser_top = max(dresser_top, dresser[i]);
i++;
}
dresser_top += ad*(kchip*bd/fd+nd);
/* chipping area is assumed to be proportional to dressing force and overlap ratio,
therefore chipping depth = [kchip*(ad*fd)*(bd/fd)]/fd */
dp = dresser_top - gp[n].z;
if (dp>=dg/2) /* non dressing */
return(0);
if (dp<=-dg/2) /* dressing */
return(kd*PI*dg*dg/4);
thta = 2*acos(fabs(2*dp/dg));
Agrit = dg*dg*(thta-sin(thta))/8;
if(dp>0)
return(kd*Agrit);
else
return(kd*(PI*dg*dg/4-Agrit));
}

```

```

/* produce wheel peripheral surface */
void wheelcutface(float far *wheel_surface, float dlta, int wlx, int I, int J, int K)
{
int i, j, k, JJ, n, idx, iy, ib, ie;
float cut_depth, iz;
div_t xf;

JJ = min(J, 5000/dlta);
for (i=1; i<I; i++)

```

```

{
for (j=1; j<JJ; j++)
{
for (k=1; k<K; k++)
{
n=i*J*K+j*K+k;
iz = gp[n].y - dg/2;
ib = max(0, iz);
iz = gp[n].y + dg/2;
ie = min(JJ*dlt, iz);
for (iy=ib; iy<ie; iy++)
{
iz=dg*dg/4-(gp[n].x-wlx)*(gp[n].x-wlx)-(gp[n].y-iy)*(gp[n].y-iy);
if (iz<0)
cut_depth= 5*dg;
else
{
cut_depth= gp[n].z - sqrt(iz);
xf = div((wlx+fd*iy/(PI*ds)),fd);
idx = xf.rem;
cut_depth = max(cut_depth, dresser[idx]);
wheel_surface[iy] = min(wheel_surface[iy], cut_depth);
}
}
}
}
}
/* end of wheelcutface */

int set_graph(void)
{
int graphdriver = DETECT, graphmode, error_code; /* Initialize graphics system; must be EGA or VGA */
if (registerbgidriver(EGAVGA_driver)<0)
exit(1); /* LINK with graph driver */

initgraph(&graphdriver, &graphmode, "");
error_code = graphresult();
if (error_code != grOk)
return(-1); /* No graphics hardware found */
if ((graphdriver != EGA) && (graphdriver != VGA))
{
closegraph();
return 0;
}
return(1); /* Graphics OK, so return "true" */
}

void calc_coords(void)
{
/* Set global variables for drawing */
max_x = getmaxx(); /* Returns maximum x-coordinate */
max_y = getmaxy(); /* Returns maximum y-coordinate */
}

void get_key(void)
{
outtextxy(50, max_y - 20, "Press any key to continue");
getch();
}

void draw_background(void)
{
/* color code for EGA
black 0; blue 1; green 2; cyan 3; red 4; magenta 5; lightgray 7; brown 20; darkgray 56;
lightblue 57; lightgreen 58; lightcyan 59; lightred 60; lightmagenta 61; yellow 62; white 63.
*/
setbkcolor(7);

```

```

setcolor(62);
outtextxy(200, 20, " The Workpiece Surface ");
outtextxy(29, 40, " ^ ");
outtextxy(max_x-31, max_y-41, " > ");
outtextxy(40, max_y-36, "0");
outtextxy(140, max_y-36, "1000");
outtextxy(240, max_y-36, "2000");
outtextxy(340, max_y-36, "3000");
outtextxy(440, max_y-36, "4000");
outtextxy(540, max_y-36, "5000 um");
line(40,max_y-40, 40, 40);
line(40, 440, max_x-20, 440);
line(37, 140, 40, 140);
line(37, 240, 40, 240);
line(37, 340, 40, 340);
line(37, 440, 40, 440);
}

```

```

void draw_graph(float far *yy, int n, float x_gain, float y_gain)
{
int i, *x, *y;

if ((x= calloc(n, sizeof(float)))==NULL)
{
closegraph();
printf ("error allocating x\n");
exit(0);
}
if ((y= calloc(n, sizeof(float)))==NULL)
{
closegraph();
printf ("error allocating y\n");
exit(0);
}
for(i=0; i<n; i++)
{
x[i]=40+i*x_gain;
y[i]=440-yy[i]*y_gain;
}
for(i=1; i<n; i++)
{
line(x[i-1], y[i-1], x[i], y[i]);
}
free(x);
free(y);
}

```

```

void draw_Ra(float far *yy, int n)
{
int i, *x, *y;
float m;

if ((x= calloc(n, sizeof(float)))==NULL)
{
closegraph();
printf ("error allocating x\n");
exit(0);
}
if ((y= calloc(n, sizeof(float)))==NULL)
{
closegraph();
printf ("error allocating y\n");
exit(0);
}
m=4000;
for (i=0; i<n;i++)
{
m= min(m, yy[i]);
}

```

```

for(i=0; i<n; i++)
    {
        x[i]=40+i;
        y[i]=440-(yy[i]-m)*10;
    }
setcolor(1);
for(i=1; i<n; i++)
    {
        line(x[i-1], y[i-1], x[i], y[i]);
    }
free(x);
free(y);
}

```

```

float Ra(float far *z, int n)
{
    float ra, mean_z;
    int i;

    mean_z=0;
    for (i=0; i<n; i++)
        {
            mean_z += z[i];
        }
    mean_z /= n;
    ra=0;
    for (i=0; i<n; i++)
        {
            ra += fabs(z[i]-mean_z);
        }
    return (ra/n);
}

```

```

float grit_length(float far *wel_face, int n, float stock)
{
    int i, j, k, flag;
    float length;

    j=0, k=0;
    length=0;
    flag=1;                /* 1 means cut, 0 means uncut */

    i=0;
    do {                    /* find first cutting point */
        i++;
    } while (stock>wel_face[i]-i*vf/vs);
    j=i;
    for (i=j; i<n-2; i++)
        {
            if (wel_face[i-2] >= wel_face[i-1] && wel_face[i-1] >= wel_face[i]
                && wel_face[i] <= wel_face[i+1] && wel_face[i+1] <= wel_face[i+2])
                {
                    if (flag==0)
                        {
                            if (stock>wel_face[i]-i*vf/vs)                /* cutting */
                                {
                                    length = length + (i-j);
                                    stock = wel_face[i]-i*vf/vs;
                                    j=i;
                                    k++;
                                    flag=1;
                                }
                        }
                    else
                        {
                            if (stock<wel_face[i]-i*vf/vs)                /* non cutting */
                                flag=0;
                        }
                }
        }
}

```

```

    }
}
printf ("Cutting point number: %d\n",k);
if (k==0) k=-1; /* to avoid divided by zero */
length= length / k;
return (length);
} /* end of grit_length() */

int grainface(float *cut, int ixb, int ix, int n, int id, float gpof, int xrand) /* dressing process */
{
div_t xf;
float iz, *dcut, *cp, dflect, gchip, ld, Fdg, Darea, maxchip, ixd, thta, omiga;
int i, j, ib, ix, ie, flag;
size_t s;

ie=ix-ixb;
if (ie <= 0)
return(ix);
ixd = xrand+x_rand[id]+fd*gp[n].y/(PI*ds);
s= fd+1;
if ((dcut= calloc(s, sizeof(float)))==NULL)
printf ("error allocating dcut in grainface\n");
if ((cp= calloc(s, sizeof(float)))==NULL)
printf ("error allocating cp in grainface\n");

ib=0;
Darea = 0;
maxchip = ad;
ld = (fd+bd)/2;
flag = ld;
gchip = 2*PI*random(flag)/ld;

for (i=0; i<ie; i++)
{
ix = ixb+i;
xf = div((ix+ixd), fd);
if (cut[i] < dresser[xf.rem] + id*ad) /* dressing */
{
iz = dg*dg/4 - (gp[n].x-ix)*(gp[n].x-ix);
if (iz<=0)
{
dcut[ib]=0;
cut[i] = 5*dg;
continue;
}
iz = gp[n].z + sqrt(iz); /* top of the grain surface */
if (dresser[xf.rem] + id*ad > iz)
{
if (iz > cut[i])
dcut[ib] = iz - cut[i];
else
dcut[ib] = 0;
cut[i] = 5*dg;
}
else
{
dcut[ib] = dresser[xf.rem] + id*ad - cut[i];
cut[i] = dresser[xf.rem] + id*ad;
}
Darea += dcut[ib];
}
else
{ /* non dressing */
dcut[ib] = 0;
}
ib++;
if (xf.rem==0 || i==ie-1)
{
j = ib;
maxchip = kchip/2*Darea*bd/fd/fd;
}
}
}

```

```

    omiga = random(20)/20 + 1;
    for (ib = 0; ib < j; ib++)
    {
        thta = gchip+2*PI*omiga*ib/ld;
        cp[ib] = maxchip*(1+sin(thta));
    }
    Fdg = kd * Darea + kd0;    /* dressing force */
    if (Fdg > 0)
    {
        dflect = kel*pow(Fdg, 0.6667);
        for (ib = 0; ib < j; ib++)
        {
            if (dcut[ib] > 0)
            {
                if (dcut[ib] > dflect)
                    cut[i+1-j+ib] += cp[ib] - dflect;
                else
                    cut[i+1-j+ib] += cp[ib] - dcut[ib];
            }
        }
    }
    if (Fdg > gpof)          /* grain brocken */
    {
        free(dcut);
        free(cp);
        ib = i+ixb-fd/2;
        ib = max(ixb, ib);
        gp[n].z = 5*dg;
        return(ib);
    }
    gchip = thta;
    ib=0;
    Darea = 0;
}
}
free(dcut);
free(cp);
return(ixe);
}

```

```

float grit_force(float cut_incre, int nd, int n, int xrand, float wly, float far *work_surface,
                float far *wheel_surface_x, float F0, float ff, int iwr, float gpof, float *F1)
{
    int id, ixb, ixe, ix, i, cn, nc;
    float cut_position, heap_area, kslp, kslp1, kslp2, h1, bg, lg, lgg, gdg, actangle, iz, avcut, maxcut, cut_area;
    double F, Fn, E, heq;
    float *cut;
    size_t s;

    id=dg+fd;          /* initial grain cutting surface */
    s=id+1;
    if ((cut = calloc(s, sizeof(float)))==NULL)
        printf ("error allocating cut in grit_force\n");

    cn = 0;
    ixb = max(0,(gp[n].x-dg/2-fd));          /* initial grain surface */
    for (i=0; i<id; i++)
    {
        ix = ixb + i;

        iz = dg*dg/4 - (gp[n].x-ix)*(gp[n].x-ix) - (gp[n].y-wly)*(gp[n].y-wly);
        if (iz>0)
        {
            /* grain shape at wly position */
            wheel_surface_x[ix] = min(wheel_surface_x[ix], gp[n].z-sqrt(iz));
            cn = i;          /* right end of the surface */
        }

        iz = dg*dg/4 - (gp[n].x-ix)*(gp[n].x-ix);
        if (iz<=0)
        {

```

```

        cut[i]=5*dg;
    }
else
    {
        cut[i] = gp[n].z - sqrt(iz);
        cut[i] = (float) max(cut[i], 1.5*dg+kchip);
    }
}

ixe = ixb+id;
ixe = min(ixe, iwr);
for (id=0; id<nd; id++)
    {
        /* dressing */
        ix = grainface(&cut[0], ixb, ix, n, id, gpof, xrand);
    }

if (ixe <= ixb)
    {
        /* dressed grain drop */
        free(cut);
        return(0);
    }

if (abs(gp[n].y-wly)<dg/2)
    {
        /* grain shape at wly position after dressing */
        for (i=0; i<ixe-ixb; i++)
            {
                if (cut[i]<5*dg)
                    wheel_surface_x[ixb+i] = max(wheel_surface_x[ixb+i],cut[i]);
            }
        for (i=ixe-ixb; i<cn; i++) wheel_surface_x[ixb+i] = 5*dg;
    }

id = ixb;
ixb = 0;
cut_area = 0;
nc=0;
cn=0;
heq=0;
F=0;
F1[0]=0;
Fn=0;
kslp1=0;
kslp2=ixe;
lg = 0;

/* grinding */
for (i=0; i<ixe-id; i++)
    {
        ix = id+i;
        cut_position = cut[i] + cut_incre;
        lgg = dg*dg/4 - (cut[i]-gp[n].z)*(cut[i]-gp[n].z) - (gp[n].x-ix)*(gp[n].x-ix);
        if (work_surface[ix]>cut_position)
            {
                if (ixb==0) ixb = ix;
                if (lgg>0)
                    {
                        lg = max(lg, sqrt(lgg)); /* max contact length of the grain*/
                        cut[i]=work_surface[ix]-cut_position; /*cut depth*/
                        cut_area += cut[i];
                        cn++;
                    }
                else
                    cut[i] = 0;
            }
    }
else
    {
        cut[i]=0;
        if (cut_area>0)
            {
                heq += cut_area;
                nc += cn;
                if (kslp1==0)

```

```

                                kslp1=ixb;
                                kslp2 = ix;
                                cn = 0;
                                cut_area=0;
                                }
                                }
if (kslp1==0)
    ixb = id;
else
    ixb = kslp1;
ixc = kslp2;
cut_area = heq;
maxcut = 0;

for (i=ixb-id; i<ixc-id; i++)
    {
        maxcut = max(maxcut, cut[i]);
    }

heq= maxcut;
nc = max(nc, 1);
avcut = maxcut;
bg = ixc - ixb;
if(cut_area>0 && bg>0)
    {
        lg = sqrt(lg*bg/2);
        kslp = 2*avcut/lg;
        gdg = avcut + lg*lg/avcut;
        actangle = asin(2*lg/gdg);
        E = 0.001*0.375*PI*lg/avcut*F0;
        Fn = cut_area*E*(cos(actangle)-ff*sin(actangle));
        Fn = max(Fn,0);
        F1[0]= Fn;
        F = E*(sin(actangle) + ff*cos(actangle));
        if (F>kd)
            {
                F = 0;
                F1[0] = F;
                free(cut);
                return(F);
            }
        else
            F += cut_area*F;
    }

if (gpof<F)
    {
        Fn = Fn*gpof/F;
        F = gpof;
        F1[0]=Fn;
    }

h1= ke]*pow(Fn, 0.6667);
heap_area = 0;
if (maxcut > 0)
    {
        for(i=ixb-id; i<ixc-id; i++)
            {
                cut[i] = cut[i] - h1;
                if (cut[i] > 0)
                    {
                        work_surface[i+id] -= cut[i];
                        heap_area += cut[i];
                    }
            }
    }

heap_area = heap_area - cut_area*kpl;
if(heap_area>0)
    pileup(ixb, ixc, iwr, heap_area, kslp, &work_surface[0]);

```

```

free(cut);
return(F);
}

/** plastic pile up */
void pileup(int ixb, int ixc, int iwr, float heap_area, float kslp, float far *work_surface)
{
float h1, h2, a1, a2, kslp1, kslp2, haa1, haa2;
int nn, ix, ixx;

kslp1=kslp;
kslp2=kslp1;

/* formular of parabola:
x^2=(h-y)*a^2/h, y=h-(h/a^2)*x^2, parabola_area = 4*a*h/3,
y'=2*h/a = 3*parabola_area/(2*a*a).
*/
if (kslp1>0 && heap_area>0) /* left side plastic deform */
{
h1= sqrt(0.1875*heap_area*kslp1); /* 0.1875=3/16 */
a1= 2*h1/kslp1; /* 0.75=3/4 */
a1 = max(a1, 0.1);
haa1= h1/(a1*a1);
nn = ixb-2*a1;
nn = max(0, nn);
for (ixx=nn+1; ixx<ixb; ixx++)
work_surface[ixx] += h1-(ixx-ixb+a1)*(ixx-ixb+a1)*haa1;
}
if (kslp2>0 && heap_area>0) /* right side plastic deform */
{
ix=ixc;
h2= sqrt(0.1875*heap_area*kslp2);
a2= 2*h2/kslp2; /* 0.75=3/4 */
a2 = max(a2, 0.1);
haa2=h2/(a2*a2);
nn= ix+2*a2;
nn=min(nn, iwr);
for (ixx=ix; ixx<nn; ixx++)
work_surface[ixx] += h2-(ixx-ix-a2)*(ixx-ix-a2)*haa2;
}
}

```

A.3. List of the Author's Relevant Published Papers

- Chen, X., Allanson, D., Thomas, A., Moruzzi, J. L., Rowe, W. B., Simulation of Plunge Grinding Cycles, Proceeding of the Conference SAMT'92, Sunderland, 1992, 13.3.
- Rowe, W. B., Chen, X., Morgan, M. N., The Identification of Dressing Strategies for Optimal Grinding Wheel Performance, Proceedings of the 30th Int. MATADOR conference, 1993, 195-202.
- Chen, X., Allanson, D., Thomas, A., Moruzzi, J. L., Rowe, W. B., Simulation of Feed Cycles for Grinding Between Centres, Int. J. Mach. Tools Manufact., 1994, v. 34, 5, 603-616.
- Rowe, W. B., Chen, X., Mills, B., Towards an Adaptive Strategy for Dressing in Grinding Operations", Proceedings of the 31st International MATADOR conference, April, 1995, 415-420.

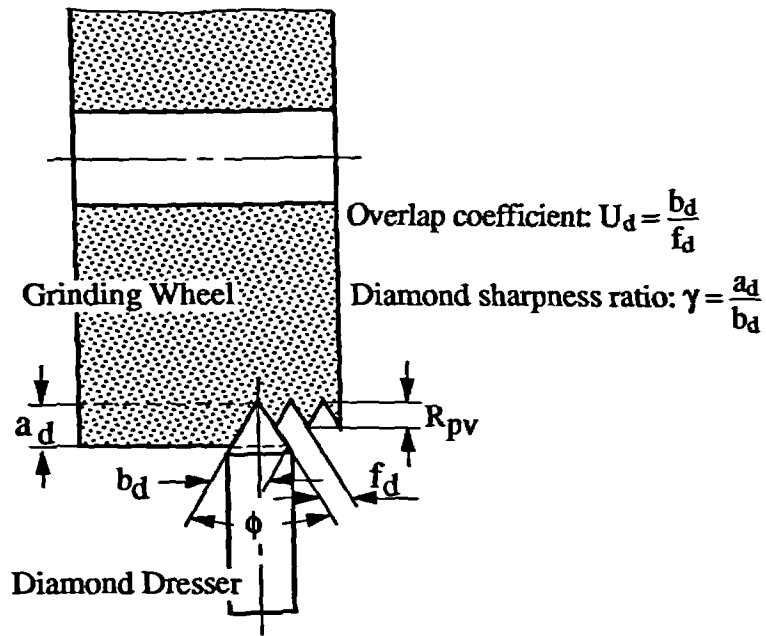


Figure 2.1 Kinematic description of dressing process

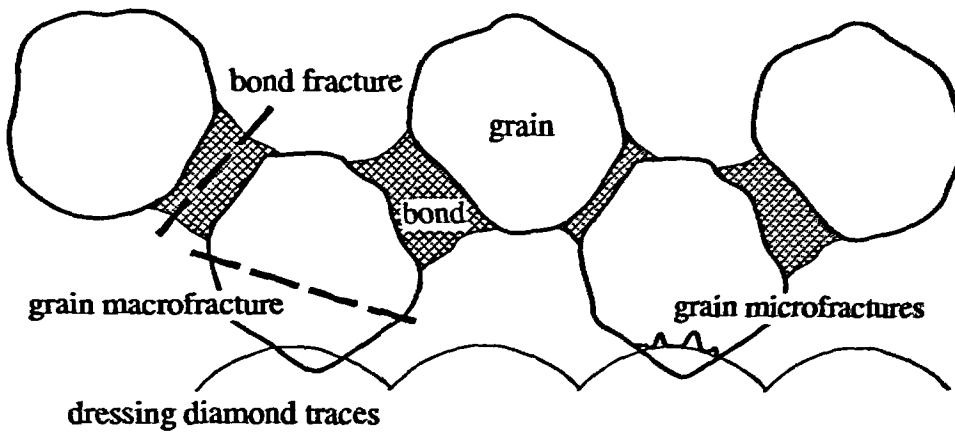


Figure 2.2 Grain fracture and bond fracture

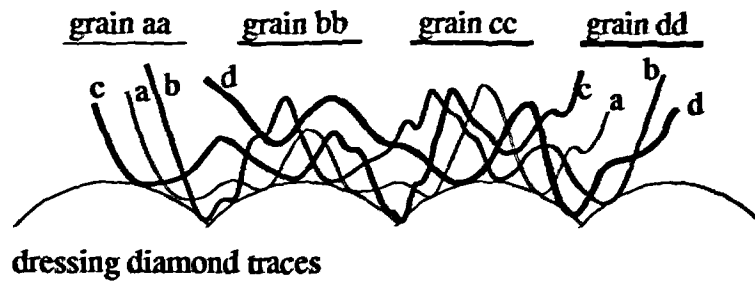


Figure 2.3 Grain surface after dressing

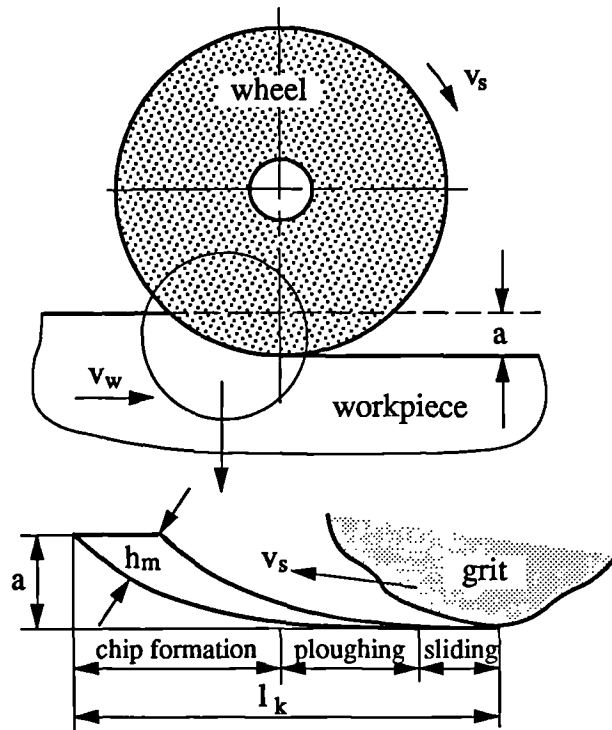


Figure 3.1 Three stages of chip generation

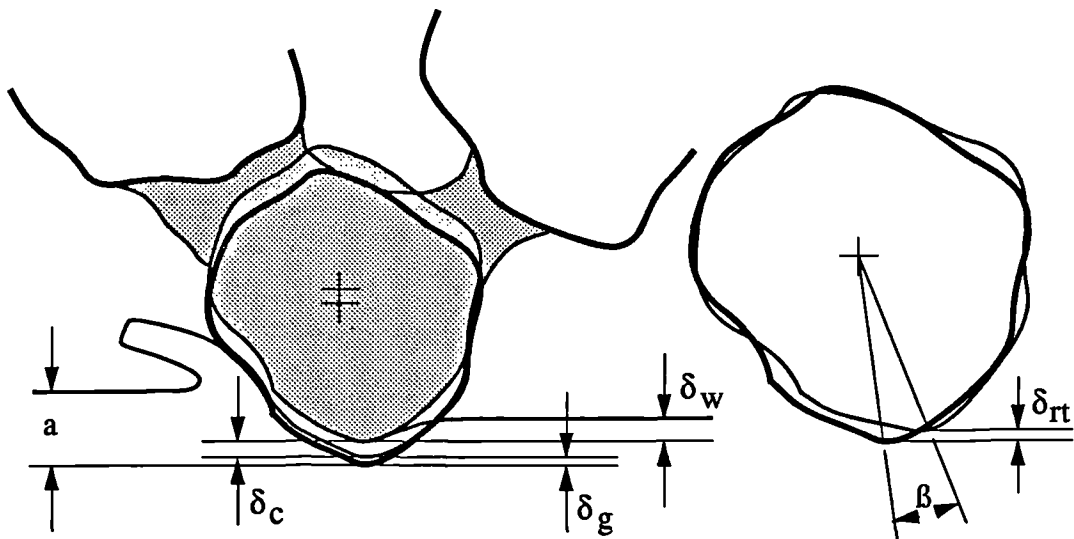


Figure 3.2 Grit deflection in grinding

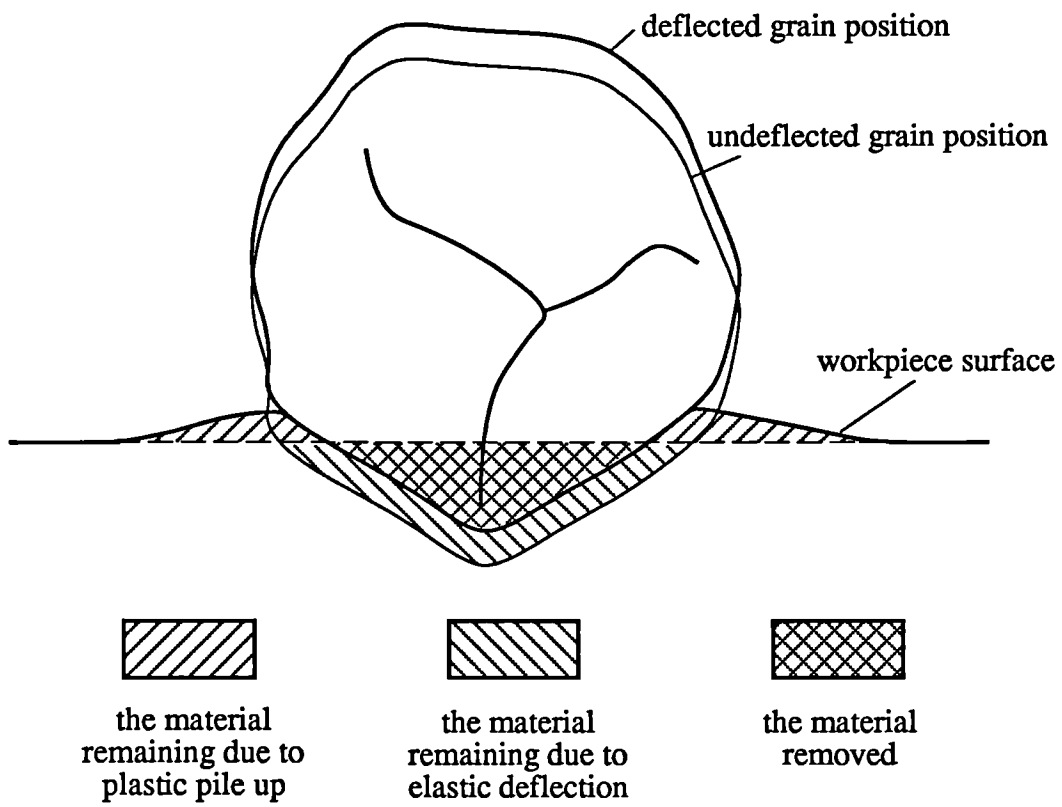


Figure 3.3 Generation of the workpiece surface in grinding

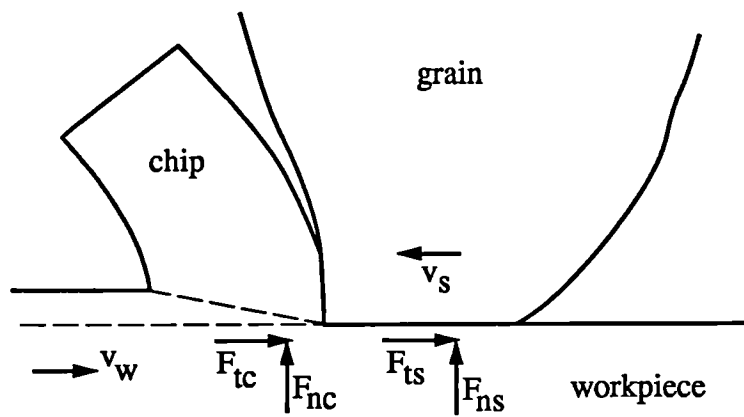


Figure 3.4 Cutting and sliding in the grinding process

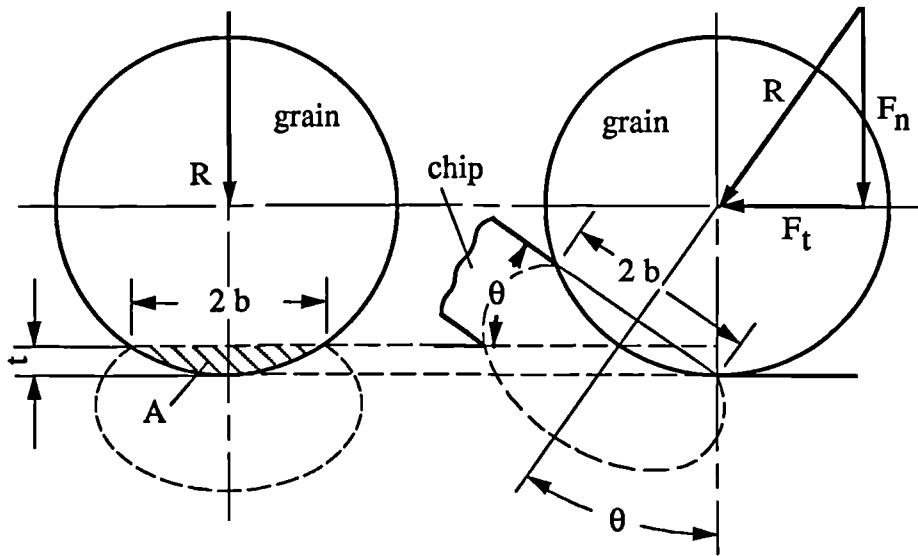


Figure 3.5 Action of a spherical grain in grinding

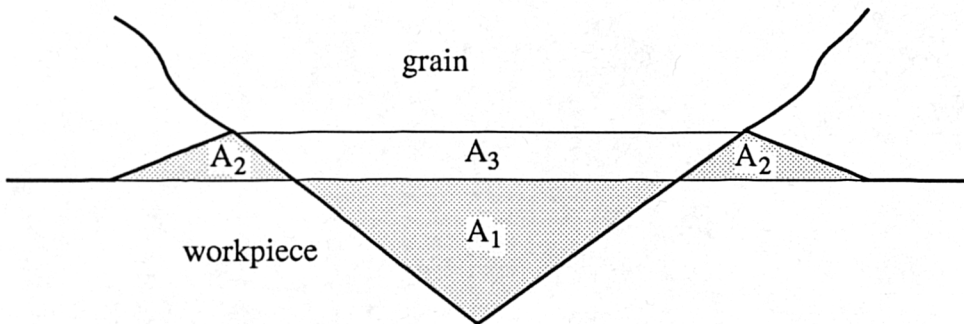


Figure 3.6 Expression of material flow under a grain in grinding

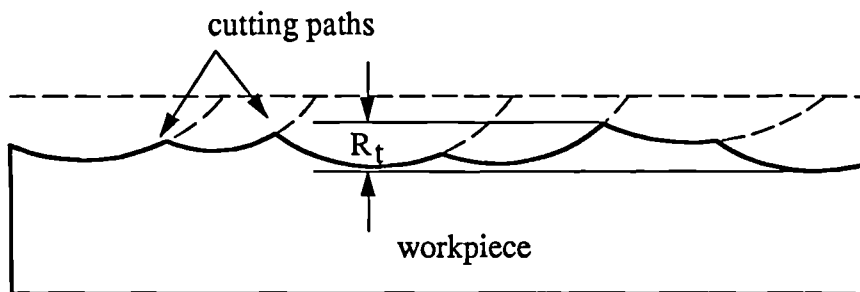


Figure 3.7 Generation of the workpiece surface due to kinematic relationships

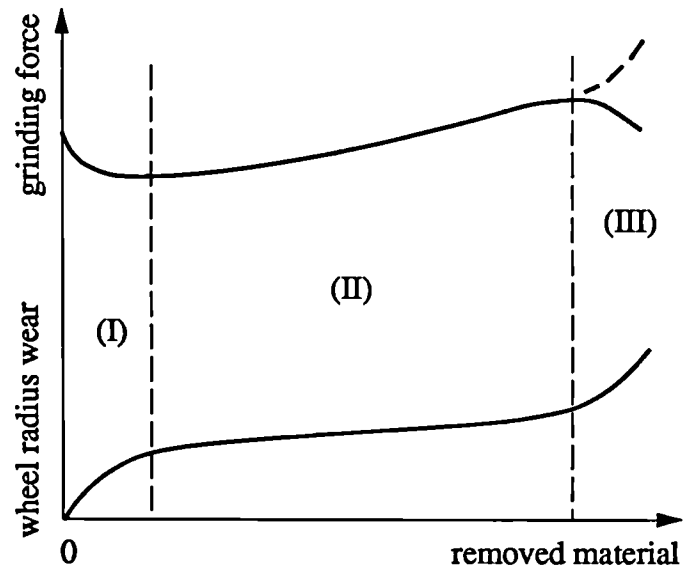


Figure 3.8 Variation of grinding force in a grinding wheel life cycle

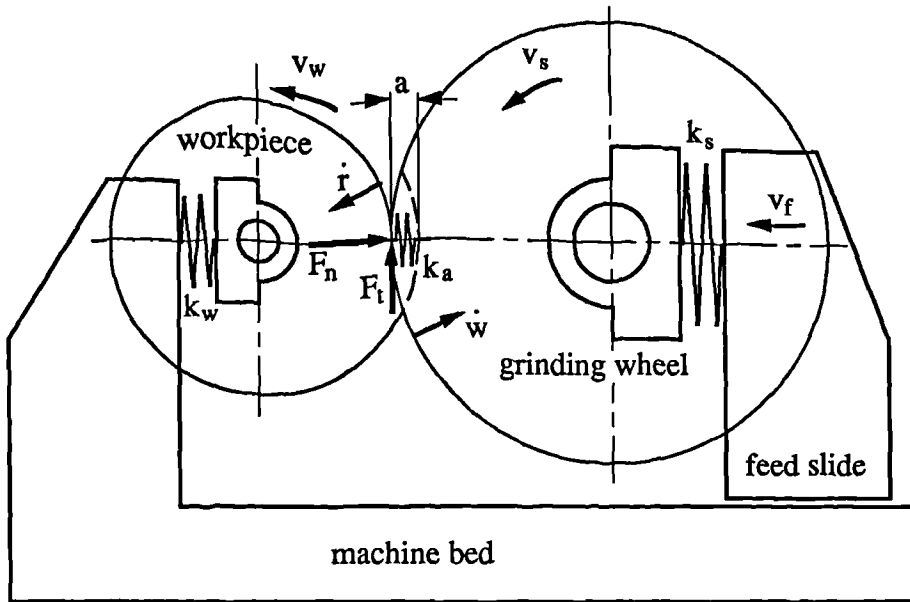


Figure 4.1 Representation of the external cylindrical plunge grinding machine system

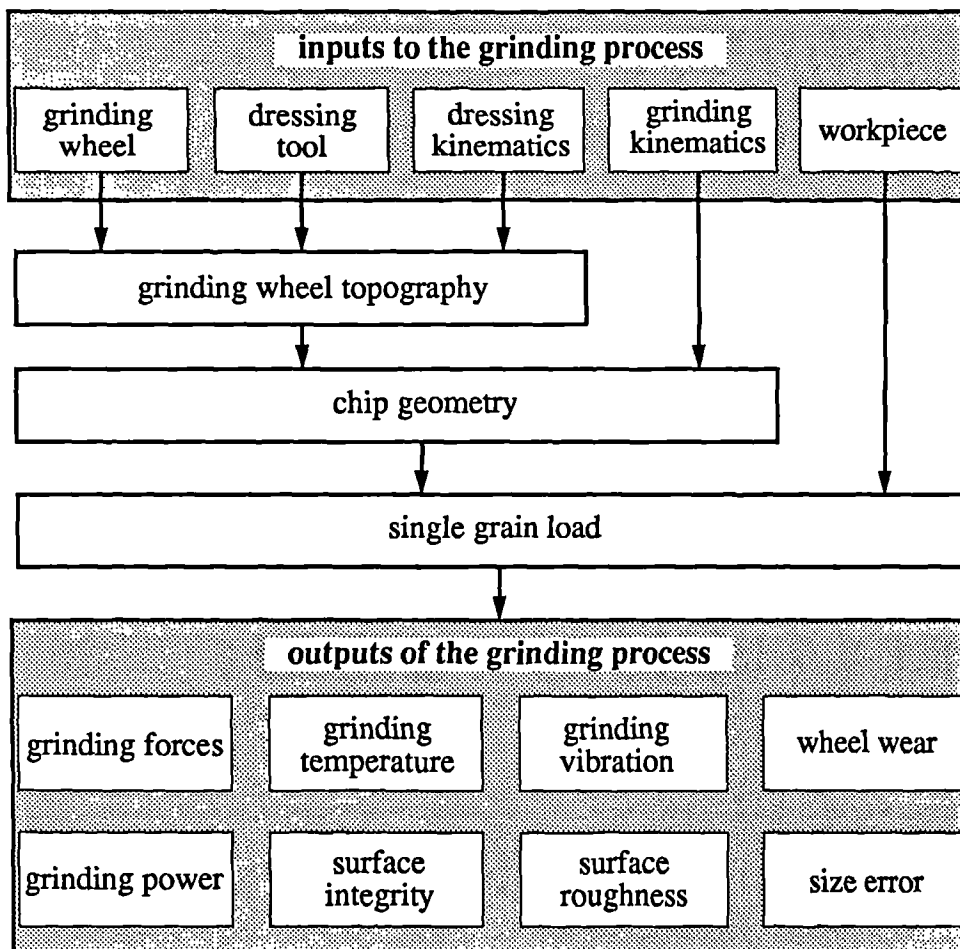


Figure 4.2 Process relationships in grinding

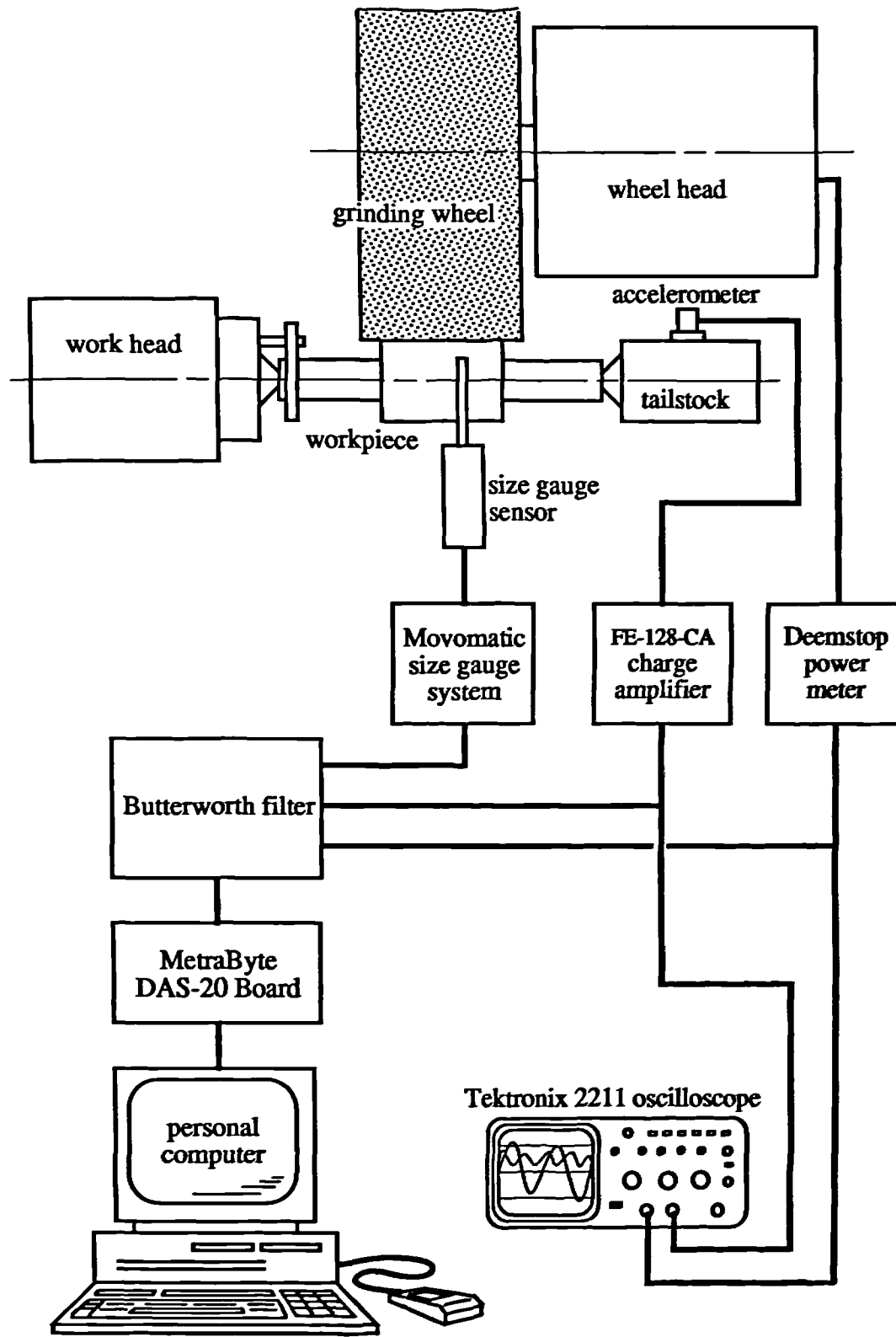


Figure 5.1 The experimental system

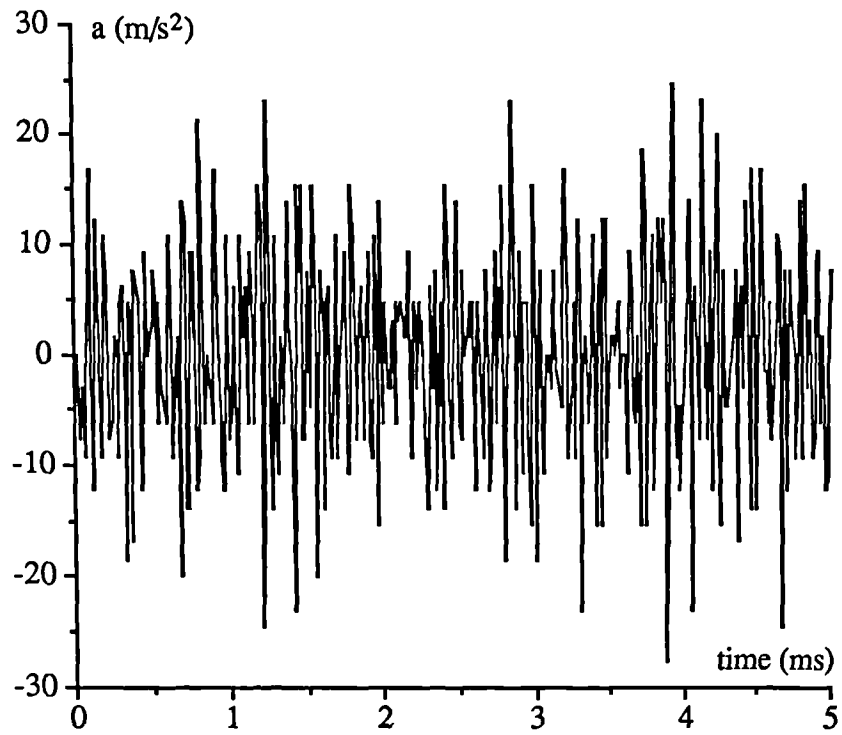


Figure 5.2 Acceleration signals of grinding vibration

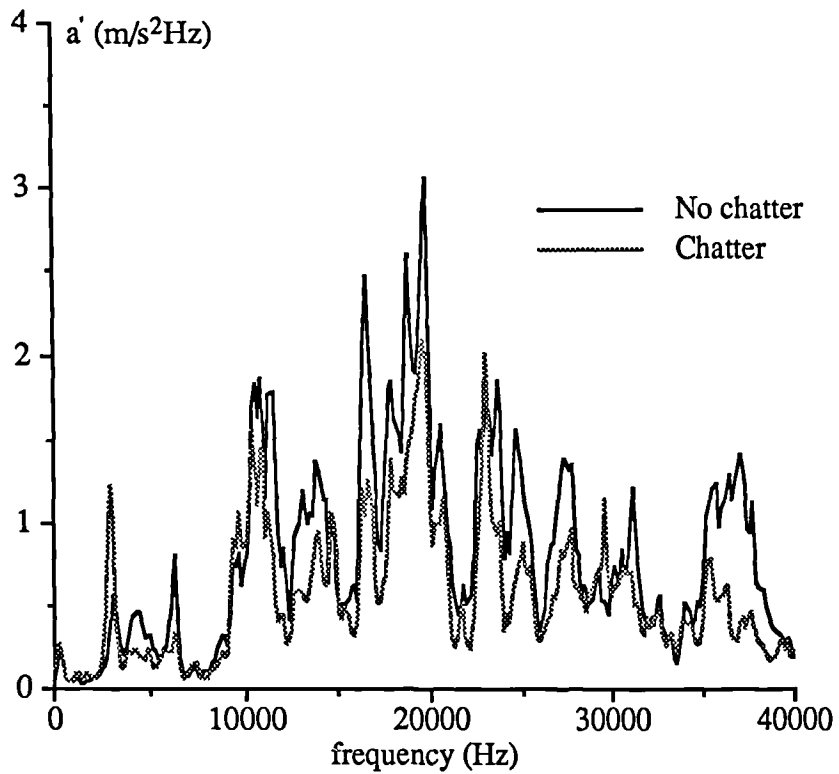


Figure 5.3 Spectrum of acceleration of grinding vibrations

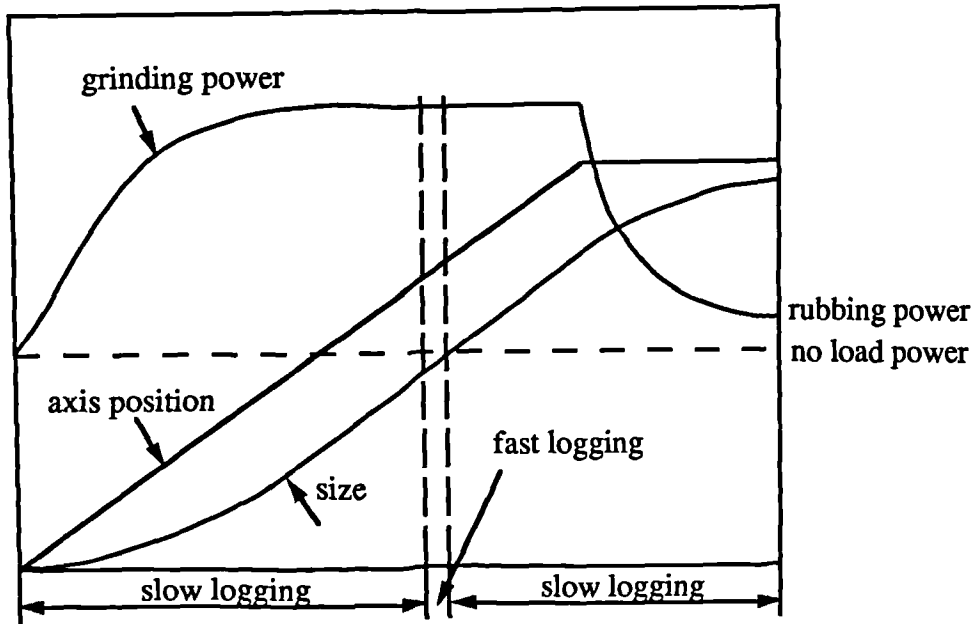


Figure 5.4 Data logging strategy

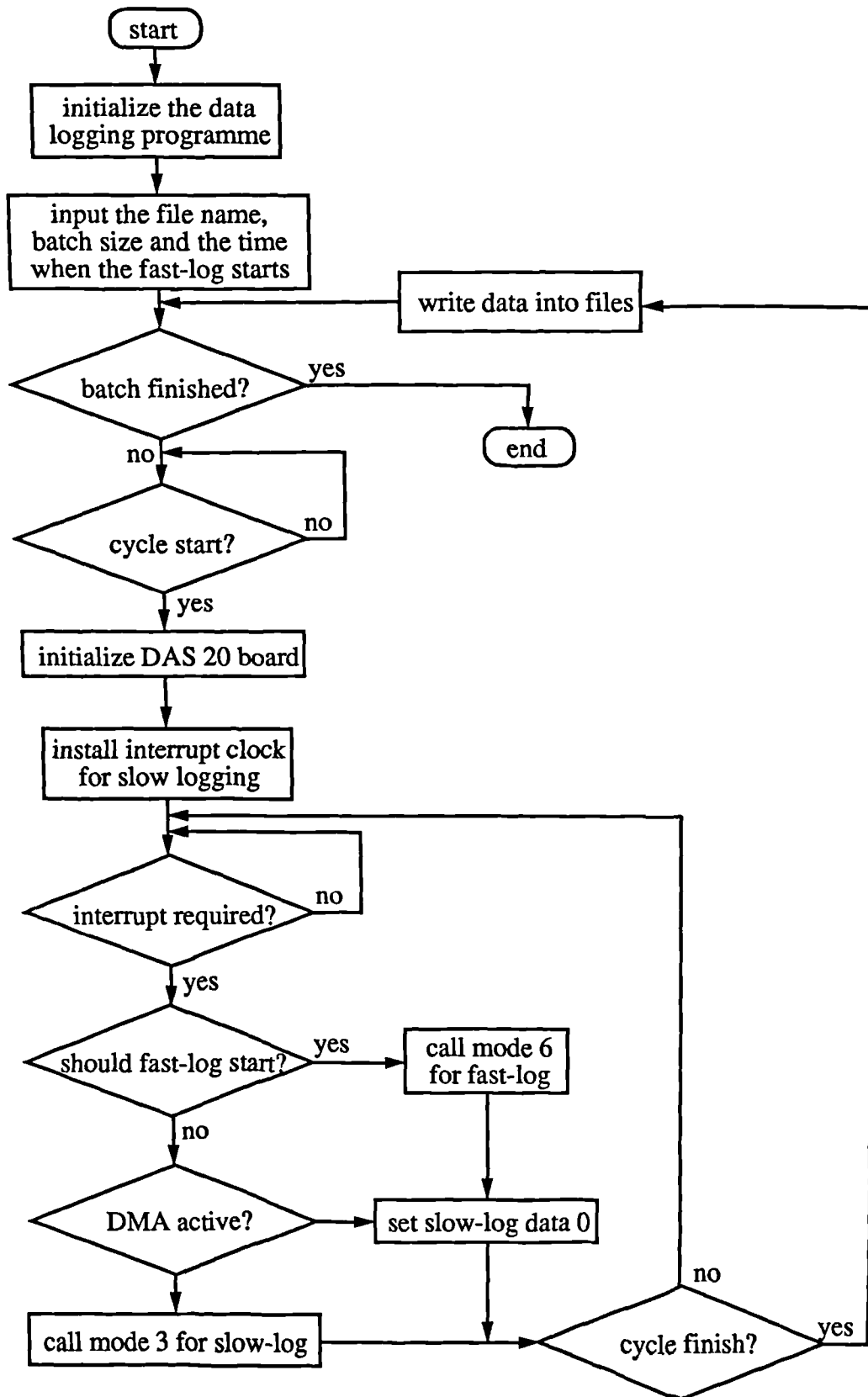


Figure 5.5 Flow chart of the data logging programme

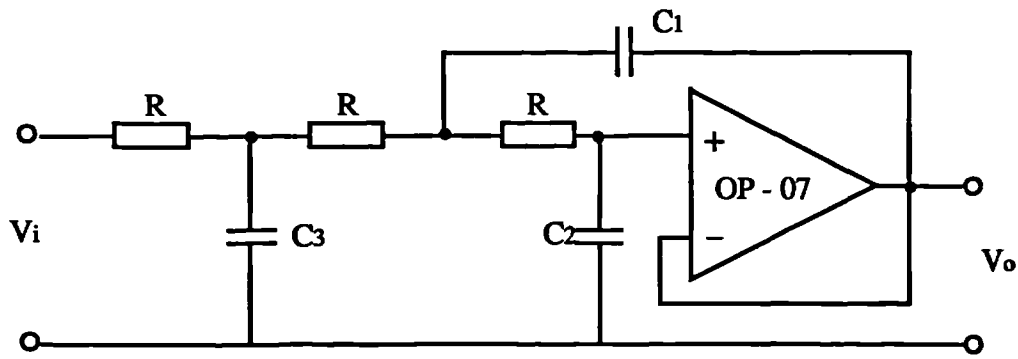


Figure 5.6 The Butterworth filter circuit

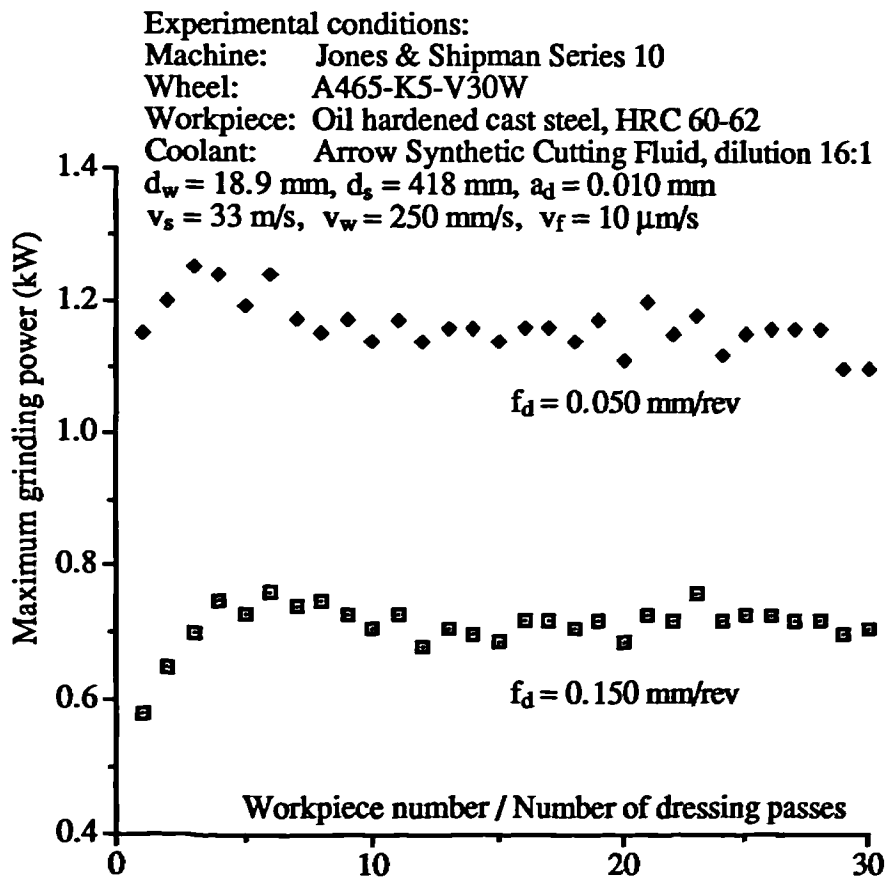


Figure 5.7 Effect of the number of dressing passes

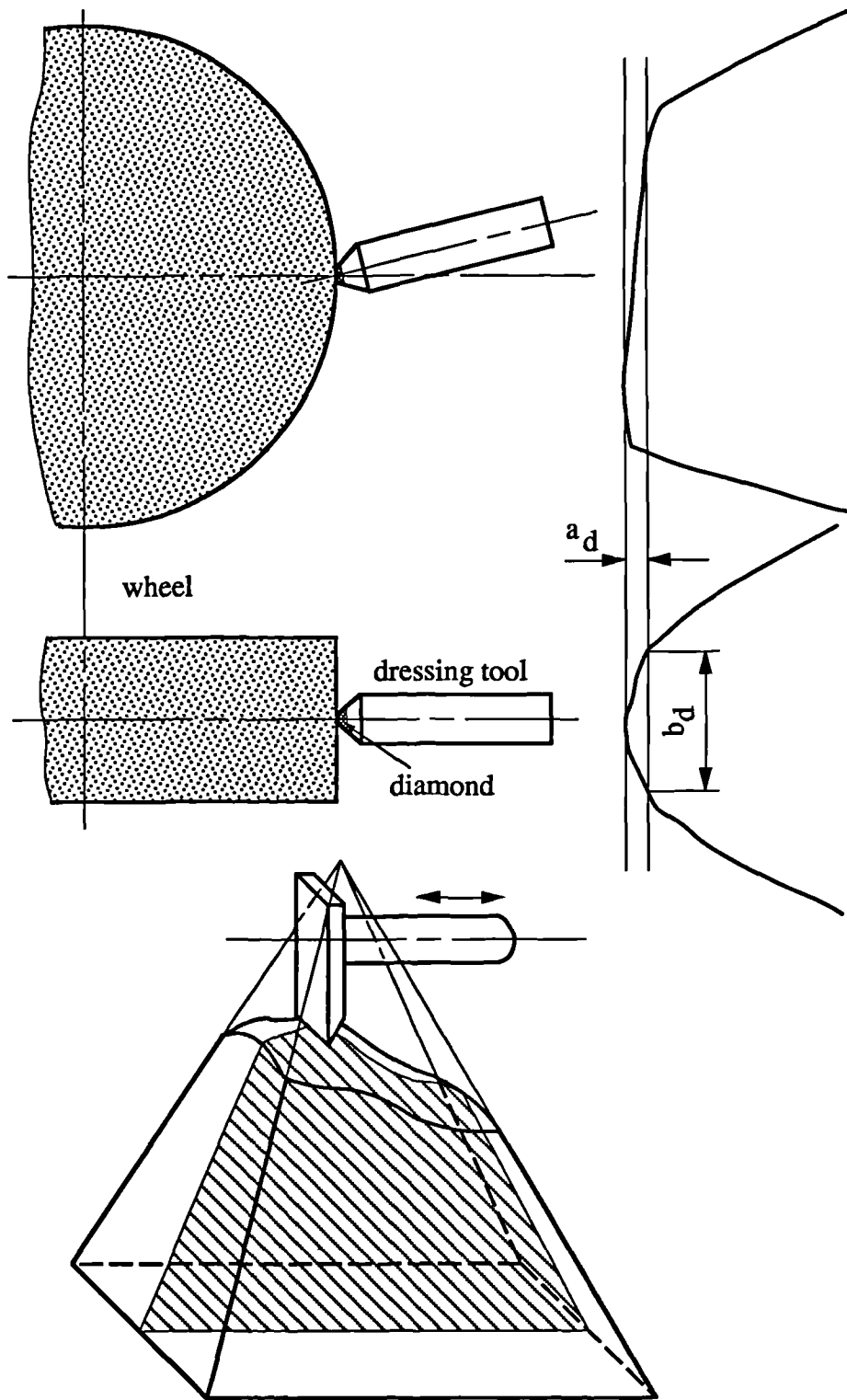


Figure 5.8. Measurement of dressing diamond shape

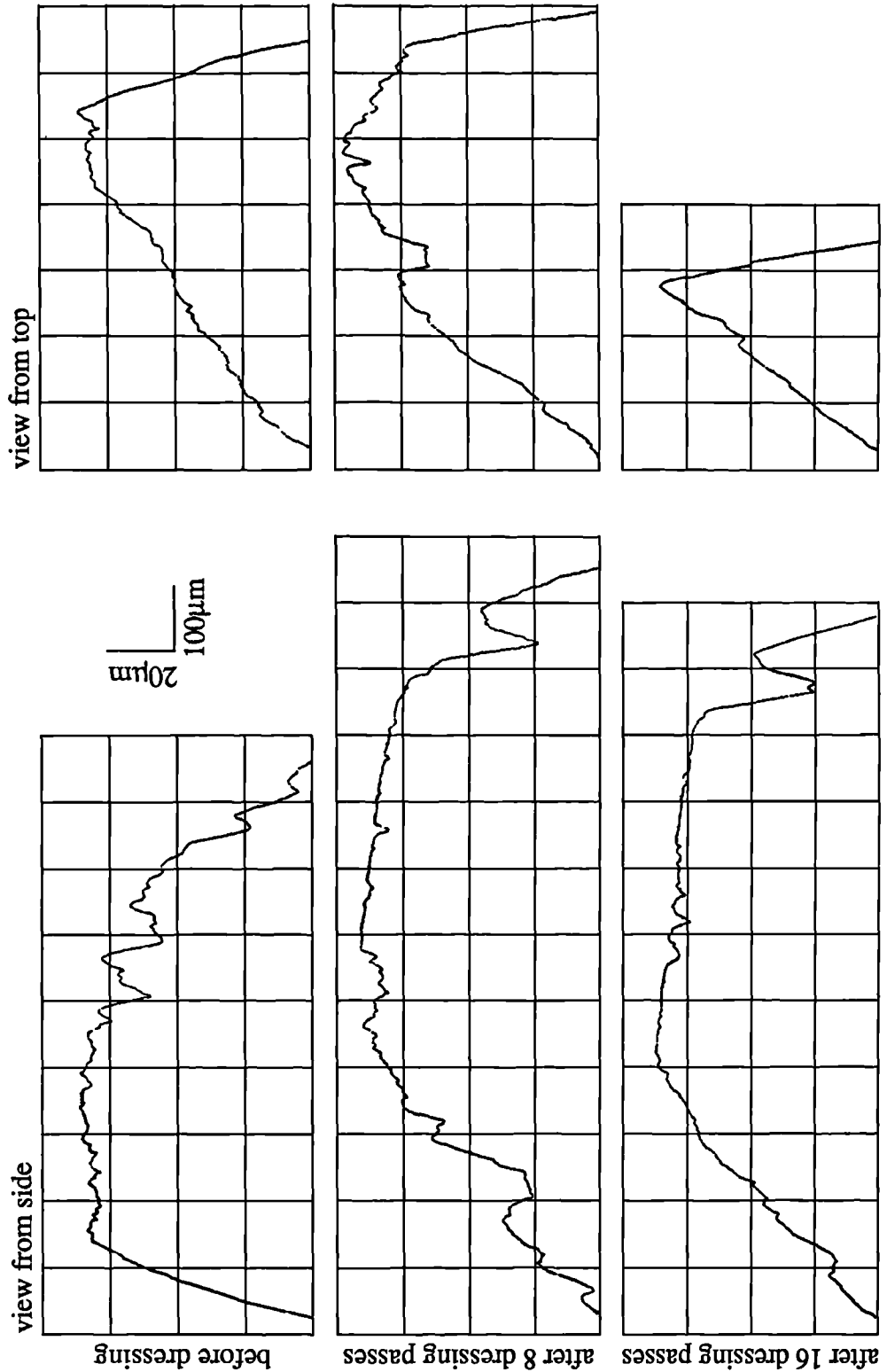


Figure 5.9 Diamond dressing tool shape affected by the dressing operation



WORN DIAMOND SURFACE X50

Figure 5.10 The surface of a worn diamond

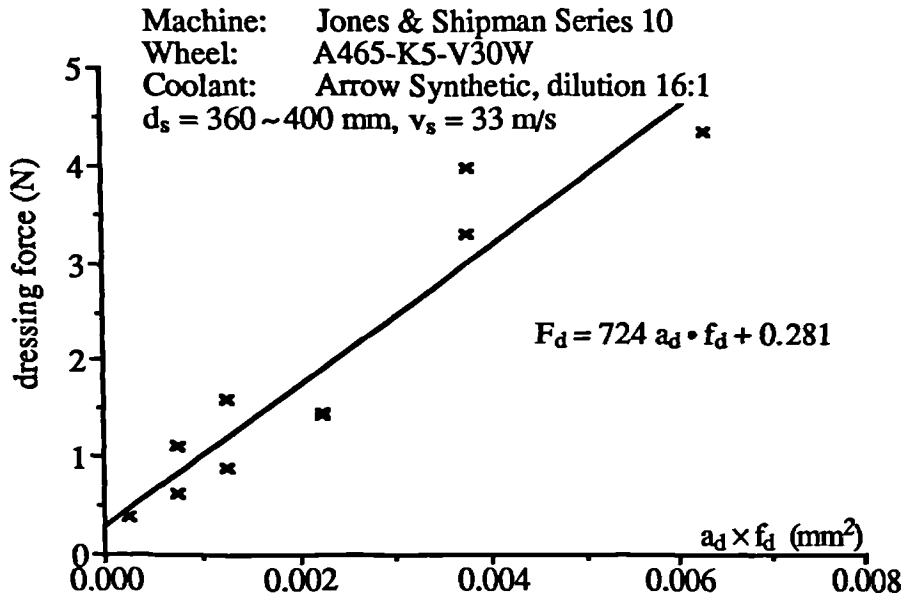


Figure 5.11 Effect of dressing condition on dressing force

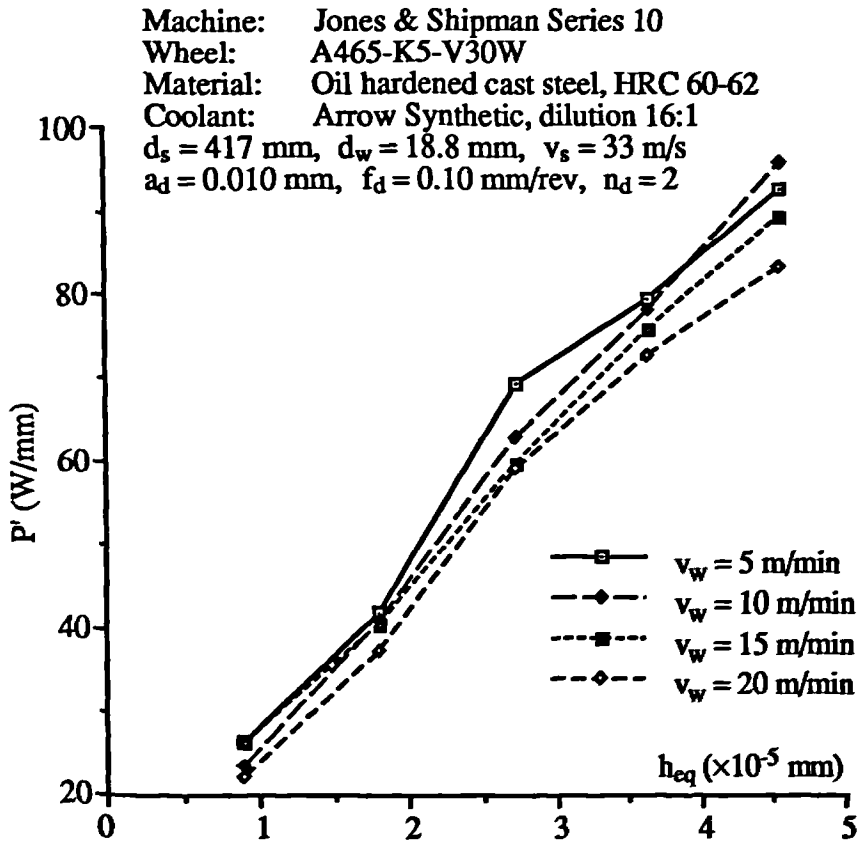


Figure 5.12 Effects of equivalent chip thickness on specific power

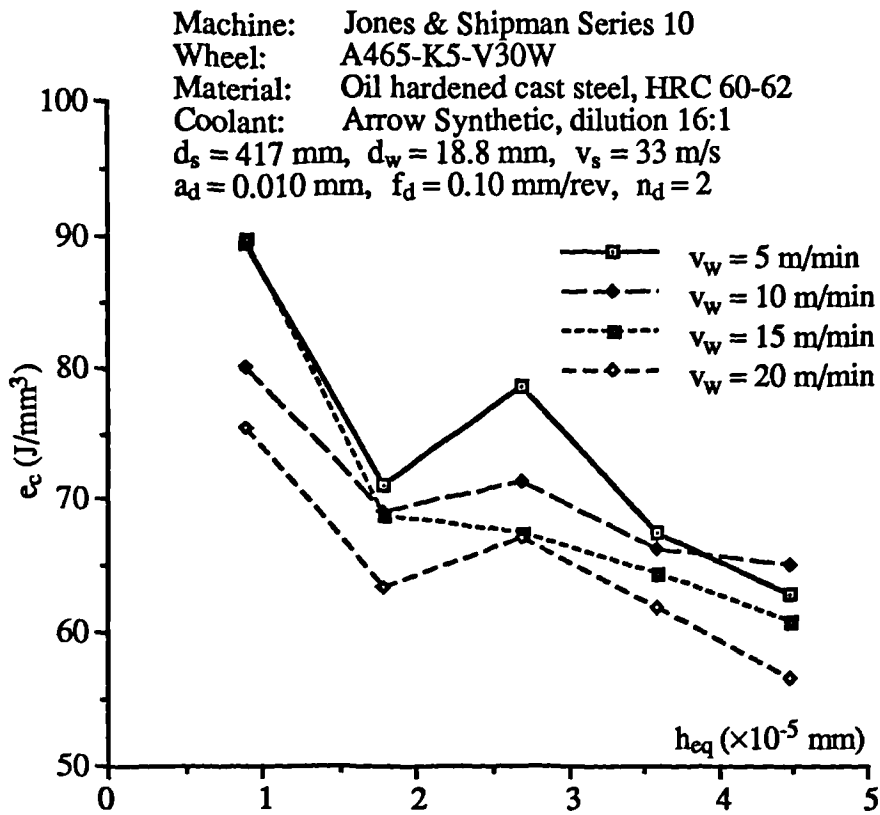


Figure 5.13 Effects of equivalent chip thickness on specific energy

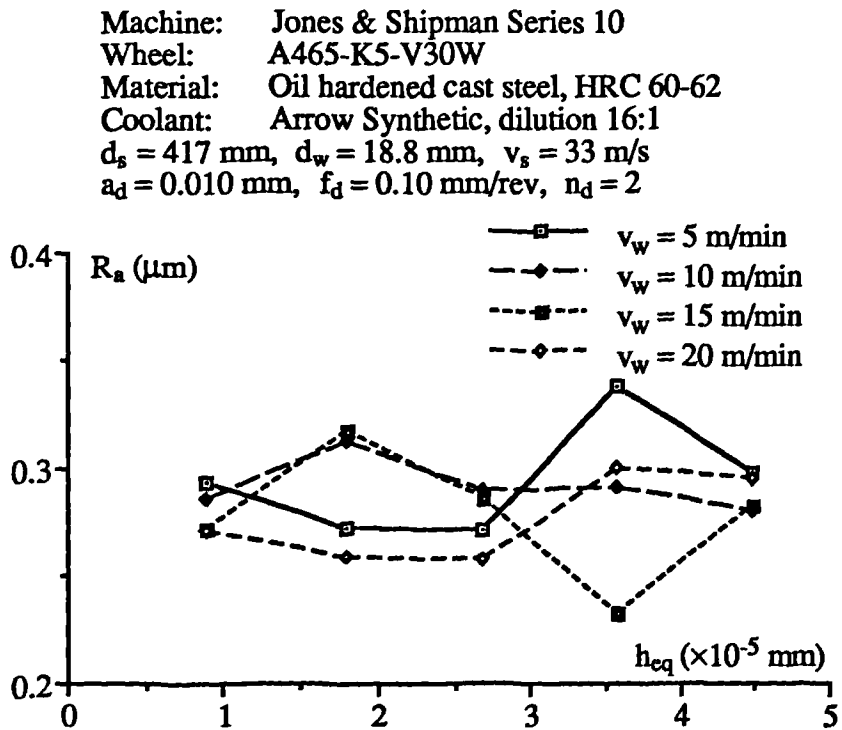
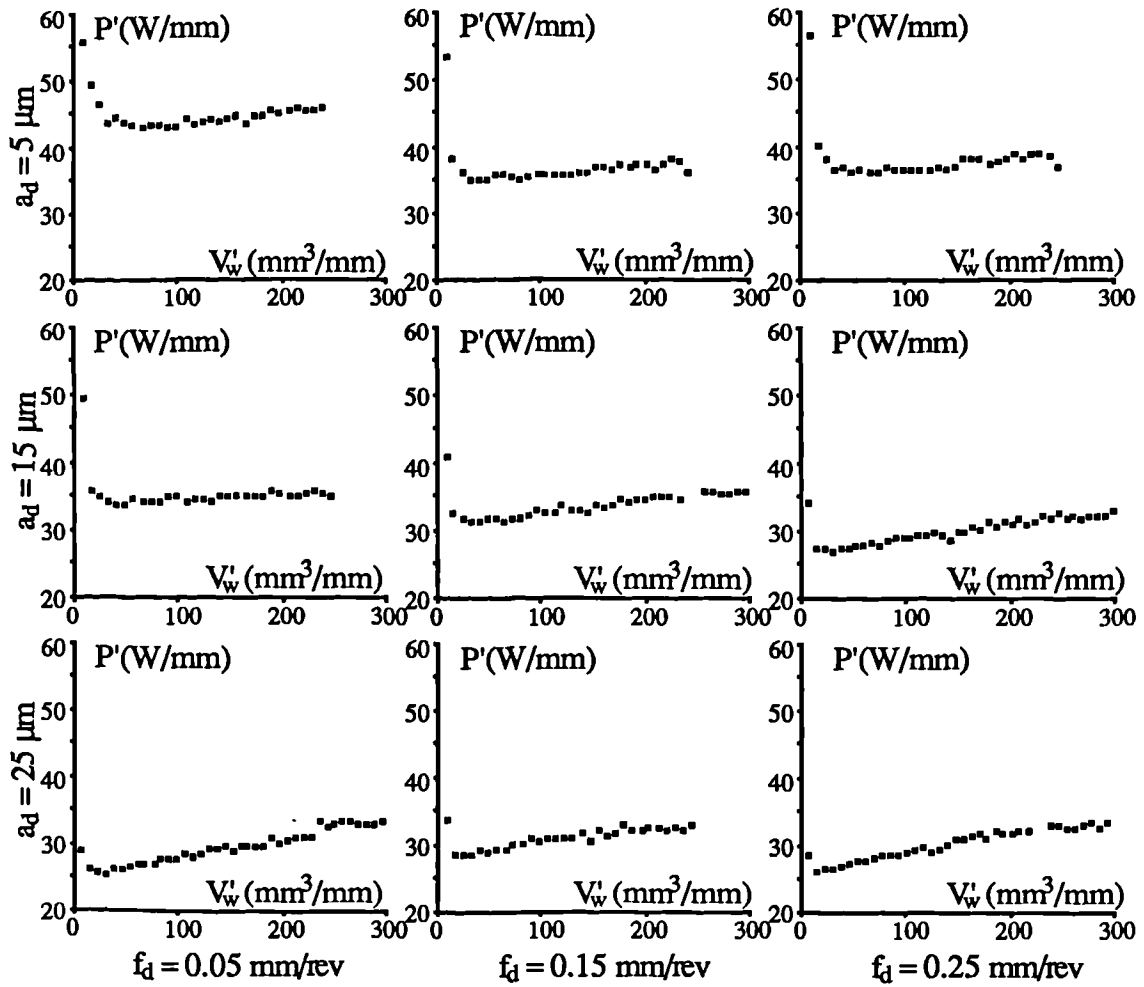
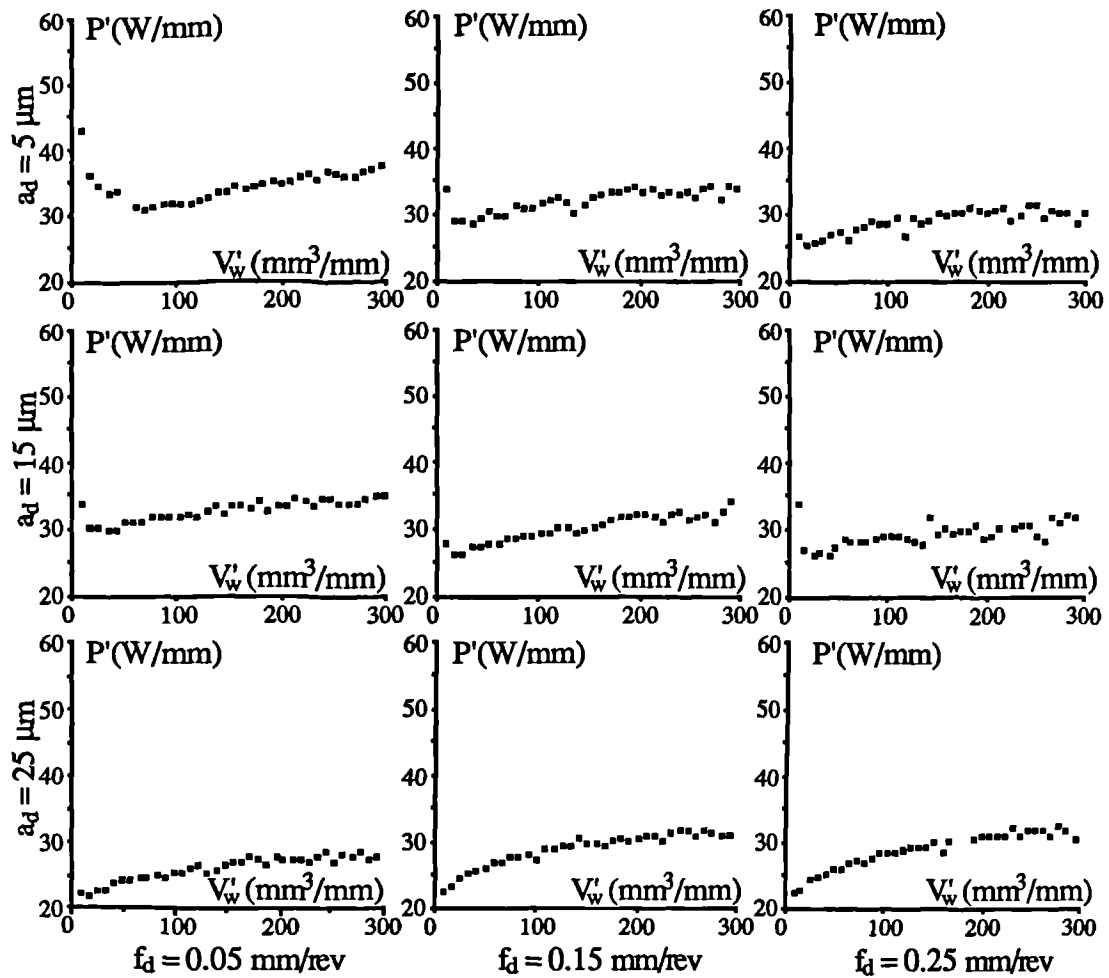


Figure 5.14 Effects of equivalent chip thickness on surface roughness



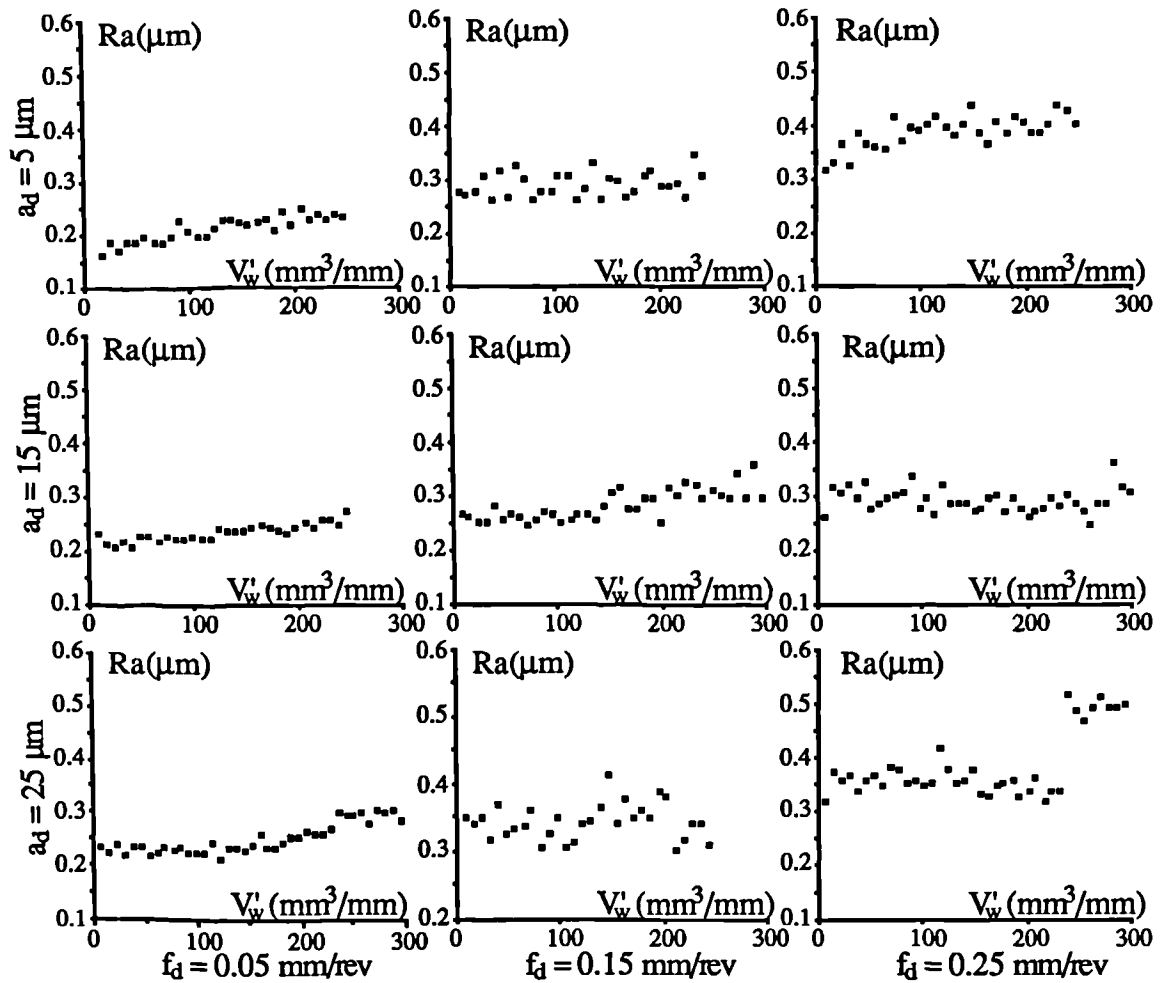
Machine: Jones & Shipman Series 10
 Wheel: A465-K5-V30W
 Material: Oil hardened cast steel, HRC 60-62
 Coolant: Arrow Synthetic, dilution 16:1
 Diamond sharpness ratio: $a_d/b_d \approx 0.05$
 $v_s = 33$ m/s, $v_w = 250$ mm/s, $v_f = 10$ $\mu\text{m/s}$
 $d_s \approx 370$ mm, $d_w \approx 17$ mm, $V_w' \approx 245$ mm³/mm

Figure 5.15 Effects of dressing condition on grinding power (sharp diamond)



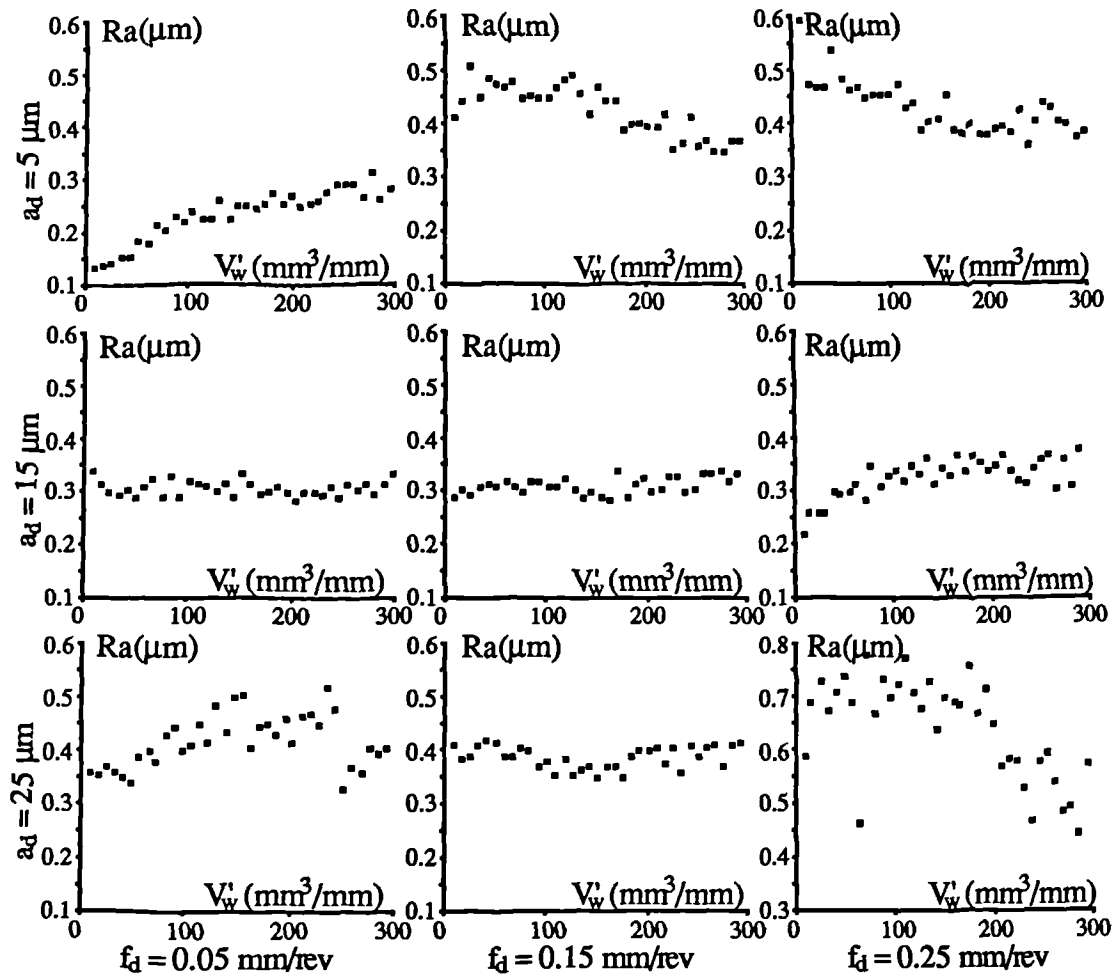
Machine: Jones & Shipman Series 10
 Wheel: A465-K5-V30W
 Material: Oil hardened cast steel, HRC 60-62
 Coolant: Arrow Synthetic, dilution 16:1
 Diamond sharpness ratio: $a_d/b_d \approx 0.02$
 $v_s = 33 \text{ m/s}$, $v_w = 250 \text{ mm/s}$, $v_f = 10 \mu\text{m/s}$
 $d_s \approx 390 \text{ mm}$, $d_w \approx 17 \text{ mm}$, $V_w' \approx 490 \text{ mm}^3/\text{mm}$

Figure 5.16 Effects of dressing condition on grinding power (blunt diamond)



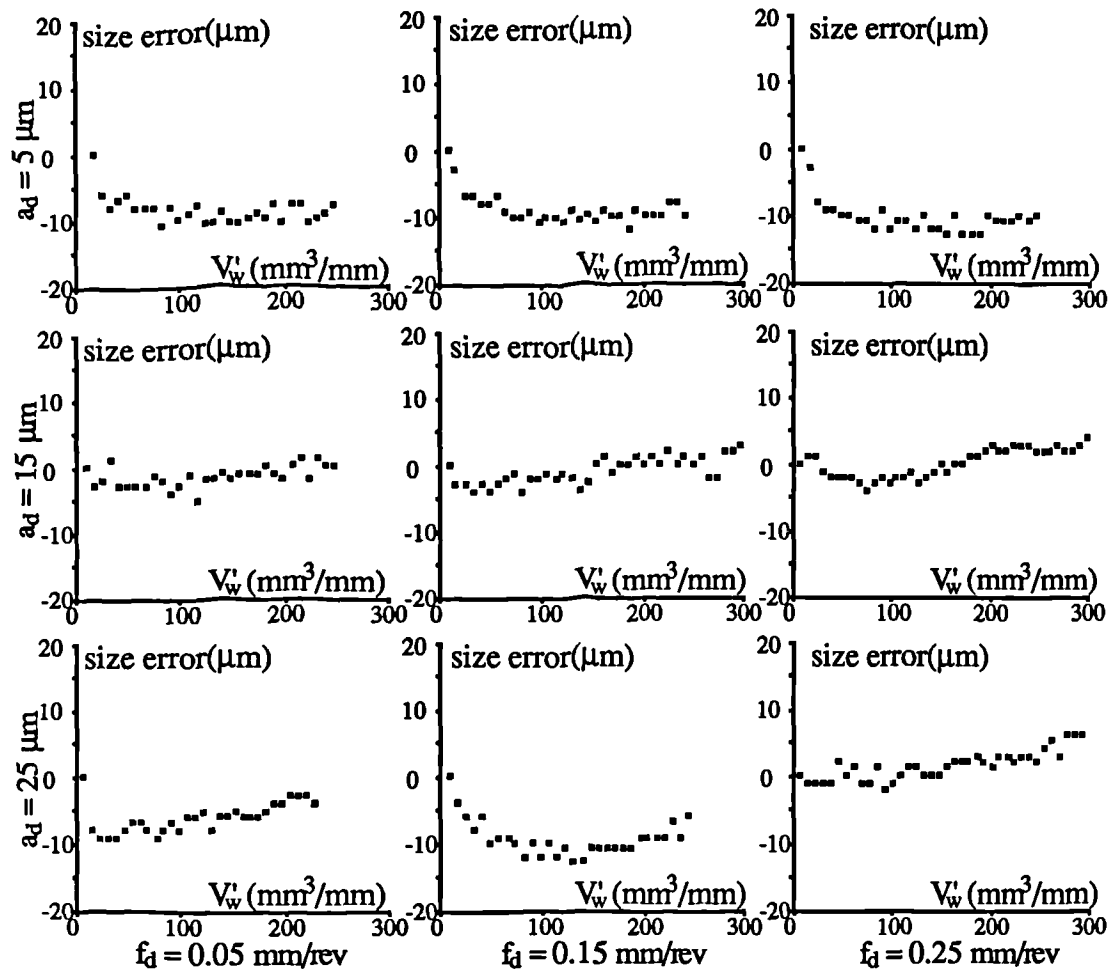
Machine: Jones & Shipman Series 10
 Wheel: A465-K5-V30W
 Material: Oil hardened cast steel, HRC 60-62
 Coolant: Arrow Synthetic, dilution 16:1
 Diamond sharpness ratio: $a_d/b_d \approx 0.05$
 $v_s = 33 \text{ m/s}$, $v_w = 250 \text{ mm/s}$, $v_f = 10 \mu\text{m/s}$
 $d_s \approx 370 \text{ mm}$, $d_w \approx 17 \text{ mm}$, $V'_w \approx 245 \text{ mm}^3/\text{mm}$

Figure 5.17 Effects of dressing condition on ground surface roughness (sharp diamond)



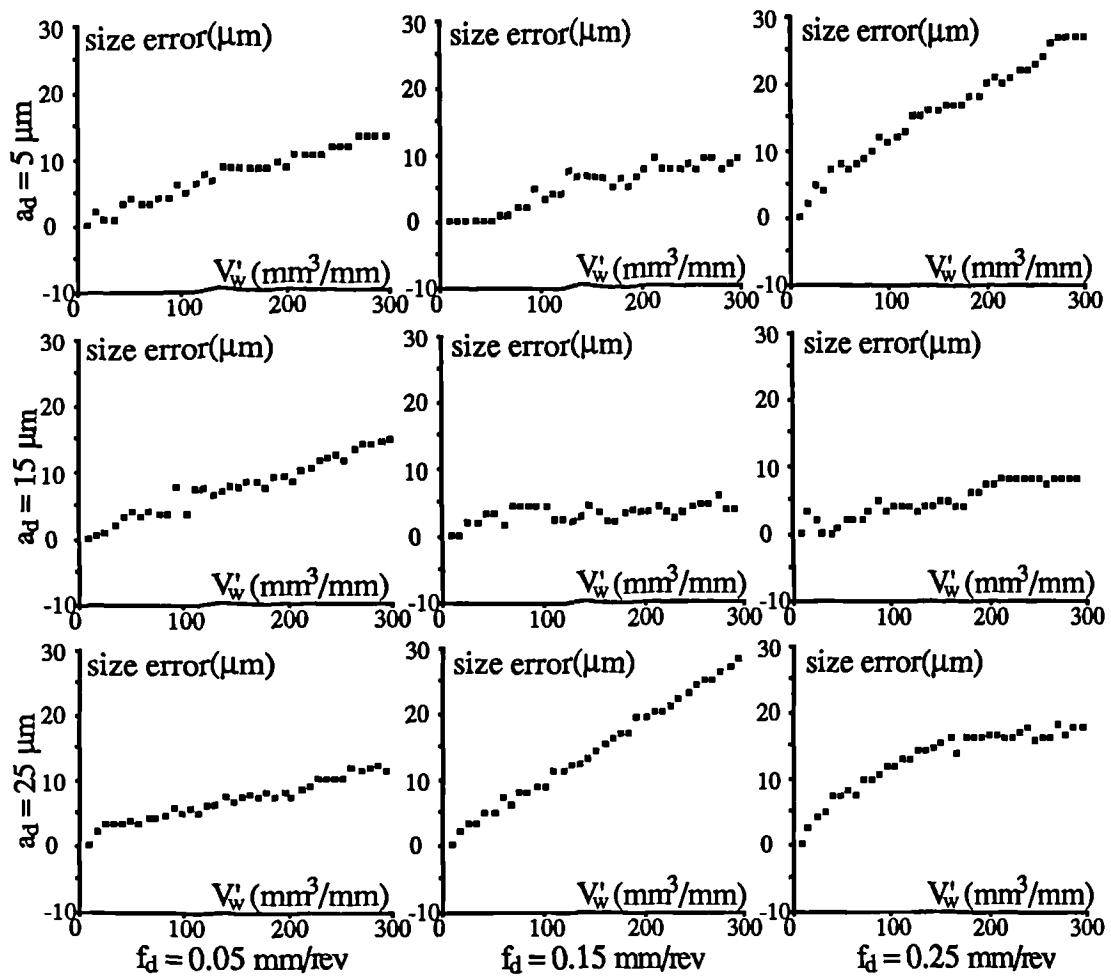
Machine: Jones & Shipman Series 10
 Wheel: A465-K5-V30W
 Material: Oil hardened cast steel, HRC 60-62
 Coolant: Arrow Synthetic, dilution 16:1
 Diamond sharpness ratio: $a_d/b_d \approx 0.02$
 $v_s = 33 \text{ m/s}$, $v_w = 250 \text{ mm/s}$, $v_f = 10 \text{ μm/s}$
 $d_s \approx 390 \text{ mm}$, $d_w \approx 17 \text{ mm}$, $V_w \approx 490 \text{ mm}^3/\text{mm}$

Figure 5.18 Effects of dressing conditions on ground surface roughness (blunt diamond)



Machine: Jones & Shipman Series 10
 Wheel: A465-K5-V30W
 Material: Oil hardened cast steel, HRC 60-62
 Coolant: Arrow Synthetic, dilution 16:1
 Diamond sharpness ratio: $a_d/b_d \approx 0.05$
 $v_s = 33 \text{ m/s}$, $v_w = 250 \text{ mm/s}$, $v_f = 10 \mu\text{m/s}$
 $d_s \approx 370 \text{ mm}$, $d_w \approx 17 \text{ mm}$, $V_w' \approx 245 \text{ mm}^3/\text{mm}$

Figure 5.19 Effects of dressing conditions on size error (sharp diamond)



Machine: Jones & Shipman Series 10
 Wheel: A465-K5-V30W
 Material: Oil hardened cast steel, HRC 60-62
 Coolant: Arrow Synthetic, dilution 16:1
 Diamond sharpness ratio: $a_d/b_d \approx 0.02$
 $v_s = 33 \text{ m/s}$, $v_w = 250 \text{ mm/s}$, $v_f = 10 \mu\text{m/s}$
 $d_s \approx 390 \text{ mm}$, $d_w \approx 17 \text{ mm}$, $V_w \approx 490 \text{ mm}^3/\text{mm}$

Figure 5.20 Effects of dressing condition on size error (blunt diamond)

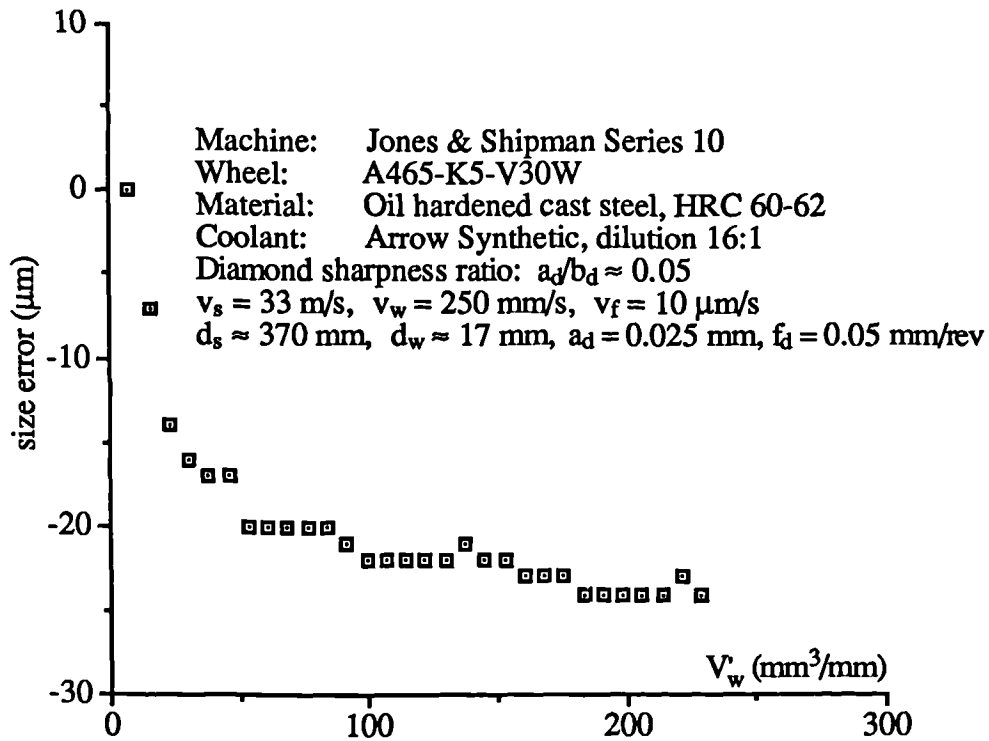


Figure 5.21 Thermal effect on size error

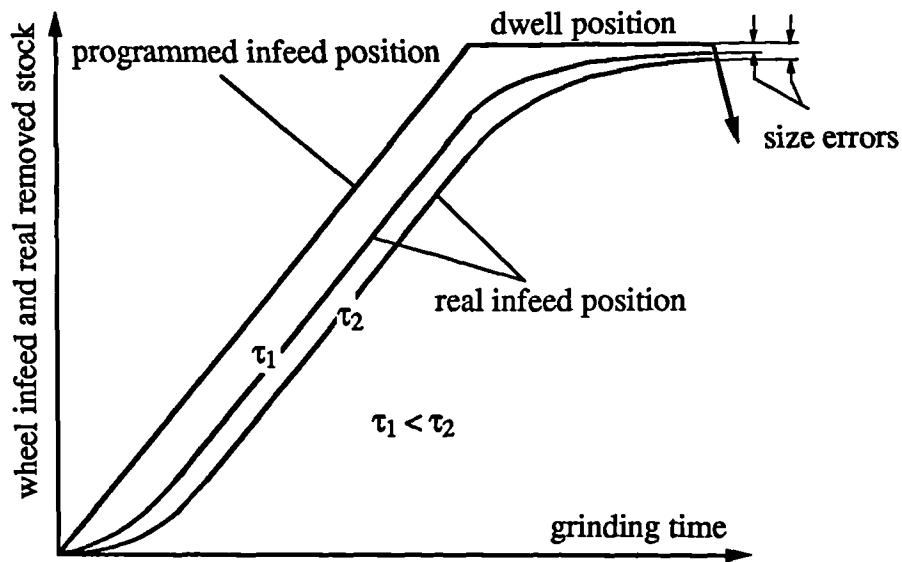
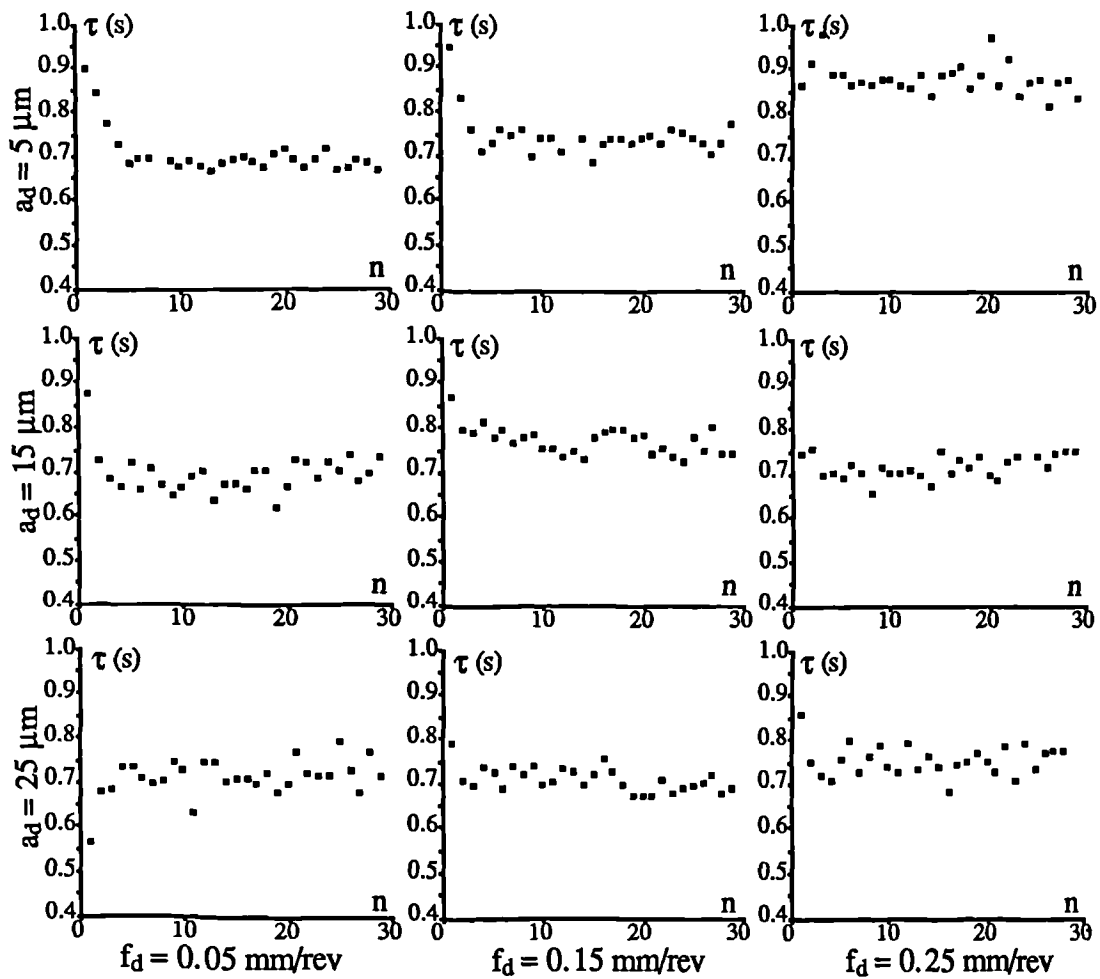
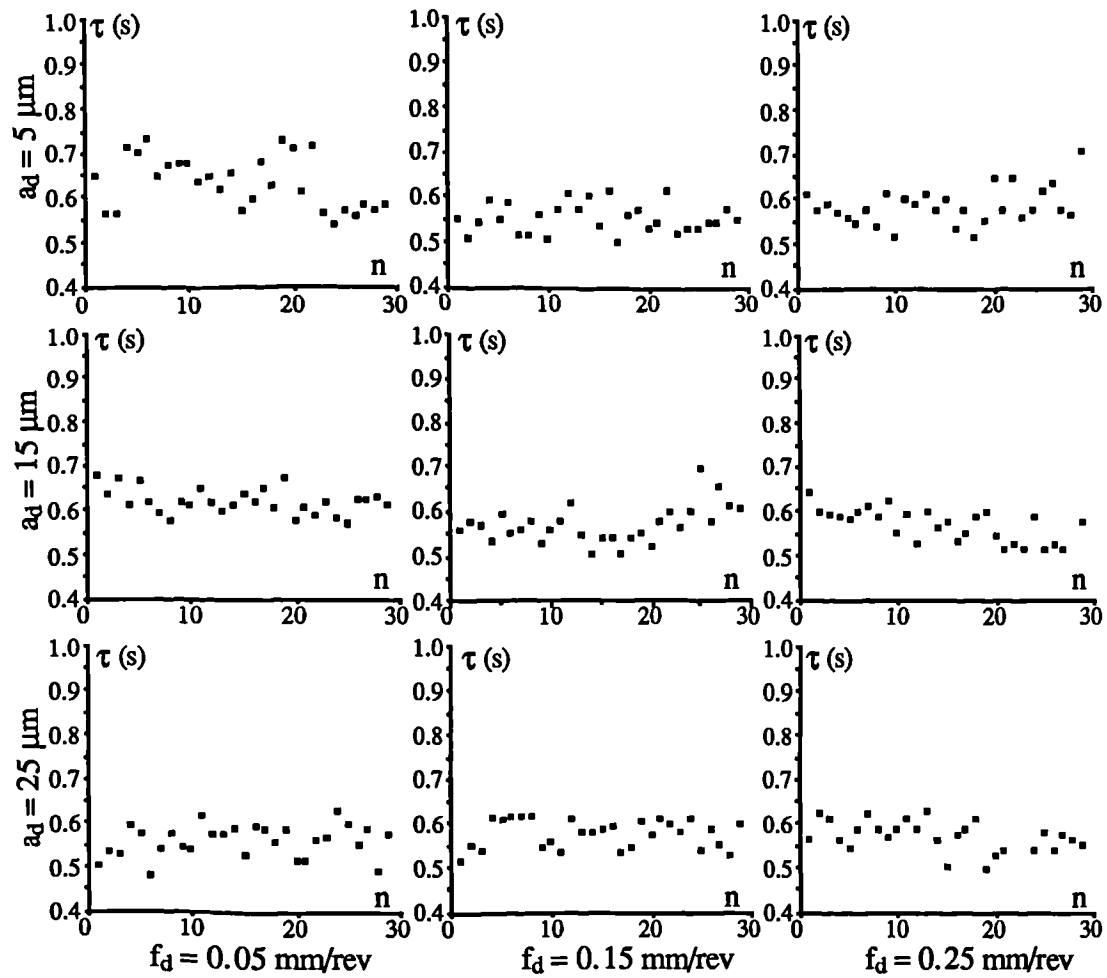


Figure 5.22 Size error generated due to variation of wheel sharpness



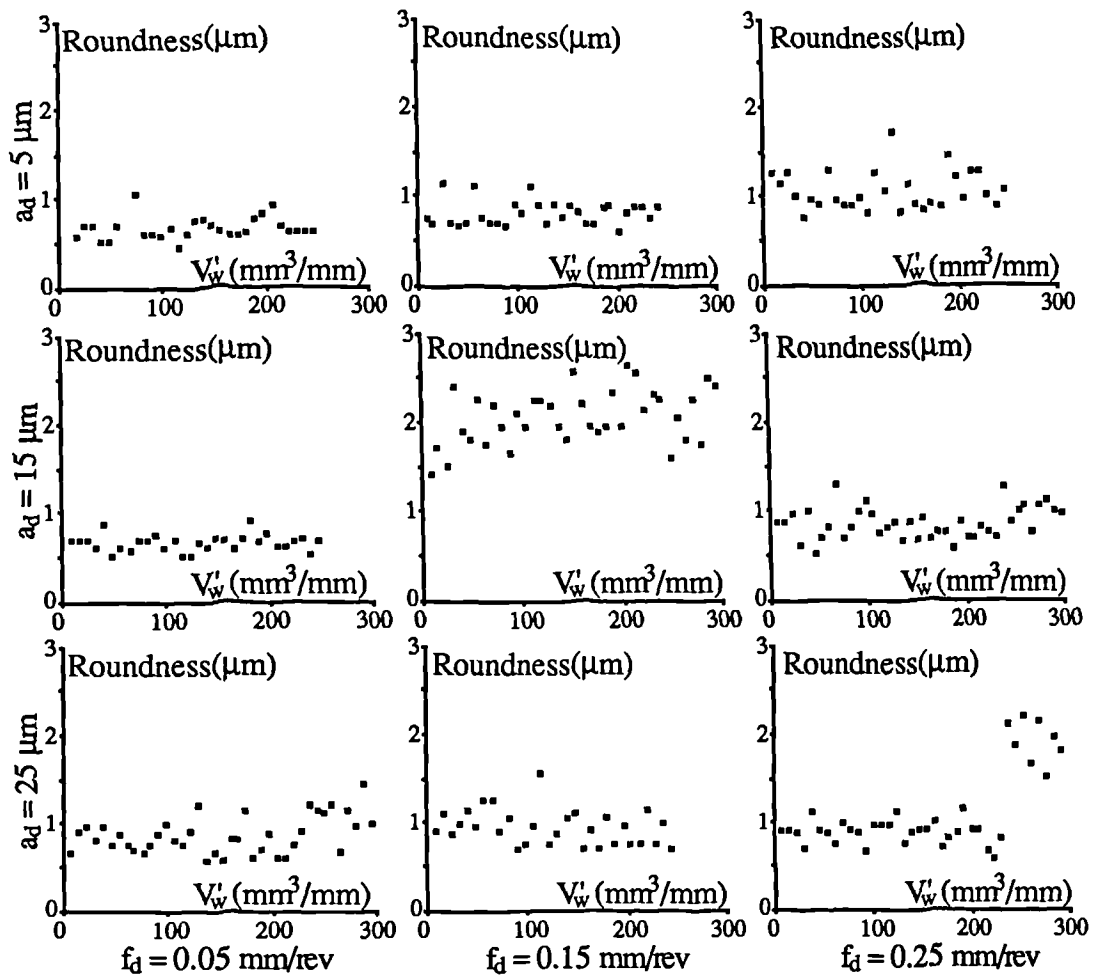
Machine: Jones & Shipman Series 10
 Wheel: A465-K5-V30W
 Material: Oil hardened cast steel, HRC 60-62
 Coolant: Arrow Synthetic, dilution 16:1
 Diamond sharpness ratio: $a_d/b_d \approx 0.05$
 $v_s = 33$ m/s, $v_w = 250$ mm/s, $v_f = 10$ μ m/s
 $d_s \approx 370$ mm, $d_w \approx 17$ mm, $V_w \approx 8.16$ (mm^3/mm)/workpiece

Figure 5.23 Variation of time constant with workpiece number in grinding for various dressing conditions (sharp diamond)



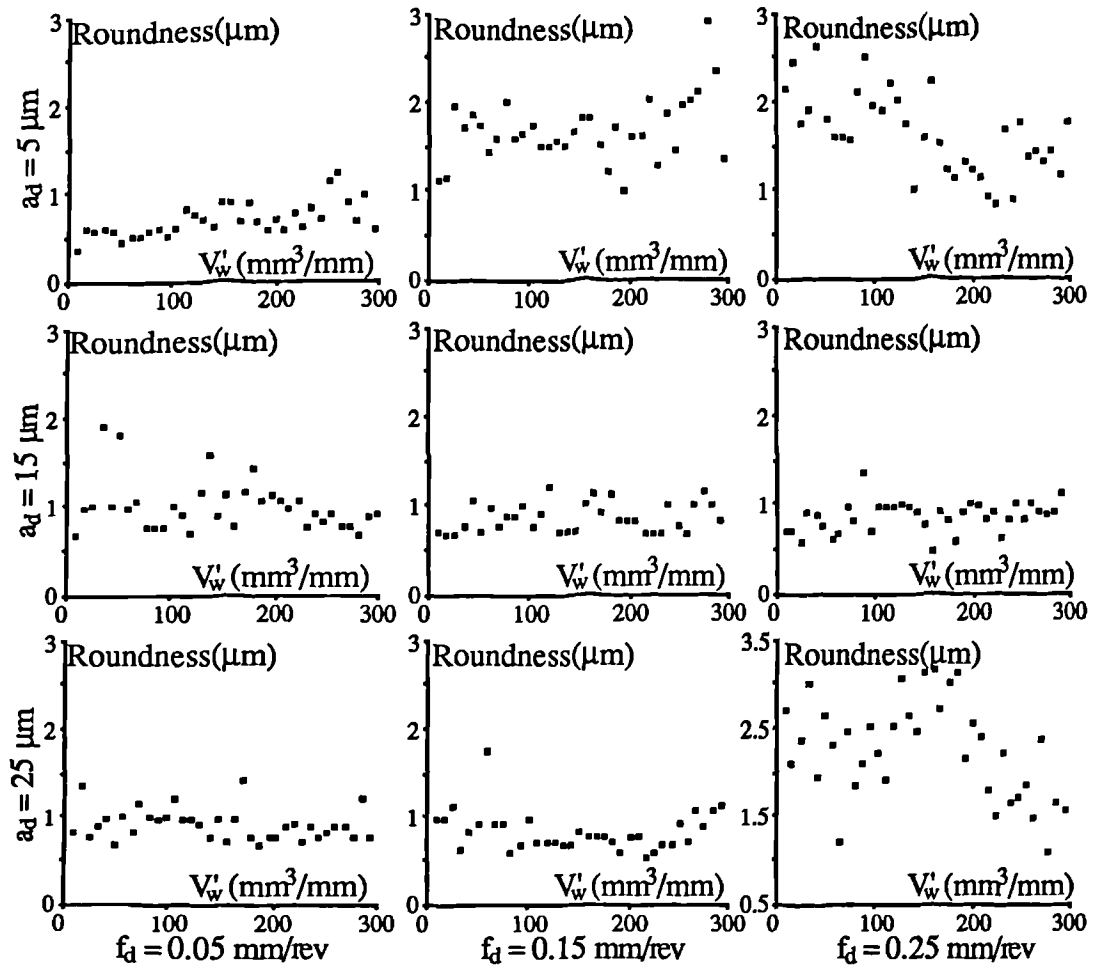
Machine: Jones & Shipman Series 10
 Wheel: A465-K5-V30W
 Material: Oil hardened cast steel, HRC 60-62
 Coolant: Arrow Synthetic, dilution 16:1
 Diamond sharpness ratio: $a_d/b_d \approx 0.02$
 $v_s \approx 33 \text{ m/s}$, $v_w = 250 \text{ mm/s}$, $v_f = 10 \text{ μm/s}$
 $d_s \approx 390 \text{ mm}$, $d_w \approx 17 \text{ mm}$, $V_w \approx 8.16 \text{ (mm}^3\text{/mm)/workpiece}$

Figure 5.24 Variation of time constant with workpiece number in grinding for various dressing conditions (blunt diamond)



Machine: Jones & Shipman Series 10
 Wheel: A465-K5-V30W
 Material: Oil hardened cast steel, HRC 60-62
 Coolant: Arrow Synthetic, dilution 16:1
 Diamond sharpness ratio: $a_d/b_d \approx 0.05$
 $v_s = 33 \text{ m/s}$, $v_w = 250 \text{ mm/s}$, $v_f = 10 \mu\text{m/s}$
 $d_s \approx 370 \text{ mm}$, $d_w \approx 17 \text{ mm}$, $V_w \approx 245 \text{ mm}^3/\text{mm}$

Figure 5.25 Effects of dressing condition on roundness (sharp diamond)



Machine: Jones & Shipman Series 10
 Wheel: A465-K5-V30W
 Material: Oil hardened cast steel, HRC 60-62
 Coolant: Arrow Synthetic, dilution 16:1
 Diamond sharpness ratio: $a_d/b_d \approx 0.02$
 $v_s = 33 \text{ m/s}$, $v_w = 250 \text{ mm/s}$, $v_f = 10 \mu\text{m/s}$
 $d_s \approx 390 \text{ mm}$, $d_w \approx 17 \text{ mm}$, $V_w' \approx 490 \text{ mm}^3/\text{mm}$

Figure 5.26 Effects of dressing condition on roundness (blunt diamond)

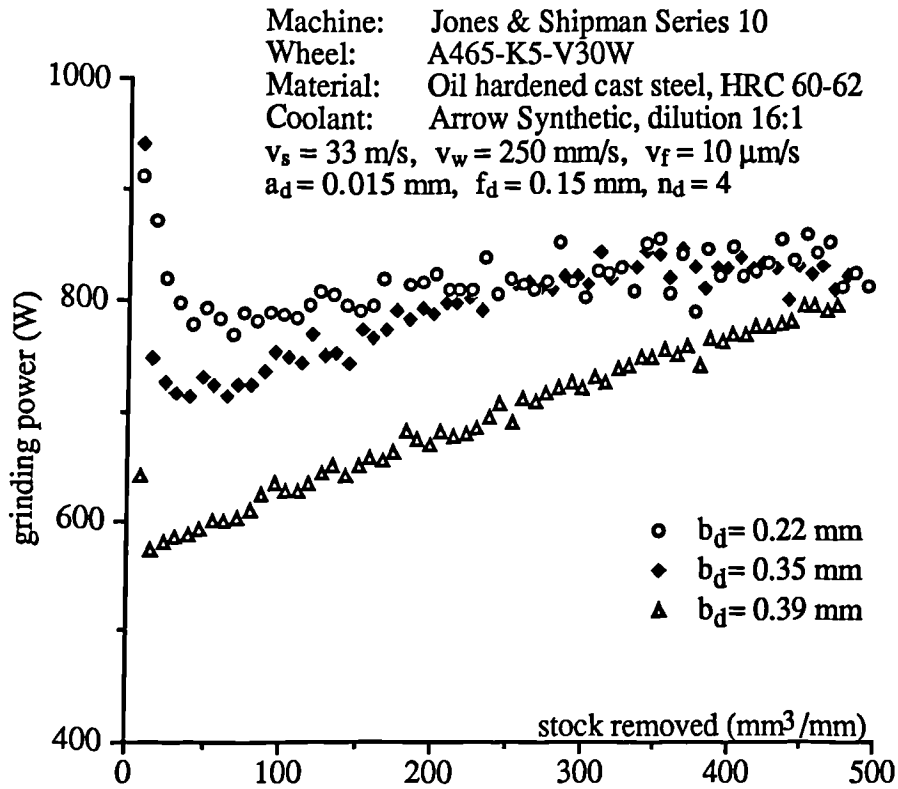


Figure 5.27 Grinding power with width of dressing diamond

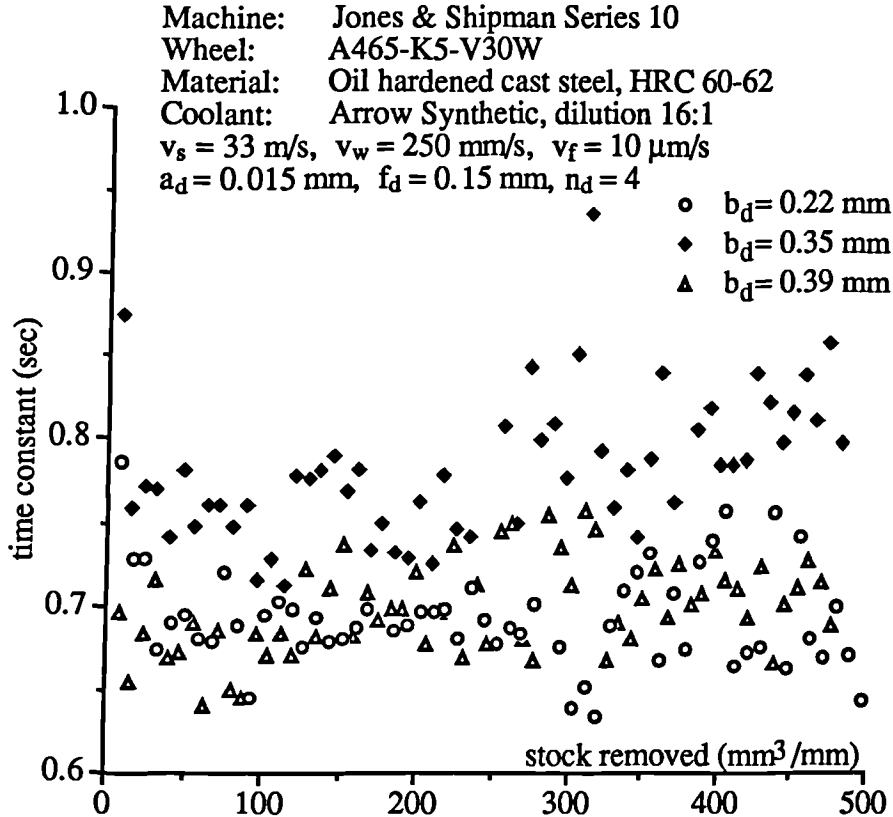


Figure 5.28 Time constant with width of dressing diamond

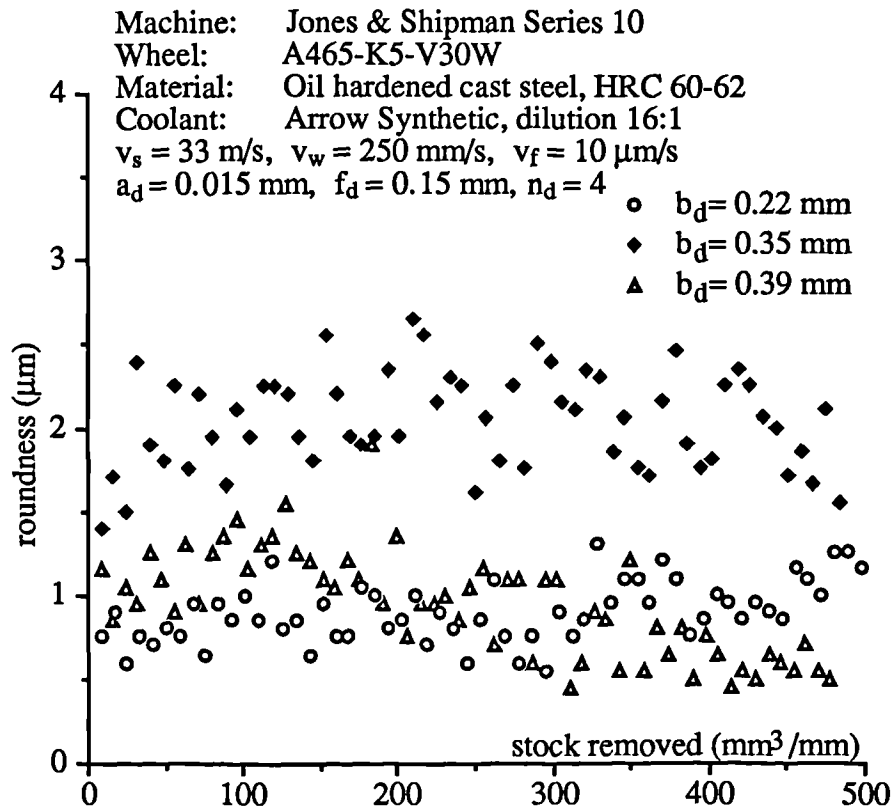


Figure 5.29 Roundness with width of dressing diamond

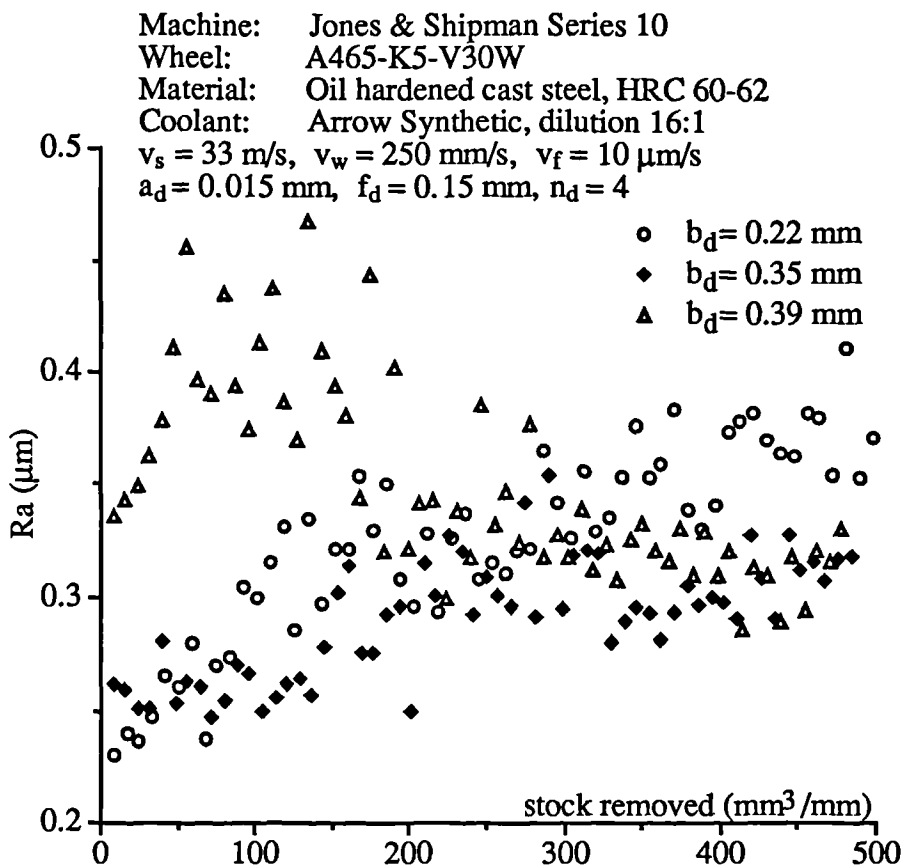


Figure 5.30 Surface roughness with width of dressing diamond

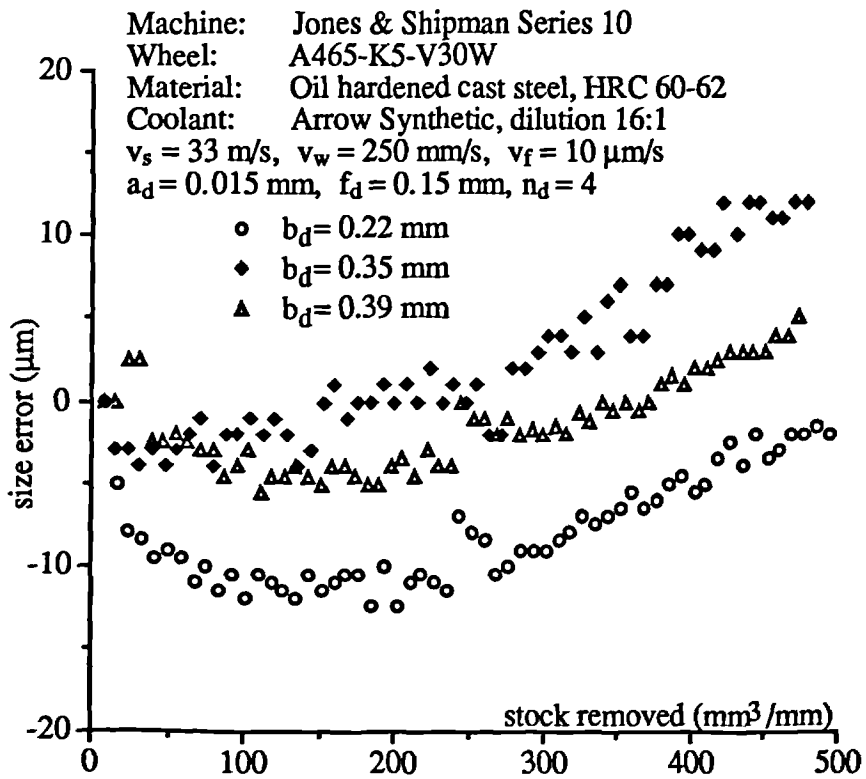
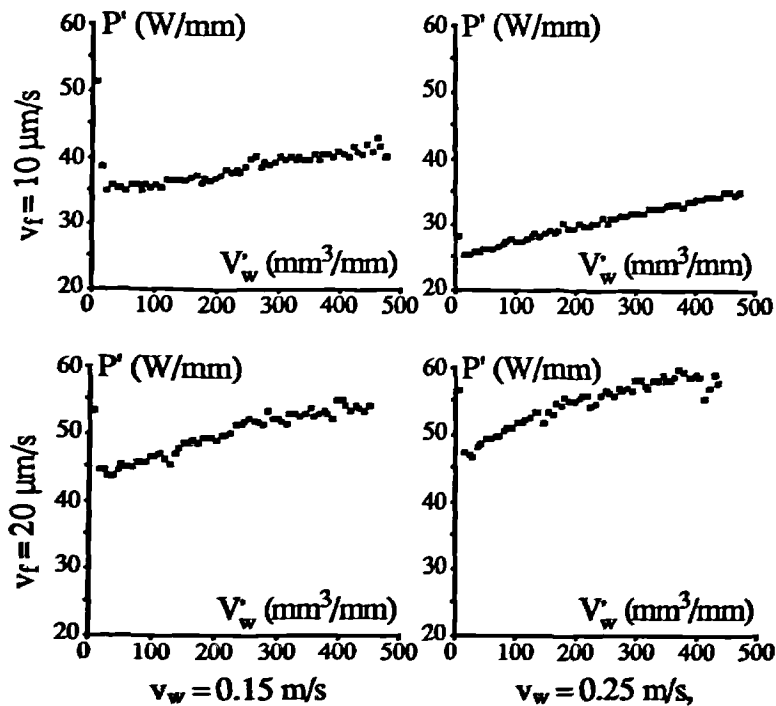
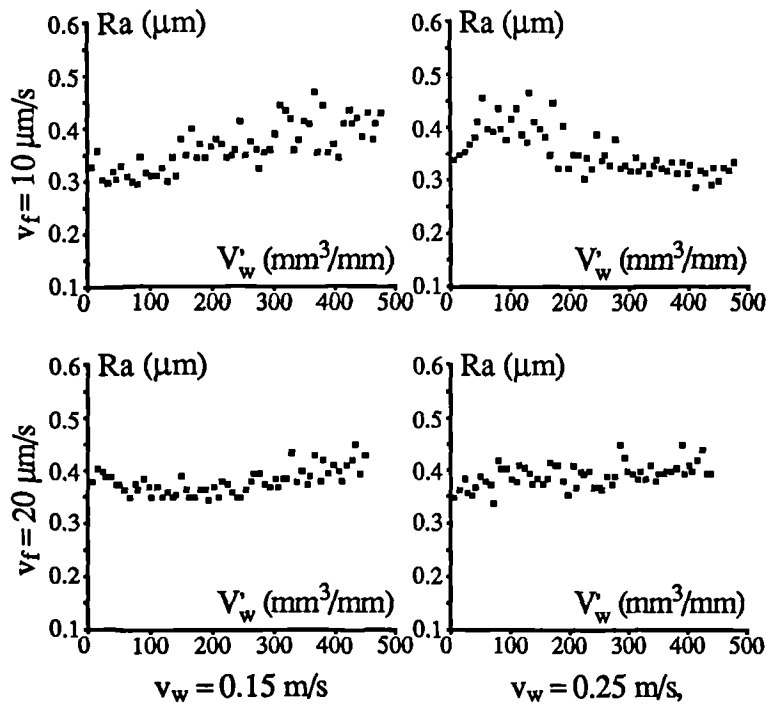


Figure 5.31 Size error with width of dressing diamond



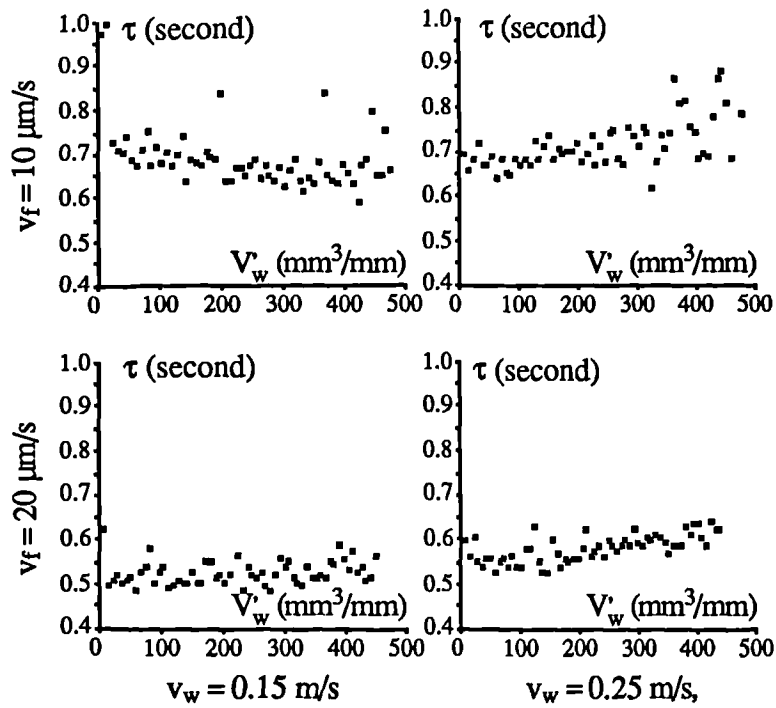
Machine: Jones & Shipman Series 10
 Wheel: A465-K5-V30W
 Material: Oil hardened cast steel, HRC 60-62
 Coolant: Arrow Synthetic, dilution 16:1
 Diamond sharpness ratio: $a_d/b_d \approx 0.05$
 $a_d = 0.015 \text{ mm}$, $f_d = 0.15 \text{ mm}$, $n_d = 4$
 $d_s \approx 365 \text{ mm}$, $d_w \approx 16 \text{ mm}$

Figure 5.32 Effect of grinding conditions on grinding power



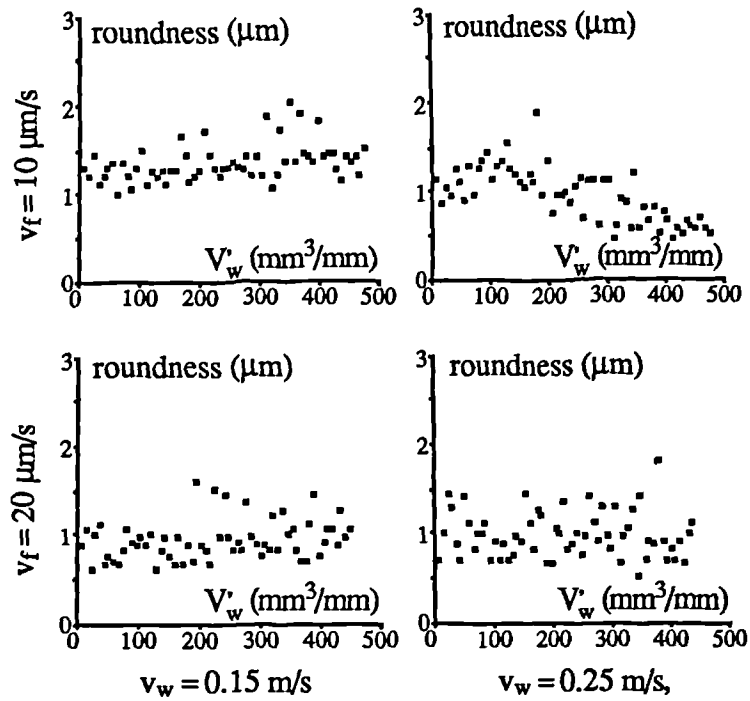
Machine: Jones & Shipman Series 10
 Wheel: A465-K5-V30W
 Material: Oil hardened cast steel, HRC 60-62
 Coolant: Arrow Synthetic, dilution 16:1
 Diamond sharpness ratio: $a_d/b_d \approx 0.05$
 $a_d = 0.015 \text{ mm}$, $f_d = 0.15 \text{ mm}$, $n_d = 4$
 $d_s \approx 365 \text{ mm}$, $d_w \approx 16 \text{ mm}$

Figure 5.33 Effect of grinding conditions on surface roughness



Machine: Jones & Shipman Series 10
 Wheel: A465-K5-V30W
 Material: Oil hardened cast steel, HRC 60-62
 Coolant: Arrow Synthetic, dilution 16:1
 Diamond sharpness ratio: $a_d/b_d \approx 0.05$
 $a_d = 0.015 \text{ mm}$, $f_d = 0.15 \text{ mm}$, $n_d = 4$
 $d_s \approx 365 \text{ mm}$, $d_w \approx 16 \text{ mm}$

Figure 5.34 Effect of grinding conditions on time constant



Machine: Jones & Shipman Series 10
 Wheel: A465-K5-V30W
 Material: Oil hardened cast steel, HRC 60-62
 Coolant: Arrow Synthetic, dilution 16:1
 Diamond sharpness ratio: $a_d/b_d \approx 0.05$
 $a_d = 0.015 \text{ mm}$, $f_d = 0.15 \text{ mm}$, $n_d = 4$
 $d_s \approx 365 \text{ mm}$, $d_w \approx 16 \text{ mm}$

Figure 5.35 Effect of grinding conditions on roundness

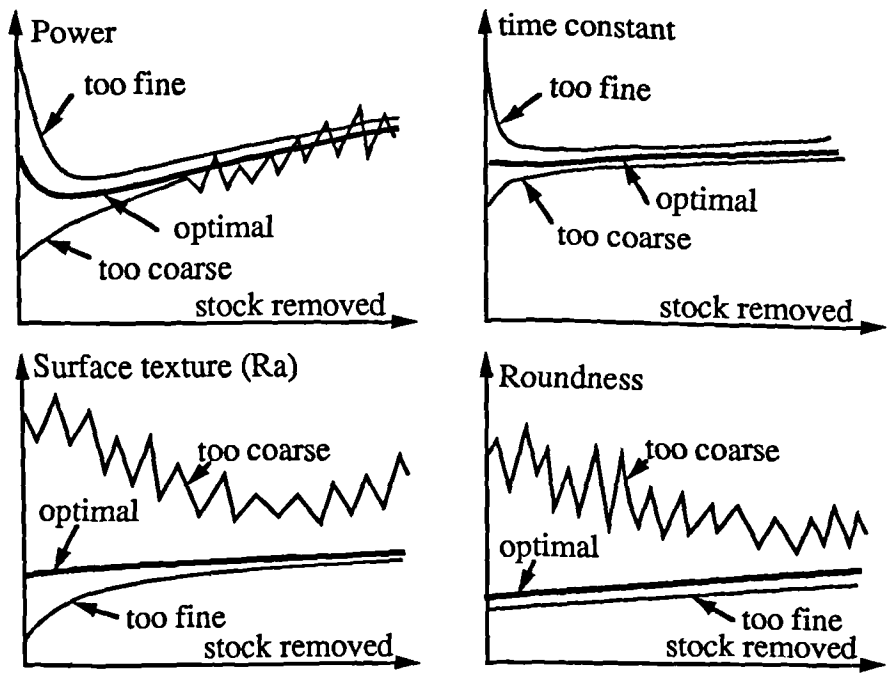


Figure 5.36 Idealized effects of dressing conditions on grinding behaviour

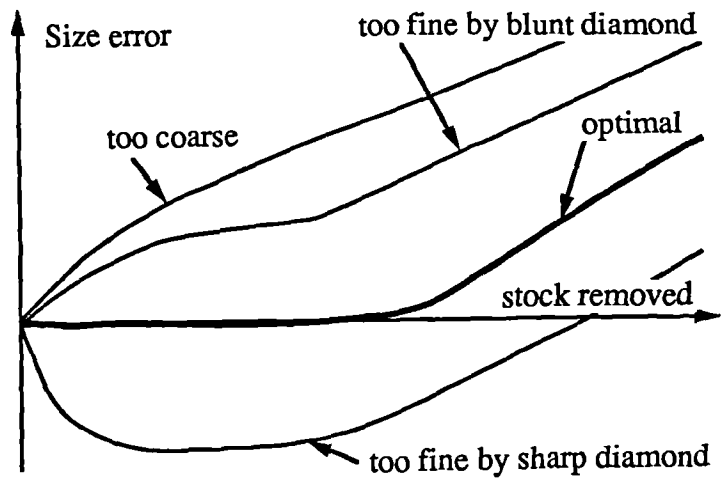


Figure 5.37 Idealized effect of dressing conditions on size error

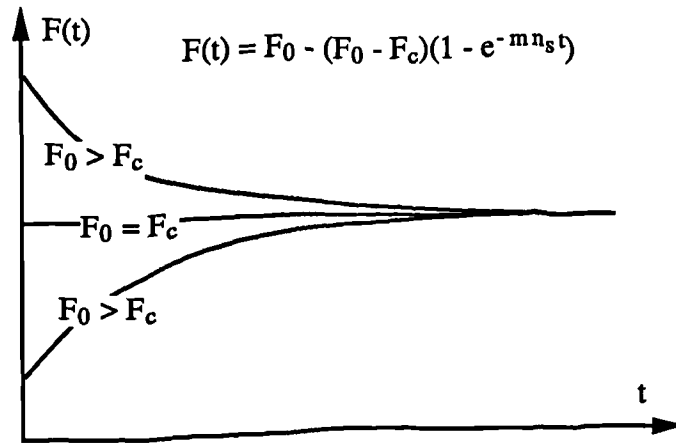


Figure 6.1 Changes of grinding force with grinding time

$$P' = [26.6 + (7.31 a_d^{-0.358} f_d^{-0.068} - 26.6) e^{-0.035 t}] h_{eq}^{0.831} \times 10^4 + 2.05 \times 10^{-4} t$$

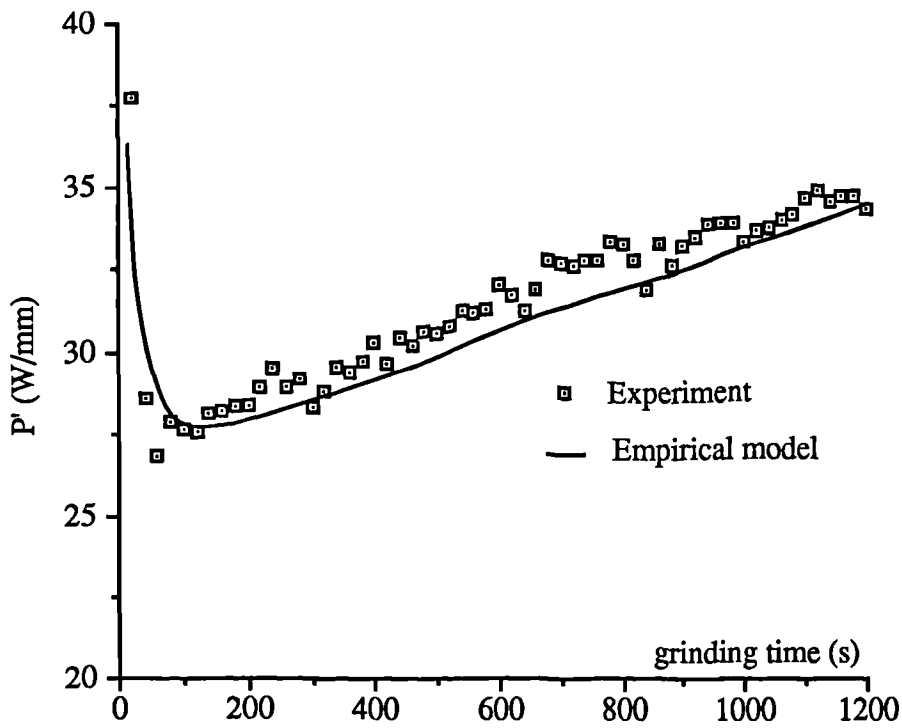


Figure 6.2 Changes of grinding power during wheel redress cycle

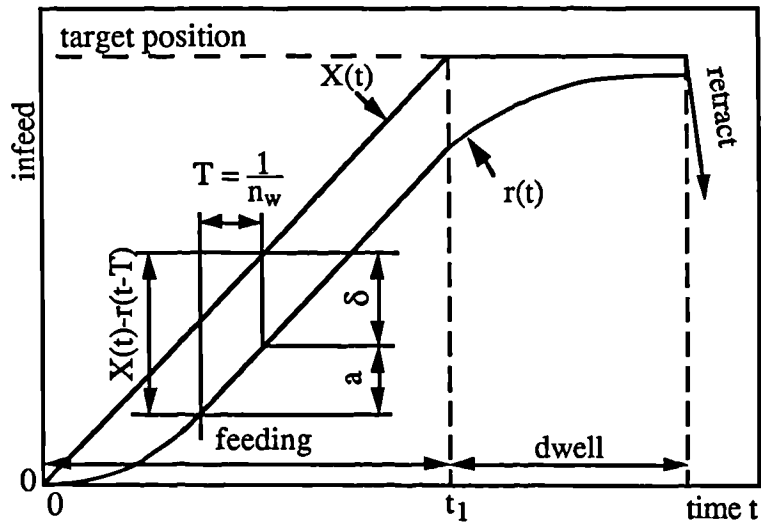


Figure 7.1 Conventional plunge grinding cycle

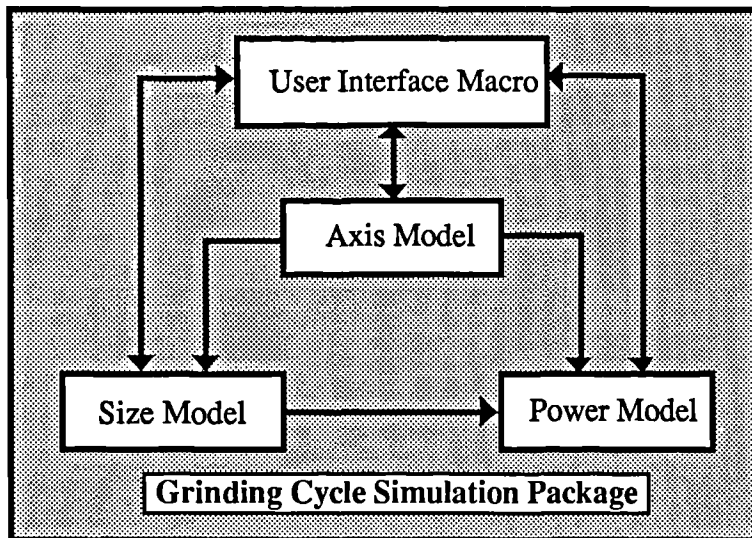


Figure 7.2 The structure of grinding cycle simulation package

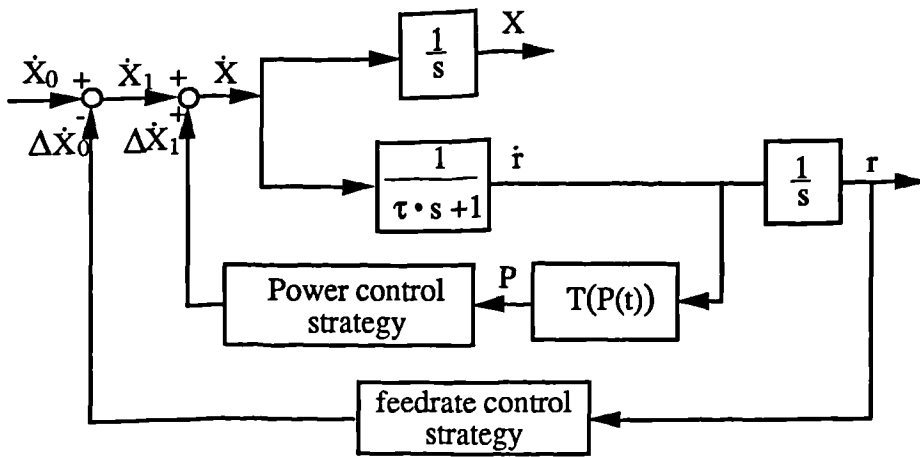


Figure 7.3 Block diagram of the simulation relationships

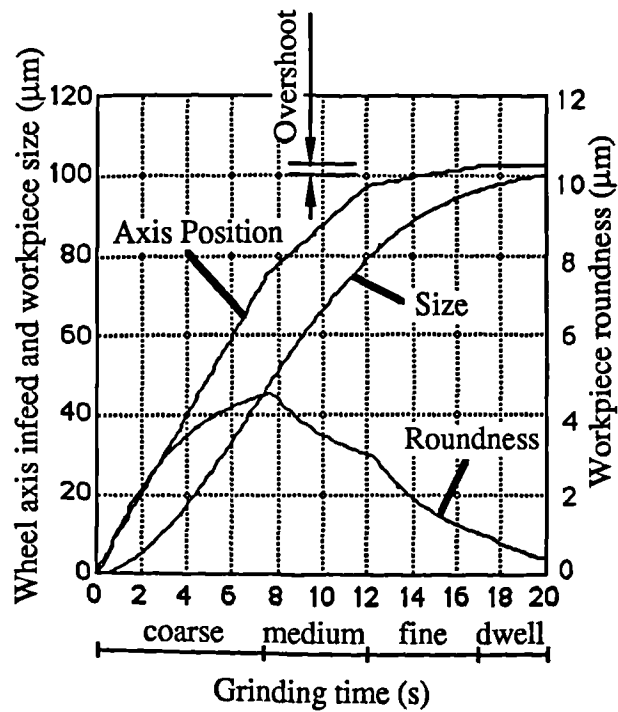
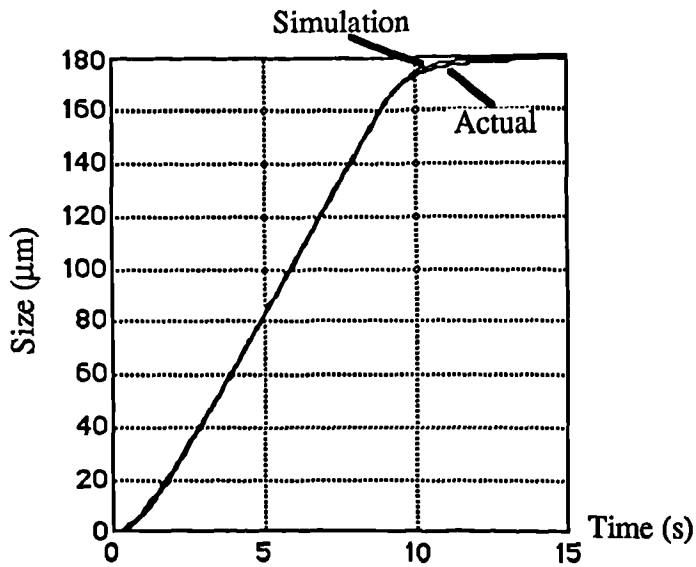


Figure 7.4 Multi-infeed and dwell cycle simulation



Machine: Jones & Shipman Series 10
 Wheel: A465-K5-V30W
 Material: Oil hardened cast steel, HRC 60-62
 Coolant: Arrow Synthetic, dilution rate 16:1
 $v_s = 33 \text{ m/s}$, $v_w = 167 \text{ mm/s}$, $v_f = 10 \text{ µm/s}$
 $a_d = 0.010 \text{ mm}$, $f_d = 0.10 \text{ mm/rev}$, $n_d = 2$
 $d_s \approx 390 \text{ mm}$, $d_w \approx 17 \text{ mm}$, $V_w \approx 490 \text{ mm}^3/\text{mm}$

Figure 7.5 Comparison between actual and simulated size reduction curves

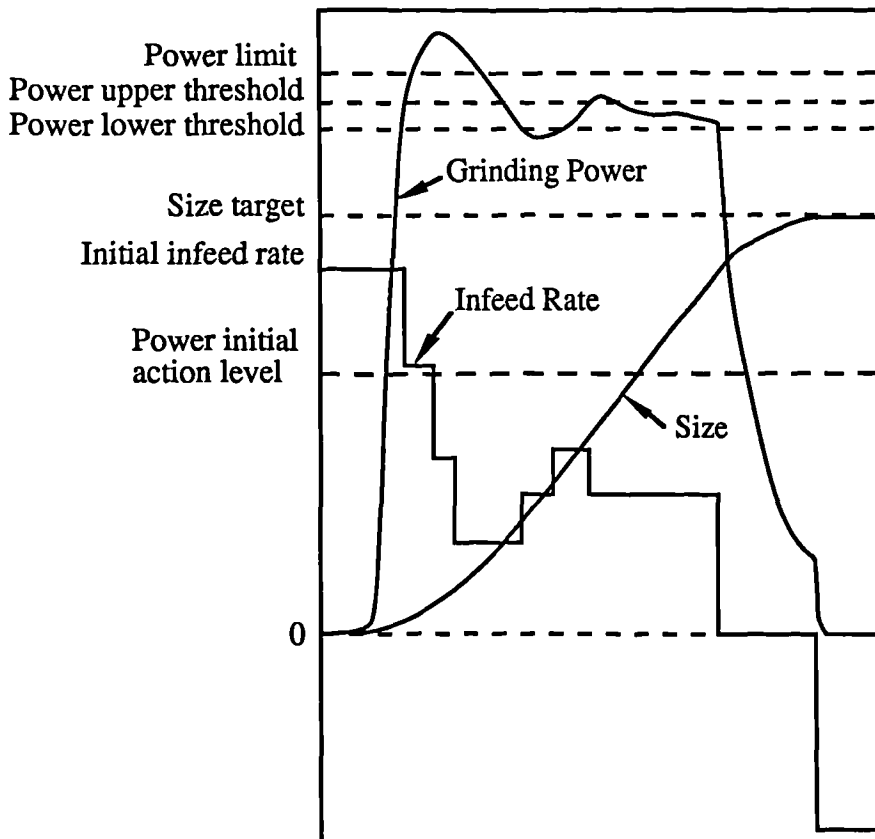


Figure 7.6 A simulated power control grinding cycle using a non-optimal in-process power control strategy

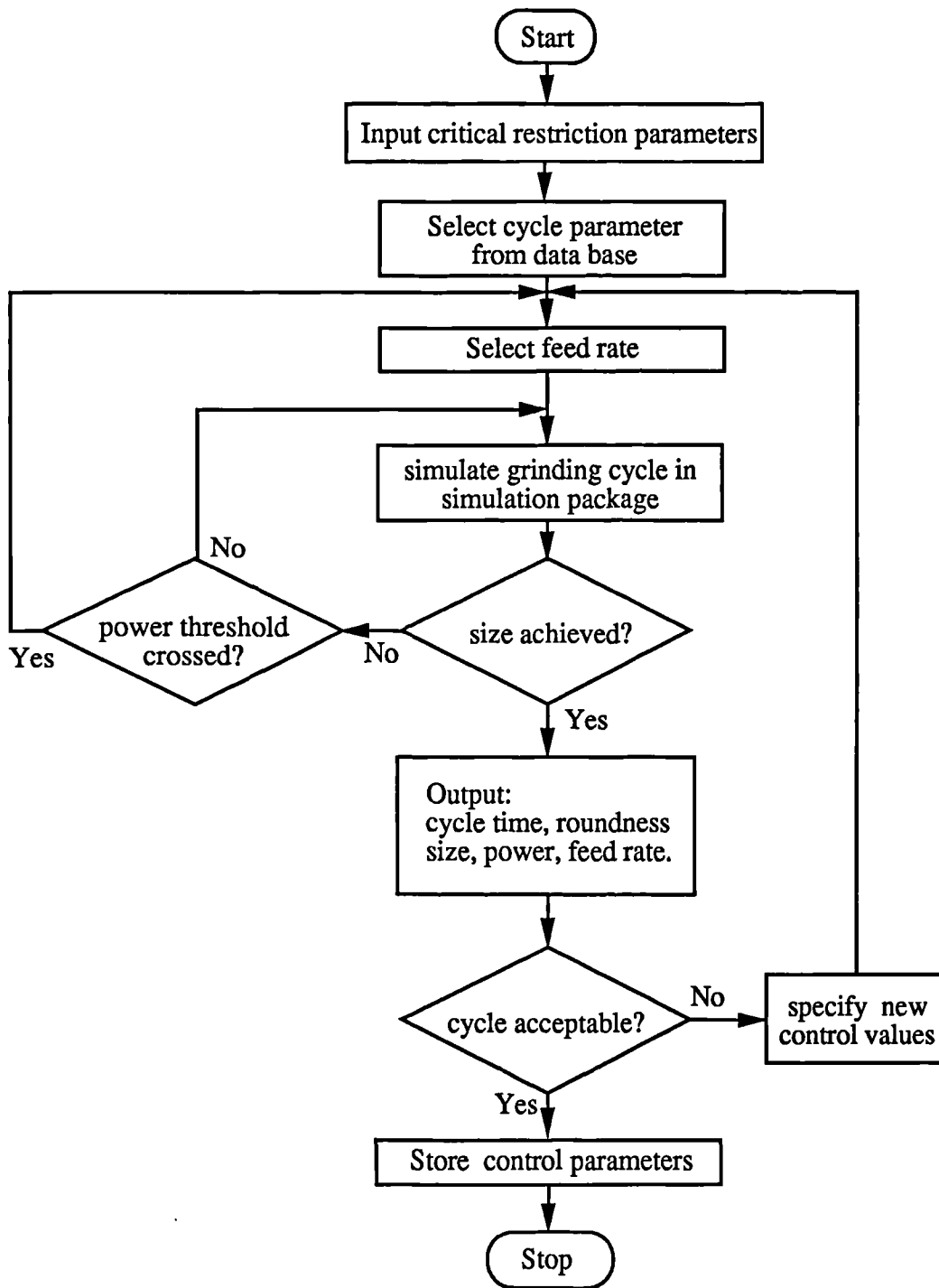


Figure 7.7 The flow chart for simulation of in-process power control

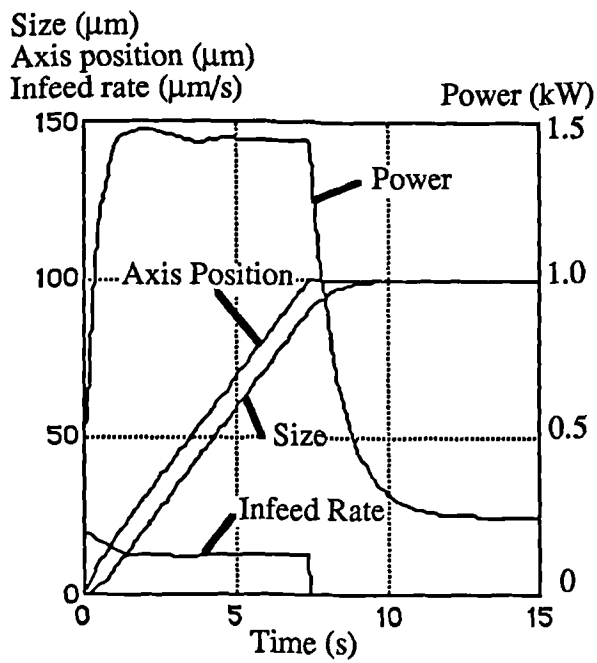


Figure 7.8 The simulated grinding cycle after optimisation

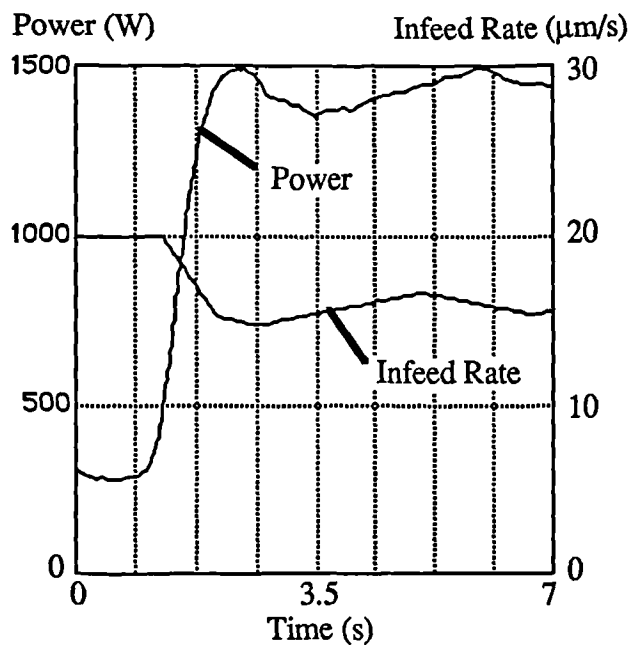


Figure 7.9 Experimental power control using the cycle determined by simulation

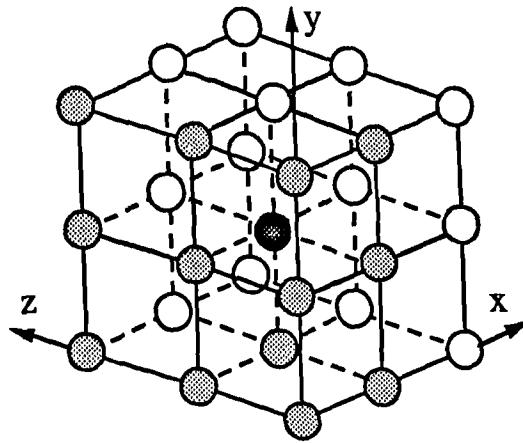


Figure 8.1 Orientation of grains for simulation of grinding

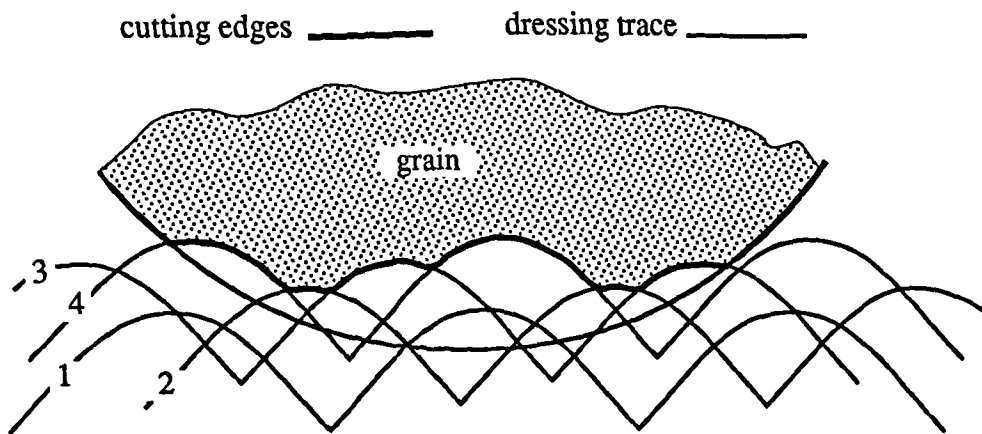


Figure 8.2 Cutting edges generated by dressing cutting

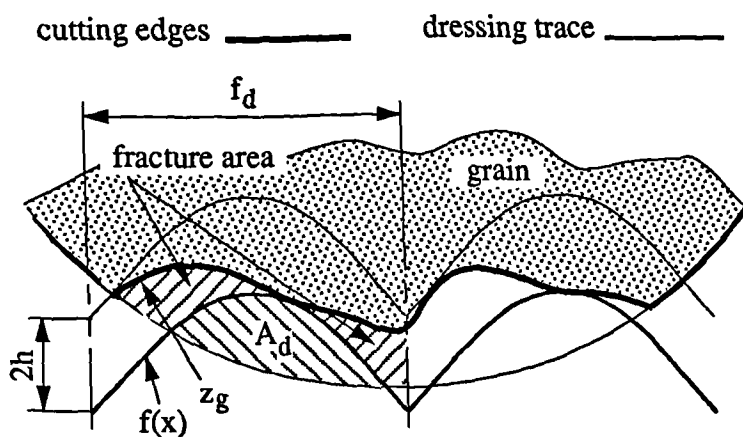


Figure 8.3 Cutting edges generated by dressing fracture

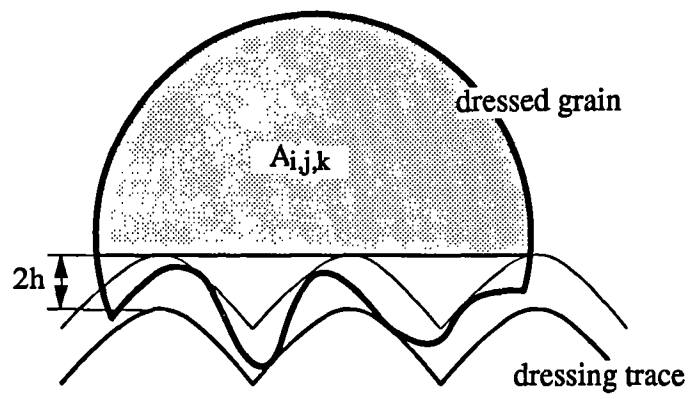


Figure 8.4 Simplified calculation of the remaining cross sectional area of the grain

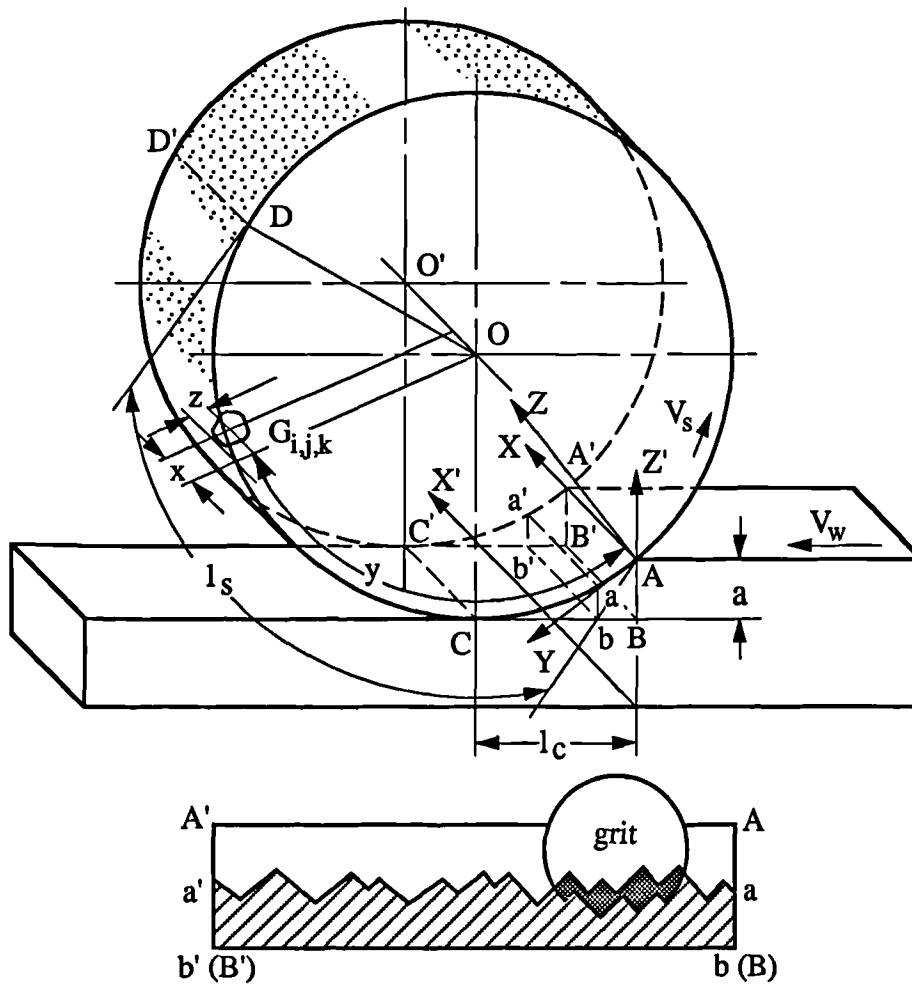


Figure 8.5 Kinematic relation between grinding wheel and workpiece

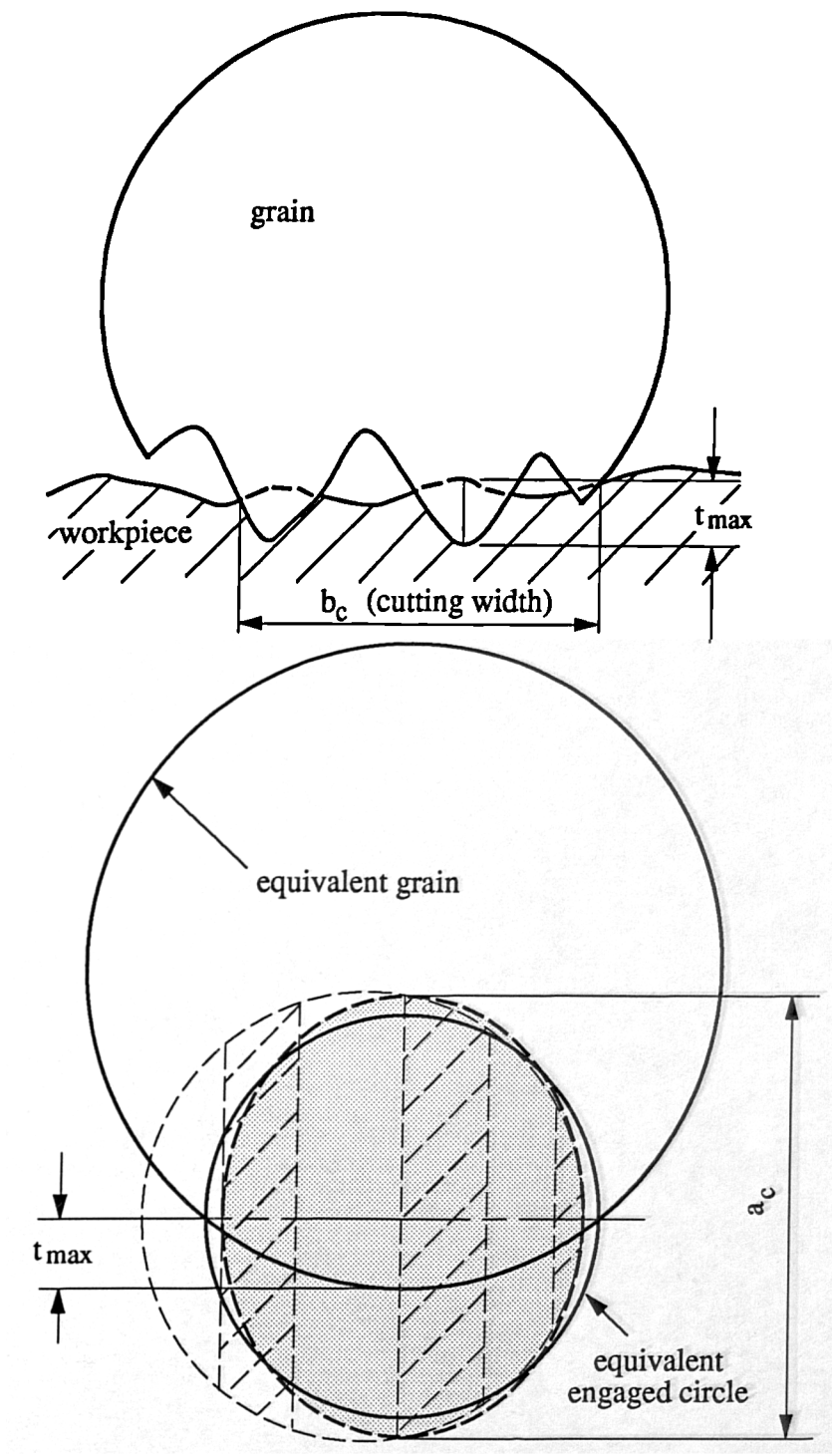


Figure 8.8 The equivalent grain in simulation

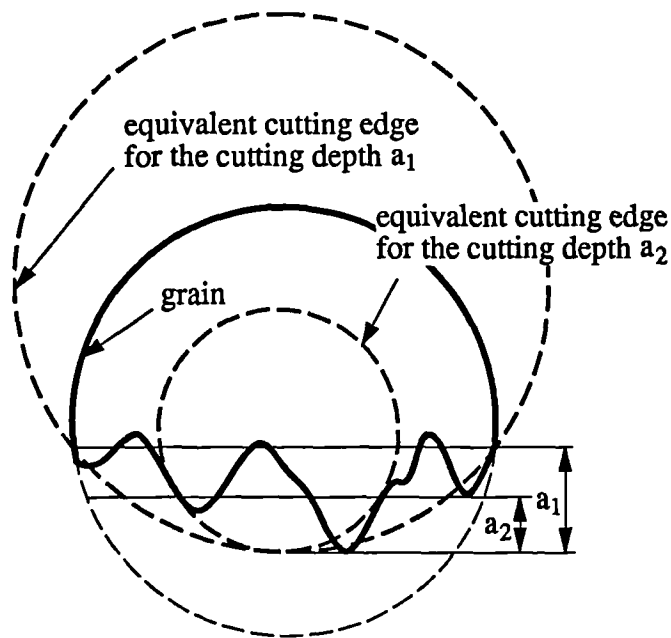


Figure 8.9 Equivalent spherical cutting edge as in sphere shape after dressing

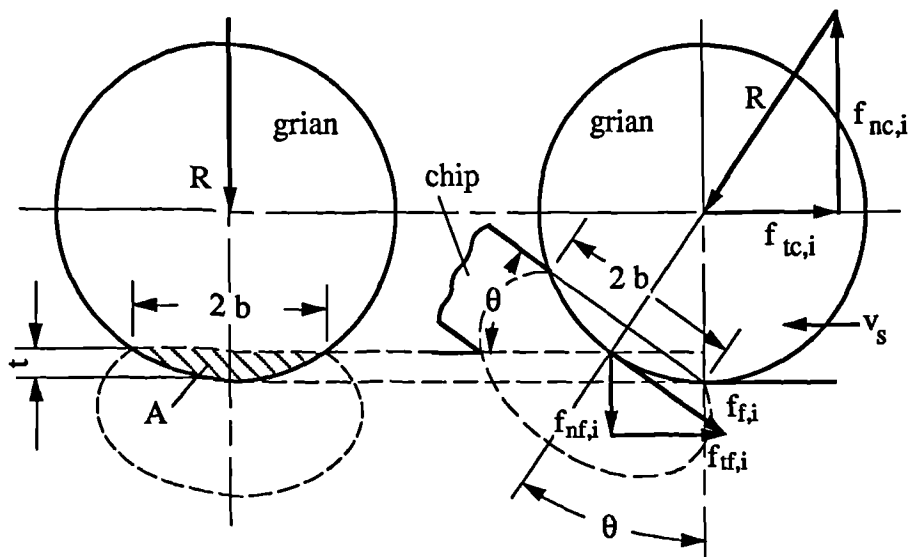


Figure 8.10 Grinding force on a spherical grain

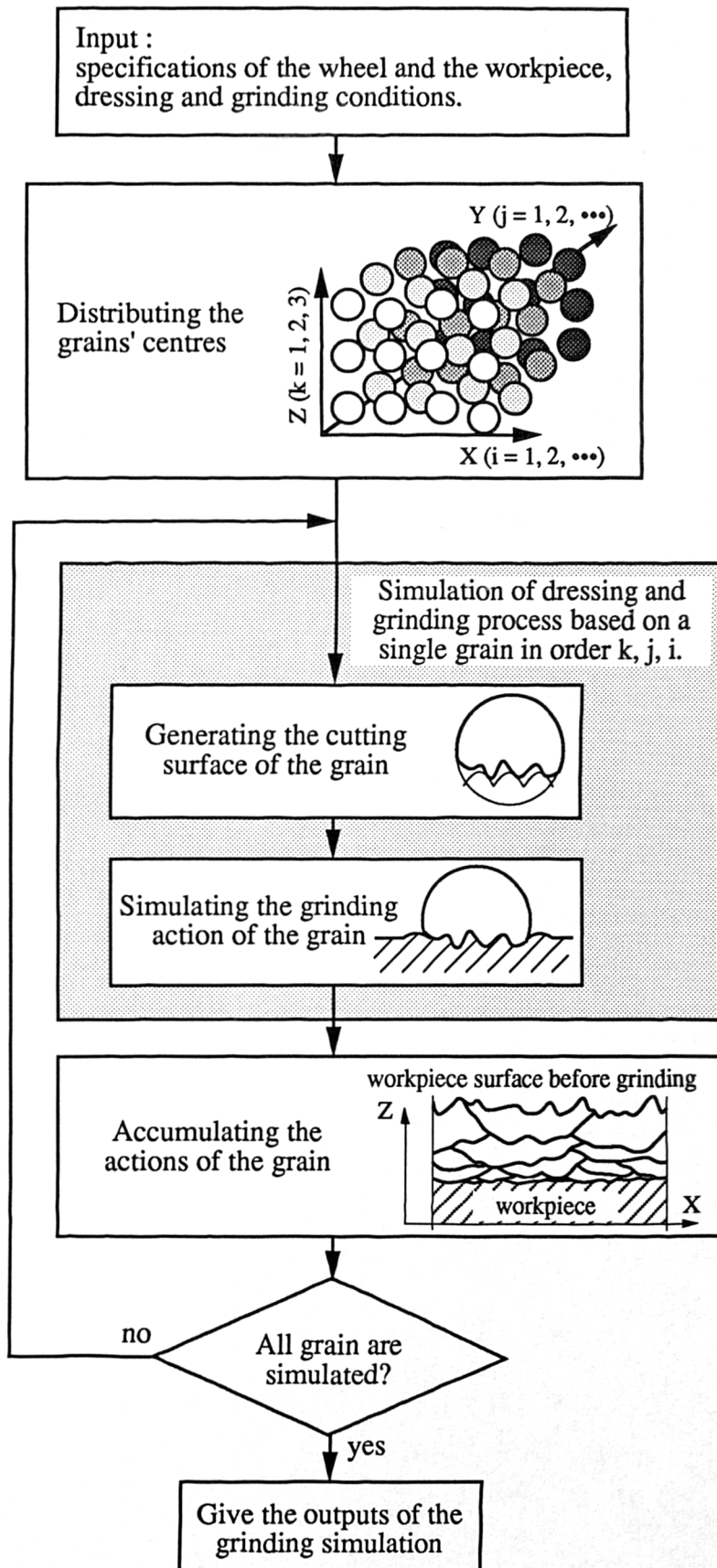


Figure 8.11 Flow chart of the dressing and grinding simulation program

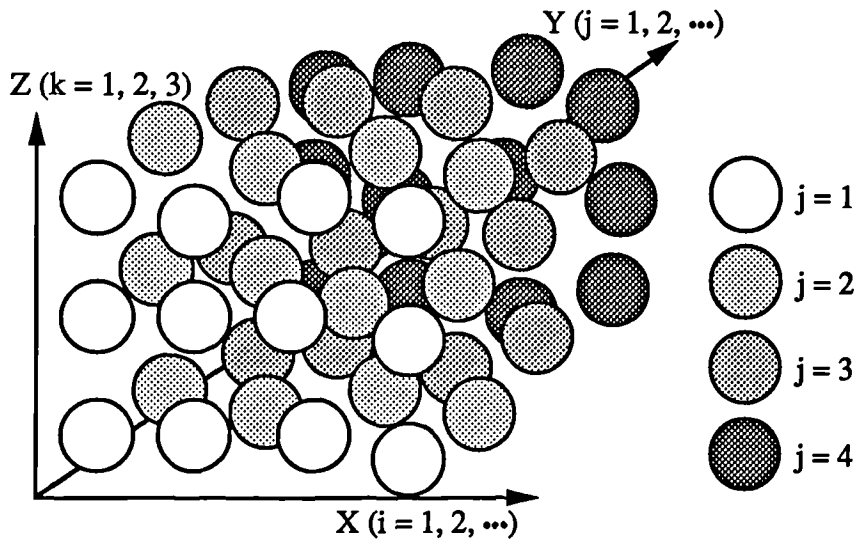


Figure 8.12 Random distribution of the grains in the simulation

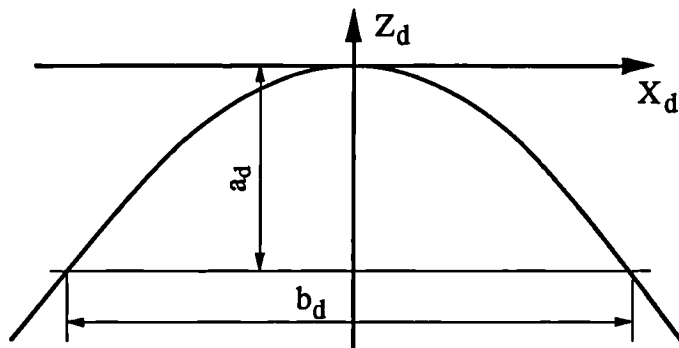


Figure 8.13 The contour of the diamond in the simulation

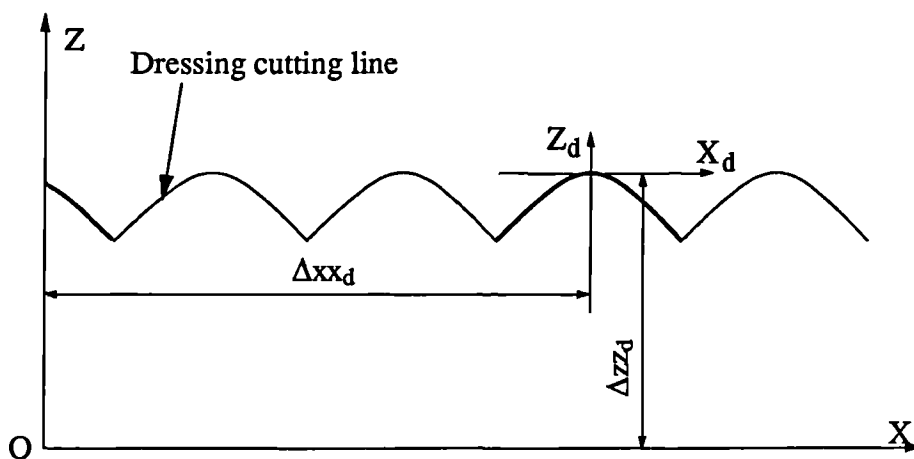


Figure 8.14 Dressing trace in the grinding wheel coordinate system

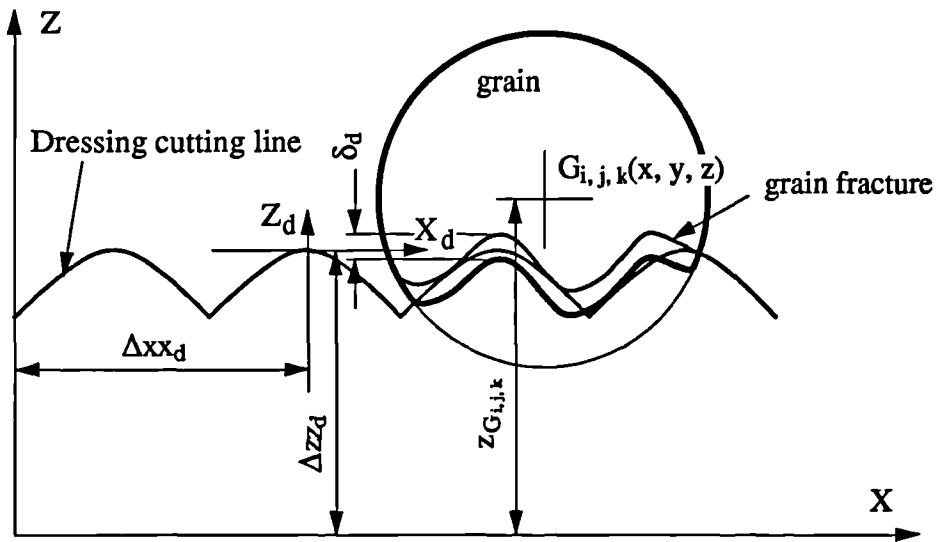


Figure 8.15 Simulation of the dressing process on a grain

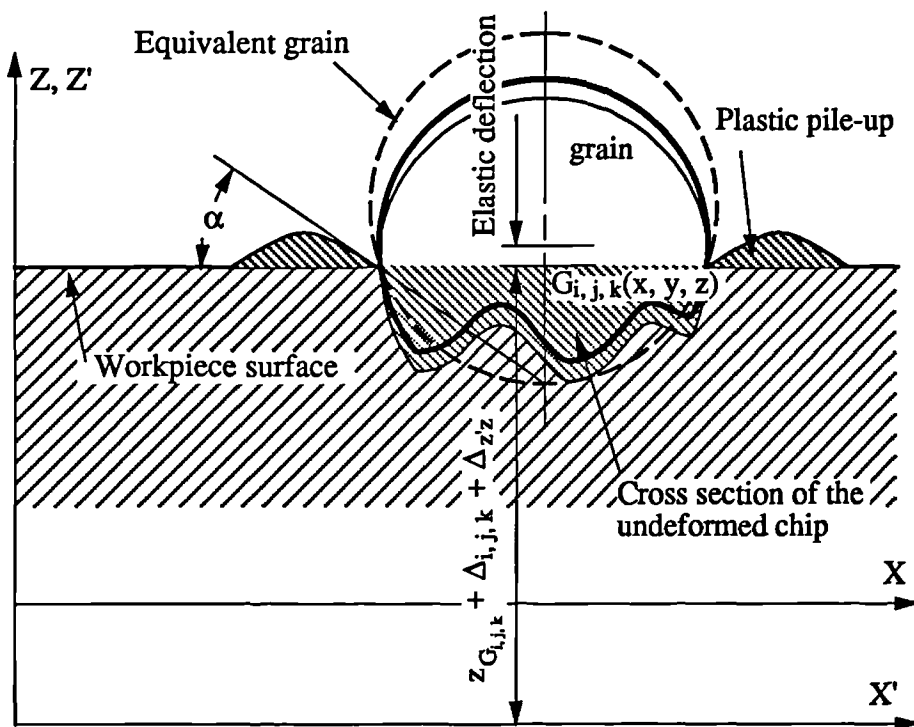


Figure 8.16 Simulation of the grinding process on a grain

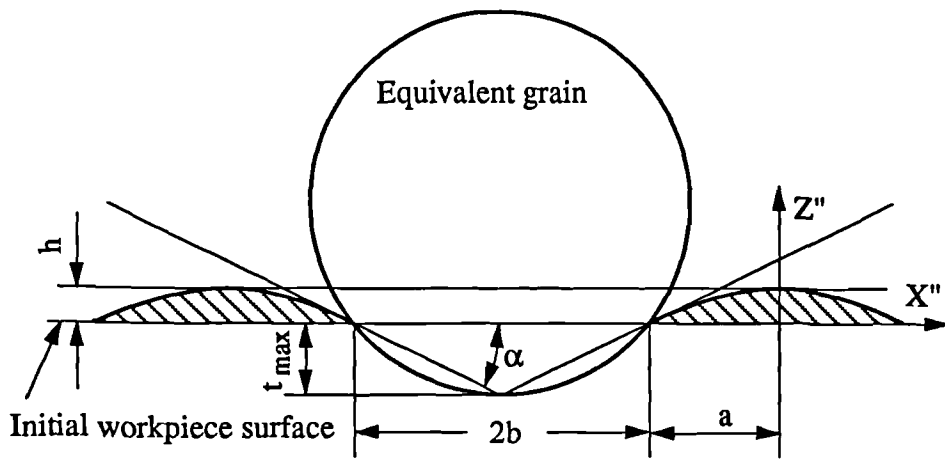


Figure 8.17 Simulation of the plastic pile up of the workpiece material

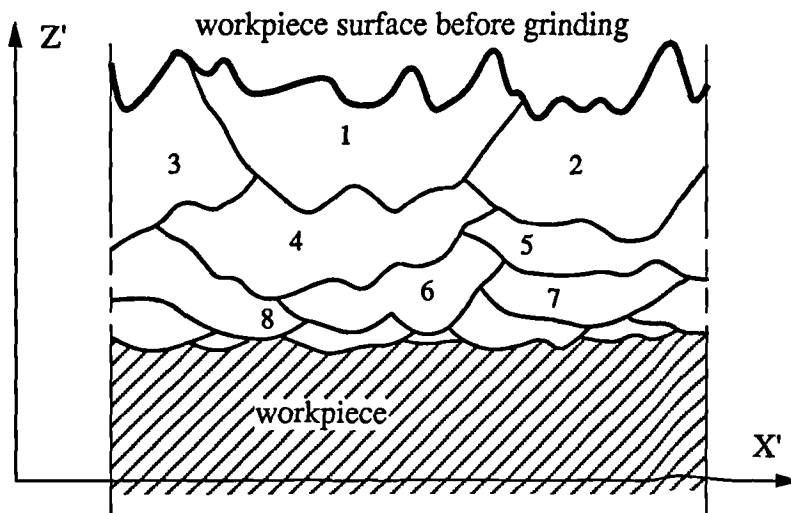


Figure 8.18 Generation of the workpiece during grinding

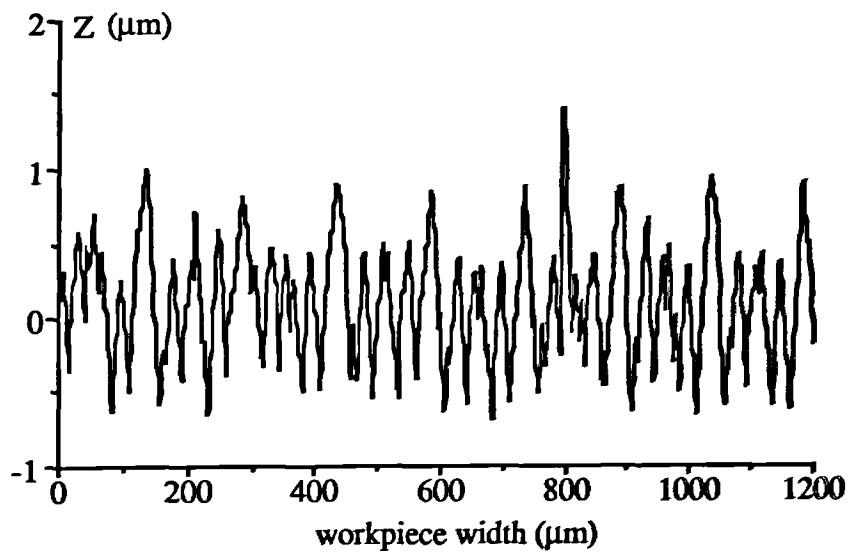


Figure 8.19 Ground surface generated from simulation

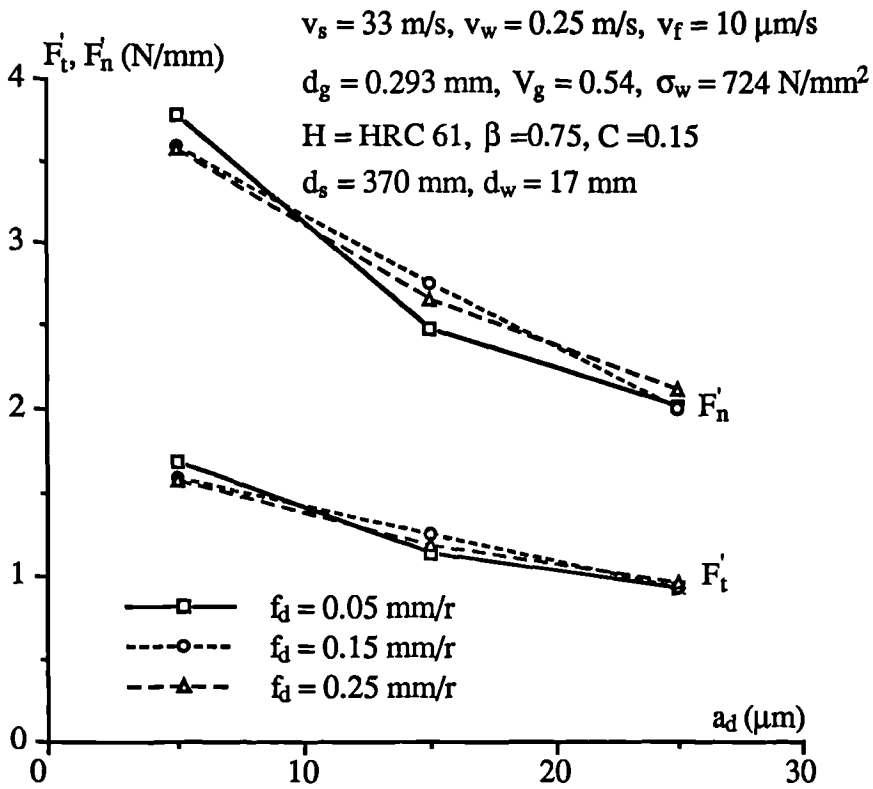


Figure 8.20 Simulated effects of dressing conditions on grinding force

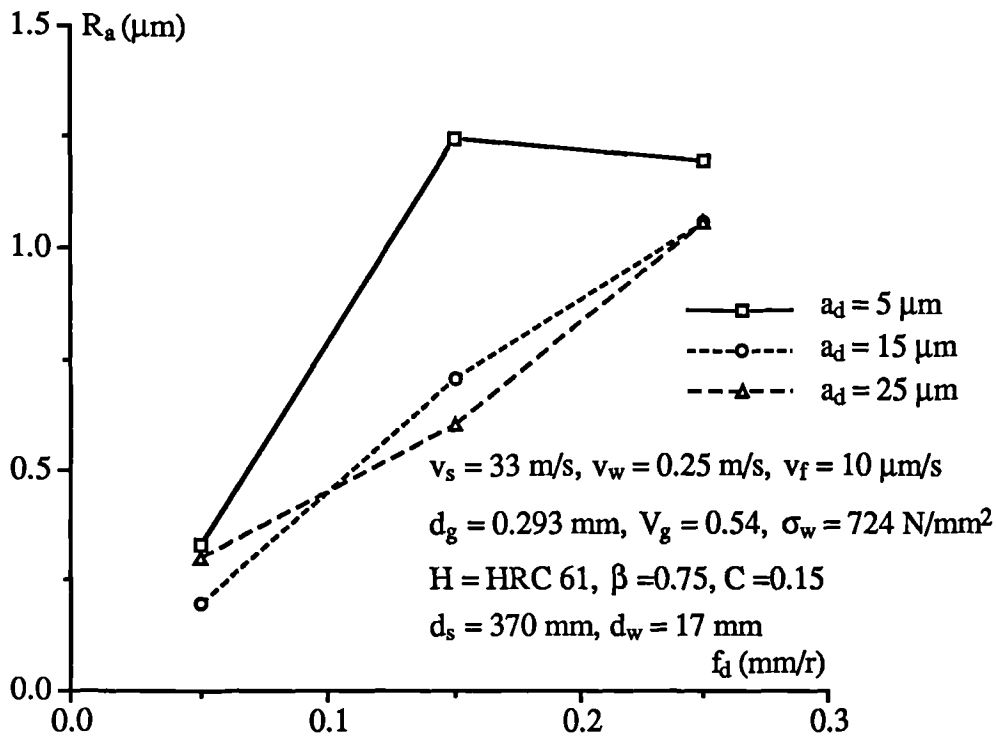


Figure 8.21 Simulated effects of dressing conditions on surface roughness

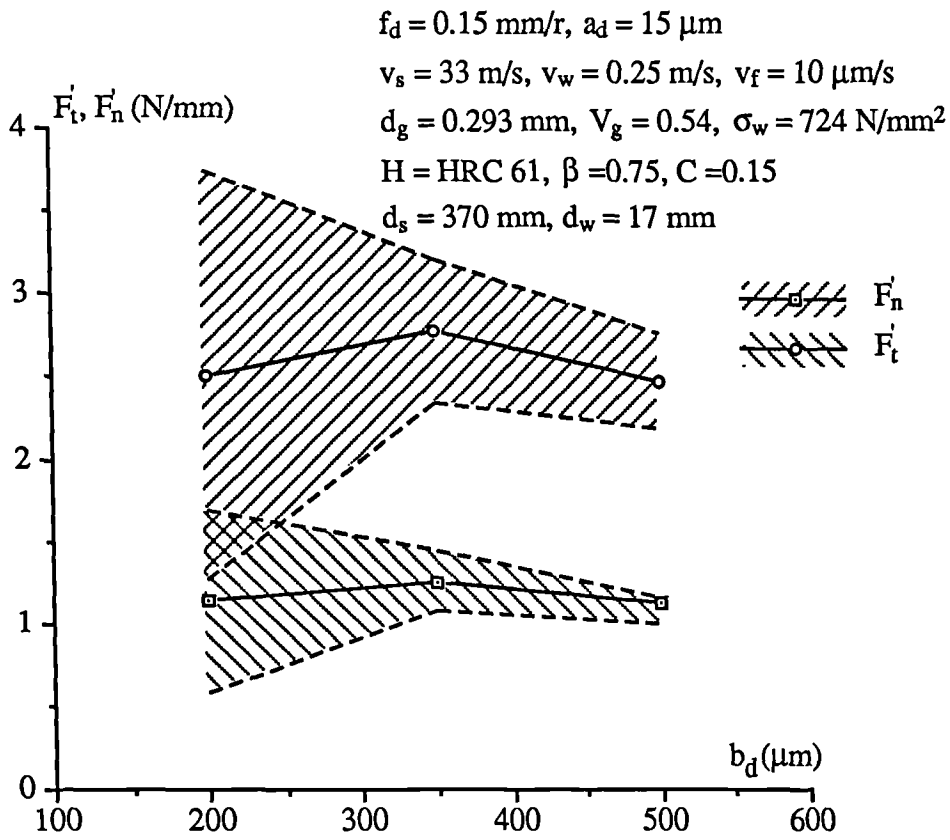


Figure 8.22 Simulated effects of diamond width on grinding force

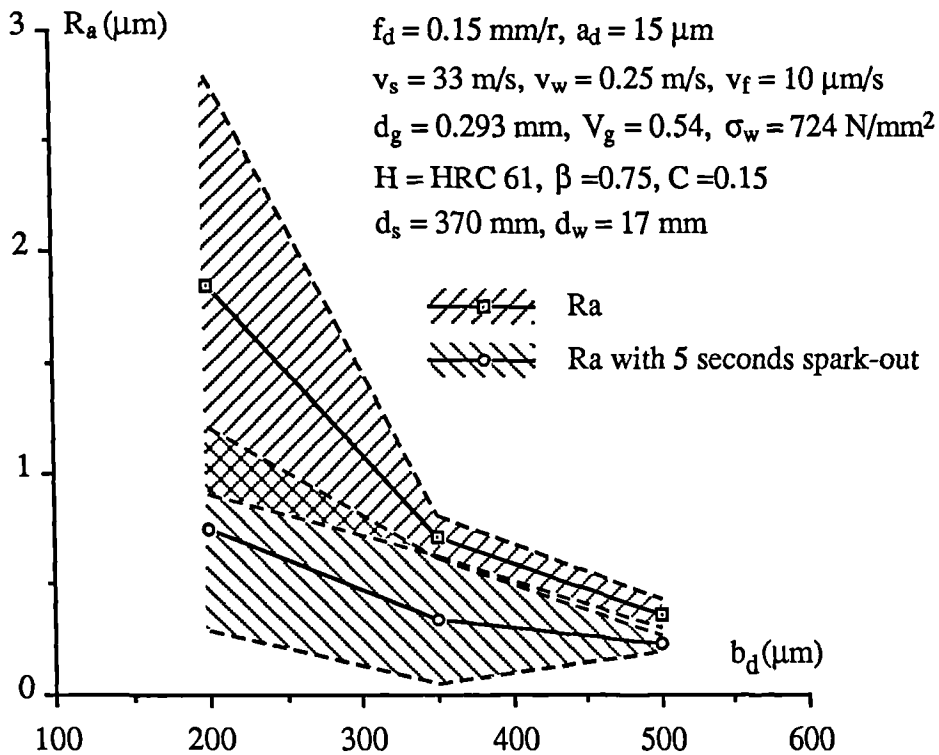


Figure 8.23 Simulated effects of diamond width on surface roughness

$v_s = 33 \text{ m/s}$, $v_w = 0.25 \text{ m/s}$, $v_f = 10 \text{ } \mu\text{m/s}$
 $d_g = 0.293 \text{ mm}$, $V_g = 0.54$, $\sigma_w = 724 \text{ N/mm}^2$
 $H = \text{HRC } 61$, $\beta = 0.75$, $C = 0.15$
 $d_s = 370 \text{ mm}$, $d_w = 17 \text{ mm}$

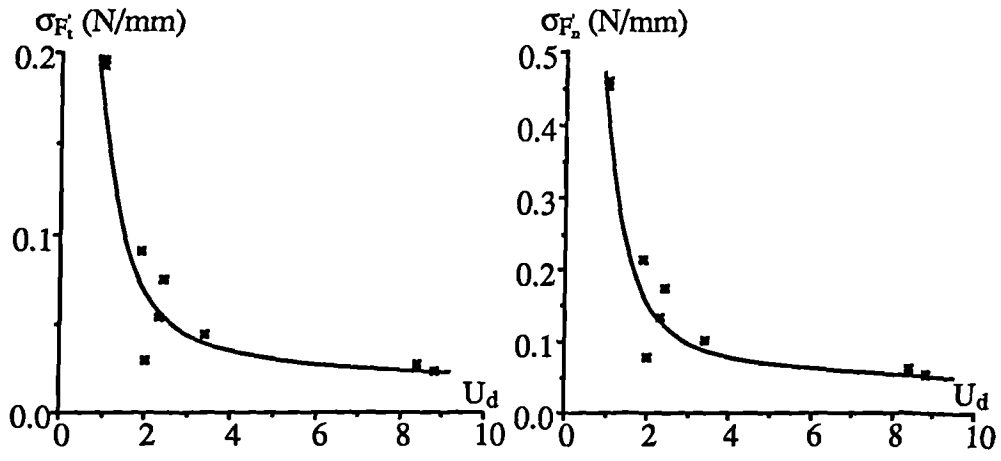


Figure 8.24 The relationship between standard deviation of grinding force and dressing overlap coefficient

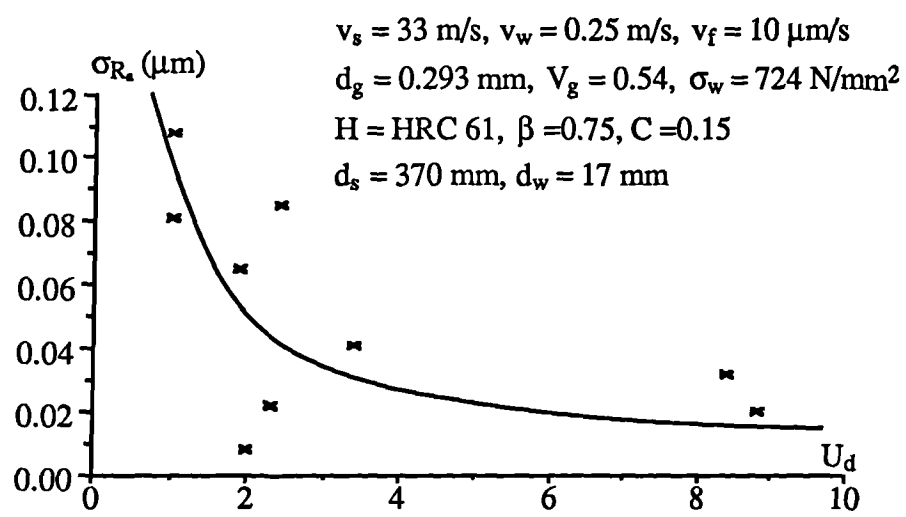


Figure 8.25 The relationship between standard deviation of surface roughness and dressing overlap coefficient

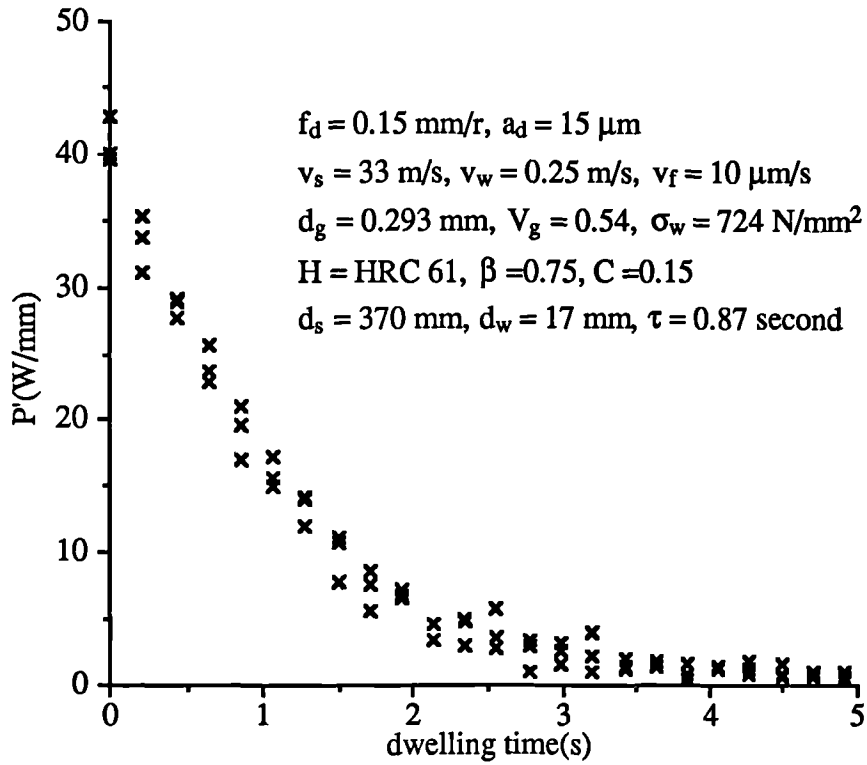


Figure 8.26 Simulated grinding power in the dwell period

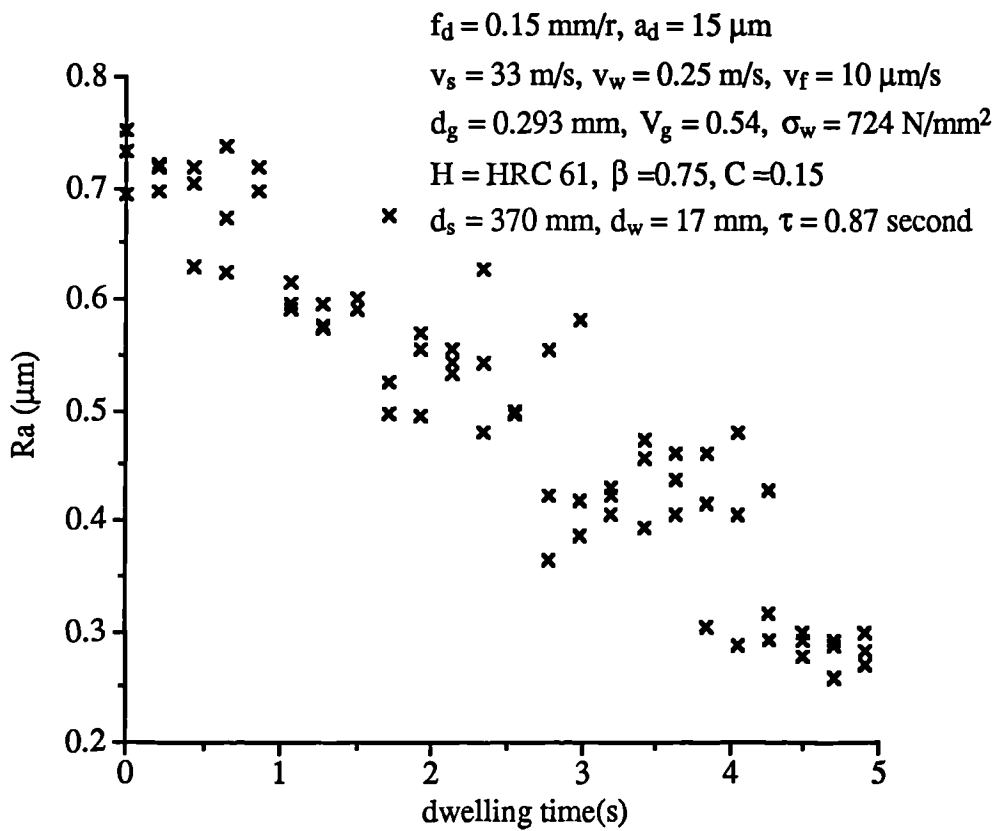


Figure 8.27 Simulated surface roughness variations in the dwell period

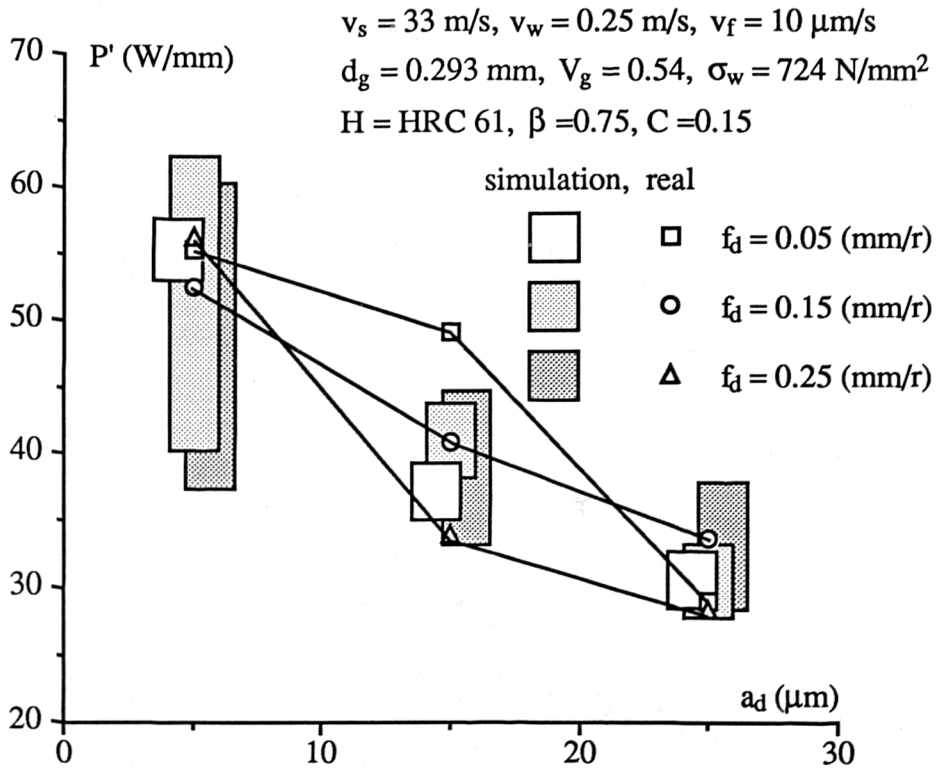


Figure 8.28 Simulated effects of dressing conditions on grinding power

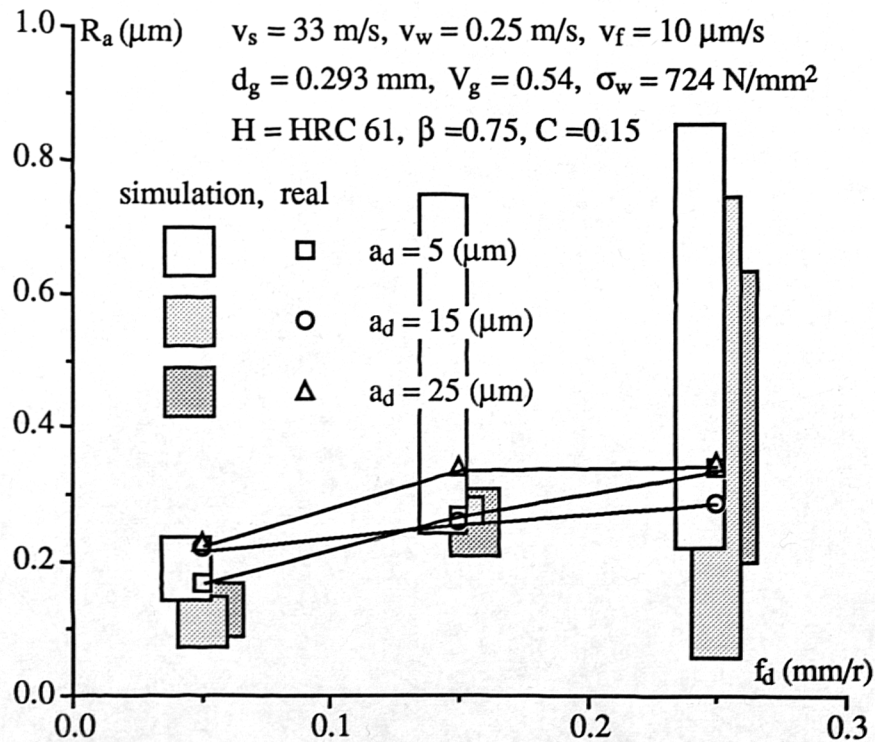


Figure 8.29 Simulated effects of dressing conditions on surface roughness (5 seconds dwell time)

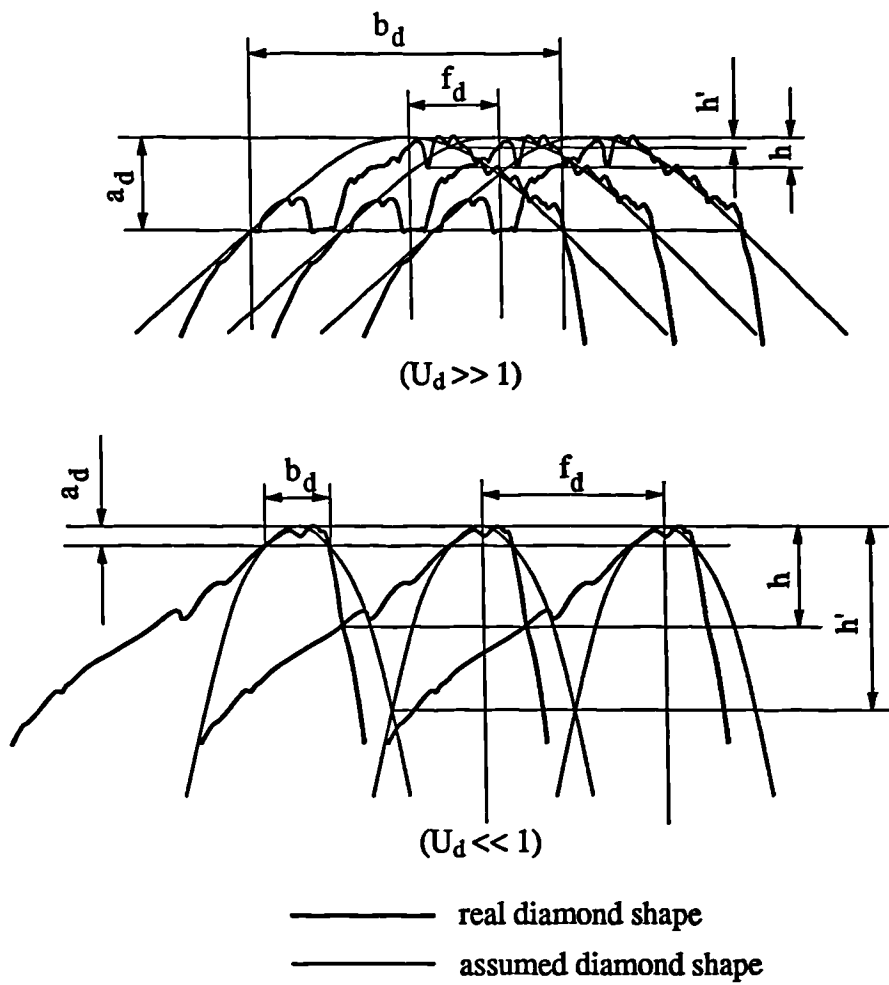


Figure 8.30 The difference between the parabola assumption and the real diamond

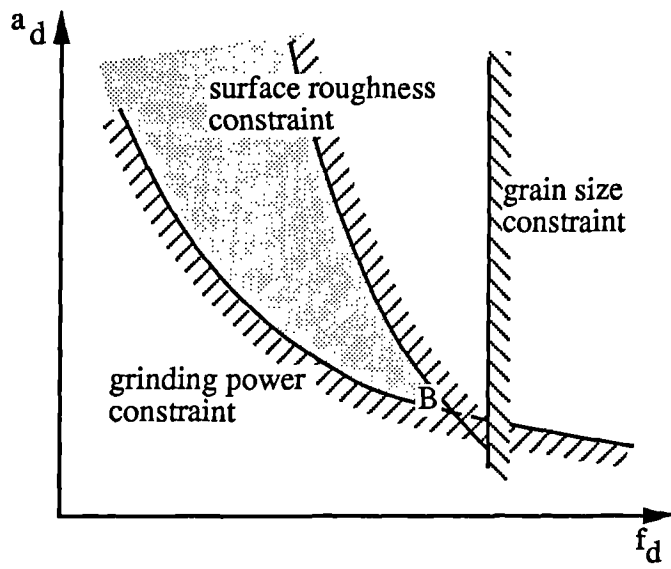


Figure 9.1 Constraints on the dressing condition

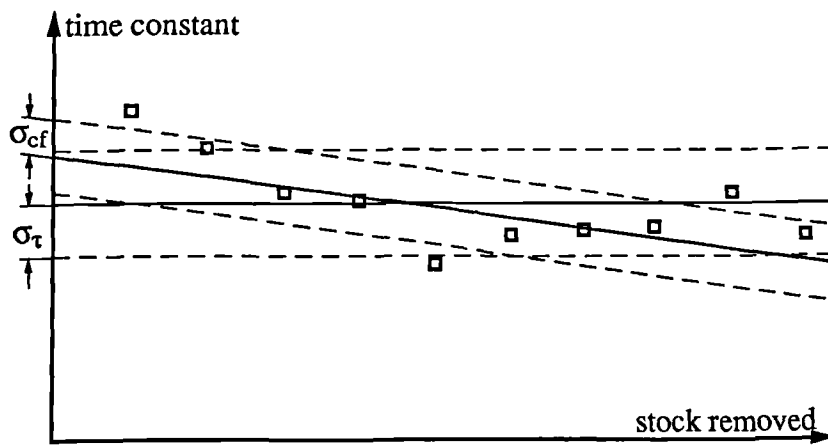


Figure 9.2 Variation of the time constant in the initial stage of grinding

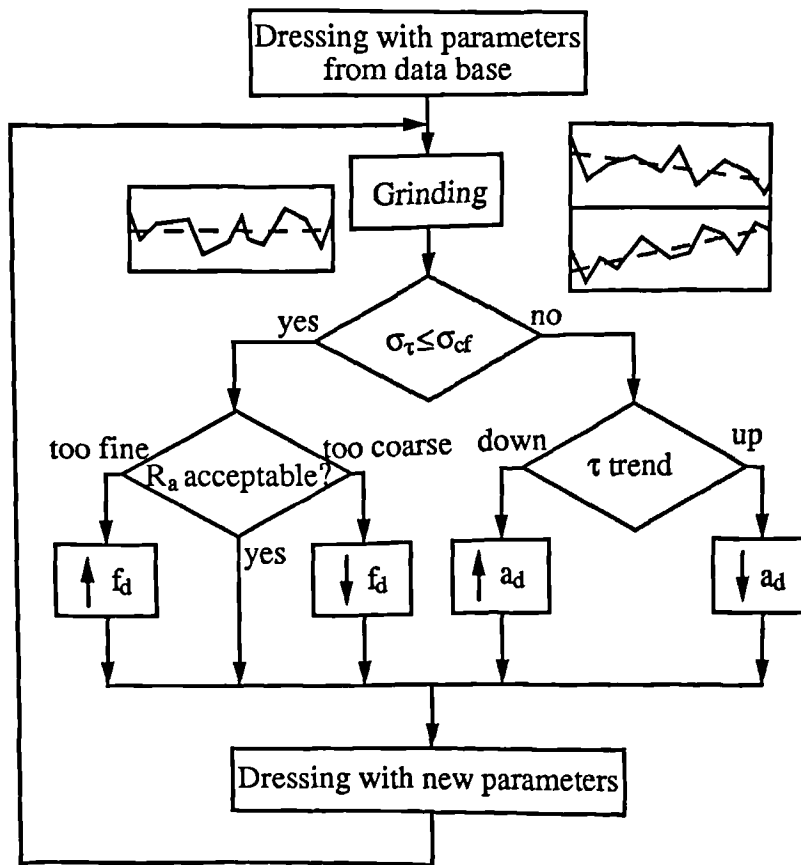


Figure 9.3 A strategy of minimizing time constant

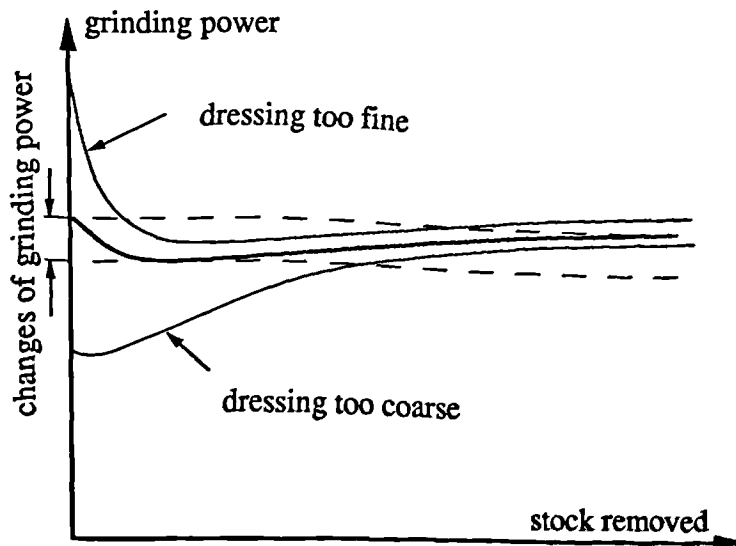


Figure 9.4 Variation of grinding power in a redress life cycle

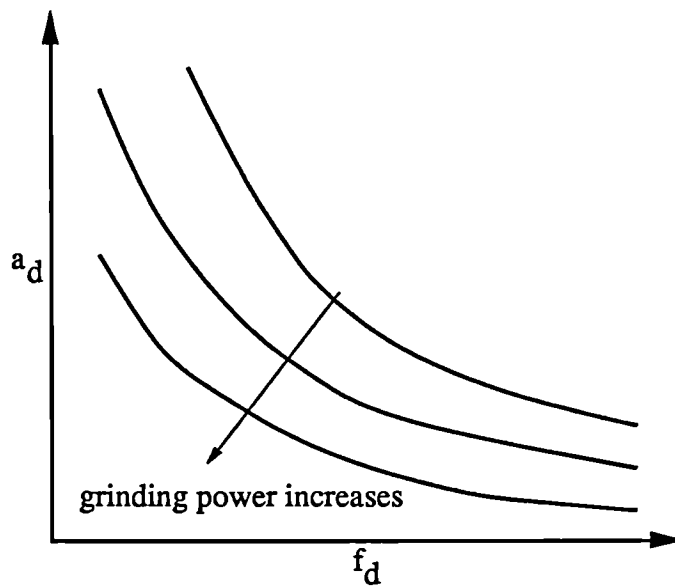


Figure 9.5 Relationship between the grinding power and dressing conditions

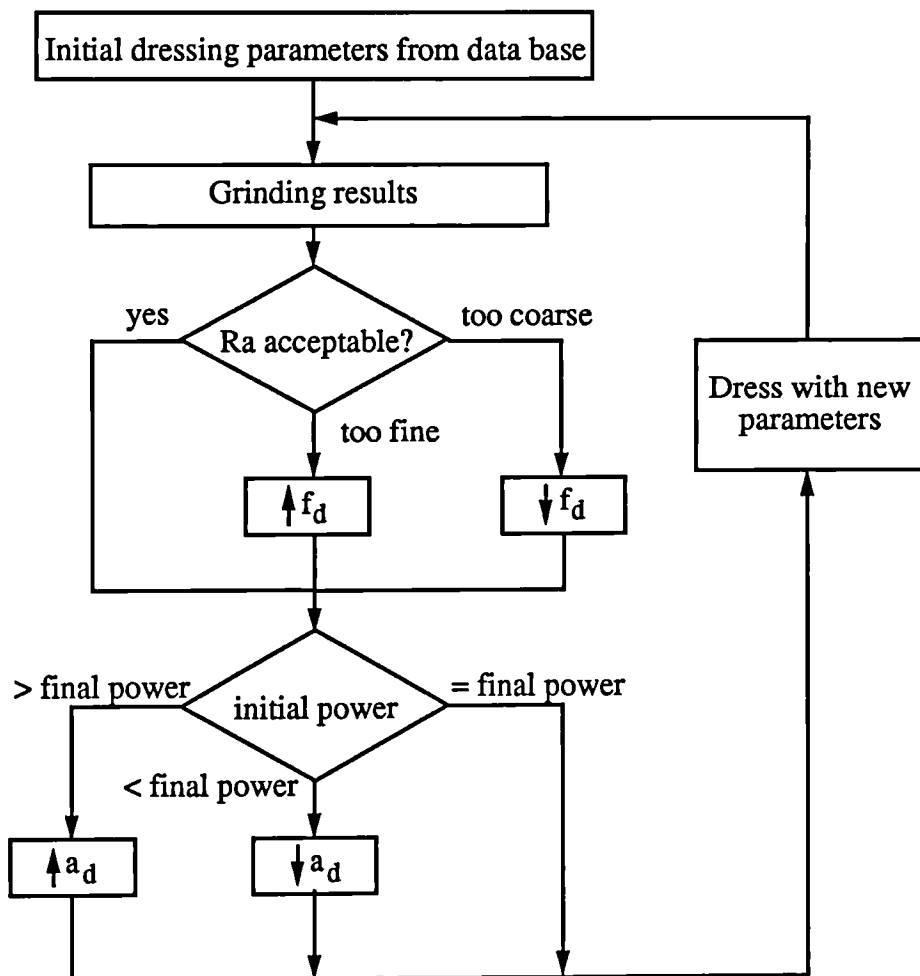


figure 9.6 Strategy to stabilise grinding power level

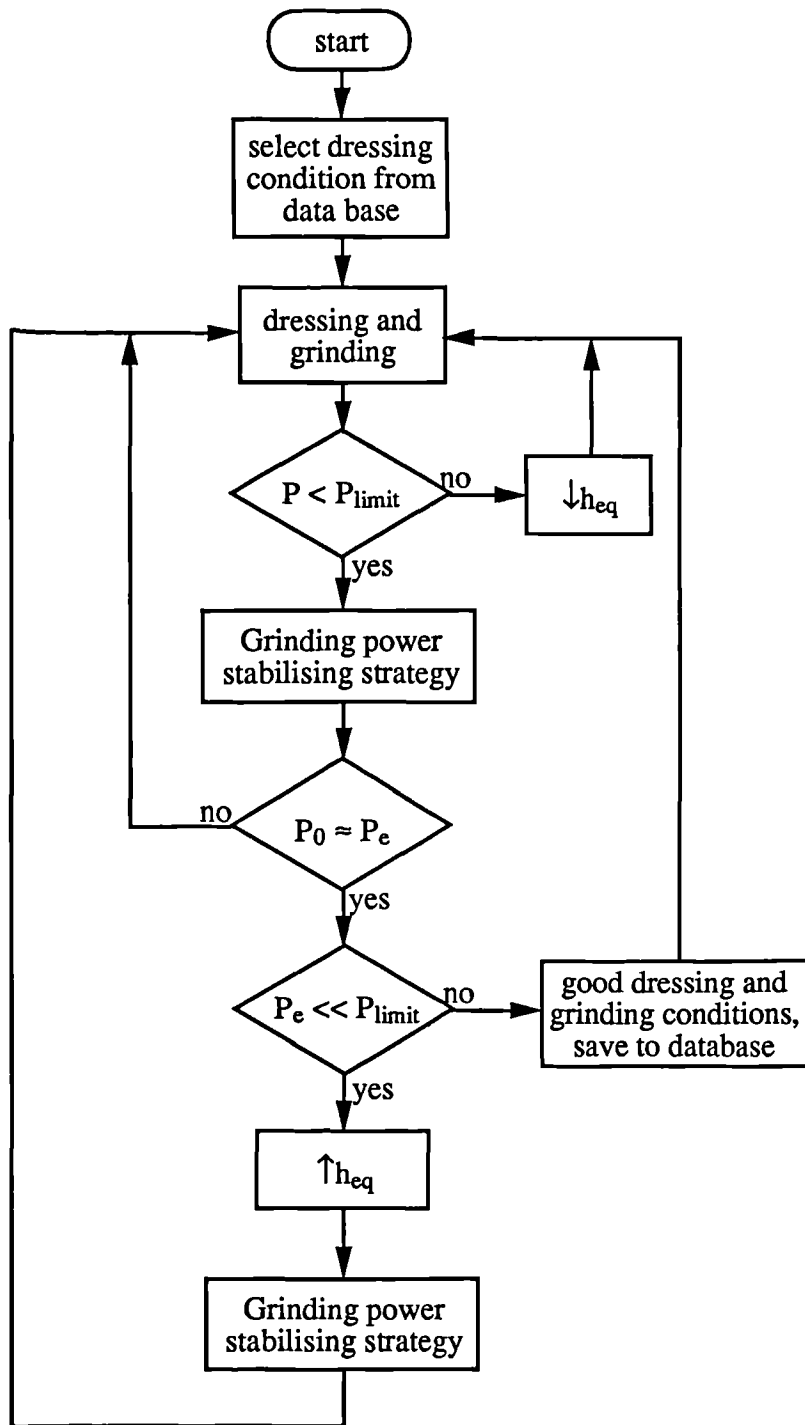


Figure 9.7 Maximum grinding power strategy for selection of dressing conditions

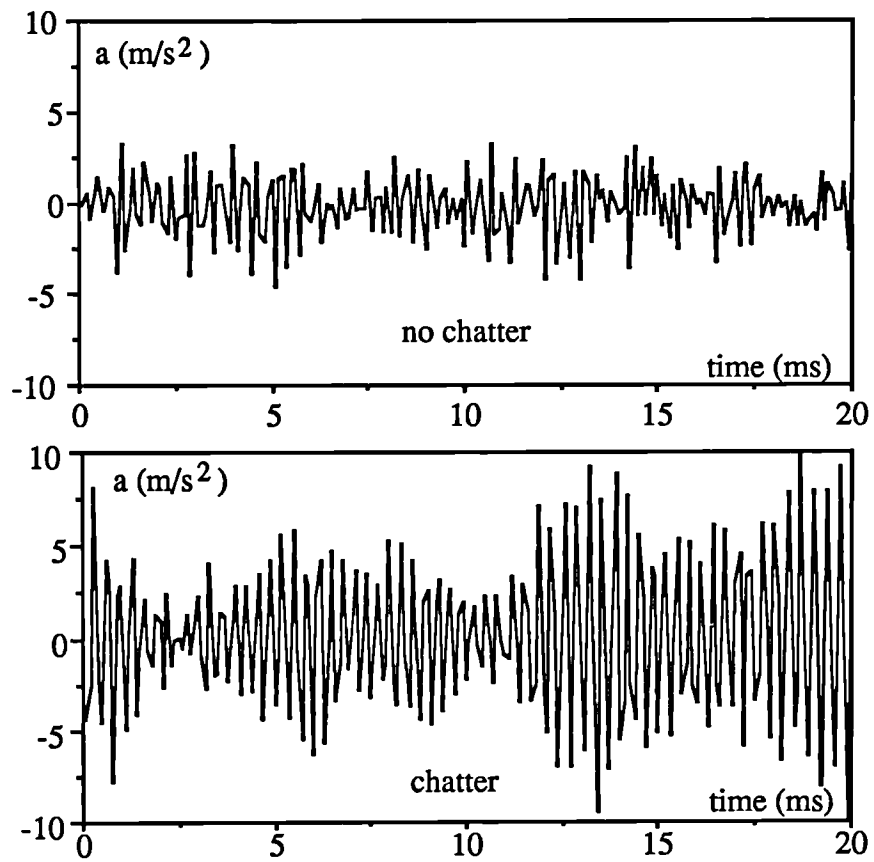
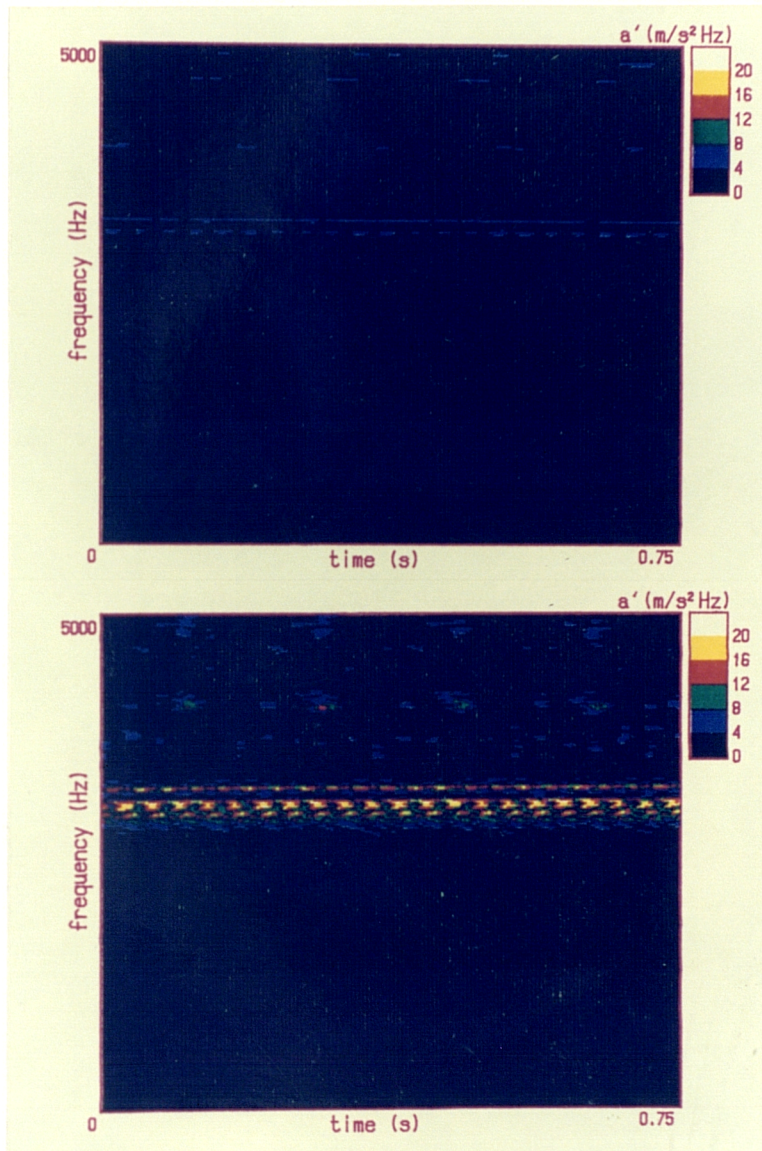


Figure 10.1 Acceleration signals of grinding vibrations



(a) No chatter

(b) Chatter

Figure 10.2 Spectra of grinding vibration

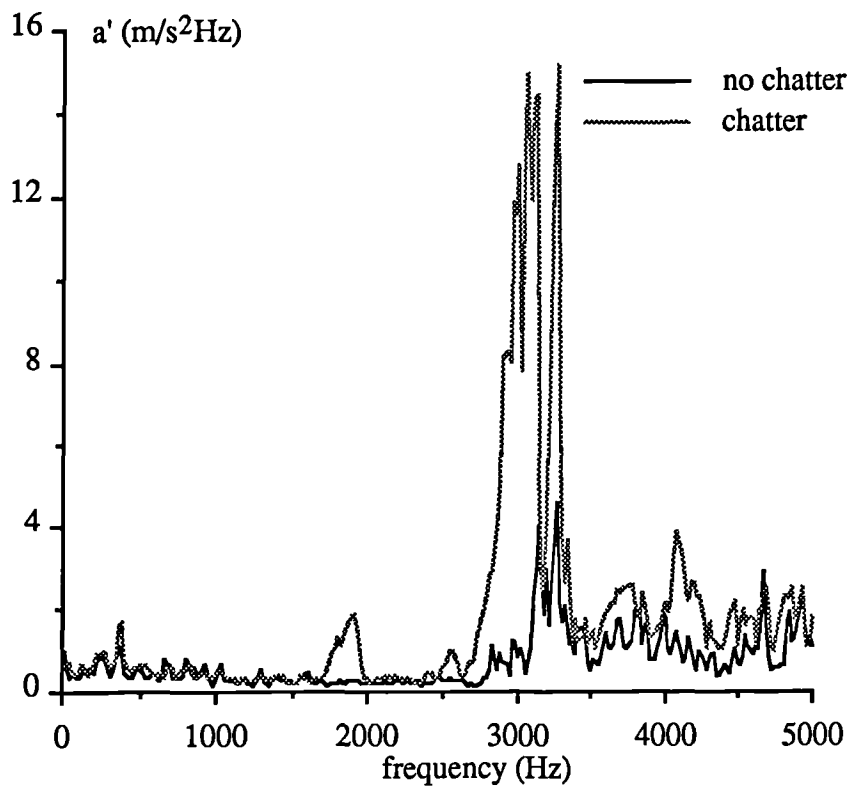


Figure 10.3 The spectrum of grinding vibrations

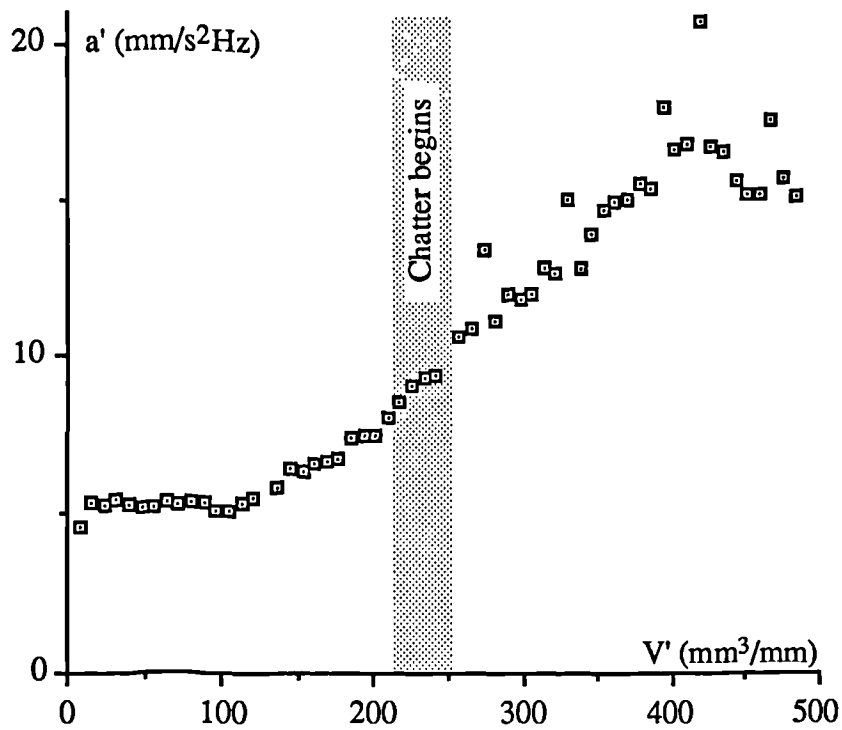


Figure 10.4 Development of the grinding vibration

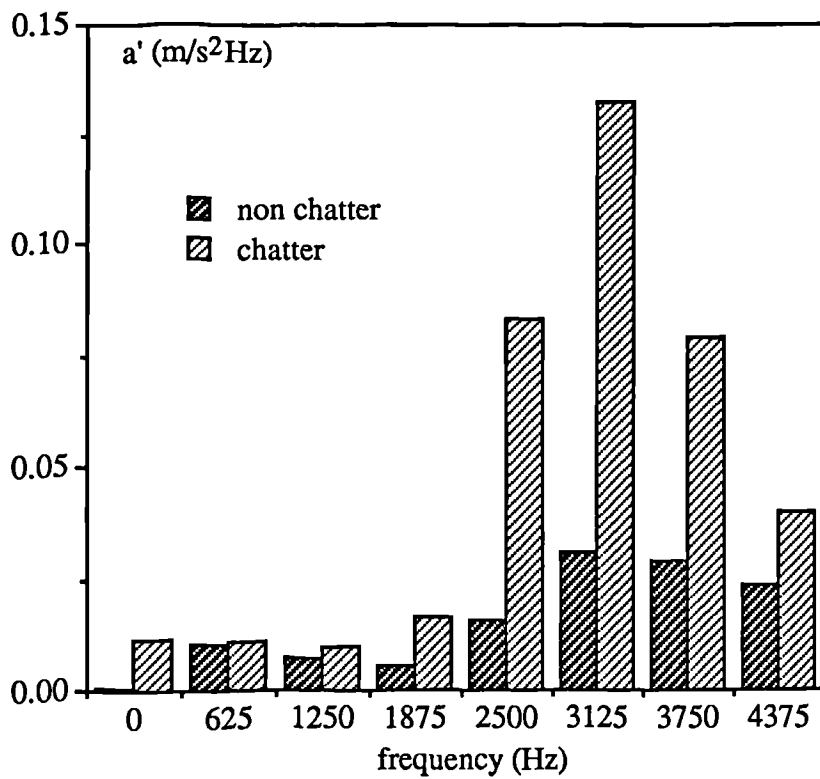


Figure 10.5 Distribution of acceleration density in eight band filters

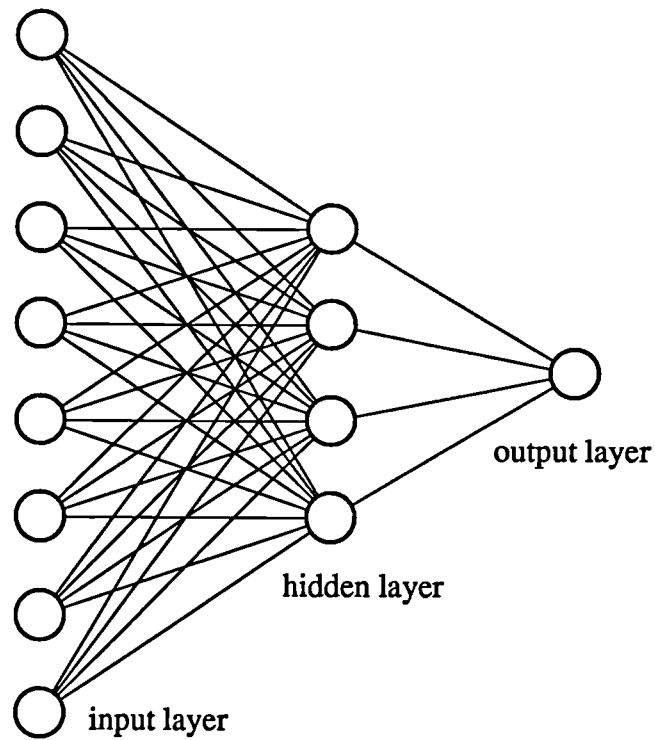


Figure 10.6 the structure of a neural network for chatter identification

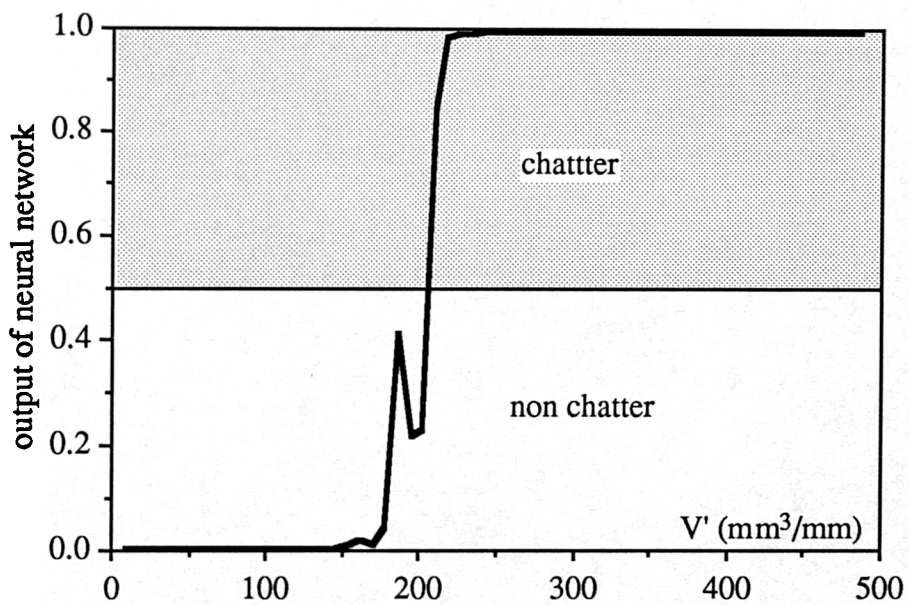


Figure 10.7 Grinding chatter recognition by neural network

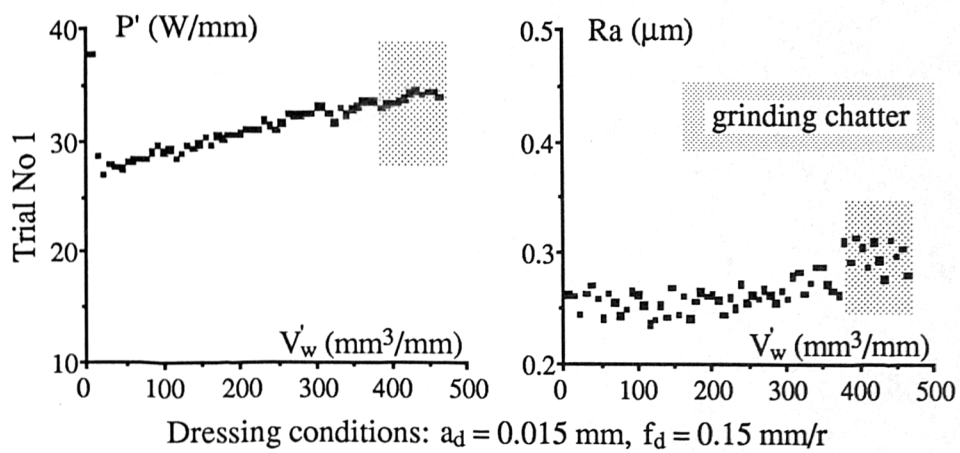


Figure 10.8 Grinding performances under initial dressing conditions

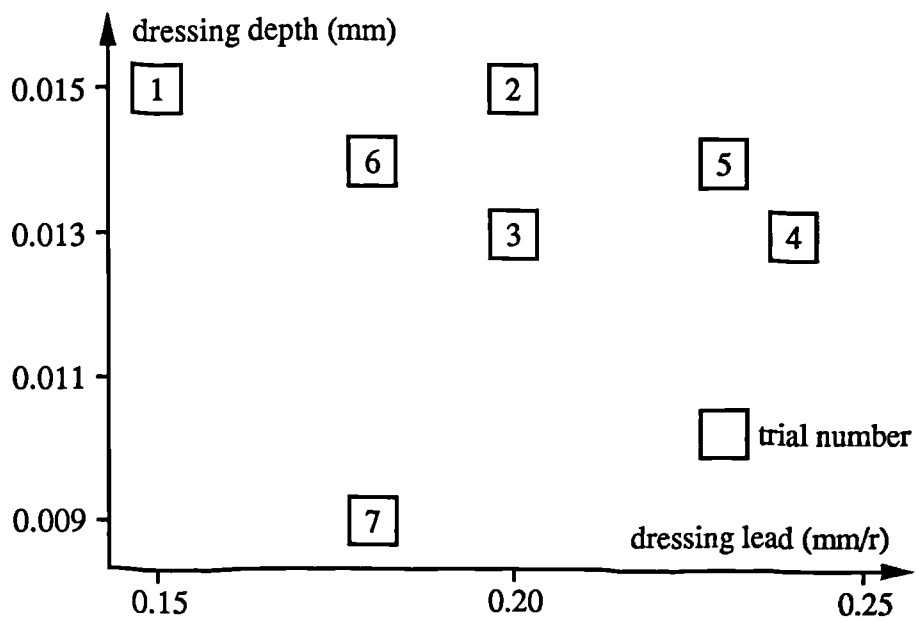


Figure 10.9 Dressing conditions recommended by dressing strategy

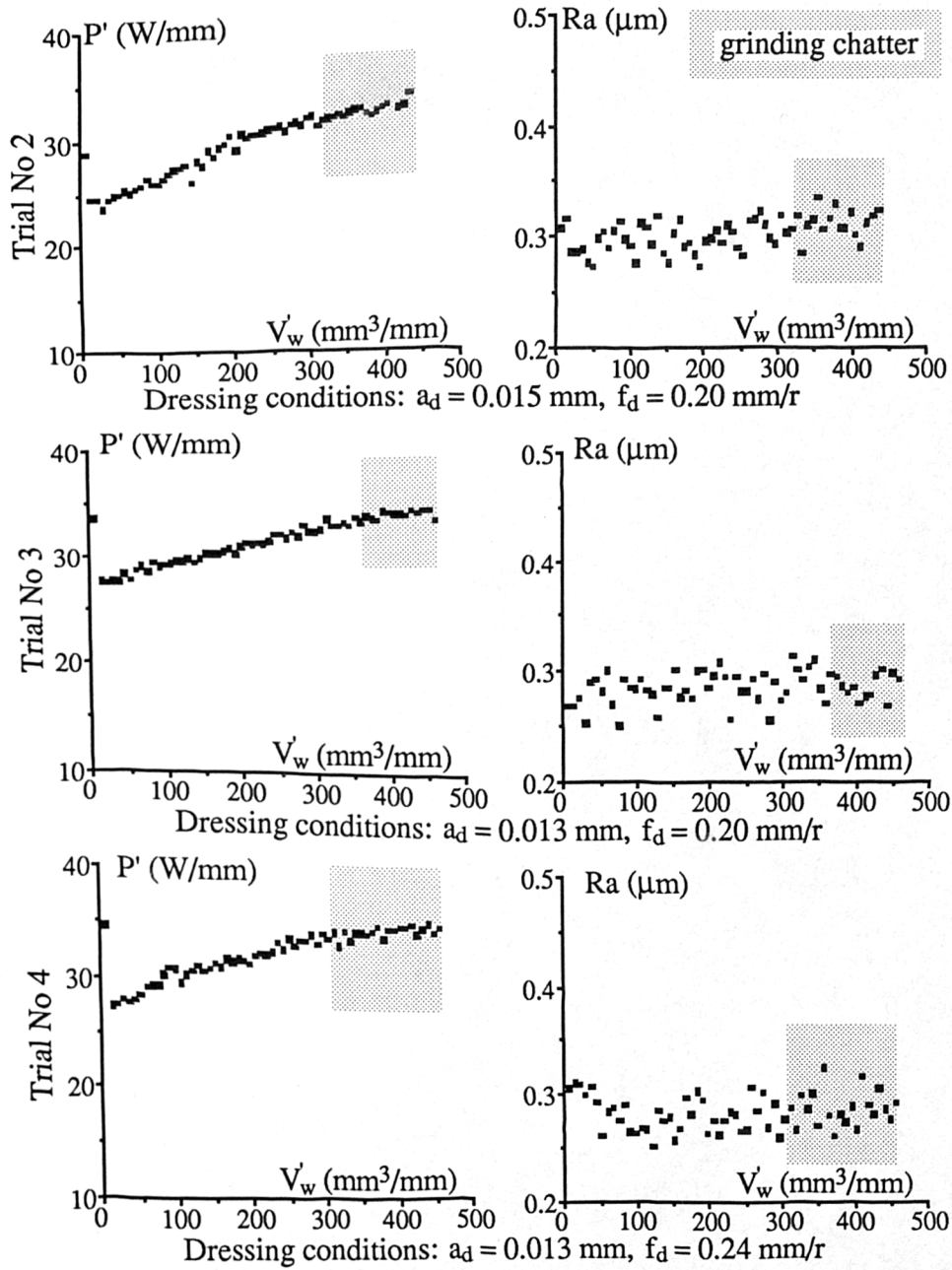


Figure 10.10 Optimization of dressing conditions by the dressing strategy

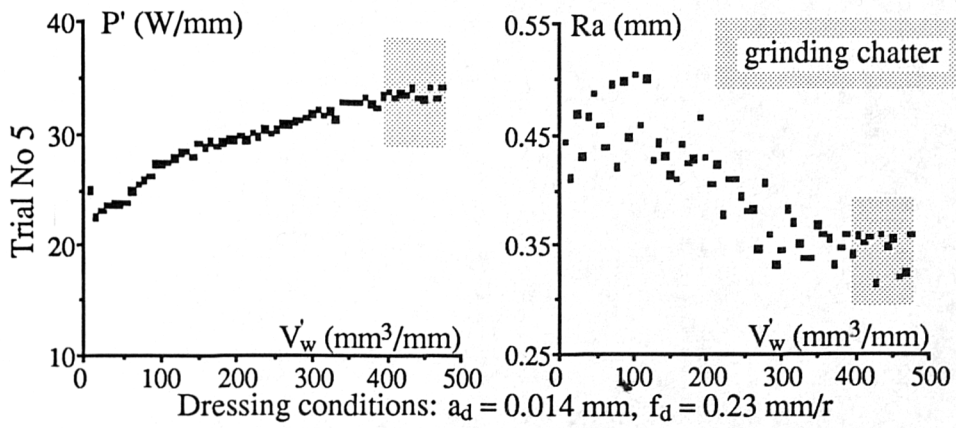


Figure 10.11 Deterioration of grinding performances due to diamond wear

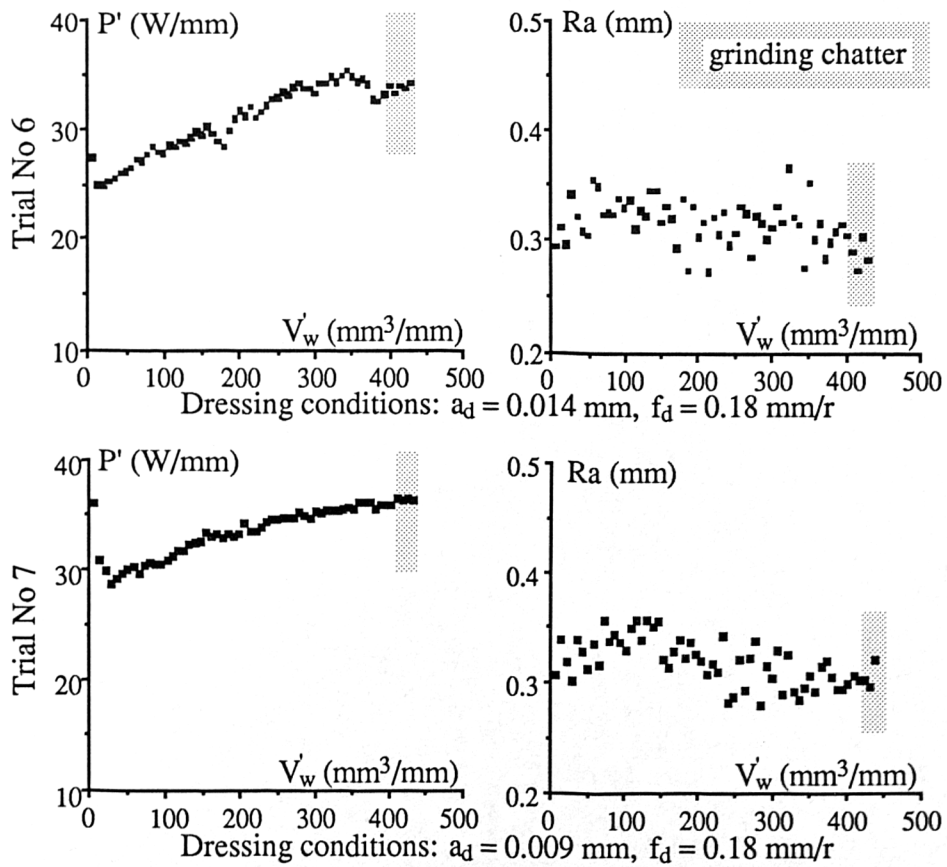


Figure 10.12 Improvement of grinding performances by dressing strategy